FACULTY OF SCIENCE
UNIVERSITY OF COPENHAGEN

Enhancement of optical nonlinearities with stationary light

Ivan Iakoupov

PhD thesis

Academic advisor: Anders S. Sørensen
This thesis has been submitted to the PhD School of The Faculty of Science, University of Copenhagen.
Submission date: December 14th, 2016

English abstract

The topic of this thesis is understanding and application of the phenomenon of stationary light. Stationary light arises in atomic ensembles with certain energy level configurations, when two counter-propagating classical drives (lasers) are applied. Probe light coupled to a different energy level transition than the classical drives can be completely stopped, while still retaining its light character. This is very different from a related phenomenon of slow light or electromagnetically induced transparency (EIT), where stopping propagation of light completely converts it into an atomic excitation instead. More generally, we will be interested in the regime of stationary light, where the probe light still propagates through the atomic ensemble, but extremely slowly. In other words, probe field has a very low group velocity, which increases its interaction time with any optical nonlinearity. Group velocity can be obtained from the dispersion relation. Therefore, the dispersion relations for various stationary light schemes are studied in detail. The study of the dispersion relations is carried out both in the continuum approximation of atomic ensembles and the discrete model where each atom is assumed to be a linear scatterer.

The enhancement of the effective nonlinear strength by stationary light is then used to propose a two-qubit (controlled-phase) quantum gate for the optical photons, which can in principle work deterministically. We do find, however, that a heralded operation of the proposed gate achieves much higher conditional fidelity (overlap of the ideal state with the actual one), since most of the error in the unconditional fidelity is due to loss of photons, which can be detected. We also find that the gate can approach the ideal limit (both in the deterministic and heralded operation) by increasing the total number of atoms in the atomic ensemble to compensate for a limited single-atom coupling strength.

Before discussing stationary light and its application, we also analyse the different fidelity measures that could be applied to the proposed gate (and related proposals). We show that all of the considered fidelity measures are (approximately) equal due to particular features of the considered physical system. This result allows one to reduce the number of expressions to be evaluated if the performance of the gate is to be analyzed for different applications at the same time.

Dansk resumé

Emnet for denne afhandling er forståelse og anvendelse af fænomenet af stationært lys. Stationært lys opstår i atomare ensemler med en bestemt konfiguration af energiniveauer, når to modpropagerende klassiske drev (lasere) er anvendt. Probelys koblet til et andet energiniveau overgang end de klassiske drev kan blive fuldstændigt stoppet men stadig bevare sin lys karakter. Det er meget forskelligt fra det relaterede fænomen af langsomt lys eller elektromagnetisk induceret gennemsigtighed (EIT), hvor standsning af lyspropagation konverterer lyset fuldstændigt til en atomar excitation i stedet for. Mere generelt vil vi være interesseret i regimet af stationært lys, hvor probelys stadig propagerer gennem det atomare ensemble, men meget langsomt. Med andre ord, probelys har en meget lav gruppehastighed, som øger dens vekselvirkningstid med enhver optisk ikke-linearitet. Gruppehastighed kan beregnes fra dispersionsrelationen. Derfor studerer vi dispersionsrelationer af forskellige former af stationært lys i detaljer. Studiet af dispersionsrelationer er udført både i kontinuumsapproksimationen af de atomare ensembler og den diskrete model, hvor hvert atom er antaget at være en lineær spreder.

Forbedring af den effektive ikke-lineære styrke med stationært lys er brugt til at foreslå en to-qubit (controlled-phase) kvantegate for de optiske fotoner, som kan i princippet fungere deterministiskt. Dog finder vi, at betinget måde at anvende gaten giver større betinget fidelity (overlap af den ideelle tilstand med den faktiske), eftersom det meste af fejlen i den ubetingede fidelity er pga. tab af fotoner, som kan detekteres. Vi også finder, at gaten kan komme arbitræt tæt på den ideelle grænse (både for deterministisk og betinget måde at anvende den) ved at øge det samlede antal atomer i ensemblet for at kompensere for en begrænset enkelt atom koblingsstyrke.

Før vi diskuterer stationært lys og dens anvendelse, vi analyserer også de forskellige slags fidelity mål, som kan blive andvendt til den foreslåede gate (og de relaterede forslag). Vi viser, at alle de betragtede fidelity mål er (approksimativt) lig med hinanden pga. bestemte egenskaber af den betragtede fysiske system. Dette resultat gør det muligt at reducere antallet af udtryk, som skal evalueres, hvis ydeevnen af gaten skal analyseres for forskellige anvendelser samtidig.

Acknowledgements

There is a number of people that I want to thank for helping me get through the PhD study. I have been fortunate to collaborate with many smart people, from whom I learned a great deal. Some of them are mentioned below in the context of specific chapters, where I have listed their contributions. In terms of collaborators, there is one name that is not specifically listed, my academic advisor Anders S. Sørensen, whose ideas and contributions are so entangled with mine throughout everything in this thesis that it will be impossible to separately list them all. I can provide the following guideline for the readers of my thesis. All the complicated mathematical derivations are almost certainly mine (unless noted otherwise), and I take full responsibility for any difficulty encountered with getting through them. For better or worse, Anders could not completely rectify my tendency to get carried away with math even after several years of working together. On the other hand, many of the insightful physical explanations following those mathematical derivations are partially or completely inspired by the ones of Anders. I would like to think that I got a hang of it in the end, and equally many of such physical explanations are genuinely mine, but it is hard to tell.

Most of the time during my PhD I was at the Niels Bohr Institute (NBI). Besides the fellow members of Anders' group, I am grateful for an opportunity to collaborate, occasionally talk or simply share the office with people from other groups doing quantum physics at NBI. For 6 short months, I have also had an opportunity to visit University of Sherbrooke as part of the PhD programme. I want to thank Alexandre Blais and the members of his group for making the stay both a great learning experience and also very enjoyable. A separate thanks goes to everyone, who joined the hockey games in the University of Sherbrooke gym.

To list everyone by name is a hopeless endeavor. Some people in the list below belong to the groups that have already been mentioned above. Others were not directly related to my work but played an important role of helping me keep my sanity through the PhD years by providing an opportunity to do something else besides physics and math. The very incomplete list is: Anders S. Sørensen, Sumanta Das, Farzana Zaman, Florentin Reiter, Johannes Borregaard, Johan R. Ott, Oleksandr Kyriienko, Julia Miroshnychenko, Luca Dellantonio, Vincent Elfving, Heidi L. Sørensen, Jean-Baptiste Béguin, Jörg Helge Müller, Jürgen Appel, Eugene S. Polzik, Alexandre Blais, Arne Grimsmo, Shruti Puri, Nicolas Quesada, Baptiste Royer, Denis Tcherniak, Yuri Borisov and Yuri Djakhan. Some of these people have been proactive about the matter and explicitly asked to be thanked in my thesis acknowledgement (you know who you are). How could I refuse?

Finally, I want to thank my parents for supporting my choice of doing a PhD in theoretical physics, and being enthusiastic about any progress I was making, even if it was often hard for me to explain in simple terms, what is it that I actually do as a physicist in theoretical quantum optics.

Contents

List of publications

- Sumanta Das, Andrey Grankin, Ivan Iakoupov, Etienne Brion, Johannes Borregaard, Rajiv Boddeda, Imam Usmani, Alexei Ourjoumtsev, Philippe Grangier and Anders S. Sørensen.
  Photonic controlled-phase gates through Rydberg blockade in optical cavities.
  Phys. Rev. A 93, 040303(R) (2016) (Ref. [1] in the text)
  (The unpublished Supplementary Material can be found in Ref. [2])

- Heidi L. Sørensen, Jean-Baptiste Béguin, Kilian W. Kluge, Ivan Iakoupov, Anders S. Sørensen, Jörg H. Müller, Eugene S. Polzik and Jürgen Appel.
  Coherent Backscattering of Light Off One-Dimensional Atomic Strings
  Phys. Rev. Lett. 117, 133604 (2016) (Ref. [3] in the text)

- Ivan Iakoupov, Johan R. Ott, Darrick E. Chang, Anders S. Sørensen,
  Dispersion relations for stationary light in one-dimensional atomic ensembles
  Phys. Rev. A 94, 053824 (2016) (Ref. [4] in the text)

- Ivan Iakoupov, Johannes Borregaard, Anders S. Sørensen,
  Controlled-phase gate for photons based on stationary light
  arXiv:1610.09206 (Ref. [5] in the text)

- Ivan Iakoupov, Anders S. Sørensen
  In preparation (based on chapter 2)

Chapter 1

Introduction

Optical photons are ideal carriers of quantum information over long distances, and such quantum communication may enable a wealth of applications [6]. Quantum information processing with photonic qubits is, however, severely limited by the lack of efficient two-qubit gates. In principle, such gates could be realized by strongly coupling photons to a single atom [7, 8]. Experiments have pushed towards realizing such strong coupling, e.g. in cavity QED structures [9–13] and optical waveguides [14–17], but the realization of gates remains challenging. An alternative approach to strong single-atom coupling is to use atomic ensembles where a large number of atoms compensates for a small coupling efficiency of the individual atoms [18]. The latter kind of systems will be the focus of this thesis. Making two-qubit gates for photons in systems consisting of many atoms is challenging, since using many atoms often decreases the effective nonlinearity. A simple explanation is that a single two-level atom can absorb exactly one photon, and hence will behave differently for the second incoming photon. An ensemble of two-level atoms can absorb as many photons as there are atoms and thus will behave linearly for a number of photons much smaller than the number of atoms. There are ways to remedy this shortcoming. One of them is to use non-local interactions between the atoms. A popular choice is the dipole-dipole interaction between Rydberg atoms [19, 20]. In a certain regime, this can make atoms within the interaction radius behave very similar to a single atom, forbidding multiple excitations. Rydberg interaction will be touched upon only briefly in this thesis. An alternative to Rydberg interaction is to make the entire atomic ensemble itself behave more like a cavity [21, 22]. Multiple excitations are then suppressed by the first photon destroying the mode-matching condition of the cavity and making it reflective. Compared to the conventional cavity QED, this avenue is not well explored and may lead to an interesting contender for an approach to implement two-qubit gates for optical photons.

Ideally, for making a cavity out of the atomic ensemble, we would like to have both strong single-atom coupling strengths and a large number of atoms. However, it seems that larger single-atom coupling strengths present in a given physical system correlate with lower total number of atoms. Hence, it is important to have a figure of merit to judge the physical systems than could be used to implement a cavity with an atomic

ensemble. One such figure of merit was found in the analysis of Ref. [22] to be the product of the single-atom coupling strength squared and the number of the atoms. Using this figure of merit, the systems with intermediate single-atom coupling strength but still a sizable number of atoms currently seem attractive. Examples of such systems are tapered optical fibers [23–27] and hollow core photonic-crystal fibers [28, 29].

The complexity with implementing two-qubit photon gates is not only due to the difficulty of engineering strong light-matter interactions. Propagating photonic wave packets are in general spread over more than than one field mode (frequency component). This lead to conjectures that gates between propagating photons are impossible, even if an optical nonlinearity is present to mediate the effective interactions [30, 31]. The usual setup in these no-go results is to send two co-propagating photons through a nonlinear medium, and it was shown that no problems seem to arise for counter-propagating photons [32–34]. Nevertheless, it is possible to side step this problem entirely by temporarily storing one or both of the photons inside the nonlinear medium. In this thesis, we will be looking at the setup, where one of the photons is stored inside the nonlinear medium and can control the scattering properties of the medium in such a way that the second photon obtains phase shift only, when the first photon was stored in the ensemble. At the end of the interaction the first photon is retrieved from the atomic ensemble. Thereby a two-qubit (controlled-phase) gate is implemented between the photons.

The structure of the thesis is as follows. In Chapter 2 we develop the formalism to evaluate the performance of controlled-phase gates for photonic qubits for a certain class of physical systems. In Chapter 3, we look at the linear properties of stationary light, which is necessary prerequisite for considering the nonlinear properties. In Chapter 4, we use the enhancement of the optical nonlinearities by stationary light to propose a controlled-phase gate for photons. In Chapter 5 we recap the major accomplishments of the thesis and provide possible directions for further research.

Chapter 2

Fidelity measures

2.1 Acknowledgements

This chapter is based on the theory of fidelity calculations that was developed for the analysis of the controlled-phase gate in Ref. [1]. The application of this general theory to the specific controlled-phase gate considered in Ref. [1] was done by Sumanta Das and Andrey Grankin. The details of the general theory can be found in the unpublished Supplemental Material [2]. In this chapter, this theory has been expanded to be able to deal with the additional complexity of the controlled-phase gate in chapter 4.

2.2 Introduction

The ultimate goal of this thesis is to propose a controlled-phase gate for photons in chapter 4. It has a sequential "store, scatter, retrieve" operation principle that is increasingly popular for proposals and implementations of photonic switches and quantum gates [1, 7, 8, 10, 35, 36]. In this chapter, we develop the theory for evaluating performance of this class of photonic quantum gates. While the analysis for the case, when the atomic ensemble consists of a single atom, can be considerably simplified, usage of many atoms is still very attractive in enhancing the linear and nonlinear interactions of a controlled-phase gate. Hence, the additional complexity can be worth it.

2.3 Preliminaries

First, we do a small review of the mathematical formalism of quantum mechanics. The most basic concept is of a *quantum state*. *Pure* states are elements (vectors) of a Hilbert space. If we denote the Hilbert space by $\mathcal{H}$, the pure states in the Dirac *ket* notation are $|\psi\rangle \in \mathcal{H}$. The Hilbert space is endowed with an *inner product* operation, where for two states $|\psi\rangle$ and $|\psi'\rangle$, the inner product is denoted by $\langle\psi|\psi'\rangle$. The inner product gives rise to the definition of *norm*. The norm of the state $|\psi\rangle$ is denoted by $\|\psi\|$ and is given by $\|\psi\| = \sqrt{\langle\psi|\psi'\rangle}$. The states $|\psi\rangle$ are usually assumed to be normalized, i.e. $\|\psi\| = 1$. In

some of the derivations below, we will also encounter states with $\|\psi\| < 1$. This is often done to model loss processes that inevitably occur in real physical systems. Presence of loss mechanisms means that the physical system is coupled to the environment, which we have little control over. In this case, representing a quantum state as a vector is, in general, not sufficient. The reason why we would want to do it anyway is to simplify calculations in specific cases, where the effective description of losses is just as valid as the full one. In fact, one of the major themes of this chapter is simplification of the fidelity calculations using exactly this type of effective description of losses. In this chapter, our goal is to compute fidelity between two quantum processes. The fidelity of quantum processes is based on the definition of fidelity of quantum states, which we can define already at this point for pure states. For two states, $|\psi\rangle$ and $|\psi'\rangle$, the fidelity is given by

$$F = |\langle\psi|\psi'\rangle|^2. \tag{2.1}$$

Continuing with our review of the formalism of quantum mechanics, we need to define how evolution of pure states is represented. In the differential form, the evolution is determined by a Hamiltonian H and the Schrödinger equation

$$i\hbar \frac{\mathrm{d}}{\mathrm{d}t} |\psi(t)\rangle = H|\psi(t)\rangle. \tag{2.2}$$

This equation can be formally integrated from the initial time t_0 to the final time t to yield

$$|\psi(t)\rangle = U|\psi(t_0)\rangle, \tag{2.3}$$

with

$$U = e^{-iH(t-t_0)/\hbar}. \tag{2.4}$$

The Hamiltonian is a Hermitian operator, i.e. $H^\dagger = H$, and hence U is a unitary operator, i.e. $U^\dagger U = I$, where I is the identity operator. Often, the state evolution is given by unitary operators directly without any reference to the Hamiltonian that has generated the evolution. Note that unitary operators preserve inner products and hence norms of the states, since any two states $|\psi\rangle$ and $|\psi'\rangle$ evolved with a unitary operator U have the inner product $\langle\psi|U^\dagger U|\psi'\rangle = \langle\psi|\psi'\rangle$. Just we have been discussing states with norm less than one, the operators representing evolution can also be non-unitary as a way to have an effective description of the loss processes. The Hamiltonians that generate them are non-Hermitian.

To describe losses in the general case, we can no longer use pure states and have to use *mixed* states instead, represented by *density matrices* (operators). A density matrix ρ is Hermitian, positive semidefinite and has trace equal to unity. The positive semidefinite property means that for any pure state (vector) $|\psi'\rangle$, it holds that $\langle\psi'|\rho|\psi'\rangle \geq 0$. This is also the definition of fidelity of a pure state $|\psi'\rangle$ and a mixed state ρ, i.e.

$$F = \langle\psi'|\rho|\psi'\rangle. \tag{2.5}$$

This definition reduces to equation (2.1), if ρ is also a pure state, i.e. $\rho = |\psi\rangle\langle\psi|$. We will not need the definition of the fidelity for two mixed states, since we want the controlled-phase gate to produce pure states as the output in the ideal limit.

Description of evolution of density matrices can be very challenging in the general case. The complexity stems from coupling to a reservoir (environment), which has a large number of degrees of freedom and usually cannot be described explicitly. Fortunately, in many situations the reservoir can be assumed to be Markovian, which basically means that the evolution only depends on the current state of the system and not on the entire history of the evolution. This allows to describe evolution of the density matrix ρ by a linear ordinary differential equation, which is usually called the *master equation*. Its general form is

$$\frac{\mathrm{d}}{\mathrm{d}t}\rho = -\frac{i}{\hbar}[H,\rho] - \frac{1}{2}\sum_j \left(L_j^\dagger L_j \rho + \rho L_j^\dagger L_j - 2L_j \rho L_j^\dagger\right), \tag{2.6}$$

where H is the Hamiltonian for the system, and the operators L_j describe incoherent decay processes. This equation can be formally integrated from the initial time t_0 with the initial condition $\rho(t_0)$ to find the density matrix for any later time t. This procedure can be used to define a *superoperator*, i.e. an operator that acts linearly on operators (density matrices) through

$$\mathcal{V}(\rho(t_0)) = \rho(t), \tag{2.7}$$

where $\rho(t)$ is computed using equation (2.6). In principle, starting from equation (2.6) is not necessary to define a superoperator. Any linear completely positive trace preserving (CPTP) map will do. One of the several equivalent definitions of a CPTP map $\mathcal{V}$ is that it can be written

$$\mathcal{V}(\rho) = \sum_l A_l \rho A_l^\dagger \tag{2.8}$$

for a set of operators A_l that fulfills $\sum_l A_l^\dagger A_l = I$, where I is the identity operator. This is the so-called Kraus (operator-sum) decomposition of a superoperator.

For every pure state $|\psi\rangle$, the density matrix is

$$\rho = |\psi\rangle\langle\psi|. \tag{2.9}$$

Therefore for pure states, the vector and the density matrix can be used interchangeably, and superoperators that, in general, act on density matrices ρ can also be thought of acting on vectors via the relation (2.9).

It is possible to write down a formal solution to equation (2.6). First we rewrite it as

$$\frac{\mathrm{d}}{\mathrm{d}t}\rho = -\frac{i}{\hbar}(H_{\mathrm{eff}}\rho - \rho H_{\mathrm{eff}}^\dagger) + \sum_j L_j \rho L_j^\dagger, \tag{2.10}$$

where

$$H_{\text{eff}} = H - \frac{i\hbar}{2}\sum_j L_j^\dagger L_j \tag{2.11}$$

is the effective non-Hermitian Hamiltonian. A formal solution to equation (2.10) is

$$\rho(t) = e^{-iH_{\text{eff}}(t-t_0)/\hbar}\rho(t_0)e^{iH_{\text{eff}}^\dagger(t-t_0)/\hbar} + \mathcal{J}(\rho(t_0)), \tag{2.12}$$

where the first term on the right hand side represents the evolution with the effective non-Hermitian Hamiltonian. The second term (the superoperator $\mathcal{J}$) can be written in terms of the definitions

$$\mathcal{S}_{tt'}(\rho) = e^{-iH_{\text{eff}}(t-t')/\hbar}\rho e^{iH_{\text{eff}}^\dagger(t-t')/\hbar}, \tag{2.13}$$

$$\mathcal{L}_j(\rho) = L_j\rho L_j^\dagger. \tag{2.14}$$

It is [37]

$$\begin{aligned}\mathcal{J}(\rho) &= \sum_j \int_{t_0}^{t} \mathrm{d}t_1 \mathcal{S}_{tt_1}\circ\mathcal{L}_j\circ\mathcal{S}_{t_1t_0}(\rho)\\ &+ \sum_j \int_{t_0}^{t}\mathrm{d}t_2\int_{t_0}^{t_2}\mathrm{d}t_1 \mathcal{S}_{tt_2}\circ\mathcal{L}_j\circ\mathcal{S}_{t_2t_1}\circ\mathcal{L}_j\circ\mathcal{S}_{t_1t_0}(\rho)\\ &+ \dots\end{aligned} \tag{2.15}$$

In the above, circles mean composition of the superoperators, so that for instance

$$\mathcal{L}_j\circ\mathcal{S}_{t_1t_0}(\rho) = L_j e^{-iH_{\text{eff}}(t_1-t_0)/\hbar}\rho e^{iH_{\text{eff}}^\dagger(t_1-t_0)/\hbar}L_j^\dagger. \tag{2.16}$$

Mathematically, the formal solution (2.12) is of the form (2.8), so equation (2.12) can be thought of as a particular Kraus decomposition of the superoperator that maps the initial state $\rho(t_0)$ to the final state $\rho(t)$. Physically, the formal solution (2.12) sums over all possible ways one can do evolution with the effective Hamiltonian H_{eff} interrupted in by abrupt jumps [38] described by the superoperators $\mathcal{L}_j$. Hence, the superoperator $\mathcal{J}$ describes the part of the evolution, where at least one quantum jump has occurred.

Often, we want to build up more complicated Hilbert spaces by combining several smaller subsystems. The operation that represents this is the *tensor product*. The tensor product of two Hilbert spaces, $\mathcal{H}_A$ and $\mathcal{H}_B$ is denoted by $\mathcal{H}_A\otimes\mathcal{H}_B$. We will be mostly interested in the case when $\mathcal{H}_A$ and $\mathcal{H}_B$ are the same Hilbert space. If $|x_A\rangle$ is the basis for $\mathcal{H}_A$ and $|x_B\rangle$ is the basis for $\mathcal{H}_B$ then any pure state $|\psi\rangle\in\mathcal{H}_A\otimes\mathcal{H}_B$ can be written

$$|\psi\rangle = \sum_{x_A,x_B} c_{x_A,x_B}|x_Ax_B\rangle, \tag{2.17}$$

Here and below, $|x_Ax_B\rangle$ means $|x_A\rangle\otimes|x_B\rangle$ (the tensor product of the states $|x_A\rangle$ and $|x_B\rangle$), however we will also use $|x_A\rangle|x_B\rangle$ for the same purpose to more clearly separate

different states. If $|\psi\rangle$ can be written as a tensor product of two states $|\psi_A\rangle \in \mathcal{H}_A$ and $|\psi_B\rangle \in \mathcal{H}_B$ (i.e. $|\psi\rangle = |\psi_A\rangle|\psi_B\rangle$), then we say that $|\psi\rangle$ is *separable*. Any state that is *not* separable is *entangled*.

In the context of tensor products, we also need to discuss the concept of *partial trace*. If we take a density matrix ρ in defined on the Hilbert space $\mathcal{H}_A \otimes \mathcal{H}_B$, then the full trace is $\mathrm{tr}(\rho) = \langle x_A x_B|\rho|x_A x_B\rangle = 1$ a number, while the partial trace with respect to the space $\mathcal{H}_B$ is $\mathrm{tr}_B(\rho) = \langle x_B|\rho|x_B\rangle = \rho_A$, which is a density matrix on $\mathcal{H}_A$. A *maximally entangled* state on a tensor product of two copies of the same Hilbert space is the one, whose density matrix after partial trace of one of them is diagonal.

The simplest non-trivial Hilbert space contains two basis states, $|0\rangle$ and $|1\rangle$. This is the Hilbert space representing a single *qubit*. As we will be considering two-qubit gates, the relevant Hilbert space is the tensor product of two copies of single-qubit Hilbert space with the basis consisting of the states $|00\rangle$, $|01\rangle$, $|10\rangle$ and $|11\rangle$. This is what we will refer to as the *computational basis*. Additionally, we will also use the *Bell basis*, consisting of the states

$$\begin{aligned}
|\phi^{00}\rangle = |\phi^{+}\rangle &= \frac{1}{\sqrt{2}}\left(|00\rangle + |11\rangle\right), \\
|\phi^{01}\rangle = |\psi^{+}\rangle &= \frac{1}{\sqrt{2}}\left(|01\rangle + |10\rangle\right), \\
|\phi^{10}\rangle = |\phi^{-}\rangle &= \frac{1}{\sqrt{2}}\left(|00\rangle - |11\rangle\right), \\
|\phi^{11}\rangle = |\psi^{-}\rangle &= \frac{1}{\sqrt{2}}\left(|01\rangle - |10\rangle\right).
\end{aligned} \tag{2.18}$$

Note that these states are the maximally entangled states in the Hilbert space of two qubits. In addition to the conventional names, we also give numbers to the Bell states, which will allow us to express summations in a simple way below.

In principle, now we have the necessary formalism to characterize the performance of the quantum gates. Since superoperators are linear maps, one can choose a basis for the quantum states (density matrices), compute the action of the superoperators representing the real and ideal physical implementations of a quantum gate on each of those basis states and thereby find the *process matrices* [39] for the superoperators. Having obtained the process matrices, any fidelity measure can be computed. This general procedure can involve complicated calculations, and our goal is to find a simpler way to calculate the different fidelity measures of a quantum gate exploiting the features of the specific physical system that we consider.

2.4 Overview of the fidelity measures

2.4.1 General approach

Our goal is to find how close a particular physical implementation of a quantum gate, represented by the superoperator $\mathcal{V}$, is to the ideal operation, represented by the su-

peroperator $\mathcal{U}$. The computation of all the fidelity measures below will follow the same pattern:

1. Choose a particular input state ρ_{in}.
2. Find the output states

$$\begin{aligned} \rho_{\mathcal{V}} &= \mathcal{V}(\rho_{\text{in}}), \\ \rho_{\mathcal{U}} &= \mathcal{U}(\rho_{\text{in}}). \end{aligned} \tag{2.19}$$

3. Find the state fidelity between $\rho_{\mathcal{V}}$ and $\rho_{\mathcal{U}}$.

Calculation of the fidelity between the output states $\rho_{\mathcal{V}}$ and $\rho_{\mathcal{U}}$ is simplified by the fact that the chosen input states $\rho_{\text{in}} = |\psi_{\text{in}}\rangle\langle\psi_{\text{in}}|$ are pure, and the ideal superoperators $\mathcal{U}$ are unitary, i.e. $\mathcal{U}(\rho) = U\rho U^{\dagger}$, where U is a unitary operator. Therefore, $\rho_{\mathcal{U}} = U|\psi_{\text{in}}\rangle\langle\psi_{\text{in}}|U^{\dagger}$ is pure and the fidelity is given by

$$F = \langle\psi_{\text{in}}|U^{\dagger}\rho_{\mathcal{V}}U|\psi_{\text{in}}\rangle. \tag{2.20}$$

For fidelities, where the operation of the controlled-phase gate is conditioned on presence of all input photons after the gate operation, the end result is that the expression above is normalized by the success probability P_{suc}. I.e., the conditional fidelities have the form

$$F_{\text{cond}} = \frac{F}{P_{\text{suc}}}. \tag{2.21}$$

The reason why we are interested in the conditional versions of all the fidelities is that in the considered class of physical implementations of the controlled-phase gate for photons, the dominant error in the unconditional fidelity is due to photon loss. If photon loss can be postselected, the end result is a heralded gate with fidelity that is much closer to unity.

The procedure outlined above makes it unnecessary to calculate the full process matrix for the superoperator, and finding action of the superoperator on a particular input state is sufficient. Initially, we will also ignore the fact each computational basis state is physically represented by a traveling photon that has a distribution of the wave vectors, and that the physical system that implements a controlled-phase gate will in general do a different transformation for the different wave vectors.

2.4.2 Fidelity of creation of a Bell state

The simplest fidelity measure that we will consider is creation of an entangled state (a Bell state) from a separable input state. Deterministic entangling operations are notoriously difficult for the photonic qubits and can only be achieved in a heralded fashion with linear optics [40, 41]. Therefore, creation of entangled states is a highly interesting application of a controlled-phase gate for photons.

As the input state, we choose

$$\begin{aligned} |\psi_{\text{in}}\rangle &= \frac{1}{2}\left(|00\rangle + |01\rangle + |10\rangle + |11\rangle\right) \\ &= \frac{1}{2}\sum_{x,x'=0}^{1} |xx'\rangle. \end{aligned} \tag{2.22}$$

To see that this state is separable, we can write it

$$|\psi_{\text{in}}\rangle = (H \otimes H)|00\rangle, \tag{2.23}$$

where H is the Hadamard operator defined by

$$H|0\rangle = (|0\rangle + |1\rangle)/\sqrt{2}, \tag{2.24}$$

$$H|1\rangle = (|0\rangle - |1\rangle)/\sqrt{2}. \tag{2.25}$$

The ideal operation of the controlled-phase gate is defined by

$$\begin{aligned} U|00\rangle &= |00\rangle, \\ U|01\rangle &= |01\rangle, \\ U|10\rangle &= |10\rangle, \\ U|11\rangle &= -|11\rangle. \end{aligned} \tag{2.26}$$

Hence, the ideal output state is

$$U|\psi_{\text{in}}\rangle = \frac{1}{2}\left(|00\rangle + |01\rangle + |10\rangle - |11\rangle\right). \tag{2.27}$$

To see that this state is entangled, it can be written

$$U|\psi_{\text{in}}\rangle = (I \otimes H)|\phi^+\rangle, \tag{2.28}$$

where I is the identity operator, and $|\phi^+\rangle$ is one of the Bell states (2.18).

Using the formal solution (2.12) for the final state of the real evolution $\rho_{\mathcal{V}}$ and defining $V = e^{-iH_{\text{eff}}(t-t_0)/\hbar}$, the fidelity (2.20) is

$$F_{\text{Bell}} = \left|\langle\psi_{\text{in}}|U^\dagger V|\psi_{\text{in}}\rangle\right|^2 + \langle\psi_{\text{in}}|U^\dagger \mathcal{J}(|\psi_{\text{in}}\rangle\langle\psi_{\text{in}}|)U|\psi_{\text{in}}\rangle. \tag{2.29}$$

We can also define a conditional fidelity using the projection (measurement) operator

$$P = \sum_{x,x'=0}^{1} |xx'\rangle\langle xx'|. \tag{2.30}$$

In the dual-rail computational basis for photons discussed in section 2.6 below, it can happen that the physical processes during operation of the controlled-phase gate bring the state of the system to a state, which is outside of the computational basis. Therefore,

in general, $P \neq I$. We can define fidelity, which is conditioned on still remaining within the computational basis. The conditional state is

$$\rho'_{\mathcal{V}} = \frac{P\rho_{\mathcal{V}}P^\dagger}{\mathrm{tr}\big(P\rho_{\mathcal{V}}P^\dagger\big)}. \tag{2.31}$$

and the conditional fidelity is $F_{\mathrm{Bell,cond}} = \langle\psi_{\mathrm{in}}|U^\dagger\rho'_{\mathcal{V}}U|\psi_{\mathrm{in}}\rangle = F_{\mathrm{Bell}}/P_{\mathrm{suc,Bell}}$ with the success probability

$$P_{\mathrm{suc,Bell}} = \mathrm{tr}\Big(P\rho_{\mathcal{V}}P^\dagger\Big)\,. \tag{2.32}$$

2.4.3 Fidelity of entanglement swap

The entanglement swap operation takes as input two Bell states, $|\phi^+\rangle_{A'A}$ and $|\phi^+\rangle_{BB'}$, where the subscripts indicate the labels of the individual qubits in the Bell states. After a unitary evolution (see figure 2.1), measurement and a single-qubit unitary correction, the ideal output is the state $|\phi^+\rangle_{A'B'}$, i.e. a Bell state, but now involving different combination of the individual qubits. This operation is central in quantum repeaters [42, 43], which can be a natural application of a controlled-phase gate for photons.

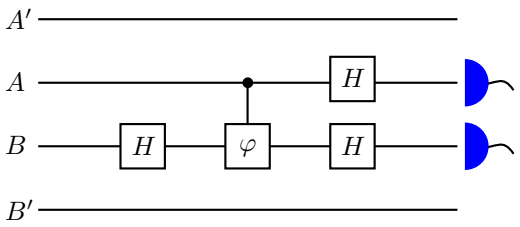

Figure 2.1: Circuit diagram for the entanglement swap operation. The letters to the left are labels of each of the four qubits. Boxes with H denote single-qubit Hadamard operations, and the box with φ on qubits A and B denotes the controlled-phase operation. Absence of a box is an implicit identity operation I. The operations represented by those boxes act sequentially on the input state, starting with the leftmost operation ($I_{A'} \otimes I_A \otimes H_B \otimes I_{B'}$, where subscripts indicate the labels of the qubits).

The fidelity of entanglement swap is a conditional fidelity measure, since the state of the qubits A and B need to be measured after the unitary evolution to determine, which kind of the unitary corrections must be applied to obtain $|\phi^+\rangle_{A'B'}$ and not any other Bell state. Here we note that both this unitary operation and the Hadamard operators in figure 2.1 will be assumed to be lossless, since our main focus is the error introduced by the controlled-phase gate. As shown below, assuming lossless Hadamard operators in figure 2.1 also makes the fidelities of the controlled-phase gate itself and the full circuit for qubits A and B in figure 2.1 equal, which reduces the complexity of the analysis. To make a distinction between the superoperators $\mathcal{U}$ and $\mathcal{V}$ for the controlled-phase gate

itself, we will also define the superoperators $\tilde{\mathcal{U}}$ and $\tilde{\mathcal{V}}$ for the full circuit for qubits A and B in figure 2.1. Hence, the maps that act on the initial state

$$|\psi_{\text{in}}\rangle = |\phi^+\rangle_{A'A}|\phi^+\rangle_{BB'} \tag{2.33}$$

are $\mathcal{I}_{A'B'} \otimes \tilde{\mathcal{U}}_{AB}$ and $\mathcal{I}_{A'B'} \otimes \tilde{\mathcal{V}}_{AB}$, where $\mathcal{I}$ is the identity superoperator. For the ideal operation, we see that $\tilde{\mathcal{U}}_{AB}(\rho) = \tilde{U}_{AB}\rho\tilde{U}_{AB}^\dagger$, where the operators $\tilde{U}_{AB}$ fulfill

$$\tilde{U}_{AB}|\phi^{xx'}\rangle_{AB} = |xx'\rangle_{AB}, \tag{2.34}$$

where $x, x' \in \{0, 1\}$ and using the numbered definitions of the Bell states (2.18) for brevity. I.e. the ideal operation of the circuit for qubits A and B in figure 2.1 is to transform Bell states into computational basis states. In this sense, this circuit accomplishes the reverse of what was considered for the fidelity of creation of a Bell state in section 2.4.2 above.

For the real evolution, the final state before the measurement is

$$\rho_{\tilde{\mathcal{V}}} = [\mathcal{I}_{A'B'} \otimes \tilde{\mathcal{V}}_{AB}]\big(|\psi_{\text{in}}\rangle\langle\psi_{\text{in}}|\big)\,. \tag{2.35}$$

The conditional nature of the entanglement swap fidelity is described by defining the quantum states conditioned on measuring states $|xx'\rangle_{AB}$ (where $x, x' \in \{0, 1\}$) after the unitary evolution. We use the projection operators $I_{A'B'} \otimes P_{xx',AB}$ with

$$P_{xx',AB} = |xx'\rangle_{AB}\langle xx'|_{AB}. \tag{2.36}$$

Hence, the states after the measurement are

$$\rho_{xx'} = \frac{(I_{A'B'} \otimes P_{xx',AB})\rho_{\tilde{\mathcal{V}}}(I_{A'B'} \otimes P_{xx',AB})^\dagger}{\text{tr}\big((I_{A'B'} \otimes P_{xx',AB})\rho_{\tilde{\mathcal{V}}}(I_{A'B'} \otimes P_{xx',AB})^\dagger\big)}. \tag{2.37}$$

Since the single-qubit correction unitary after measurement is assumed to be lossless, for defining fidelity, we can skip this step and directly project the states (2.37) onto the appropriate Bell state. Therefore, for each of these states, we define the conditional fidelities

$$F_{xx'} = \langle\phi^{xx'}|_{A'B'}\text{tr}_{AB}(\rho_{xx'})|\phi^{xx'}\rangle_{A'B'}, \tag{2.38}$$

where we first take a partial trace over the qubits A and B and then project the remaining qubits A' and B' onto the expected Bell state.

Due to the definition (2.36), we can write the fidelity (2.38)

$$F_{xx'} = \frac{\langle\phi^{xx'}|_{A'B'}\langle xx'|_{AB}\rho_{\tilde{\mathcal{V}}}|xx'\rangle_{AB}|\phi^{xx'}\rangle_{A'B'}}{P_{\text{suc},xx'}}, \tag{2.39}$$

which is of the form (2.21) with the success probability

$$P_{\text{suc},xx'} = \text{tr}\Big((I_{A'B'} \otimes P_{xx',AB})\rho_{\tilde{\mathcal{V}}}(I_{A'B'} \otimes P_{xx',AB})^\dagger\Big)\,. \tag{2.40}$$

In the ideal limit, $P_{\mathrm{suc},xx'} = 1/4$, so that the total success probability

$$P_{\mathrm{suc,swap}} = \sum_{x,x'=0}^{1} P_{\mathrm{suc},xx'} \tag{2.41}$$

is unity. In expression (2.39), we have ignored the multi-mode nature of the computational basis states discussed in section 2.6 below, which affects the definition of trace.

Finally, we can define the average entanglement swap fidelity by

$$F_{\mathrm{swap}} = \frac{1}{4} \sum_{x,x'=0}^{1} F_{xx'}. \tag{2.42}$$

2.4.4 Choi-Jamiolkowski fidelity

The Choi-Jamiolkowski fidelity is among the "general purpose" fidelities recommended by Ref. [39] (also known as "Jamiolkowski process fidelity" [39] and "entanglement fidelity" [44, 45]). This fidelity measure is based on the fact that every superoperator can be mapped onto a density matrix on a higher-dimensional space by the Choi-Jamiolkowski isomorphism [46, 47]. The Choi-Jamiolkowski fidelity of two superoperators $\mathcal{U}$ and $\mathcal{V}$ is then the state fidelity of the two density matrices $\rho_{\mathcal{U}}$ and $\rho_{\mathcal{V}}$ that correspond to the superoperators. To compute $\rho_{\mathcal{U}}$ and $\rho_{\mathcal{V}}$, we take the modified superoperators $\mathcal{I} \otimes \mathcal{U}$ and $\mathcal{I} \otimes \mathcal{V}$ (tensor products with the identity superoperator $\mathcal{I}$), and let them act on a particular input state $|\Phi\rangle$. If $\mathcal{H}$ the Hilbert space, for which $\mathcal{U}$ and $\mathcal{V}$ are defined, then $|\Phi\rangle \in \mathcal{H} \otimes \mathcal{H}$, i.e. $|\Phi\rangle$ is an element on the tensor product of the original Hilbert space with a copy of itself.

By the discussion above, besides extending the Hilbert space and redefining the superoperators, the computation of the Choi-Jamiolkowski fidelity is no different from the more specialized fidelity measures discussed earlier. In the general case, the input state for $\mathcal{I} \otimes \mathcal{U}$ and $\mathcal{I} \otimes \mathcal{V}$ can be written [39]

$$|\Phi\rangle = \sum_{x} |x\rangle|x\rangle/\sqrt{d}, \tag{2.43}$$

where $\{|x\rangle\}$ is an orthonormal basis set for the considered Hilbert space $\mathcal{H}$, and d is its dimension. Thus, $|\Phi\rangle$ is a maximally entangled state on $\mathcal{H} \otimes \mathcal{H}$. We will only be concerned with the two-qubit case, where $d = 4$. Using the formal solution (2.12) for the final state of the real evolution $\rho_{\mathcal{V}}$ and defining $V = e^{-iH_{\mathrm{eff}}(t-t_0)/\hbar}$, the final states (2.19) are

$$\begin{aligned} \rho_{\mathcal{U}} &= [\mathcal{I} \otimes \mathcal{U}]\big(|\Phi\rangle\langle\Phi|\big) = (I \otimes U)|\Phi\rangle\langle\Phi|(I \otimes U^\dagger), \\ \rho_{\mathcal{V}} &= [\mathcal{I} \otimes \mathcal{V}]\big(|\Phi\rangle\langle\Phi|\big) = (I \otimes V)|\Phi\rangle\langle\Phi|(I \otimes V^\dagger) + [\mathcal{I} \otimes \mathcal{J}](|\Phi\rangle\langle\Phi|). \end{aligned} \tag{2.44}$$

Hence, the expression (2.20) for Choi-Jamiolkowski fidelity is

$$F_{\mathrm{CJ}} = \Big|\langle\Phi|(I \otimes U^\dagger V)|\Phi\rangle\Big|^2 + \langle\Phi|(I \otimes U^\dagger)[\mathcal{I} \otimes \mathcal{J}](|\Phi\rangle\langle\Phi|)(I \otimes U)|\Phi\rangle. \tag{2.45}$$

The conditional Choi-Jamiolkowski fidelity using the projection operator $I \otimes P$ with P given by equation (2.30) is $F_{\mathrm{CJ,cond}} = F_{\mathrm{CJ}}/P_{\mathrm{suc,CJ}}$ with the success probability

$$P_{\mathrm{suc,CJ}} = \mathrm{tr}\Big((I \otimes P)\rho_{\mathcal{V}}(I \otimes P)^{\dagger}\Big). \tag{2.46}$$

We will show that for the considered class of physical systems, the Choi-Jamiolkowski fidelity of a controlled-phase gate is the same as the fidelity of creation of a Bell state. The conditional versions of those two fidelities will be shown to be equal to the entanglement swap fidelity in certain limit. Relating Choi-Jamiolkowski fidelity to the fidelity of creation of a Bell state is best seen in the computational basis, where the input state (2.43) can be written

$$\begin{aligned} |\Phi\rangle &= \frac{1}{2}\big(|00\rangle|00\rangle + |01\rangle|01\rangle + |10\rangle|10\rangle + |11\rangle|11\rangle\big) \\ &= \frac{1}{2}\sum_{x,x'=0}^{1} |xx'\rangle|xx'\rangle. \end{aligned} \tag{2.47}$$

On the other hand, the relation to the entanglement swap fidelity will use the Bell basis (2.18) instead, in which the input state (2.43) can be written

$$\begin{aligned} |\Phi\rangle &= \frac{1}{2}\Big(|\phi^+\rangle|\phi^+\rangle + |\psi^+\rangle|\psi^+\rangle + |\phi^-\rangle|\phi^-\rangle + |\psi^-\rangle|\psi^-\rangle\Big) \\ &= \frac{1}{2}\sum_{x,x'=0}^{1} |\phi^{xx'}\rangle|\phi^{xx'}\rangle. \end{aligned} \tag{2.48}$$

The similarity of the conditional Choi-Jamiolkowski fidelity and the entanglement swap fidelity can be seen from the fact that the initial state for the entanglement swap operation (2.33) can be written

$$\begin{aligned} |\phi^+\rangle_{A'A}|\phi^+\rangle_{BB'} = \frac{1}{2}\Big(&|\phi^+\rangle_{A'B'}|\phi^+\rangle_{AB} + |\psi^+\rangle_{A'B'}|\psi^+\rangle_{AB} \\ &+ |\phi^-\rangle_{A'B'}|\phi^-\rangle_{AB} + |\psi^-\rangle_{A'B'}|\psi^-\rangle_{AB}\Big) \\ = |\Phi\rangle_{A'B'AB}&, \end{aligned} \tag{2.49}$$

which is the same as the input state for calculating the Choi-Jamiolkowski fidelity given by equation (2.48). Not only is the input state the same, but the evolution has the same structure of a tensor product with identity. The only difference are (lossless) Hadamard operators in the evolution of entanglement swap operation compared to just a controlled-phase gate.

2.5 Interlude: Electromagnetically induced transparency and Rydberg atoms

To have a concrete physical system to refer to while we are developing the abstract formalism below, we briefly discuss the electromagnetically induced transparency (EIT) [48,

49] and Rydberg dipole-dipole interactions [19, 20]. These phenomena are the key ingredients in the implementations of the controlled-phase gate in Ref. [1].

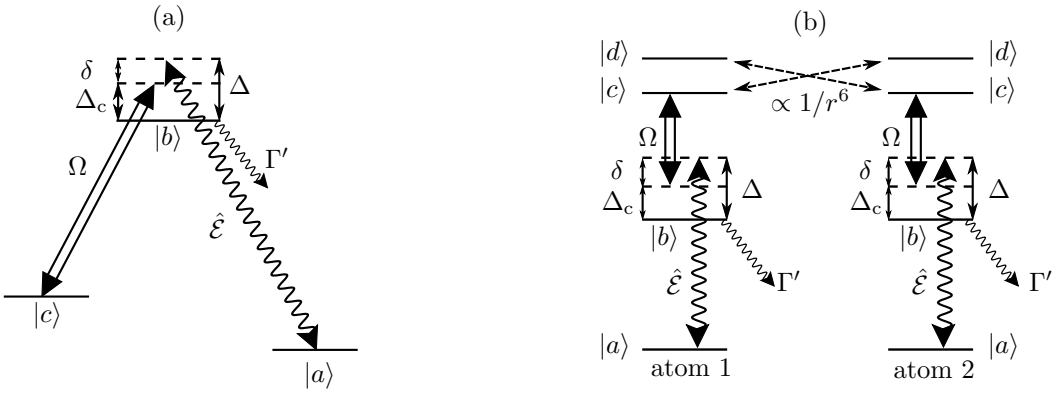

Figure 2.2: (a) Level diagram of a Λ-type atom. (b) Level diagrams of two Rydberg atoms. Two different Rydberg levels, $|c\rangle$ and $|d\rangle$, for each atom are shown. If one of the atoms is initialized in state $|d\rangle$, the state $|c\rangle$ of another atom will experience an energy shift $\propto 1/r^6$.

The phenomenon of EIT arises in three-level Λ-type atoms (see figure 2.2(a)). EIT is often implemented in such a way that $|a\rangle$ and $|c\rangle$ are the two hyperfine levels of the atom, which ensures that state $|c\rangle$ has very long lifetime (meta-stable). Hence, in the theoretical models in this thesis, the spontaneous emission from state $|c\rangle$ will be neglected. Presence of a classical drive (with the Rabi frequency Ω) on the transition $|b\rangle \leftrightarrow |c\rangle$ renders the transition $|a\rangle \leftrightarrow |b\rangle$ transparent for incoming probe light (labeled by the electric field operator $\hat{\mathcal{E}}$) for the two-photon detuning $\delta = 0$. Additionally, the group velocity of the probe light is greatly reduced compared to free space. The group velocity can be further reduced to zero and thereby store the probe pulse in state $|c\rangle$ [50–52]. Importantly, the qualitatively different behavior of Λ-type atoms compared to two-level atoms happens only for a certain range of frequencies. Outside of the (possibly narrow) EIT window, the atom behaves like a two-level atom.

EIT can also be implemented such that state $|c\rangle$ is the Rydberg state (see figure 2.2(b)). Rydberg states have a very high principal quantum number and a lifetime much longer than the excited state $|b\rangle$ (e.g. a lifetime of ~ 50 ns for state $|b\rangle$ compared to a lifetime of ~ 2.65 μs for state $|c\rangle$ [1]). Hence, also in this case we assume that state $|c\rangle$ has negligible spontaneous emission for simplicity. The Rydberg levels of different atoms have dipole-dipole interactions, which amounts to an energy shift $\propto 1/r^6$ of the states, where two atoms close to each other are both in a Rydberg level. This energy shift can be used to change the behavior of nearby Rydberg atoms by shifting them out of the EIT resonance window. In figure 2.2(b), two different Rydberg levels, $|c\rangle$ and $|d\rangle$ for each atom are indicated. In this way, an excitation stored in level $|d\rangle$ can be completely decoupled from the EIT dynamics by ensuring that the classical drive in EIT does not couple to state $|d\rangle$.

The spontaneous decay rates Γ' from the excited state $|b\rangle$ indicated in figure 2.2 are described in the master equation (2.6) by operators

$$L_j = \sqrt{\Gamma'}|a_j\rangle\langle b_j|, \tag{2.50}$$

where j is the index of the atom. Hence, the assumption is that spontaneous emission from the excited state $|b\rangle$ brings the atom to the state $|a\rangle$. After the spontaneous emission process (a quantum jump), the system is effectively decoupled from the dynamics, since the classical drive is only coupled to the transition $|b\rangle \leftrightarrow |c\rangle$. Hence, the final state (with formal solution (2.12)) will have an incoherent part (described by the superoperator $\mathcal{J}$) that consists solely of vacuum state.

For the level diagram of figure 2.2(a), spontaneous emission can also make the atom in state $|b\rangle$ transition to the meta-stable state $|c\rangle$. In this case, the state of the system is not decoupled from the dynamics, since the the state can be excited by the classical drive. Looking at the solution (2.12), we see that this results in additional non-vacuum incoherent terms in the final density matrix. In the regime, where there are many atoms in the ensemble, the photonic wavepackets propagating through the ensemble will be spread over many atoms to reach the regime of low losses. On the other hand, a quantum jump caused by the operators (2.50) will localize the excitation in a single atom. Due to the lack of mode-matching, such localized excitation cannot exit the ensemble with high efficiency and will be instead repeatedly reabsorbed by other atoms. At each reabsorption, there is a chance that spontaneous emission will transition the atom to the ground state $|a\rangle$ thereby decoupling from the dynamics. Hence, the non-vacuum incoherent terms in equation (2.12) in this case are expected to be negligible.

2.6 Computational basis states

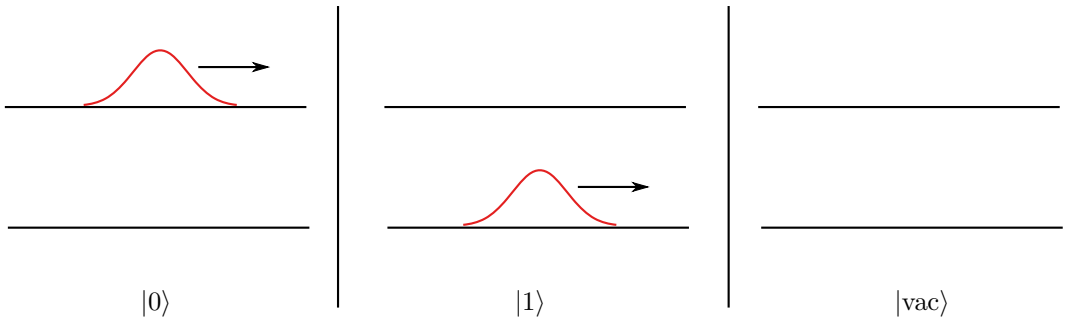

Figure 2.3: Dual-rail computational basis states ($|0\rangle$ and $|1\rangle$). The vacuum state $|\text{vac}\rangle$ is outside of the computational basis.

We will use the dual-rail encoding of the photonic qubits. In this encoding, the two states of the qubit, $|0\rangle$ and $|1\rangle$, correspond to a single photon traveling along either one

or the other path (rail) in the photonic circuit (see figure 2.3). Importantly, the vacuum state $|\text{vac}\rangle$ is outside of the computational basis, and this gives a straightforward way to detect the photon loss errors: if no photons are detected for any pair of rails that represent a single photonic qubit, then an error must have occurred.

Another thing to note about the encoding is that, in general, only using states $|0\rangle$ and $|1\rangle$ is a too simplistic way to describe the actual physical system. Any traveling photon will necessarily have a distribution of wave vectors, and this distribution can change during the operations on the logical states. We will only look at the one-dimensional case, where the wave vectors are scalars. We can define the annihilation operators $\hat{a}_0(k)$ and $\hat{a}_1(k)$ for modes with the wave vector k in the rail corresponding to the logical states $|0\rangle$ and $|1\rangle$ respectively. The commutation relation is $[\hat{a}_x(k), \hat{a}^\dagger_{x'}(k')] = \delta_{x,x'}\delta(k-k')$, where $\delta_{x,x'}$ is the Kronecker delta, and $\delta(k-k')$ is the Dirac delta function. Also, here and for the rest of this section, x and x' mean either 0 or 1. The wave vector k is related to the frequency ω_k by some dispersion relation, which in the simplest case of vacuum is $\omega_k = |k|c$, where c is the speed of light. Then we can write the logical states

$$|x\rangle = \int_{-\infty}^{\infty} \phi(k)\hat{a}^\dagger_x(k)|\text{vac}\rangle \,\mathrm{d}k, \tag{2.51}$$

where the wave function (wave vector distribution in this case) ϕ fulfills the normalization condition

$$\int_{-\infty}^{\infty} |\phi(k)|^2 \,\mathrm{d}k = 1. \tag{2.52}$$

This function ϕ can, in principle, be different for the two logical states, but we assume it to be the same for simplicity.

The free evolution under the Hamiltonian

$$\hat{H}_{\text{free}} = \hbar \sum_{x=0}^{1} \int_{-\infty}^{\infty} \omega_k \hat{a}^\dagger_x(k)\hat{a}_x(k) \,\mathrm{d}k \tag{2.53}$$

results in time dependence of the logical states given by

$$|x(t)\rangle = \int_{-\infty}^{\infty} \phi(k)e^{-i\omega_k t}\hat{a}^\dagger_x(k)|\text{vac}\rangle \,\mathrm{d}k. \tag{2.54}$$

The basis states can also be regarded in real space by doing the Fourier transform of the operators

$$\hat{a}_x(z) = \frac{1}{\sqrt{2\pi}} \int_{-\infty}^{\infty} \hat{a}_x(k)e^{ikz} \,\mathrm{d}k. \tag{2.55}$$

With this definition we have

$$|x(t)\rangle = \int_{-\infty}^{\infty} \phi(z,t)\hat{a}^\dagger_x(z)|\text{vac}\rangle \,\mathrm{d}z, \tag{2.56}$$

where

$$\phi(z,t) = \frac{1}{\sqrt{2\pi}} \int_{-\infty}^{\infty} \phi(k) e^{ikz} e^{-i\omega_k t} \, \mathrm{d}k. \tag{2.57}$$

In the case of the vacuum dispersion relation, if ϕ is sharply peaked around some large positive k_0, then we can approximate $\omega_k = kc$ (where c is speed of light in vacuum or more generally group velocity in the waveguide), since the contribution of the negative k can be neglected, and we get $\phi(z,t) = \phi(z-ct)$. If ϕ were centered on $-k_0$, then we could have approximated $\omega_k = -kc$ and obtained $\phi(z,t) = \phi(z+ct)$. This property is usually the motivation for treating the right- and left-moving fields completely separately [53].

To make two-qubit gates, the photons need to interact, and to induce the interaction, we will assume that one of the photons is stored in the atomic medium, then the second photon is scattered off the ensemble, and finally the first photon is retrieved. Therefore, we first look at the storage and retrieval of the first photon without scattering of the second photon. Storage and retrieval is assumed to use EIT, although there many variations of EIT storage and retrieval [54, 55]. We do not specify the exact protocol in this chapter and limit ourselves to the discussion in terms of general storage and retrieval kernels.

Even if the input state before storage is pure, the output after storage and retrieval is, in general, a mixed state due to imperfections. Another complication is that storage and retrieval can depend on some classical stochastic parameters. This can be fluctuations in power and phase of the applied classical drives (lasers), inhomogeneous broadening of atoms due to trapping lasers, positions of the atoms (assumed classical) within the trapping potential etc. Below, a single realization of the atomic ensemble will be assumed to have some definite values for these classically fluctuating parameters. For storage and retrieval of a single photon, the output state for a realization n of the atomic ensemble, results in the output state

$$\rho_{x,\mathrm{out},n} = |x_{\mathrm{out},n}\rangle\langle x_{\mathrm{out},n}| + (1-\eta_{\mathrm{EIT},n})|\mathrm{vac}\rangle\langle\mathrm{vac}|, \tag{2.58}$$

where the part $|x_{\mathrm{out},n}\rangle\langle x_{\mathrm{out},n}|$ is in the single-photon manifold (spanned by the states $\hat{a}_x^\dagger(z)|\mathrm{vac}\rangle$), and $\eta_{\mathrm{EIT},n} = \langle x_{\mathrm{out},n}|x_{\mathrm{out},n}\rangle$ is the efficiency of the EIT storage and retrieval this realization of the atomic ensemble. The output state should be statistically averaged over all the different realizations. In practice, we can consider a large finite number N_r of randomly chosen different realizations, such that the averaged output state is

$$\rho_{x,\mathrm{out}} = \frac{1}{N_\mathrm{r}} \sum_{n=1}^{N_\mathrm{r}} \rho_{x,\mathrm{out},n}. \tag{2.59}$$

Hence, this can be thought of as a kind of a Monte Carlo method to describe the classical fluctuations.

For calculation of some of the fidelity measures below, one also has to choose pure computational basis states to use as the reference. For the photon that is stored and

then retrieved, we will make the choice

$$|x_{\text{out}}\rangle = \frac{1}{\mathcal{N}} \sum_n |x_{\text{out},n}\rangle, \tag{2.60}$$

where $\mathcal{N}$ is chosen such that the state $|x_{\text{out}}\rangle$ is normalized, and the index n runs over the different realizations of the atomic ensemble. If there is only a single realization, $\mathcal{N}^2$ is the EIT storage and retrieval efficiency. For more than one realization, the average EIT storage and retrieval efficiency

$$\eta_{\text{EIT}} = \sum_n \eta_{\text{EIT},n} = \sum_n \langle x_{\text{out},n}|x_{\text{out},n}\rangle \tag{2.61}$$

is different from

$$\mathcal{N}^2 = \sum_{n,n'} \langle x_{\text{out},n}|x_{\text{out},n'}\rangle, \tag{2.62}$$

since the states $|x_{\text{out},n}\rangle$ are, in general, not orthogonal.

For the calculations of the fidelities, we will need to find inner products between real and ideal photonic states. By the definition of the states in equation (2.56), the inner products of two such states,

$$|x_{\text{out,real}}(t)\rangle = \int_{-\infty}^{\infty} \phi_{\text{out,real}}(z,t)\hat{a}_x^\dagger(z)|\text{vac}\rangle \,\mathrm{d}z, \tag{2.63}$$

$$|x_{\text{out,ideal}}(t)\rangle = \int_{-\infty}^{\infty} \phi_{\text{out,ideal}}(z,t)\hat{a}_x^\dagger(z)|\text{vac}\rangle \,\mathrm{d}z, \tag{2.64}$$

is given by

$$\langle x_{\text{out,real}}(t)|x_{\text{out,ideal}}(t)\rangle = \int_{-\infty}^{\infty} \phi^*_{\text{out,real}}(z,t)\phi_{\text{out,ideal}}(z,t) \,\mathrm{d}z. \tag{2.65}$$

The limits for integration in the above expression are infinite, but we can argue that in a specific situation, we can impose finite limits on physical grounds. We need to compare the states after they have interacted with the atomic ensemble. Suppose that the ensemble is placed in the interval $z \in [0, L]$ (see figure 2.4), and that the photons enter the ensemble from the left ($z < 0$) and exit from the right ($z > L$). For the sake of illustration, we can assume that we are calculating fidelity of single photon storage and retrieval, i.e. compared to efficiency we also want a particular shape of the retrieved photon wave packet given by $\phi_{\text{out,ideal}}$. We want to calculate the inner product (2.65) at a time t large enough that all of the photon has exited the ensemble. Hence, the lower bound in equation (2.65) can be set to L. On the other hand, if we assume that the excitation was entirely within the the ensemble at $t = 0$, then by causality, the upper limit in equation (2.65) is $L + ct$.

After imposing finite limits of integration in equation (2.65), we would like to switch from integration over z to integration over t, since in the discussion of the operation of

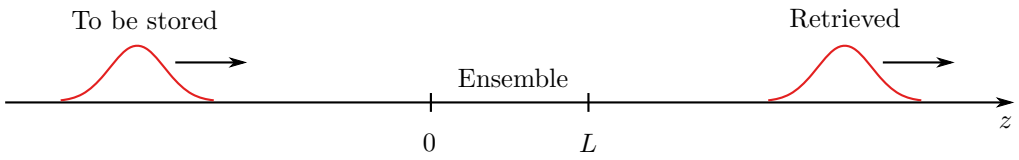

Figure 2.4: The setup of storage and forward retrieval of a single photon.

the controlled-phase gate below, interactions of the incoming or outgoing field with the atomic ensemble are formulated in terms of time-dependent signals at a fixed position. This view is entirely equivalent to the spatial one, since in vacuum (outside of the atomic ensemble), the electric field evolves according to the Hamiltonian (2.53), that simply makes the wave function propagate either in the positive or the negative direction. For retrieved photons propagating to the right, as discussed above, we have $\phi_{\text{out}}(z,t) = \phi_{\text{out}}(L, t-(z-L)/c)$. Hence, equation (2.65) with finite limits of integration is

$$\begin{aligned}\langle x_{\text{out,real}}(t)|x_{\text{out,ideal}}(t)\rangle &= \int_L^{L+ct} \phi^*_{\text{out,real}}(L,t-(z-L)/c)\phi_{\text{out,ideal}}(L,t-(z-L)/c)\,\mathrm{d}z \\ &= \int_0^t \phi^*_{\text{out,real}}(L,t')\phi_{\text{out,ideal}}(L,t')\,\mathrm{d}t'.\end{aligned} \tag{2.66}$$

The details of the storage and retrieval setup can vary. For instance, retrieval could happen such that the outgoing photon is to the left of the ensemble ($z < 0$) instead of being to the right ($z > L$) as indicated in figure 2.4. The bottom line is the same: the photonic wavepackets can be described by time-dependent signals at a particular fixed position. Below, this fixed position will be implicit, since it depends on the particular setup.

2.7 Ideal and real operation of the controlled-phase gate

The operation of the controlled-phase gate between two photonic qubits is assumed to be sequential. The first photon is stored in the atomic ensemble, the second photon is scattered by the ensemble and obtains a conditional-phase shift, and finally the the first photon is retrieved.

Both the controlled-phase gates in Ref. [1] and chapter 4 are applied to the entanglement swap operation shown as a circuit in figure 2.1. In the dual-rail encoding, the setup for qubits A and B can be implemented as shown in figure 2.5. Each line of figure 2.1 needs to be represented by two rails in figure 2.5. Hadamard operators are implemented with beam splitters, and the controlled-phase gate is implemented by two ensembles (represented by triangles) and a beam splitter. In the setup of figure 2.5, photon A is stored and retrieved, and photon B is scattered by the lower atomic ensemble or passes through a beam splitter with transmission coefficient t_{b} (explained below). Out of the

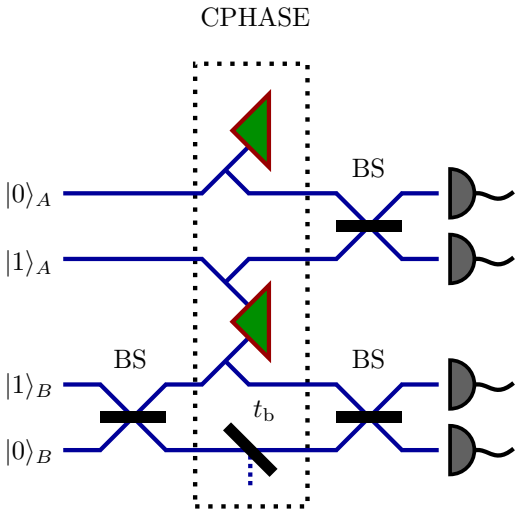

Figure 2.5: Entanglement swap in the dual-rail encoding. The labels of the individual rails indicate, where the photonic wavepacket is present for the shown basis state. The elements corresponding to the controlled-phase gate are within the dotted rectangle with the label "CPHASE", where triangles represent atomic ensembles (coupled to some linear optics elements). After exiting the atomic ensembles, the photons take the path at the intersections as to continue propagation to the right. This diagram corresponds to the circuit for the qubits A and B in figure 2.1. The Hadamard operators are implemented by beam splitters (BS). In the implementation of the controlled-phase gate, there is an additional beam splitter with transmission coefficient t_b. The photons propagate from left to right and get affected by the linear and nonlinear optics elements.

two ensembles, the upper one (coupled to the rail corresponding to state $|0\rangle_A$) only functions a memory, while the lower one (coupled to the rails corresponding to states $|1\rangle_A$ and $|1\rangle_B$) functions both as a memory for photon A and a scatterer for photon B. The need for two ensembles is due to the fact that the state of photon A can be in a superposition, and both of the states $|0\rangle_A$ and $|1\rangle_A$ need to be stored before scattering photon B. The ensembles could be coupled to linear optics elements (an optical cavity like in Ref. [1] or a Sagnac interferometer like in chapter 4).

The role of the beam splitter in the implementation of the controlled-phase gate shown in figure 2.5 is to add loss in the heralded operation of the gate, which can improve conditional fidelity at the expense of decreasing success probability. To explain the intuition behind improvement of conditional fidelity by additional loss, consider the fidelity of creation of creation of a Bell state with the input state (2.22). The output state of the controlled-phase gate using the effective description of loss and written in the simplified single-mode basis is

$$|\psi_{\text{out}}\rangle = \frac{1}{2}\left(t_{\text{b}}|00\rangle_{AB} + R_0|01\rangle_{AB} + t_{\text{b}}|10\rangle_{AB} + R_1|11\rangle_{AB}\right), \tag{2.67}$$

where t_{b} is the transmission coefficient of the beam splitter in figure 2.5 and R_0 (R_1) is the reflection coefficient of the atomic ensemble without (with) a stored photon. If we set $t_{\text{b}} = R_0 = -R_1$, the output state (2.67) is proportional to the ideal state (2.27). Hence, the operation has unit conditional fidelity. Due to the multi-mode nature of the traveling photons, it may not be possible to reach unit conditional fidelity, but adding loss can allow us to cancel lower order error terms in the conditional fidelity and thus make it is closer to unity (see chapter 4 for a concrete example).

Another note here is that we only talk about the reflection coefficients R_0 and R_1 and not the transmission coefficients for example. This is mainly to be consistent with the setups of Ref. [1] and chapter 4. In those setups, the linear optics elements coupled to the ensemble (one-sided cavity and Sagnac interferometer respectively) are such that everything is reflected in the same rail as the incident photon or dissipated. In general, R_0 and R_1 are just factors that the respective photonic basis states acquire as a result of interactions with the atomic ensemble. Below, we will continue calling these "the reflection coefficients" for simplicity.

Now we discuss the real and ideal evolution of the controlled-phase gate using the multi-mode computational basis as described in section 2.6. Since photon A is stored and retrieved, and photon B is scattered, it is most natural to describe the former as a time-dependent signal and the latter through a frequency distribution. We define $\hat{a}^\dagger_{A,0}(t_A)$ and $\hat{a}^\dagger_{A,1}(t_A)$ to be the creation operators for photon A at time t_A, corresponding respectively to the states $|0\rangle_A$ and $|1\rangle_A$. These operators have the commutation relations

$$[\hat{a}_{A,x}(t_A), \hat{a}^\dagger_{A,x'}(t'_A)] = \delta_{x,x'}\delta(t_A - t'_A), \tag{2.68}$$

where $x, x' \in \{0, 1\}$. For photon B, the operators corresponding to the states $|0\rangle_B$ and $|1\rangle_B$ are respectively $\hat{a}^\dagger_{B,0}(\omega_B)$ and $\hat{a}^\dagger_{B,1}(\omega_B)$, where ω_B is the frequency of the photon.

They have commutation relations

$$[\hat{a}_{B,x}(\omega_B), \hat{a}^\dagger_{B,x'}(\omega'_B)] = \delta_{x,x'}\delta(\omega_B - \omega'_B), \tag{2.69}$$

where $x, x' \in \{0, 1\}$. For notational convenience, we define the states $|0_{t_A}\rangle = \hat{a}^\dagger_{A,0}(t_A)|\text{vac}\rangle$, $|1_{t_A}\rangle = \hat{a}^\dagger_{A,1}(t_A)|\text{vac}\rangle$, $|0_{\omega_B}\rangle = \hat{a}^\dagger_{B,0}(\omega_B)|\text{vac}\rangle$, and $|1_{\omega_B}\rangle = \hat{a}^\dagger_{B,1}(\omega_B)|\text{vac}\rangle$. With these definitions, the initial computational basis states can be written

$$\begin{aligned}
|00\rangle_{AB} &= \int\int \phi_{A,\text{in}}(t_A)\phi_B(\omega_B)|0_{t_A}0_{\omega_B}\rangle \,\mathrm{d}t_A \,\mathrm{d}\omega_B, \\
|01\rangle_{AB} &= \int\int \phi_{A,\text{in}}(t_A)\phi_B(\omega_B)|0_{t_A}1_{\omega_B}\rangle \,\mathrm{d}t_A \,\mathrm{d}\omega_B, \\
|10\rangle_{AB} &= \int\int \phi_{A,\text{in}}(t_A)\phi_B(\omega_B)|1_{t_A}0_{\omega_B}\rangle \,\mathrm{d}t_A \,\mathrm{d}\omega_B, \\
|11\rangle_{AB} &= \int\int \phi_{A,\text{in}}(t_A)\phi_B(\omega_B)|1_{t_A}1_{\omega_B}\rangle \,\mathrm{d}t_A \,\mathrm{d}\omega_B.
\end{aligned} \tag{2.70}$$

We define the ideal unitary evolution corresponding to the controlled-phase gate such that the effects of EIT storage and retrieval of photon A are included. Hence, the input photon wave function $\phi_{A,\text{in}}$ is transformed into output wave function $\phi_{A,\text{out}}$ in addition to the phase transformation according to equation (2.26). The intermediate step is that the photon is stored inside the ensemble in the single excitation states. For the EIT setup in figure 2.2, the single excitation states are the ones, where atom with the index j is in state $|c\rangle$, and all the rest are in state $|a\rangle$. We denote these states $|c_j a\rangle$.

The relation between the input wave functions and the output wave functions of the photons does, in general, depend on the values of the classically fluctuating parameters. For a given realization of the atomic ensemble n, we can define

$$\phi_{A,\text{out},n,0}(t_A) = \sum_j \int K_{\text{r},n,0,j}(t_A) K_{\text{s},n,0,j}(t'_A)\phi_{A,\text{in}}(t'_A) \,\mathrm{d}t'_A, \tag{2.71}$$

where $K_{\text{s},n,0,j}$ and $K_{\text{r},n,0,j}$ are the EIT storage and retrieval kernels respectively, the index j runs over the individual atoms, and the label "0" on the state and kernels indicates that storage and retrieval happens using the upper ensemble in figure 2.5. This distinction is due to the fact that, if we have two atomic ensembles with classically fluctuating parameters, then for each realization they will, in general, have different values of those parameters. If the only stochastic parameter is the positions of the atoms, storage and retrieval for each realization will be approximately the same in the limit of small coupling strength of the individual atoms and a large number of them. This is the basis of the continuum approximation that is often used to describe EIT storage and retrieval [55]. We note that after storage, the atoms are in the state $\rho_{\text{stored},0,n} = |\psi_{\text{stored},0,n}\rangle\langle\psi_{\text{stored},0,n}| + (1 - \eta_{\text{storage}})|a\rangle^N\langle a|^N$, where

$$|\psi_{\text{stored},0,n}\rangle = \sum_j \left(\int K_{\text{s},n,0,j}(t'_A)\phi_{A,\text{in}}(t'_A) \,\mathrm{d}t'_A \right) |c_j a\rangle, \tag{2.72}$$

$|a\rangle^N$ is the state, where all atoms in the ensemble are in state $|a\rangle$, and

$$\eta_{\text{storage}} = \langle \psi_{\text{stored},0,n} | \psi_{\text{stored},0,n} \rangle. \tag{2.73}$$

According to equation (2.60) we take the reference wave function to be

$$\phi_{A,\text{out},0}(t_A) = \sum_{n=1}^{N_\text{r}} \phi_{A,\text{out},n,0}(t_A), \tag{2.74}$$

where N_r is the number of realizations of atomic ensemble that we sample over. The states below will be properly normalized below by adding factors of

$$\mathcal{N} = \sqrt{\int |\phi_{A,\text{out},0}(t_A)|^2 \, \mathrm{d}t_A}. \tag{2.75}$$

Having defined $\phi_{A,\text{out},0}$, we can now define the action of the unitary operator U_{AB} for the ideal evolution on the basis states. It is

$$\begin{aligned}
U_{AB}|00\rangle_{AB} &= \frac{1}{\mathcal{N}} \int\int \phi_{A,\text{out},0}(t_A)\phi_B(\omega_B)|0_{t_A}0_{\omega_B}\rangle \, \mathrm{d}t_A \, \mathrm{d}\omega_B, \\
U_{AB}|01\rangle_{AB} &= \frac{1}{\mathcal{N}} \int\int \phi_{A,\text{out},0}(t_A)\phi_B(\omega_B)|0_{t_A}1_{\omega_B}\rangle \, \mathrm{d}t_A \, \mathrm{d}\omega_B, \\
U_{AB}|10\rangle_{AB} &= \frac{1}{\mathcal{N}} \int\int \phi_{A,\text{out},0}(t_A)\phi_B(\omega_B)|1_{t_A}0_{\omega_B}\rangle \, \mathrm{d}t_A \, \mathrm{d}\omega_B, \\
U_{AB}|11\rangle_{AB} &= -\frac{1}{\mathcal{N}} \int\int \phi_{A,\text{out},0}(t_A)\phi_B(\omega_B)|1_{t_A}1_{\omega_B}\rangle \, \mathrm{d}t_A \, \mathrm{d}\omega_B.
\end{aligned} \tag{2.76}$$

When defining the ideal evolution in equation (2.76), we have taken the ideal output wave packets for photon A to be the ones, which are obtained after storage and retrieval in the absence of scattering. For photon B, we take the ideal frequency distribution to be equal to the input frequency distribution. This is a natural choice, but there may exist more optimal wave functions which give better fidelities.

The operator U_{AB} above can be used to define a map acting on the density matrices instead of states, i.e. $\mathcal{U}_{AB}(\rho) = U_{AB}\rho U_{AB}^\dagger$. The real physical implementation of the controlled-phase gate, can, in general, be written only as such a map $\mathcal{V}_{AB}$, due to incoherent processes. Generalizing equation (2.12) to many realizations of the atomic ensemble, the map $\mathcal{V}_{AB}$ can written

$$\mathcal{V}_{AB}(\rho) = \frac{1}{N_\text{r}} \sum_{n=1}^{N_\text{r}} \left(V_{n,AB}\rho V_{n,AB}^\dagger + \mathcal{J}_{n,AB}(\rho) \right), \tag{2.77}$$

where $V_{n,AB} = e^{-iH_{\text{eff},n}(t-t_0)/\hbar}$ is the operator describing the evolution under the effective non-Hermitian Hamiltonian $H_{\text{eff},n}$ (for a particular realization n of the atomic ensemble), and the superoperators $\mathcal{J}_{n,AB}$ describe the processes, where at least one quantum jump

occurs. We do not need to calculate the exact form of the superoperators $\mathcal{J}_{n,AB}$, since we assume that they produce states with zero overlap with the computational basis, i.e.

$$\langle x_{t'_A} x'_{\omega'_B} | \mathcal{J}_{n,AB}(\rho) | y_{t_A} y'_{\omega_B} \rangle = 0 \tag{2.78}$$

for $x, x', y, y' \in \{0, 1\}$. This statement is another way of putting the result of the discussion in section 2.5 above, where we have argued that spontaneous emission in the atoms will bring the atom into a state that is decoupled from the dynamics and ultimately result in a vacuum state, which is outside of the computational basis.

After solving the scattering problem, the action of the operators $V_{n,AB}$ on the basis states can be written

$$\begin{aligned}
V_{n,AB}|00\rangle_{AB} &= t_\mathrm{b} \int\int \phi_{A,\mathrm{out},n,0}(t_A)\phi_B(\omega_B)|0_{t_A}0_{\omega_B}\rangle \,\mathrm{d}t_A \,\mathrm{d}\omega_B, \\
V_{n,AB}|01\rangle_{AB} &= \int\int R_{0,n}(\omega_B)\phi_{A,\mathrm{out},n,0}(t_A)\phi_B(\omega_B)|0_{t_A}1_{\omega_B}\rangle \,\mathrm{d}t_A \,\mathrm{d}\omega_B, \\
V_{n,AB}|10\rangle_{AB} &= t_\mathrm{b} \int\int \phi_{A,\mathrm{out},n,10}(t_A)\phi_B(\omega_B)|1_{t_A}0_{\omega_B}\rangle \,\mathrm{d}t_A \,\mathrm{d}\omega_B, \\
V_{n,AB}|11\rangle_{AB} &= \int\int \phi_{A,\mathrm{out},n,11}(t_A, \omega_B)\phi_B(\omega_B)|1_{t_A}1_{\omega_B}\rangle \,\mathrm{d}t_A \,\mathrm{d}\omega_B,
\end{aligned} \tag{2.79}$$

where

$$\phi_{A,\mathrm{out},n,10}(t_A) = \sum_j \int K_{\mathrm{r},n,1,j}(t_A) K_{\mathrm{s},n,1,j}(t'_A) \phi_{A,\mathrm{in}}(t'_A) \,\mathrm{d}t'_A, \tag{2.80}$$

$$\phi_{A,\mathrm{out},n,11}(t_A, \omega_B) = \sum_j \int K_{\mathrm{r},n,1,j}(t_A) R_{1,n,j}(\omega_B) K_{\mathrm{s},n,1,j}(t'_A) \phi_{A,\mathrm{in}}(t'_A) \,\mathrm{d}t'_A. \tag{2.81}$$

The only difference between $\phi_{A,\mathrm{out},n,10}$ in equation (2.80) and $\phi_{A,\mathrm{out},n,0}$ in equation (2.71) is that $\phi_{A,\mathrm{out},n,0}$ results from storage and retrieval in the upper ensemble in figure 2.5 (subscript "0" in the storage and retrieval kernels), while $\phi_{A,\mathrm{out},n,10}$ results from storage and retrieval in the lower ensemble (subscript "1" in the storage and retrieval kernels). As discussed above, for each realization, the two ensembles will have different values of the stochastic parameters, which can influence storage and retrieval. If no stochastic parameters are assumed in the model, $\phi_{A,\mathrm{out},n,10}$ and $\phi_{A,\mathrm{out},n,0}$ are the same.

The wave function $\phi_{A,\mathrm{out},n,11}$ in equation (2.81) additionally contains the reflection coefficient $R_{1,n,j}(\omega_B)$, which describes scattering of photon B, while photon A is stored in the ensemble. The reflection coefficient $R_{1,n,j}(\omega_B)$, in general, depends on the position (index j) of the atom, where photon A was stored. It is, however, assumed to be diagonal, i.e. scattering of photon B does not redistribute the stored photon A among the atoms. Physically, this can be realized by storing photon A in internal states of the atom that are decoupled from the dynamics during scattering as discussed in section 2.5 above for Rydberg atoms and similarly for the controlled-phase gate in chapter 4.

The action of operators $V_{n,AB}$ in equation (2.79) illustrates the fact that real physical systems usually act differently on the different frequency components of the photons, which makes a single-mode computational basis insufficient for description of the problem. Another remark is that the errors of the real evolution described by equations (2.79) never make the states of the computational basis transition to other states within the basis. In other words, the evolution of the real physical system preserves the diagonal property of the ideal controlled-phase evolution (2.76). This is a consequence of sequential operation of the gate and the dual-rail encoding. Only the rails corresponding to states $|1\rangle_A$ and $|1\rangle_B$ could possibly mix, which could introduce logic errors. The sequential operation makes it possible to filter any leakage during scattering of photon B into the rail corresponding to state $|1\rangle_A$, since photon A is stored in the atomic ensemble at this point. The diagonal property of V_{AB} will be important for showing that the different fidelity measures are equal to each other.

Having defined the evolution of the states for the multi-mode basis states, we also need to discuss the projection operators corresponding to the conditional fidelities. The multi-mode version of the projection operator (2.30) is

$$P_{AB} = \sum_{x,x'=0}^{1} \int\int |x_{t_A} x'_{\omega_B}\rangle\langle x_{t_A} x'_{\omega_B}| \, \mathrm{d}t_A \, \mathrm{d}\omega_B. \tag{2.82}$$

Physically, this corresponds to a quantum nondemolition (QND) measurement of photon number without projecting on any particular computational basis state. Doing such a QND measurement efficiently is challenging, and hence conditional fidelity of creation of a Bell state and conditional Choi-Jamiolkowski fidelity can be considered in the abstract sense.

For entanglement swap, the multi-mode version of the projection operators (2.36) are $I_{A'B'} \otimes P_{xx',AB}$ with

$$P_{xx',AB} = \int\int |x_{t_A} x'_{\omega_B}\rangle\langle x_{t_A} x'_{\omega_B}| \, \mathrm{d}t_A \, \mathrm{d}\omega_B. \tag{2.83}$$

Compared to equation (2.82), the projection operators in equation (2.83) project onto a particular computational basis state. This is implemented by having a (destructive) single-photon detector at the end of each of the 4 rails in figure 2.5. Such detectors are routinely used and can reach very high efficiencies [56].

Another thing to note about the projection operators (2.82) and (2.83) is that we have not specified the range of frequencies and times for integration. In principle, the integration limits may be different from the the limits in the definition of the basis states and their evolution in equations (2.70), (2.76) and (2.79) (where the integration limits are also implicit). For simplicity we will assume that the limits of integration in all the mentioned equations are the same. For the frequency variable ω_B, we assume integration over the whole real line. For the time variable t_A, by the discussion at the end of section 2.6 above, the integration is from 0 to some final time t. Using these limits in the projection operators (2.82) and (2.83) means in particular that we assume

the detector to perform with unit efficiency across all frequencies and times, which is an idealization. Non-unit efficiency dependent on frequency or time could be modeled by using a weight function in the integrands of equations (2.82) and (2.83). Frequency and time independent non-unit efficiency of the detector η_{detector} can be introduced in the model by e.g. replacing P by $\sqrt{\eta_{\text{detector}}}P$ in equations (2.31) and (2.32). We see that such a replacement will only decrease the success probability, while the conditional fidelity will remain the same.

For the calculation of some of the fidelities and success probabilities, we will also need a definition of the Hadamard operator in the multi-mode basis. It is

$$\begin{aligned} H_A|0_{t_A}\rangle &= (|0_{t_A}\rangle + |1_{t_A}\rangle)/\sqrt{2}, \\ H_A|1_{t_A}\rangle &= (|0_{t_A}\rangle - |1_{t_A}\rangle)/\sqrt{2} \end{aligned} \tag{2.84}$$

for photon A, and

$$\begin{aligned} H_B|0_{\omega_B}\rangle &= (|0_{\omega_B}\rangle + |1_{\omega_B}\rangle)/\sqrt{2}, \\ H_B|1_{\omega_B}\rangle &= (|0_{\omega_B}\rangle - |1_{\omega_B}\rangle)/\sqrt{2} \end{aligned} \tag{2.85}$$

for photon B. These two definitions reduce to the original definition (2.24) for the input basis states (2.70).

2.8 Fidelities in the multi-mode basis

Using the above definitions, we can now find the fidelities and success probabilities. The details of the derivation are in appendix A. The fidelity for creation of a Bell state F_{Bell} and the Choi-Jamiolkowski fidelity F_{CJ} are the same and can be calculated using the expression

$$\begin{aligned} F_{\text{Bell}} = F_{\text{CJ}} = \frac{1}{16N_{\text{r}}\mathcal{N}^2}\sum_{n=1}^{N_{\text{r}}}\Bigg| & \left(t_{\text{b}} + \int R_{0,n}(\omega_B)|\phi_B(\omega_B)|^2\,\mathrm{d}\omega_B\right) \\ & \times \int \phi^*_{A,\text{out},0}(t_A)\phi_{A,\text{out},n,0}(t_A)\,\mathrm{d}t_A \\ & + t_{\text{b}}\int \phi^*_{A,\text{out},0}(t_A)\phi_{A,\text{out},n,10}(t_A)\,\mathrm{d}t_A \\ & - \int\int \phi^*_{A,\text{out},0}(t_A)\phi_{A,\text{out},n,11}(t_A,\omega_B)|\phi_B(\omega_B)|^2\,\mathrm{d}t_A\,\mathrm{d}\omega_B\Bigg|^2. \end{aligned} \tag{2.86}$$

The conditional fidelities are $F_{\text{Bell,cond}} = F_{\text{Bell}}/P_{\text{suc}}$ and $F_{\text{CJ,cond}} = F_{\text{CJ}}/P_{\text{suc}}$, with the same success probability

$$P_{\text{suc}} = \frac{1}{4N_{\text{r}}} \sum_{n=1}^{N_{\text{r}}} \Bigg(\left(t_{\text{b}}^2 + \int |R_{0,n}(\omega_B)|^2 |\phi_B(\omega_B)|^2 \, \mathrm{d}\omega_B \right) \int |\phi_{A,\text{out},n,0}(t_A)|^2 \, \mathrm{d}t_A + t_{\text{b}}^2 \int |\phi_{A,\text{out},n,10}(t_A)|^2 \, \mathrm{d}t_A + \int\int |\phi_{A,\text{out},n,11}(t_A,\omega_B)|^2 |\phi_B(\omega_B)|^2 \, \mathrm{d}t_A \, \mathrm{d}\omega_B \Bigg). \tag{2.87}$$

Hence, we also have that $F_{\text{Bell,cond}} = F_{\text{CJ,cond}}$. The entanglement swap fidelity is slightly different and has the expression

$$F_{\text{swap}} = \frac{1}{16N_{\text{r}}P_{\text{suc}}} \sum_{n=1}^{N_{\text{r}}} \int\int |\phi_B(\omega_B)|^2 \Big| \big(t_{\text{b}} + R_{0,n}(\omega_B)\big) \, \phi_{A,\text{out},n,0}(t_A) + t_{\text{b}} \phi_{A,\text{out},n,10}(t_A) - \phi_{A,\text{out},n,11}(t_A,\omega_B) \Big|^2 \, \mathrm{d}t_A \, \mathrm{d}\omega_B, \tag{2.88}$$

where the success probability is given by the same expression (2.87). Compared to $F_{\text{Bell,cond}}$ and $F_{\text{CJ,cond}}$, the difference is that for calculation of F_{swap}, no projection is made on a reference wave function, and the terms are integrals over all the time and frequency components of the output photons.

Using the Cauchy-Schwarz inequality

$$\left| \int\int u^*(t_A,\omega_B) v(t_A,\omega_B) \, \mathrm{d}t_A \, \mathrm{d}\omega_B \right|^2 \leq \int |u(t_A,\omega_B)|^2 \, \mathrm{d}t_A \, \mathrm{d}\omega_B \int |v(t_A,\omega_B)|^2 \, \mathrm{d}t_A \, \mathrm{d}\omega_B \tag{2.89}$$

on functions

$$u(t_A,\omega_B) = \phi_{A,\text{out},0}(t_A)\phi_B(\omega_B), \tag{2.90}$$

$$v(t_A,\omega_B) = \phi_B(\omega_B) \Big(\big(t_{\text{b}} + R_{0,n}(\omega_B)\big) \phi_{A,\text{out},n,0}(t_A) + t_{\text{b}} \phi_{A,\text{out},n,10}(t_A) - \phi_{A,\text{out},n,11}(t_A,\omega_B) \Big), \tag{2.91}$$

we see that $F_{\text{Bell,cond}} = F_{\text{CJ,cond}} \leq F_{\text{swap}}$.

2.9 Further simplifications

Here we discuss the simplifications in the case when there is only a single realization of the atomic ensemble, i.e. storage and scattering does not depend on any classical

stochastic parameters. There are only two output wave functions to consider,

$$\phi_{A,\mathrm{out},0}(t_A) = \sum_j \int K_{\mathrm{r},j}(t_A) K_{\mathrm{s},j}(t'_A) \phi_{A,\mathrm{in}}(t'_A)\, \mathrm{d}t'_A, \tag{2.92}$$

$$\phi_{A,\mathrm{out},1}(t_A, \omega_B) = \sum_j \int K_{\mathrm{r},j}(t_A) R_{1,j}(\omega_B) K_{\mathrm{s},j}(t'_A) \phi_{A,\mathrm{in}}(t'_A)\, \mathrm{d}t'_A. \tag{2.93}$$

The wave function $\phi_{A,\mathrm{out},0}$ has the same definition as $\phi_{A,\mathrm{out},n,0}$ in equation (2.71), and the wave function $\phi_{A,\mathrm{out},1}$ has the same definition as $\phi_{A,\mathrm{out},n,11}$ in equation (2.81). We omit the index of realization n and use "1" instead of "11", since there is no wave function with the subscript "01". The storage and retrieval kernels ($K_{\mathrm{s},j}$ and $K_{\mathrm{r},j}$ respectively) are the same for both ensembles. The storage and retrieval efficiency is $\eta_{\mathrm{EIT}} = \int |\phi_{A,\mathrm{out},0}(t_A)|^2\, \mathrm{d}t_A$ (i.e. $\eta_{\mathrm{EIT}} = \mathcal{N}^2$, where $\mathcal{N}$ is given by equation (2.75))

Using above definitions, equation (2.86) simplifies to

$$\begin{aligned} F_{\mathrm{Bell}} = F_{\mathrm{CJ}} = \frac{\eta_{\mathrm{EIT}}}{16} \Bigg| 2t_{\mathrm{b}} + \int R_0(\omega_B) |\phi_B(\omega_B)|^2\, \mathrm{d}\omega_B \\ - \frac{1}{\eta_{\mathrm{EIT}}} \int\int \phi^*_{A,\mathrm{out},0}(t_A) \phi_{A,\mathrm{out},1}(t_A, \omega_B) |\phi_B(\omega_B)|^2\, \mathrm{d}t_A\, \mathrm{d}\omega_B \Bigg|^2, \end{aligned} \tag{2.94}$$

equation (2.87) simplifies to

$$\begin{aligned} P_{\mathrm{suc}} = \frac{\eta_{\mathrm{EIT}}}{4} \Bigg(2|t_{\mathrm{b}}|^2 + \int |R_0(\omega_B)|^2 |\phi_B(\omega_B)|^2\, \mathrm{d}\omega_B \\ + \frac{1}{\eta_{\mathrm{EIT}}} \int\int |\phi_{A,\mathrm{out},1}(t_A, \omega_B)|^2 |\phi_B(\omega_B)|^2\, \mathrm{d}t_A\, \mathrm{d}\omega_B \Bigg), \end{aligned} \tag{2.95}$$

and equation (2.88) simplifies to

$$F_{\mathrm{swap}} = \frac{1}{16 P_{\mathrm{suc}}} \int\int |\phi_B(\omega_B)|^2 \Big| \left(2t_{\mathrm{b}} + R_0(\omega_B)\right) \phi_{A,\mathrm{out},0}(t_A) - \phi_{A,\mathrm{out},1}(t_A, \omega_B) \Big|^2\, \mathrm{d}t_A\, \mathrm{d}\omega_B. \tag{2.96}$$

Here we also note that F_{swap} can be equal to $F_{\mathrm{Bell,cond}}$ and $F_{\mathrm{CJ,cond}}$ for certain conditions. This happens, when the non-zero bandwidth of the photon B is neglected by assuming $|\phi_B(\omega_B)|^2 = \delta(\omega_B - \omega_0)$ and

$$\phi_{A,\mathrm{out},1}(t_A, \omega_B) = R_1(\omega_B) \phi_{A,\mathrm{out},0}(t_A), \tag{2.97}$$

instead of the definition (2.93). These two assumptions result in

$$F_{\mathrm{Bell,cond}} = F_{\mathrm{CJ,cond}} = F_{\mathrm{swap}} = \frac{\eta_{\mathrm{EIT}}}{16 P_{\mathrm{suc}}} \Big| 2t_{\mathrm{b}} + R_0(\omega_0) - R_1(\omega_0) \Big|^2. \tag{2.98}$$

The assumption (2.97) is satisfied if $R_{1,j}$ in equation (2.93) is independent of the index of the atom j, i.e. $R_{1,j} = R_1$. Alternatively, that assumption can be satisfied if it is possible to do filtering of the retrieved excitation, e.g. by use of an optical cavity coupled to the ensemble (as in Ref. [1]). In the latter case, the general form of the storage and retrieval kernels could be written

$$K_{\mathrm{s},j}(t_A) = \phi^*_{A,\mathrm{in,ref}}(t_A) S_j, \tag{2.99}$$

$$K_{\mathrm{r},j}(t_A) = \phi_{A,\mathrm{out,ref}}(t_A) S^*_j. \tag{2.100}$$

The above expressions are designed to model the fact that presence of an optical cavity restricts storage of only a single mode of the incident photon [54] with temporal shape $\phi_{A,\mathrm{in,ref}}(t_A)$, so that the coefficients of the state (2.72) are all weighted by the projection of $\phi_{A,\mathrm{in}}(t_A)$ and $\phi_{A,\mathrm{in,ref}}(t_A)$. Hence, the highest storage efficiency is obtained if we choose $\phi_{A,\mathrm{in}}(t_A) = \phi_{A,\mathrm{in,ref}}(t_A)$. The coefficients of the single excitation states inside the ensemble are set by S_j, which describe the single spatial mode of the ensemble that the incident photon can be stored into. During retrieval, again only this spatial mode given by the coefficients S_j can be retrieved in the output photon, so that application of the retrieval kernel is effectively a projection of any state inside the ensemble onto this spatial mode. The end result is that insertion of equations (2.99) and (2.100) into equations (2.92) and (2.93) gives

$$\phi_{A,\mathrm{out},0}(t_A) = \left(\sum_j |S_j|^2 \right) \phi_{A,\mathrm{out,ref}}(t_A) \int \phi^*_{A,\mathrm{in,ref}}(t_A) \phi_{A,\mathrm{in}}(t'_A)\, \mathrm{d}t'_A, \tag{2.101}$$

$$\phi_{A,\mathrm{out},1}(t_A, \omega_B) = \left(\sum_j |S_j|^2 R_{1,j}(\omega_B) \right) \phi_{A,\mathrm{out,ref}}(t_A) \int \phi^*_{A,\mathrm{in,ref}}(t_A) \phi_{A,\mathrm{in}}(t'_A)\, \mathrm{d}t'_A. \tag{2.102}$$

These equations satisfy equation (2.97) with

$$R_1(\omega_B) = \frac{\sum_j |S_j|^2 R_{1,j}(\omega_B)}{\sum_j |S_j|^2}. \tag{2.103}$$

2.10 Discussion

The main result of this chapter are the fidelity expressions in sections 2.8 and 2.9, which were used in Ref. [1] and will be used in chapter 4. On a more general note, we have illustrated the difficulties of defining the meaning of fidelity for photon gates, which is mainly a consequence of the multi-mode nature of the traveling photon wavepackets. Among other things, this gives a lot more freedom in the choice of the input states. In the single-mode case, the general pure two-qubit input state is

$$|\psi_{\mathrm{in}}\rangle = c_{00}|00\rangle + c_{01}|01\rangle + c_{10}|10\rangle + c_{11}|10\rangle \tag{2.104}$$

for some complex numbers c_{00}, c_{01}, c_{10} and c_{11}, which are only constrained by the normalization condition $\|\psi_{\text{in}}\| = 1$. For the multi-mode case, the input state can be written

$$\begin{aligned}|\psi_{\text{in}}\rangle = \int\int \big(&\phi_{00}(t_A,\omega_B)|0_{t_A}0_{\omega_B}\rangle + \phi_{01}(t_A,\omega_B)|0_{t_A}1_{\omega_B}\rangle \\ &+ \phi_{10}(t_A,\omega_B)|1_{t_A}0_{\omega_B}\rangle + \phi_{10}(t_A,\omega_B)|1_{t_A}0_{\omega_B}\rangle\big)\,\mathrm{d}t_A\,\mathrm{d}\omega_B,\end{aligned} \tag{2.105}$$

where the choice is now over complex-valued *functions* ϕ_{00}, ϕ_{01}, ϕ_{10} and ϕ_{11} (also constrained by the normalization condition).

In chapter 4, we find the optimal input wave packets of the photons for a single operation of the gate, but the analysis of the scenario, when the output the controlled-phase gate is used in further computation (possibly as an input for another controlled-phase gate) is out of scope for this thesis. It is clear that the multi-mode nature of the photons will greatly complicate the analysis of such a scenario. However, it is not obvious, whether such analysis is needed, since repeated application of entangling gates (e.g. controlled-phase gates) on the same quantum state is only needed in the so-called circuit model of the quantum computation (i.e. representable by a circuit similar to figure 2.1 but arbitrarily complicated), which may be not a good fit for qubits encoded in photons.

For comparison, the best bet to achieve general purpose quantum information processing with linear optics seems to be using measurement-based computation [57, 58], where the entanglement is generated offline in a probabilistic but still efficient manner similar in some sense to quantum repeaters, and the final state is measured is a particular way to implement quantum computation equivalent to a circuit. This might also be a viable path forward for the class of controlled-phase gates for photons discussed in this chapter, since they can be operated in a heralded fashion with higher fidelities, as exemplified by Ref. [1] and chapter 4.

Chapter 3

Dispersion relations for stationary light

3.1 Acknowledgements

This chapter is based on the material published in Ref. [4]. The derivation of the dispersion relations for the continuum model is based on the one by Johan R. Ott. One of the dispersion relations for the discrete model (quadratic, with $N_{\mathrm{u}} = 2$) has already been obtained in the Master's thesis [59].

3.2 Overview

The controlled-phase gate in chapter 4 uses the phenomenon of stationary light for enhancement of the nonlinear interaction strength of the photons. To use stationary light for enhancement of the nonlinear interactions, it is essential to first understand the linear properties (dispersion relations), which is the focus of this chapter. Since, we have already discussed EIT in section 2.5, we first remark, why EIT in itself is not enough to get enhancement of the nonlinear interaction strength. The relevant figure of merit is the interaction time of the photons, which is proportional to the inverse of the group velocity. For EIT, decreasing the group velocity of the polaritons (coupled light-matter excitations) simultaneously makes them increasingly atomic and less photonic in character [52] thus also decreasing the optical nonlinearity. These two effects cancel each other, which results in no enhancement of the effective nonlinear interaction strength. In this context, proposals for "stationary light" have emerged as a way of creating polaritons with very small (or even vanishing) group velocities within the atomic medium, while retaining a non-zero photonic component [60, 61]. Building upon the enhanced nonlinear interactions, it is in principle possible to observe the rich physics of nonlinear optics at the level of a few photons [22, 62].

We will consider the dispersion relation for three different stationary light schemes (see figure 3.1). The dispersion relation gives the frequency (two-photon detuning) δ in

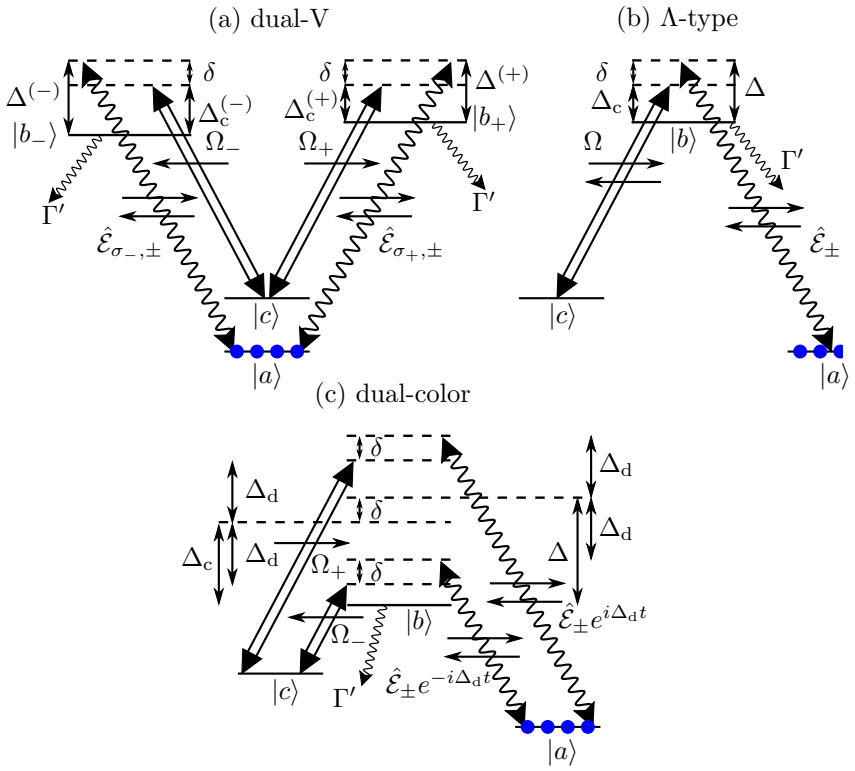

Figure 3.1: Level diagrams of the three schemes that we consider. The blue circles on state $|a\rangle$ indicate that the atoms are assumed to be initialized in this state. The arrows with small wiggly lines originating on the excited states $|b_\pm\rangle$ and $|b\rangle$ indicate spontaneous emission with a decay rate Γ'. The arrows between different states indicate either quantum fields (wiggly lines), or classical drives (double straight lines). The small horizontal arrows on each of these coupling arrows indicate the propagation direction. All the transitions are assumed to couple equally to both the right-moving and left-moving fields, but the arrows pointing only in a single direction on the classical drives for dual-V and dual-color schemes instead indicate that the externally applied drives propagate in the shown direction. The excited level $|b\rangle$ for the dual-color scheme is shifted vertically in order to be able to clearly show all the different detunings.

terms of the Bloch vector q. From the dispersion relation, the group velocity $v_g = \frac{\partial \delta}{\partial q}$ can be readily obtained, and by the discussion above, it can therefore provide an intuition about how strong the nonlinear interaction strength is expected to be. For the analysis, we will use two different theoretical models. The first is the continuum model, in which the atomic operators are defined for any real position coordinate z between 0 and L (the total length of the ensemble). The second is the discrete model, where each atom is a linear point scatterer. The latter model is motivated by a growing interest in considering systems, where the number of atoms is relatively small, while the coupling strength and control over placement of the individual atoms are greatly improved. Examples are tapered optical fibers [23–27] and photonic crystal waveguides [16, 63]. In the discrete model, we find that placing the atoms in a particular way provides an additional handle for controlling the dispersion relation [64, 65].

The dispersion relations for the continuum model have already been derived elsewhere [66–68]. However, as we will show below, the results of the discrete model can be understood better, if they are set in context by rederiving the results of the continuum model in a different way compared to the previous publications. Additionally, even when restricted to the continuum model, treating every stationary light scheme in the same framework allows for a much easier comparison of the schemes and also for tracking the various (physically motivated) approximations that are employed in the derivations. By doing numerical calculations with the discrete model afterwards, we can test the validity of some of these approximations. We will show that for some of the stationary light schemes, the dispersion relations derived analytically using the continuum model, can also be obtained numerically as limiting cases of the discrete model with randomly placed atoms.

We will consider one-dimensional ensembles of atoms with three different level and coupling schemes where stationary light can be observed (see figure 3.1). We will focus on the case of cold atoms, although for completeness we will also briefly discuss hot Λ-type atoms, which was the scheme used for the first prediction and observation of stationary light [60, 61]. Common to all stationary light schemes is the presence of two counter-propagating classical drives which couple the right-moving and left-moving modes of the quantum field through four-wave mixing [66]. One way to explain the origin of the four-wave mixing is that an incident photon of the quantum field will be temporarily mapped to the meta-stable state $|c\rangle$ by the classical drive propagating in the same direction. The other classical drive can then retrieve this temporary excitation into a photon of the quantum field propagating in the opposite direction. In this picture, stationary light can be viewed as simultaneous EIT storage and retrieval in both the forward and backward directions [55].

For the Λ-type scheme (figure 3.1(b)), a different intuitive explanation of stationary light can be given in terms of Bragg scattering. In this scheme, the two counter-propagating classical drives produce a standing wave, which modulates the refractive index of the ensemble such that it behaves as a Bragg grating. Hence, the coupling of the right-moving and left-moving modes of the quantum field happens due to the reflection of one into the other by the Bragg grating. The dynamics of the cold Λ-type

scheme is, however, more complicated, which can be illustrated in terms of the allowed processes. Since both counter-propagating drives are applied on the same transition $|b\rangle \leftrightarrow |c\rangle$, it is possible for the atom to be excited by one of the classical drives and de-excited by the other. This leads to the build up of higher order Fourier components of the atomic coherence resulting in a rich and complicated physics of stationary light for cold Λ-type atoms [69–74]. We will show that depending on the precise details of the system and the approximations used, it is possible to get dispersion relations with three different scalings close to the two-photon resonance ($\delta = 0$): $\delta \propto q^2$ (quadratic dispersion relation of stationary light), $\delta \propto \pm q$ (EIT-like linear dispersion relation), and $\delta \propto \pm|q|^{4/3}$ [68]. In the derivations below, the first two cases will arise in the continuum model due to different truncations of the set of higher order modes of the atomic coherence. Afterwards, in the discrete model, we will show that these truncations can actually be realized physically by positioning the atoms in certain ways. The dispersion relation $\delta \propto |q|^{4/3}$ is obtained in the continuum model, when all the higher order Fourier components of the atomic coherence are summed to infinite order [68]. In the discrete model, such a scaling can be reproduced in the limit of an infinite number of randomly placed atoms.

A common trait of the two other schemes for stationary light, dual-V [67] and dual-color [66] (figures 3.1(a) and 3.1(c) respectively) is the separation of the right-moving and left-moving fields (both classical and quantum) into different modes, either with different polarizations for dual-V or with different frequencies for dual-color. The main purpose of this separation is to suppress the higher order Fourier components of the atomic coherence since excitation and de-excitation with two different classical fields are no longer allowed. The end result of this, is that both the dual-V and dual-color schemes have quadratic dispersion relations $\delta \propto q^2$, just like stationary light in hot Λ-type atoms, where the higher order Fourier components of the atomic coherence are washed away by the thermal motion of the atoms [60, 61].

3.3 Continuum model

3.3.1 Dispersion relations for cold dual-V atoms

The dual-V scheme as shown in figure 3.1(a) has already been studied in Ref. [67] and was shown to have a quadratic dispersion relation. Here we do a different derivation of this result to serve as the context for the discussion of the other stationary light schemes. We take the dual-V scheme as the starting point, because the derivation of the dispersion relation is more straightforward, even if the additional atomic energy level and two different polarizations of the electric fields make the setup of the problem more complicated. In the course of the derivation we will introduce most of the definitions that we will also use for the other schemes (Λ-type and dual-color).

The atomic ensemble is assumed to be a one-dimensional medium of length L consisting of N atoms. In the continuum model, the atomic density $n_0 = N/L$ is assumed to be constant throughout the length of the ensemble. The atoms are described by the

collective operators

$$\hat{\sigma}_{\alpha\beta}(z) = \frac{1}{n_0}\sum_j \delta(z - z_j)\hat{\sigma}_{\alpha\beta,j} \tag{3.1}$$

where $\hat{\sigma}_{\alpha\beta,j} = |\alpha_j\rangle\langle\beta_j|$ is the atomic coherence ($\alpha \neq \beta$) or population ($\alpha = \beta$) of atom j. These collective operators have the equal time commutation relations

$$[\hat{\sigma}_{\alpha\beta}(z), \hat{\sigma}_{\alpha'\beta'}(z')] = \frac{1}{n_0}\delta(z - z')(\delta_{\beta,\alpha'}\hat{\sigma}_{\alpha\beta'} - \delta_{\beta',\alpha}\hat{\sigma}_{\alpha'\beta}). \tag{3.2}$$

Throughout this chapter (and the next one), all operators are defined to be slowly-varying in time, since we work in the interaction picture relative to the carrier frequencies of the fields.

The dual-V scheme has two excited states, $|b_+\rangle$ and $|b_-\rangle$, which both couple to the ground state $|a\rangle$ but with the different polarization modes, σ_+ and σ_-, of the quantum field. The σ_+ mode only couples the $|a\rangle \leftrightarrow |b_+\rangle$ transition, and the σ_- mode only couples the $|a\rangle \leftrightarrow |b_-\rangle$ transition. The operator for the total quantum field $\hat{\mathcal{E}}_{\sigma_\pm}$ for the different polarizations can be decomposed as

$$\hat{\mathcal{E}}_{\sigma_\pm} = \hat{\mathcal{E}}_{\sigma_\pm,+}e^{ik_0 z} + \hat{\mathcal{E}}_{\sigma_\pm,-}e^{-ik_0 z}, \tag{3.3}$$

where k_0 is the wave vector corresponding to the carrier frequency of the quantum fields ω_0, i.e. $k_0 = \omega_0/c$. For the σ_+ fields, $\hat{\mathcal{E}}_{\sigma_+,+}(z)$ is the spatially slowly-varying annihilation operator at position z for the field moving to the right (positive direction), and $\hat{\mathcal{E}}_{\sigma_+,-}(z)$ is the operator for the field moving to the left (negative direction). Analogous definitions hold for the σ_- fields. We will be concerned with the dynamics within a frequency interval around atomic resonances that is much smaller than the carrier frequencies of the fields. Therefore, the right-moving and left-moving quantum fields (for each polarization mode) can be regarded as being completely separate [53] with the equal time commutation relations

$$[\hat{\mathcal{E}}_\alpha(z), \hat{\mathcal{E}}^\dagger_\beta(z')] = \delta_{\alpha\beta}\delta(z - z'), \tag{3.4}$$

where α and β each denote one of the four possible combinations of polarization ($\sigma_\pm$) and propagation direction ($\pm$).

The transition frequencies between the atomic energy levels $|\alpha\rangle$ and $|\beta\rangle$ will be denoted by $\omega_{\alpha\beta}$. The quantum fields are detuned from the atomic transition frequencies by $\Delta_0^{(\pm)} = \omega_0 - \omega_{ab_\pm}$. The excited states $|b_+\rangle$ and $|b_-\rangle$ are assumed to have the same incoherent decay rate Γ' to modes other than the forward and backward propagating ones. We account for Γ' by making the detunings complex: $\tilde{\Delta}_0^{(\pm)} = \Delta_0^{(\pm)} + i\Gamma'/2$. In the calculations below, we will employ Fourier transformation, where the Fourier frequencies ω will be defined relative to the carrier frequency ω_0. For ease of notation we therefore define the detunings $\Delta^{(\pm)} = \Delta_0^{(\pm)} + \omega$. As opposed to the detunings of the carrier frequency $\Delta_0^{(\pm)}$, the detunings $\Delta^{(\pm)}$ additionally include the shift due to the finite bandwidth of the quantum field.

The two counter-propagating classical drives are in the two different polarization modes. Here, the polarization and the propagation direction are chosen such that Ω_+ is the Rabi frequency of the σ_+ classical drive propagating in the positive direction that couples the transition $|b_+\rangle \leftrightarrow |c\rangle$, and Ω_- is the Rabi frequency of the σ_- classical drive propagating in the negative direction that couples the transition $|b_-\rangle \leftrightarrow |c\rangle$. The classical drives have frequency ω_c and are detuned from the respective transitions by $\Delta_\mathrm{c}^{(\pm)} = \omega_\mathrm{c} - \omega_{b_\pm c}$. Furthermore, we define the two-photon detuning $\delta_0 = \omega_0 - \omega_\mathrm{c} - \omega_{ac}$, which has a unique definition, since the quantum fields have the same carrier frequency (ω_0) for both polarizations, and the classical drives have the same frequency (ω_c) for both polarizations. In terms of $\Delta_0^{(\pm)}$ and $\Delta_\mathrm{c}^{(\pm)}$ above, we also have $\delta_0 = \Delta_0^{(+)} - \Delta_\mathrm{c}^{(+)} = \Delta_0^{(-)} - \Delta_\mathrm{c}^{(-)}$. Similar to $\Delta^{(\pm)}$ above, there is a complementary definition of the two-photon detuning $\delta = \delta_0 + \omega$ that takes into account the finite bandwidth of the quantum field. The wave vector of the classical drive is $k_\mathrm{c} = \omega_\mathrm{c}/c$, but throughout our calculations we are going to assume $k_\mathrm{c} \approx k_0$.

The Hamiltonian for the dual-V scheme can be decomposed as $\hat{H}_\mathrm{V} = \hat{H}_\mathrm{V,a} + \hat{H}_\mathrm{V,i} + \hat{H}_\mathrm{V,p}$, where $\hat{H}_\mathrm{V,a}$ describes the atoms, $\hat{H}_\mathrm{V,p}$ describes the photons, and $\hat{H}_\mathrm{V,i}$ describes the light-matter interactions. In the interaction picture and the rotating wave approximation, the parts are

$$\hat{H}_\mathrm{V,a} = -\hbar n_0 \int \left[\sum_{\alpha\in\{+,-\}} \tilde{\Delta}_0^{(\alpha)} \hat{\sigma}_{b_\alpha b_\alpha}(z) + \delta_0 \hat{\sigma}_{cc}(z) \right] \mathrm{d}z, \tag{3.5a}$$

$$\hat{H}_\mathrm{V,i} = -\hbar n_0 \int \sum_{\alpha\in\{+,-\}} \left\{ \left[\hat{\sigma}_{b_\alpha c}(z) \Omega_\alpha e^{\alpha i k_\mathrm{c} z} + \mathrm{H.c.} \right] + g\sqrt{2\pi} \left[\hat{\sigma}_{b_\alpha a}(z) \hat{\mathcal{E}}_{\sigma_\alpha}(z) + \mathrm{H.c.} \right] \right\} \mathrm{d}z, \tag{3.5b}$$

$$\hat{H}_\mathrm{V,p} = -i\hbar c \int \sum_{\alpha\in\{+,-\}} \left[\hat{\mathcal{E}}^\dagger_{\sigma_\alpha,+}(z) \frac{\partial \hat{\mathcal{E}}_{\sigma_\alpha,+}(z)}{\partial z} - \hat{\mathcal{E}}^\dagger_{\sigma_\alpha,-}(z) \frac{\partial \hat{\mathcal{E}}_{\sigma_\alpha,-}(z)}{\partial z} \right] \mathrm{d}z, \tag{3.5c}$$

where $g = \mu\sqrt{\omega_{ab_\pm}/(4\pi\hbar\epsilon_0 A)}$ (in this constant, we assume that $\omega_{ab_+} \approx \omega_{ab_-}$), μ is the matrix element of the atomic dipole, and A is the effective area of the electric field mode.

The Heisenberg equations of motion for the electric field operators are given by

$$\left(\frac{\partial}{\partial t} \pm c \frac{\partial}{\partial z} \right) \mathcal{E}_{\sigma_+,\pm} = ig\sqrt{2\pi} n_0 \sigma_{ab_+} e^{\mp i k_0 z}. \tag{3.6a}$$

$$\left(\frac{\partial}{\partial t} \pm c \frac{\partial}{\partial z} \right) \mathcal{E}_{\sigma_-,\pm} = ig\sqrt{2\pi} n_0 \sigma_{ab_-} e^{\mp i k_0 z}. \tag{3.6b}$$

Here and in the following we will omit the hats above the operators as soon as the Heisenberg equations of motion are found, since we will be considering linear effects for which the operator character does not play any role. The noise operators, normally included in the Heisenberg equations of motion whenever incoherent losses are present ($\Gamma' > 0$), are also omitted, since they can be shown to not have any effect [54, 55, 67].

The equations of motion for the atoms are found under the assumption that the probe field is weak and that the ensemble is initially prepared in the ground state. Hence, we set $\hat{\sigma}_{aa} \approx 1$, $\hat{\sigma}_{b_\pm b_\pm} \approx \hat{\sigma}_{b_\pm b_\mp} \approx \hat{\sigma}_{cc} \approx \hat{\sigma}_{b_\pm c} \approx 0$, and get the equations

$$\frac{\partial \sigma_{ab_\pm}}{\partial t} = i\tilde{\Delta}_0^{(\pm)}\sigma_{ab_\pm} + i\Omega_\pm \sigma_{ac} e^{\pm ik_c z} + ig\sqrt{2\pi}\mathcal{E}_{\sigma_\pm}, \tag{3.7a}$$

$$\frac{\partial \sigma_{ac}}{\partial t} = i\delta_0 \sigma_{ac} + i\Omega_+^* \sigma_{ab_+} e^{-ik_c z} + i\Omega_-^* \sigma_{ab_-} e^{ik_c z}. \tag{3.7b}$$

We note that it is in equations (3.7) that the continuum approximation is first applied, since both the Hamiltonian (3.5) and equations (3.6) in principle retain the discrete nature of the atoms due to the definition (3.1). Equations (3.7) are derived under the approximation $\sigma_{aa} \approx 1$, which can be viewed as two separate approximations. The first is that $\sigma_{aa,j} \approx 1$ for all the individual atoms j. Together with the definition (3.1), we see that $\sigma_{aa} \approx 1$ also means approximating $\sum_j \delta(z - z_j) \approx n_0$, and this is what we mean by the continuum approximation. In the analysis done in Ref. [75] it was shown in a perturbative calculation that this is a good approximation for randomly placed atoms. Using the discrete model in section 3.4 below, we will verify it explicitly without any perturbative assumptions.

We make two assumptions for simplicity and to be able to relate this derivation to the secular approximation for Λ-type atoms, which we discuss below. First, we assume equal atomic transition frequencies, $\omega_{b_+c} = \omega_{b_-c}$, so that $\Delta_0^{(+)} = \Delta_0^{(-)} = \Delta_0$, and $\Delta_c^{(+)} = \Delta_c^{(-)} = \Delta_c$. Second, we assume equal classical drive strengths, $\Omega_+ = \Omega_- = \Omega_0/2$.

With the above assumptions and defining the slowly-varying versions of $\sigma_{ab\pm}$ by

$$\sigma_{ab}^\pm = \sigma_{ab\pm} e^{\mp ik_0 z}, \tag{3.8}$$

the equations of motion become

$$\frac{\partial \sigma_{ab}^\pm}{\partial t} = i\tilde{\Delta}_0 \sigma_{ab}^\pm + i\frac{\Omega_0}{2}\sigma_{ac} + ig\sqrt{2\pi}\mathcal{E}_{\sigma_\pm} e^{\mp ik_0 z}, \tag{3.9a}$$

$$\frac{\partial \sigma_{ac}}{\partial t} = i\delta_0 \sigma_{ac} + i\frac{\Omega_0^*}{2}(\sigma_{ab}^+ + \sigma_{ab}^-), \tag{3.9b}$$

and after the Fourier transform in time,

$$0 = i\tilde{\Delta}\sigma_{ab}^\pm + i\frac{\Omega_0}{2}\sigma_{ac} + ig\sqrt{2\pi}\mathcal{E}_{\sigma_\pm} e^{\mp ik_0 z}, \tag{3.10a}$$

$$0 = i\delta\sigma_{ac} + i\frac{\Omega_0^*}{2}(\sigma_{ab}^+ + \sigma_{ab}^-). \tag{3.10b}$$

Here, we have absorbed the Fourier frequency variable ω into the detunings by defining $\tilde{\Delta} = \tilde{\Delta}_0 + \omega$ and $\delta = \delta_0 + \omega$. Isolating σ_{ac} from equation (3.10b) and inserting into equations (3.10a) gives two coupled equations

$$0 = \left(1 - \frac{\delta_S}{2\delta}\right)\sigma_{ab}^\pm - \frac{\delta_S}{2\delta}\sigma_{ab}^\mp + \frac{g\sqrt{2\pi}}{\tilde{\Delta}}\mathcal{E}_{\sigma_\pm} e^{\mp ik_0 z}. \tag{3.11}$$

Here, we have introduced

$$\delta_{\mathrm{S}} = \frac{|\Omega_0|^2}{2\tilde{\Delta}}. \tag{3.12}$$

For $\delta, \Gamma' \ll \Delta_{\mathrm{c}}$, $\delta_{\mathrm{S}} \approx |\Omega_0|^2/(2\Delta_{\mathrm{c}})$ is the total AC Stark shift induced by the classical drives on the state $|c\rangle$. We will focus on the case when $|\delta| \ll |\delta_{\mathrm{S}}|$. For $|\delta| \gtrsim |\delta_{\mathrm{S}}|$, the frequency is outside the scale of the strongest effect induced by the classical drives. Therefore, the dispersion relations for the different schemes all cross over to the dispersion relation corresponding to a two-level atom, as can be seen in figure 3.2.

Solving equations (3.11), we find

$$\sigma_{ab}^{\pm} = -\frac{g\sqrt{2\pi}}{\tilde{\Delta}}\left[\frac{\delta - \delta_{\mathrm{S}}/2}{\delta - \delta_{\mathrm{S}}}\mathcal{E}_{\sigma_\pm} e^{\mp ik_0 z} + \frac{\delta_{\mathrm{S}}/2}{\delta - \delta_{\mathrm{S}}}\mathcal{E}_{\sigma_\mp} e^{\pm ik_0 z}\right]. \tag{3.13}$$

We insert equations (3.13) into the Fourier transformed versions of equations (3.6) and remove terms with rapid spatial variation, i.e. terms containing factors $e^{ink_0 z}$ with the integer n fulfilling $|n| > 0$. As a consequence, $\mathcal{E}_{\sigma_+,+}$ and $\mathcal{E}_{\sigma_-,-}$ form a closed set of equations, separate from $\mathcal{E}_{\sigma_+,-}$ and $\mathcal{E}_{\sigma_-,+}$. We therefore find

$$\left(-i\frac{\omega}{cn_0} \pm \frac{1}{n_0}\frac{\partial}{\partial z}\right)\mathcal{E}_{\sigma_\pm,\pm} = -i\frac{\Gamma_{1\mathrm{D}}}{2\tilde{\Delta}}\left[\frac{\delta - \delta_{\mathrm{S}}/2}{\delta - \delta_{\mathrm{S}}}\mathcal{E}_{\sigma_\pm,\pm} + \frac{\delta_{\mathrm{S}}/2}{\delta - \delta_{\mathrm{S}}}\mathcal{E}_{\sigma_\mp,\mp}\right], \tag{3.14a}$$

$$\left(-i\frac{\omega}{cn_0} \mp \frac{1}{n_0}\frac{\partial}{\partial z}\right)\mathcal{E}_{\sigma_\pm,\mp} = -i\frac{\Gamma_{1\mathrm{D}}}{2\tilde{\Delta}}\frac{\delta - \delta_{\mathrm{S}}/2}{\delta - \delta_{\mathrm{S}}}\mathcal{E}_{\sigma_\pm,\mp}, \tag{3.14b}$$

where we have introduced the decay rate $\Gamma_{1\mathrm{D}} = 4\pi g^2/c$ which describes the photon emission rate into the one-dimensional modes (the sum of right-moving and left-moving) from the atoms. The total decay rate of an excited atom is then $\Gamma = \Gamma' + \Gamma_{1\mathrm{D}}$. In the absence of inhomogeneous broadening, the decay rate $\Gamma_{1\mathrm{D}}$ is related to the resonant optical depth d_{opt} through $d_{\mathrm{opt}} = 2N\Gamma_{1\mathrm{D}}/\Gamma$.

Since the Hamiltonian (3.5) is periodic in space with period $2\pi/k_0$, we can invoke Bloch's theorem and look for solutions to equations (3.14) of the form

$$\mathcal{E}_{\sigma_\pm}(z,\omega) = \left(\mathcal{E}_{\sigma_\pm,+}(0,\omega)e^{ik_0 z} + \mathcal{E}_{\sigma_\pm,-}(0,\omega)e^{-ik_0 z}\right)e^{iqz}. \tag{3.15}$$

In general by Bloch's theorem, equation (3.15) should have been a product of a periodic function and the factor e^{iqz}, where q is the Bloch vector. In equation (3.15) we have effectively written the periodic function as a Fourier series and kept only the ± 1 terms, which were then identified with the components $\mathcal{E}_{\sigma_\pm,+}$ and $\mathcal{E}_{\sigma_\pm,-}$ at $z = 0$. Removing higher order modes is justified, since we are interested in the dynamics, for which $|k_0| = |\omega_0/c| \gg |q|$. Effectively, after applying the derivative $\partial/\partial z$ in equations (3.14), the higher order modes will have an energy difference that is multiple of ck_0, which corresponds to a multiple of the optical frequency of the atomic transition.

On the other hand, the frequency ω in equations (3.14) is relative to the carrier frequency ω_0 and is assumed to fulfill $|\omega/c| \ll |q|$, i.e. within the narrow frequency

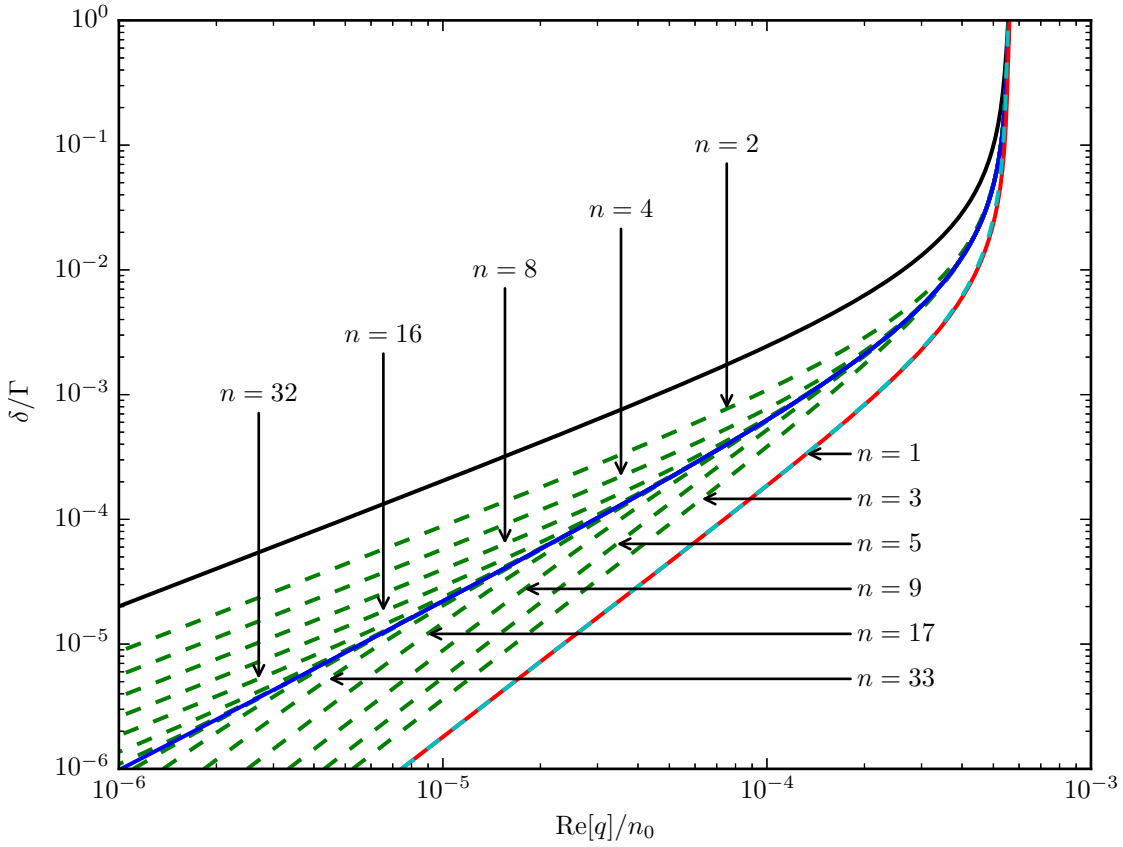

Figure 3.2: Log-log plot of the dispersion relations for the different setups. The upper solid black curve is for EIT (see equation (3.29)). The lower solid red curve is the quadratic dispersion relation for the dual-V setup (or the secular approximation for the Λ-type scheme) given by equation (3.23). The dashed green curves are the dispersion relations for the truncations of equations (3.33) with increasing number of the Fourier components of σ_{ab} and σ_{ac}. The dispersion relations for small $\mathrm{Re}[q]/n_0$ alternate between linear and quadratic depending on the truncation. The solid blue curve is the analytical limit of these dispersion relations given by equation (3.48). The lower dashed cyan curve is for the dual-color scheme with $\Delta_\mathrm{d}/\Gamma = 1$. It overlaps the quadratic dual-V curve, so that the difference is not visible. The common parameters for all the curves are $\Gamma_{1\mathrm{D}}/\Gamma = 0.1$, $\Delta_\mathrm{c}/\Gamma = -90$, and $\Omega_0/\Gamma = 1$. The curves are obtained by using a real δ, calculating complex q and then plotting δ/Γ as a function of $\mathrm{Re}[q]/n_0$. The alternative approach: using real q, calculating complex δ and then plotting $\mathrm{Re}[\delta]/\Gamma$ as a function of q/n_0 will produce results that are indistinguishable for this parameter regime (big Δ_c/Γ and $\Delta_\mathrm{d}/|\delta_\mathrm{S}|$). For all the dispersion relations we pick the branches such that $\mathrm{Re}[q]/n_0 > 0$.

range of interest, the stationary light dispersion is the dominant contribution to the dispersion relation, and the vacuum dispersion relation can be neglected. Therefore, we remove the terms $\omega/(cn_0)$ in the following.

The form of equation (3.15) implies that we should insert

$$\mathcal{E}_{\sigma_\pm,\pm}(z,\omega) = \mathcal{E}_{\sigma_\pm,\pm}(0,\omega)e^{iqz}, \tag{3.16}$$

into equations (3.14a) and

$$\mathcal{E}_{\sigma_\pm,\mp}(z,\omega) = \mathcal{E}_{\sigma_\pm,\mp}(0,\omega)e^{iqz}, \tag{3.17}$$

into equations (3.14b). After removing terms with rapid spatial variation, this gives

$$\pm\frac{q}{n_0}\mathcal{E}_{\sigma_\pm,\pm} = -\frac{\Gamma_{1D}}{2\tilde{\Delta}}\left[\frac{\delta-\delta_S/2}{\delta-\delta_S}\mathcal{E}_{\sigma_\pm,\pm} + \frac{\delta_S/2}{\delta-\delta_S}\mathcal{E}_{\sigma_\mp,\mp}\right], \tag{3.18a}$$

$$\mp\frac{q}{n_0}\mathcal{E}_{\sigma_\pm,\mp} = -\frac{\Gamma_{1D}}{2\tilde{\Delta}}\frac{\delta-\delta_S/2}{\delta-\delta_S}\mathcal{E}_{\sigma_\pm,\mp}. \tag{3.18b}$$

The equations above describe coupling between the different electric field modes. We first solve for the field modes moving in the opposite direction compared to the classical fields of the same polarization ($\mathcal{E}_{\sigma_\pm,\mp}$). Due to momentum conservation (or equivalently the lack of mode matching), these do not couple to any other field modes. As a consequence, we essentially have two separate Λ-systems. One of them involves the states $|a\rangle$, $|b_+\rangle$, and $|c\rangle$, which are coupled by the fields $\mathcal{E}_{\sigma_+,-}$ and Ω_+. The other one involves the states $|a\rangle$, $|b_-\rangle$, and $|c\rangle$, which are coupled by the fields $\mathcal{E}_{\sigma_-,+}$ and Ω_-. From equations (3.18b) we immediately find the dispersion relations

$$\frac{q}{n_0} = \pm\frac{\Gamma_{1D}}{2\tilde{\Delta}}\frac{\delta-\delta_S/2}{\delta-\delta_S}. \tag{3.19}$$

Solving these equations for δ and expanding for small q/n_0 gives

$$\delta \approx \frac{\delta_S}{2} \mp \frac{|\Omega_0|^2}{2\Gamma_{1D}}\frac{q}{n_0}. \tag{3.20}$$

This is the regular EIT dispersion relation (c.f. equations (3.29) and (3.30) below) only shifted by the AC Stark shift of the classical drive not participating in the EIT (since it is only shifted by one of the fields, the shift is $\delta_S/2$).

The quadratic dispersion relation is obtained from equations (3.18a). Here, the forward and backward propagation are coupled and can be written in matrix form as

$$\begin{pmatrix} \alpha_1 + \frac{q}{n_0} & \alpha_2 \\ \alpha_2 & \alpha_1 - \frac{q}{n_0} \end{pmatrix}\begin{pmatrix} \mathcal{E}_{\sigma_+,+} \\ \mathcal{E}_{\sigma_-,-} \end{pmatrix} = \begin{pmatrix} 0 \\ 0 \end{pmatrix} \tag{3.21}$$

with

$$\alpha_1 = \left(\frac{\Gamma_{1D}}{2\tilde{\Delta}}\right)\frac{\delta-\delta_S/2}{\delta-\delta_S}, \quad \alpha_2 = \left(\frac{\Gamma_{1D}}{2\tilde{\Delta}}\right)\frac{\delta_S/2}{\delta-\delta_S}. \tag{3.22}$$

In order for equation (3.21) to have non-trivial solutions, the determinant of the matrix on the left hand side has to be zero. This produces the equation

$$\left(\frac{q}{n_0}\right)^2 = \left(\frac{\Gamma_{1D}}{2\tilde{\Delta}}\right)^2 \frac{\delta}{\delta - \delta_S}, \tag{3.23}$$

which determines the dispersion relation. Solving equation (3.23) for δ, and expanding the solution for small q/n_0, we get the quadratic dispersion relation

$$\delta \approx \frac{1}{2m}\left(\frac{q}{n_0}\right)^2 \tag{3.24}$$

with the effective mass

$$m = -\frac{\Gamma_{1D}^2}{4(\Delta_c + i\Gamma'/2)|\Omega_0|^2}. \tag{3.25}$$

The quadratic dispersion relation (3.24) is the same as for the original stationary light in hot Λ-type atoms [60, 61] (see below for a discussion of the connection between cold dual-V and hot Λ-type schemes). We plot the full dispersion relation given by equation (3.23) in figure 3.2 as the solid red curve.

Having gone through the derivation, we now return to highlight some important parts, which will be of relevance later. We note that when solving the atomic equations (equations (3.9)), the full spatial dependence of the field was included, i.e. no attempt was made to remove fast-varying terms at this level. Such a procedure was only made after substituting the atomic solutions into the Fourier transforms of the field equations (3.6). We will show below, that for the cold Λ-type atoms, it is very important, at which point and how the removal of the fast-varying terms is performed.

3.3.2 Dispersion relations for cold Λ-type atoms

We now turn to the Λ-type scheme shown in figure 3.1(b). The atoms have fewer energy levels than in the dual-V scheme, but the dynamics in the case of cold atoms is complicated by presence of higher order Fourier components of the atomic coherence [69–74]. The dispersion relation for the cold Λ-type scheme, that effectively sums all the Fourier components to the infinite order, has been found in Ref. [68]. However, the result in Ref. [68] does not provide much intuition about the underlying physics. Here, we will do a different derivation that explicitly tracks the different Fourier components of the atomic coherence. This will illustrate the differences from the dual-V scheme and lead to the discussion of the "secular approximation" for the Λ-type scheme, which makes the two schemes equivalent. This derivation will also serve as a connection between the continuum and discrete models of the Λ-type scheme. In short, the different truncations of the infinite set of Fourier components that we will discuss in the continuum model can physically be implemented by positioning the atoms in the discrete model the certain way (see section 3.4.5). For completeness, we will also do a second derivation of the

dispersion relation for the Λ-type scheme that is more similar to Ref. [68], but with more focus on the off-resonant regime ($\Delta_c \neq 0$, $\delta \neq 0$).

Compared to the dual-V scheme, the Λ-type atoms have only one excited state $|b\rangle$, and there is only one polarization mode for both the quantum and the classical fields. The quantum field has detuning Δ_0 from the $|a\rangle \leftrightarrow |b\rangle$ transition, and the classical drive has detuning Δ_c from the $|b\rangle \leftrightarrow |c\rangle$ transition. The operator for the total quantum field $\hat{\mathcal{E}}$ can be decomposed as $\hat{\mathcal{E}} = \hat{\mathcal{E}}_+ e^{ik_0 z} + \hat{\mathcal{E}}_- e^{-ik_0 z}$, where $\hat{\mathcal{E}}_\pm$ are the spatially slowly-varying components. The classical drive is given by the sum of the two parts moving in both directions, $\Omega(z) = \Omega_0 \cos(k_0 z)$ (assuming $k_c \approx k_0$). Similar to the dual-V scheme and using the definitions above, the Hamiltonian is $\hat{H}_3 = \hat{H}_{3,a} + \hat{H}_{3,i} + \hat{H}_{3,p}$ (sum of the atomic, interaction, and photonic parts), where

$$\hat{H}_{3,a} = -\hbar n_0 \int \left[\tilde{\Delta}_0 \hat{\sigma}_{bb}(z) + \delta_0 \hat{\sigma}_{cc}(z)\right] \mathrm{d}z \tag{3.26a}$$

$$\hat{H}_{3,i} = -\hbar n_0 \int \left\{ \left[\hat{\sigma}_{bc}(z)\Omega(z) + \text{H.c.}\right] + g\sqrt{2\pi} \left[\hat{\sigma}_{ba}(z)\hat{\mathcal{E}}(z) + \text{H.c.}\right] \right\} \mathrm{d}z \tag{3.26b}$$

$$\hat{H}_{3,p} = -i\hbar c \int \left[\hat{\mathcal{E}}_+^\dagger(z) \frac{\partial \hat{\mathcal{E}}_+(z)}{\partial z} - \hat{\mathcal{E}}_-^\dagger(z) \frac{\partial \hat{\mathcal{E}}_-(z)}{\partial z}\right] \mathrm{d}z. \tag{3.26c}$$

With this Hamiltonian, the Heisenberg equations of motion for the electric field operators and the atomic operators are given by

$$\left(\frac{\partial}{\partial t} \pm c\frac{\partial}{\partial z}\right) \mathcal{E}_\pm = ig\sqrt{2\pi} n_0 \sigma_{ab} e^{\mp ik_0 z}, \tag{3.27}$$

and

$$\frac{\partial \sigma_{ab}}{\partial t} = i\tilde{\Delta}_0 \sigma_{ab} + i\Omega\sigma_{ac} + ig\sqrt{2\pi}\mathcal{E}, \tag{3.28a}$$

$$\frac{\partial \sigma_{ac}}{\partial t} = i\delta_0 \sigma_{ac} + i\Omega^* \sigma_{ab}. \tag{3.28b}$$

If Ω were independent of position ($\Omega(z) = \Omega_0$), equations (3.28) would describe the usual EIT system, which can be shown to have the dispersion relation

$$\frac{q}{n_0} = \pm \frac{\Gamma_{1D}}{2\tilde{\Delta}} \frac{\delta}{\delta - 2\delta_S}, \tag{3.29}$$

or for small q/n_0,

$$\delta \approx \pm \frac{2|\Omega_0|^2}{\Gamma_{1D}} \frac{q}{n_0}. \tag{3.30}$$

We note that for the Λ-type scheme, δ_S has a different meaning. For EIT with $\Omega(z) = \Omega_0$, it is a half of the AC Stark shift induced by the field. For $\Omega(z) = \Omega_0 \cos(k_0 z)$ below, it

is the average of the AC Stark shift. Also note that the group velocity (factor in front of q) in equation (3.30) differs by a factor of 4 from the group velocity in equation (3.20). This difference arises from the fact that the strength of the field participating in the EIT in that case is given by $\Omega_\pm = \Omega_0/2$.

We now calculate the dispersion relation for the case when Ω is a standing wave ($\Omega(z) = \Omega_0 \cos(k_0 z)$). The Fourier transform in time of equations (3.28) gives

$$0 = i\tilde{\Delta}\sigma_{ab} + i\Omega\sigma_{ac} + ig\sqrt{2\pi}\mathcal{E}, \tag{3.31a}$$

$$0 = i\delta\sigma_{ac} + i\Omega^*\sigma_{ab}, \tag{3.31b}$$

where, as before, we have absorbed the Fourier frequency variable ω into the detunings by defining $\tilde{\Delta} = \tilde{\Delta}_0 + \omega$ and $\delta = \delta_0 + \omega$.

By Bloch's theorem, σ_{ab}, σ_{ac} and $\mathcal{E}$ need to be periodic functions in space multiplied by the factor e^{iqz}, with q being the Bloch vector. The periodic parts have the same periodicity as $\Omega(z)$, and we write each one of them as a Fourier series

$$\sigma_{ab}(z,\omega) = \sum_{n=-\infty}^{\infty} \sigma_{ab}^{(n)}(\omega) e^{ink_0 z} e^{iqz}, \tag{3.32a}$$

$$\sigma_{ac}(z,\omega) = \sum_{n=-\infty}^{\infty} \sigma_{ac}^{(n)}(\omega) e^{ink_0 z} e^{iqz}, \tag{3.32b}$$

$$\mathcal{E}(z,\omega) = \left(\mathcal{E}_+(0,\omega)e^{ik_0 z} + \mathcal{E}_-(0,\omega)e^{-ik_0 z}\right) e^{iqz}, \tag{3.32c}$$

where we have kept only the lowest order terms in the Fourier series for the field, similar to equation (3.15).

After inserting equations (3.32a) and (3.32b) into equations (3.31) and collecting the terms with equal exponents of $ink_0 z$, we obtain an infinite set of coupled equations

$$0 = i\tilde{\Delta}\sigma_{ab}^{(n)} + i\frac{\Omega_0}{2}\left(\sigma_{ac}^{(n+1)} + \sigma_{ac}^{(n-1)}\right) + ig\sqrt{2\pi}\left(\mathcal{E}_+\delta_{n,1} + \mathcal{E}_-\delta_{n,-1}\right), \tag{3.33a}$$

$$0 = i\delta\sigma_{ac}^{(n)} + i\frac{\Omega_0^*}{2}\left(\sigma_{ab}^{(n+1)} + \sigma_{ab}^{(n-1)}\right), \tag{3.33b}$$

where $\delta_{j,j'}$ is the Kronecker delta.

From the above equations, we see the crucial difference between the dual-V scheme and the cold Λ-type scheme. In the dual-V scheme, described in equations (3.10), there are only two components of the atomic coherence for the excited states ($\sigma_{ab\pm}$). For the cold Λ-type atoms, by writing σ_{ab} as a Fourier series, we have obtained an infinite set of coupled components. This can be explained by the fact that a dual-V atom in state $|c\rangle$ can transition to state $|b_+\rangle$ (i.e. be excited) by absorbing a photon of the classical drive propagating in the positive direction, and can only transition back to state $|c\rangle$ (i.e. be de-excited) by emitting a photon in the same direction. On the other hand, a cold Λ-type atom in state $|c\rangle$ can transition to state $|b\rangle$ by a photon of the classical drive coming from one direction and transition back to state $|c\rangle$ by emitting a photon in the

opposite direction. This couples a Fourier component $\sigma_{ab}^{(n)}$ with a certain wave number n to components differing by two wave numbers, i.e. $\sigma_{ab}^{(n\pm2)}$ (through $\sigma_{ac}^{(n\pm1)}$), and leads to an infinite set of coupled equations.

To obtain any results from equations (3.33), truncation of the Fourier components of σ_{ab} and σ_{ac} is needed. The smallest non-trivial truncated set of equations involves $\sigma_{ab}^{(\pm1)}$ and $\sigma_{ac}^{(0)}$ and can be written

$$0 = i\tilde{\Delta}\sigma_{ab}^{(\pm1)} + i\frac{\Omega_0}{2}\sigma_{ac}^{(0)} + ig\sqrt{2\pi}\mathcal{E}_{\pm}, \tag{3.34a}$$

$$0 = i\delta\sigma_{ac}^{(0)} + i\frac{\Omega_0^*}{2}\left(\sigma_{ab}^{(+1)} + \sigma_{ab}^{(-1)}\right). \tag{3.34b}$$

This particular truncation is also known as the "secular approximation" in the literature [67, 70]. If we had approximated $\mathcal{E}_{\sigma_\pm}e^{\mp ik_0z} \approx \mathcal{E}_{\sigma_\pm,\pm}$ in equations (3.10) (which would not have changed the quadratic dispersion relation for the dual-V scheme), then equations (3.34) would have had exactly the same form as equations (3.10).

The equations for the electric field (3.27), in principle, contain all the Fourier components $\sigma_{ab}^{(n)}$, but, as for the dual-V scheme, we will make the approximation, where we remove terms with rapid spatial variation. This effectively means that we approximate $\sigma_{ab}e^{\mp ik_0z} \approx \sigma_{ab}^{(\pm1)}e^{iqz}$ in equations (3.27). Fourier transforming these equations, we end up with

$$\left(-i\omega \pm c\,\frac{\partial}{\partial z}\right)\mathcal{E}_{\pm} = ig\sqrt{2\pi}n_0\sigma_{ab}^{(\pm1)}e^{iqz}. \tag{3.35}$$

Proceeding as for the dual-V case, equations (3.34) and equations (3.35) together with the sought form of the Bloch solutions

$$\mathcal{E}_{\pm}(z,\omega) = \mathcal{E}_{\pm}(0,\omega)e^{iqz}, \tag{3.36}$$

which is similar to equations (3.16) and (3.17) for the dual-V scheme, result in the coupled equations for the fields

$$\begin{pmatrix} \alpha_1 + \frac{q}{n_0} & \alpha_2 \\ \alpha_2 & \alpha_1 - \frac{q}{n_0} \end{pmatrix}\begin{pmatrix} \mathcal{E}_+ \\ \mathcal{E}_- \end{pmatrix} = \begin{pmatrix} 0 \\ 0 \end{pmatrix}. \tag{3.37}$$

This is the same as equation (3.21) with the same α_1 and α_2 (but with different definitions of the electric fields). Hence, exactly the same quadratic dispersion relation (3.24) is obtained.

A completely different dispersion relation can be found by considering the next smallest truncated set of equations. That set additionally involves $\sigma_{ac}^{(\pm2)}$, so that the system of equations is

$$0 = i\tilde{\Delta}\sigma_{ab}^{(\pm1)} + i\frac{\Omega_0}{2}\left(\sigma_{ac}^{(0)} + \sigma_{ac}^{(\pm2)}\right) + ig\sqrt{2\pi}\mathcal{E}_{\pm}, \tag{3.38a}$$

$$0 = i\delta\sigma_{ac}^{(0)} + i\frac{\Omega_0^*}{2}\left(\sigma_{ab}^{(+1)} + \sigma_{ab}^{(-1)}\right), \tag{3.38b}$$

$$0 = i\delta\sigma_{ac}^{(\pm2)} + i\frac{\Omega_0^*}{2}\sigma_{ab}^{(\pm1)}. \tag{3.38c}$$

Following the same procedure as above, we get the dispersion relation

$$\left(\frac{q}{n_0}\right)^2 = \left(\frac{\Gamma_{1D}}{2\tilde{\Delta}}\right)^2 \frac{\delta^2}{(\delta - \delta_S/2)(\delta - 3\delta_S/2)}, \tag{3.39}$$

which for small q/n_0 can be approximated by

$$\delta \approx \pm \frac{\sqrt{3}|\Omega_0|^2}{2\Gamma_{1D}} \frac{q}{n_0}. \tag{3.40}$$

This dispersion relation is linear instead of quadratic. Comparing it with the dispersion relation for EIT (3.30), we observe that equation (3.40) only differs by a constant factor.

One could continue calculating dispersion relations for even higher order truncations. As the analytical calculations quickly become complicated, we only do it numerically, as described in appendix B. The resulting dispersion relations are shown in figure 3.2. We find that truncations which contain Fourier components up to and including $\sigma_{ab}^{(\pm n)}$ with odd n, result in a quadratic dispersion relation for small q/n_0. On the other hand, truncations that contain Fourier components up to and including $\sigma_{ac}^{(\pm n)}$ with even n, result in a linear dispersion relation for small q/n_0.

It is possible to find the limiting dispersion relation ($n \to \infty$) analytically [68]. To derive it, we will not use the Fourier series representation in equations (3.32a) and (3.32b), but instead solve equations (3.31) directly. Isolating σ_{ac} from equation (3.31b) and inserting in equation (3.31a) gives

$$\sigma_{ab}(z, \omega) = -\frac{g\sqrt{2\pi}}{\tilde{\Delta}} \gamma(k_0 z) \mathcal{E}(z, \omega), \tag{3.41}$$

where we have defined the dimensionless position dependent coupling parameter

$$\gamma(k_0 z) = \frac{1}{1 - (2\delta_S/\delta)\cos^2(k_0 z)}. \tag{3.42}$$

We then introduce the Fourier series of γ, i.e.

$$\gamma(k_0 z) = \sum_{\ell=-\infty}^{\infty} \gamma^{(\ell)} e^{2i\ell k_0 z}, \tag{3.43}$$

with

$$\gamma^{(\ell)} = \frac{1}{\pi} \int_{-\frac{\pi}{2}}^{\frac{\pi}{2}} \gamma(k_0 z) e^{-2i\ell k_0 z} \, \mathrm{d}(k_0 z) = {}_3\tilde{F}_2 \left[\left\{ \frac{1}{2}, 1, 1 \right\}, \{1 - \ell, 1 + \ell\}, (2\delta_S/\delta) \right], \tag{3.44}$$

where ${}_p\tilde{F}_q$ is the regularized generalized hypergeometric function. The terms with $\ell = 0$ and $\ell = \pm 1$ are

$$\gamma^{(0)} = \frac{1}{\sqrt{1 - (2\delta_S/\delta)}}, \tag{3.45a}$$

$$\gamma^{(\pm 1)} = -\frac{2\sqrt{1 - (2\delta_S/\delta)} + (2\delta_S/\delta) - 2}{(2\delta_S/\delta)\sqrt{1 - (2\delta_S/\delta)}}. \tag{3.45b}$$

Inserting equation (3.43) into equation (3.41) we can write

$$\sigma_{ab} = -\frac{g\sqrt{2\pi}}{\tilde{\Delta}} \sum_{\ell=-\infty}^{\infty} [\gamma^{(\ell)}\mathcal{E}_+ + \gamma^{(\ell+1)}\mathcal{E}_-]e^{i(2\ell+1)k_0 z}. \tag{3.46}$$

In equations (3.35), we only need the terms from equation (3.46) that have the factors $e^{\pm ik_0 z}$, i.e. the terms corresponding to $\ell = 0$ and $\ell = -1$. Inserting those terms into equations (3.35) and proceeding as for the previous calculations we get two coupled equations for the fields as in equations (3.37), but with the different α_1 and α_2:

$$\alpha_1 = \frac{\Gamma_{1D}}{2\tilde{\Delta}}\gamma^{(0)}, \quad \alpha_2 = \frac{\Gamma_{1D}}{2\tilde{\Delta}}\gamma^{(\pm 1)}. \tag{3.47}$$

Finally, we get the dispersion relation

$$\left(\frac{q}{n_0}\right)^2 = \left(\frac{\Gamma_{1D}}{2\tilde{\Delta}}\right)^2 \left(\frac{4\left(-1+\sqrt{1-(2\delta_S/\delta)}\right)^2}{\sqrt{1-(2\delta_S/\delta)}(2\delta_S/\delta)^2} \right) \tag{3.48}$$

which for small real q/n_0 can be approximated by

$$\delta \approx \frac{(-\Delta_c - i\Gamma'/2)^{1/3}|\Omega_0|^2}{\Gamma_{1D}^{4/3}} \left|\frac{q}{n_0}\right|^{4/3}, \tag{3.49}$$

where we have restricted the solution to the branch with $\mathrm{Re}[\delta]$ having the same sign as $-\Delta_c$ ($\Delta_c \neq 0$), and $(-\Delta_c - i\Gamma'/2)^{1/3}$ means third root of $-\Delta_c - i\Gamma'/2$ such that $\mathrm{Re}[(-\Delta_c - i\Gamma'/2)^{1/3}]$ has the same sign as $-\Delta_c$.

We see that for small q/n_0, the dispersion relation is neither quadratic, nor linear, but goes as $\delta \propto |q|^{4/3}$. The dispersion relation (3.48) is shown by the solid blue curve in figure 3.2. It is seen to lie in between the curves for the EIT and dual-V results and is the limiting case as we increase the number of Fourier components for the atomic coherence.

3.3.3 Dispersion relations for cold dual-color atoms

We now consider the dual-color scheme shown in figure 3.1(c). The dispersion for this scheme has been originally derived in Ref. [66] under the secular approximation. Using the secular approximation for this scheme makes the dual-color scheme equivalent to the dual-V scheme. However, in the analysis below, we want to illustrate the fact that the dynamics of the dual-color scheme can potentially be much more complex compared to the dual-V and Λ-type schemes.

The atomic level structure of the dual-color scheme is the same as for the Λ-type scheme, but the two counter-propagating classical drives are at two different frequencies instead of only one. The detuning Δ_c now has a different meaning—it is relative to

the mean of the two frequencies. Hence, if $\omega_{c\pm}$ are the frequencies of the two classical drives, then $\Delta_c = (\omega_{c+} + \omega_{c-})/2 - \omega_{bc}$. We also define the detuning $\Delta_d = |\omega_{c+} - \omega_{c-}|/2$, which measures how far the two frequencies are separated from each other. With the modified definition of Δ_c, the Hamiltonian is the same as for the Λ-type atom, i.e. it is given by equations (3.26), but with $\Omega(z,t) = \Omega_0 \cos(\Delta_d t + k_c z)$. The Heisenberg equations of motion are also the same as for the Λ-type scheme (equations (3.27) and equations (3.28)), just with the different definition of $\Omega(z,t)$.

Compared to the Λ-type scheme, the dual-color scheme has a time-dependent Hamiltonian, but since it is periodic in time, it allows us to use Floquet's theorem in addition to Bloch's theorem [76, 77]. According to the two theorems, σ_{ab}, σ_{ac} and $\mathcal{E}$ need to be periodic functions in space and time multiplied by the factor $e^{iqz - i\omega_q t}$, with q being the Bloch vector, and ω_q being the Floquet quasi-energy divided by $\hbar$. The periodic parts have the same periodicity as $\Omega(z,t)$, and we write each one of them as a Fourier series

$$\sigma_{ab}(z,t) = \sum_{n_1=-\infty}^{\infty} \sum_{n_2=-\infty}^{\infty} \sigma_{ab}^{(n_1,n_2)} e^{in_1 k_0 z} e^{in_2 \Delta_d t} e^{iqz - i\omega_q t}, \tag{3.50a}$$

$$\sigma_{ac}(z,t) = \sum_{n_1=-\infty}^{\infty} \sum_{n_2=-\infty}^{\infty} \sigma_{ac}^{(n_1,n_2)} e^{in_1 k_0 z} e^{in_2 \Delta_d t} e^{iqz - i\omega_q t}, \tag{3.50b}$$

$$\mathcal{E}(z,t) = \left(\mathcal{E}_+(0,0) e^{ik_0 z + i\Delta_d t} + \mathcal{E}_-(0,0) e^{-ik_0 z - i\Delta_d t}\right) e^{iqz - i\omega_q t}, \tag{3.50c}$$

where we have kept only two terms in the Fourier series for the electric field and removed all other terms. The justification for removing the terms with $e^{\mp ik_0 z \pm i\Delta_d t}$ is that we expect them to only add separate linear dispersion bands, similar to the linear bands for $\mathcal{E}_{\sigma_\pm,\mp}$ for the dual-V scheme. Also, we have not included other $n\Delta_d$ terms except the ones for $n = \pm 1$, since the other terms will not contribute to the dynamics for $\Delta_d \gg |\delta_S|$.

Inserting equations (3.50) into equations (3.28), and collecting terms of equal exponents gives

$$0 = i(\tilde{\Delta} - n\Delta_d)\sigma_{ab}^{(n)} + i\frac{\Omega_0}{2}\left(\sigma_{ac}^{(n+1)} + \sigma_{ac}^{(n-1)}\right) + ig\sqrt{2\pi}\left(\mathcal{E}_+ \delta_{n,1} + \mathcal{E}_- \delta_{n,-1}\right), \tag{3.51a}$$

$$0 = i(\delta - n\Delta_d)\sigma_{ac}^{(n)} + i\frac{\Omega_0^*}{2}\left(\sigma_{ab}^{(n+1)} + \sigma_{ab}^{(n-1)}\right), \tag{3.51b}$$

where by $\sigma_{ab}^{(n)}$ and $\sigma_{ac}^{(n)}$ we mean $\sigma_{ab}^{(n,n)}$ and $\sigma_{ac}^{(n,n)}$ respectively. The absence of $\sigma_{ab}^{(n_1,n_2)}$ and $\sigma_{ac}^{(n_1,n_2)}$ for $n_1 \neq n_2$ in this system of equations is a consequence of the classical drive only coupling the Fourier terms to the ones with both an increased (decreased) wave vector and increased (decreased) detuning, combined with only considering the lowest order quantum field components in equation (3.50c). We have absorbed ω_q into the detunings by defining $\tilde{\Delta} = \tilde{\Delta}_0 + \omega_q$ and $\delta = \delta_0 + \omega_q$. The only but important difference from equations (3.33) is that the frequencies of the different Fourier components are shifted by $n\Delta_d$ in equations (3.51). The result of this difference is that the higher order Fourier components of the atomic coherence contribute little for $\Delta_d \gg |\delta_S|$ and therefore can be neglected, thus giving the same effect as in the secular approximation. Hence, the

dispersion relation will be the same as the quadratic dispersion relation of the dual-V scheme. We verify numerically (see figure 3.2 and appendix B) that this is the case for $\Delta_{\mathrm{d}}/\Gamma = 1$ and $|\delta_{\mathrm{S}}|/\Gamma \approx 10^{-2}$.

The summary of the discussion in section 3.3.2 is that the reason for the difference in the dispersion relation between dual-V and the cold Λ-type schemes is that the cold Λ-type scheme allows excitations and de-excitations by the classical fields from different directions, whereas the dual-V does not due to separation of the different directions into different polarization modes. For the dual-color scheme, such mismatched excitations and de-excitations are suppressed by the frequency difference between the right-moving and left-moving fields.

3.3.4 Dispersion relations for hot Λ-type atoms

Stationary light was first considered for hot Λ-type atoms, where a quadratic dispersion relation was predicted [60, 61]. For completeness, we will briefly discuss how this result arises from the results of the dual-color scheme [74]. The main difference between the cold atoms and the hot atoms is that the latter ones move and hence have an associated Doppler shift in the transition frequency. In the one-dimensional approximation this amounts to having the right propagating fields being shifted by ω_{D}, and the left propagating fields being shifted by $-\omega_{\mathrm{D}}$, where ω_{D} is the Doppler shift that is determined by the velocity of the atoms. For each individual velocity class with the same ω_{D}, the dynamics will be completely equivalent to the dual-color setup, where instead of Δ_{d} we now have ω_{D}. That is, the system is described by equations (3.27) and equations (3.28) with $\Omega(z,t) = \Omega_0 \cos(\omega_{\mathrm{D}} t + k_{\mathrm{c}} z)$. Hence, for $\omega_{\mathrm{D}} \gg |\delta_{\mathrm{S}}|$, the quadratic dispersion relation is valid. If the width of the distribution of ω_{D} is much bigger than $|\delta_{\mathrm{S}}|$, then the contribution of the velocity classes, where $\omega_{\mathrm{D}} \gg |\delta_{\mathrm{S}}|$ is not fulfilled, is small, and the quadratic dispersion relation (3.24) should be true for the ensemble as a whole.

In the original derivations of stationary light [60, 61] the dispersion relation was obtained by arguing that the thermal motion of the atoms washes out any spatial coherences with Fourier components $|n| \geq 2$. This argument is essentially equivalent to the Doppler shift argument above, except that it is formulated in time rather than frequency. As originally noted in Ref. [67] the level structure of the dual-V scheme does not allow these higher order Fourier components. Hence, the dispersion relation (3.24) originally derived for hot Λ-type atoms also applies for the dual-V system regardless of the temperature.

3.4 Discrete model

3.4.1 Scattering matrix for Λ-type atoms

To support some of the conclusions reached above and to provide additional possibilities for how the dispersion relation can be controlled, we will now consider a model where we account for the individual atoms instead of using the continuum model. The discrete model will use the (multi-mode) transfer matrix formalism, which we will discuss in detail

below. In this and the following sections we will first derive the scattering coefficients for the Λ-type and dual-V atoms respectively, which is the necessary first step in applying the transfer matrix formalism.

The derivation of the scattering matrix (i.e. the reflection and transmission coefficients) for a Λ-type atom (see figure 3.1(b)) is based on Ref. [65]. The electric field is given by the operator

$$\hat{\mathcal{E}}(z) = \hat{\mathcal{E}}_+(z)e^{ik_0(z-z_j)} + \hat{\mathcal{E}}_-(z)e^{-ik_0(z-z_j)}. \tag{3.52}$$

Compared to the continuum model, we have shifted the spatial phases such that they vanish at the position of the atom z_j (j is the index of the atom). The effects of the propagation phases will be accounted for separately by the transfer matrices of free propagation.

The Hamiltonian (3.26), which we have used for the continuum model, can also be used to describe a single Λ-type atom, since the discrete nature of the atoms is still present due to the definition of the atomic operators given by equation (3.1). Because of considering only a single atom, equation (3.1) becomes $\hat{\sigma}_{\alpha\beta}(z) = \frac{1}{n_0}\delta(z - z_j)\hat{\sigma}_{\alpha\beta,j}$, and inserting this into equations (3.26) results in

$$\hat{H}_{3,\mathrm{a}} = -\hbar\left[\tilde{\Delta}_0\hat{\sigma}_{bb,j} + \delta_0\hat{\sigma}_{cc,j}\right], \tag{3.53a}$$

$$\hat{H}_{3,\mathrm{i}} = -\hbar\left[\hat{\sigma}_{bc,j}\Omega(z_j) + \mathrm{H.c.}\right] - \hbar g\sqrt{2\pi}\left[\hat{\sigma}_{ba,j}\hat{\mathcal{E}}(z_j) + \mathrm{H.c.}\right], \tag{3.53b}$$

$$\hat{H}_{3,\mathrm{p}} = -i\hbar c\int\left[\hat{\mathcal{E}}_+^\dagger(z)\,\frac{\partial\hat{\mathcal{E}}_+(z)}{\partial z} - \hat{\mathcal{E}}_-^\dagger(z)\,\frac{\partial\hat{\mathcal{E}}_-(z)}{\partial z}\right]\mathrm{d}z. \tag{3.53c}$$

From the Hamiltonian, we get the Heisenberg equations for the atom

$$\frac{\partial\sigma_{ab,j}}{\partial t} = i\tilde{\Delta}_0\sigma_{ab,j} + i\Omega(z_j)\sigma_{ac,j} + ig\sqrt{2\pi}\mathcal{E}(z_j,t), \tag{3.54a}$$

$$\frac{\partial\sigma_{ac,j}}{\partial t} = i\delta_0\sigma_{ac,j} + i\Omega^*(z_j)\sigma_{ab,j}. \tag{3.54b}$$

These equations are similar to equations (3.28), except that here we do not make the continuum approximation.

For the electric field we have the equations

$$\left(\frac{\partial}{\partial t} \pm c\,\frac{\partial}{\partial z}\right)\mathcal{E}_\pm(z,t) = ig\sqrt{2\pi}\delta(z - z_j)\sigma_{ab,j}, \tag{3.55}$$

which are exactly the same as equations (3.27) due the definition (3.1). In this form, however, we can formally solve them [21], so that we obtain

$$\mathcal{E}_\pm(z,t) = \mathcal{E}_{\pm,\mathrm{in}}(z \mp ct) + \frac{ig\sqrt{2\pi}}{c}\theta\big(\pm(z - z_j)\big)\,\sigma_{ab,j}\left(t \mp \frac{z - z_j}{c}\right), \tag{3.56}$$

where $\mathcal{E}_{\pm,\mathrm{in}}(z \pm ct)$ are the input fields, and θ is the Heaviside theta function.

Since the scattering problem is symmetric, and since the equations are linear, we can gain full information about the scattering by setting $\mathcal{E}_{+,\mathrm{in}}(z-ct) = 1$ and $\mathcal{E}_{-,\mathrm{in}}(z+ct) = 0$ in equations (3.56). Then we find the total electric field (3.52) to be

$$\mathcal{E}(z_j, t) = 1 + \frac{ig\sqrt{2\pi}}{c}\sigma_{ab,j}\,(t) \tag{3.57}$$

Upon inserting this expression into (3.54a), we obtain

$$\frac{\partial \sigma_{ab,j}}{\partial t} = i\left(\tilde{\Delta}_0 + i\frac{\Gamma_{1\mathrm{D}}}{2}\right)\sigma_{ab,j} + i\Omega(z_j)\sigma_{ac,j} + ig\sqrt{2\pi}. \tag{3.58}$$

After Fourier transforming equations (3.56) we get the reflection and transmission coefficients

$$r_j = \mathcal{E}_-(z_j^-, \omega) = \frac{ig\sqrt{2\pi}}{c}\sigma_{ab,j}(\omega), \tag{3.59a}$$

$$t_j = \mathcal{E}_+(z_j^+, \omega) = 1 + r_j, \tag{3.59b}$$

where $z_j^+ = z_j + \epsilon$ and $z_j^- = z_j - \epsilon$ in the limit $\epsilon \to 0$. This limit expresses the fact that the atoms are assumed to be point scatterers with no spatial extent.

We also Fourier transform equation (3.54b) and equation (3.58) and get

$$0 = i\left(\tilde{\Delta} + i\frac{\Gamma_{1\mathrm{D}}}{2}\right)\sigma_{ab,j} + i\Omega(z_j)\sigma_{ac,j} + ig\sqrt{2\pi}, \tag{3.60a}$$

$$0 = i\delta\sigma_{ac,j} + i\Omega^*(z_j)\sigma_{ab,j}, \tag{3.60b}$$

where, as before, we have absorbed the Fourier frequency variable ω into the detunings by defining $\tilde{\Delta} = \tilde{\Delta}_0 + \omega$ and $\delta = \delta_0 + \omega$.

Now we solve equations (3.59) and (3.60) and find

$$r_j = -\frac{i(\Gamma_{1\mathrm{D}}/2)\delta}{(\tilde{\Delta} + i\Gamma_{1\mathrm{D}}/2)\delta - |\Omega(z_j)|^2}, \tag{3.61a}$$

$$t_j = \frac{\tilde{\Delta}\delta - |\Omega(z_j)|^2}{(\tilde{\Delta} + i\Gamma_{1\mathrm{D}}/2)\delta - |\Omega(z_j)|^2}. \tag{3.61b}$$

Below, transfer matrices will be written in terms a single parameter β_j, which in this case is

$$\beta_j = -\frac{r_j}{t_j} = \frac{i(\Gamma_{1\mathrm{D}}/2)\delta}{\tilde{\Delta}\delta - |\Omega(z_j)|^2}. \tag{3.62}$$

3.4.2 Scattering matrix for the dual-V atoms.

The derivation of the scattering matrix for the dual-V atoms proceeds in a similar manner as the derivation for the Λ-type atoms in section 3.4.1. Similar to equation (3.52) we define the electric field operators

$$\hat{\mathcal{E}}_{\sigma_\pm}(z) = \hat{\mathcal{E}}_{\sigma_\pm,+}(z)e^{ik_0(z-z_j)} + \hat{\mathcal{E}}_{\sigma_\pm,-}(z)e^{-ik_0(z-z_j)}. \tag{3.63}$$

The Hamiltonian for a single dual-V atom interacting with light is given by equations (3.5) with the atomic operators $\hat{\sigma}_{\alpha\beta}(z) = \frac{1}{n_0}\delta(z - z_j)\hat{\sigma}_{\alpha\beta,j}$ (special case of the definition (3.1)). Therefore, equations (3.5) can be written

$$\hat{H}_{\mathrm{V,a}} = -\hbar \left[\sum_{\alpha\in\{+,-\}} \tilde{\Delta}_0^{(\alpha)} \hat{\sigma}_{b_\alpha b_\alpha,j} + \delta_0 \hat{\sigma}_{cc,j} \right], \tag{3.64a}$$

$$\hat{H}_{\mathrm{V,i}} = -\hbar \sum_{\alpha\in\{+,-\}} \left\{ \left[\hat{\sigma}_{b_\alpha c,j} \Omega_\alpha e^{\alpha i k_\mathrm{c} z_j} + \mathrm{H.c.} \right] + g\sqrt{2\pi} \left[\hat{\sigma}_{b_\alpha a,j} \hat{\mathcal{E}}_{\sigma_\alpha}(z_j) + \mathrm{H.c.} \right] \right\}, \tag{3.64b}$$

$$\hat{H}_{\mathrm{V,p}} = -i\hbar c \int \sum_{\alpha\in\{+,-\}} \left[\hat{\mathcal{E}}^\dagger_{\sigma_\alpha,+}(z) \frac{\partial \hat{\mathcal{E}}_{\sigma_\alpha,+}(z)}{\partial z} - \hat{\mathcal{E}}^\dagger_{\sigma_\alpha,-}(z) \frac{\partial \hat{\mathcal{E}}_{\sigma_\alpha,-}(z)}{\partial z} \right] \mathrm{d}z. \tag{3.64c}$$

From the Hamiltonian, the equations for the atom are

$$\frac{\partial \sigma_{ab_\pm,j}}{\partial t} = i\tilde{\Delta}_0^{(\pm)} \sigma_{ab_\pm,j} + i\Omega_\pm \sigma_{ac,j} e^{\pm i k_\mathrm{c} z_j} + ig\sqrt{2\pi} \mathcal{E}_{\sigma_\pm}(z_j, t), \tag{3.65a}$$

$$\frac{\partial \sigma_{ac,j}}{\partial t} = i\delta_0 \sigma_{ac,j} + i\Omega_+^* \sigma_{ab_+,j} e^{-i k_\mathrm{c} z_j} + i\Omega_-^* \sigma_{ab_-,j} e^{i k_\mathrm{c} z_j}. \tag{3.65b}$$

The formal solutions to the equations for the field are

$$\mathcal{E}_{\sigma_+,\pm}(z,t) = \mathcal{E}_{\sigma_+,\pm,\mathrm{in}}(z \mp ct) + \frac{ig\sqrt{2\pi}}{c} \theta\big(\pm(z - z_j)\big)\, \sigma_{ab_+,j}\left(t \mp \frac{z - z_j}{c} \right), \tag{3.66a}$$

$$\mathcal{E}_{\sigma_-,\pm}(z,t) = \mathcal{E}_{\sigma_-,\pm,\mathrm{in}}(z \mp ct) + \frac{ig\sqrt{2\pi}}{c} \theta\big(\pm(z - z_j)\big)\, \sigma_{ab_-,j}\left(t \mp \frac{z - z_j}{c} \right). \tag{3.66b}$$

Because of the symmetry of the system, we only need to consider two cases: $\mathcal{E}_{\sigma_+,+,\mathrm{in}}(z_j - ct) = 1$ with the rest of the input fields being zero, and $\mathcal{E}_{\sigma_-,+,\mathrm{in}}(z_j - ct) = 1$ with the rest of the input fields being zero.

Starting with the first case ($\mathcal{E}_{\sigma_+,+,\mathrm{in}}(z_j - ct) = 1$) and Fourier transforming, equations (3.65) become

$$0 = i\tilde{\Delta}_{\mathrm{tot}}^{(+)} \sigma_{ab_+,j} + i\Omega_+ \sigma_{ac,j} e^{i k_\mathrm{c} z_j} + ig\sqrt{2\pi}, \tag{3.67a}$$

$$0 = i\tilde{\Delta}_{\mathrm{tot}}^{(-)} \sigma_{ab_-,j} + i\Omega_- \sigma_{ac,j} e^{-i k_\mathrm{c} z_j}, \tag{3.67b}$$

$$0 = i\delta \sigma_{ac,j} + i\Omega_+^* \sigma_{ab_+,j} e^{-i k_\mathrm{c} z_j} + i\Omega_-^* \sigma_{ab_-,j} e^{i k_\mathrm{c} z_j}, \tag{3.67c}$$

with $\tilde{\Delta}_{\mathrm{tot}}^{(\pm)} = \tilde{\Delta}_0^{(\pm)} + i(\Gamma_{1\mathrm{D}}/2) + \omega$ defined for notational convenience, such that we have now absorbed the total decay rate $\Gamma = \Gamma' + \Gamma_{1\mathrm{D}}$ into $\tilde{\Delta}_{\mathrm{tot}}^{(\pm)}$; and $\delta = \delta_0 + \omega$. From equations (3.66) we have the relations

$$r_{j,++} = \mathcal{E}_{\sigma_+,-}(z_j^-, \omega) = \frac{ig\sqrt{2\pi}}{c} \sigma_{ab_+,j}(\omega), \tag{3.68a}$$

$$t_{j,++} = \mathcal{E}_{\sigma_+,+}(z_j^+,\omega) = 1 + r_{j,++}, \tag{3.68b}$$

$$r_{j,+-} = \mathcal{E}_{\sigma_-,-}(z_j^-,\omega) = \frac{ig\sqrt{2\pi}}{c}\sigma_{ab_-,j}(\omega), \tag{3.68c}$$

$$t_{j,+-} = \mathcal{E}_{\sigma_-,+}(z_j^+,\omega) = r_{j,+-}. \tag{3.68d}$$

After solving equations (3.67) and (3.68) (with $k_c \approx k_0$) we get

$$r_{j,++} = -\frac{i(\Gamma_{1D}/2)\left(\tilde{\Delta}_{tot}^{(-)}\delta - |\Omega_-|^2\right)}{\tilde{\Delta}_{tot}^{(+)}\tilde{\Delta}_{tot}^{(-)}\delta - \tilde{\Delta}_{tot}^{(+)}|\Omega_-|^2 - \tilde{\Delta}_{tot}^{(-)}|\Omega_+|^2}, \tag{3.69a}$$

$$t_{j,++} = 1 + r_{j,++}, \tag{3.69b}$$

$$r_{j,+-} = t_{j,+-} = \frac{\Omega_-\Omega_+^* e^{-2ik_0 z_j}}{\tilde{\Delta}_{tot}^{(-)}\delta - |\Omega_-|^2} r_{j,++}. \tag{3.69c}$$

For the second case ($\mathcal{E}_{\sigma_-,+,in}(z_j - ct) = 1$), instead of equations (3.67) we have

$$0 = i\tilde{\Delta}_{tot}^{(+)}\sigma_{ab_+,j} + i\Omega_+\sigma_{ac,j}e^{ik_c z_j}, \tag{3.70a}$$

$$0 = i\tilde{\Delta}_{tot}^{(-)}\sigma_{ab_-,j} + i\Omega_-\sigma_{ac,j}e^{-ik_c z_j} + ig\sqrt{2\pi}, \tag{3.70b}$$

$$0 = i\delta\sigma_{ac,j} + i\Omega_+^*\sigma_{ab_+,j}e^{-ik_c z_j} + i\Omega_-^*\sigma_{ab_-,j}e^{ik_c z_j}. \tag{3.70c}$$

Instead of equations (3.69) we have

$$r_{j,--} = \mathcal{E}_{\sigma_-,-}(z_j^-,\omega) = \frac{ig\sqrt{2\pi}}{c}\sigma_{ab_-,j}(\omega), \tag{3.71a}$$

$$t_{j,--} = \mathcal{E}_{\sigma_-,+}(z_j^+,\omega) = 1 + r_{j,--}, \tag{3.71b}$$

$$r_{j,-+} = \mathcal{E}_{\sigma_+,-}(z_j^-,\omega) = \frac{ig\sqrt{2\pi}}{c}\sigma_{ab_+,j}(\omega), \tag{3.71c}$$

$$t_{j,-+} = \mathcal{E}_{\sigma_+,+}(z_j^+,\omega) = r_{j,-+}. \tag{3.71d}$$

After solving equations (3.70) and (3.71) we get

$$r_{j,--} = -\frac{i(\Gamma_{1D}/2)\left(\tilde{\Delta}_{tot}^{(+)}\delta - |\Omega_+|^2\right)}{\tilde{\Delta}_{tot}^{(+)}\tilde{\Delta}_{tot}^{(-)}\delta - \tilde{\Delta}_{tot}^{(+)}|\Omega_-|^2 - \tilde{\Delta}_{tot}^{(-)}|\Omega_+|^2}, \tag{3.72a}$$

$$t_{j,--} = 1 + r_{j,--}, \tag{3.72b}$$

$$r_{j,-+} = t_{j,-+} = \frac{\Omega_+\Omega_-^* e^{2ik_0 z_j}}{\tilde{\Delta}_{tot}^{(+)}\delta - |\Omega_+|^2} r_{j,--}. \tag{3.72c}$$

In terms of equations (3.69) and (3.72), the blocks of the scattering matrix in equation (3.77) with the definition of the fields in equation (3.76) are

$$S_{j,t} = S_{j,11} = S_{j,22} = \begin{pmatrix} t_{j,++} & t_{j,-+} \\ t_{j,+-} & t_{j,--} \end{pmatrix}, \tag{3.73a}$$

$$S_{j,r} = S_{j,12} = S_{j,21} = \begin{pmatrix} r_{j,++} & r_{j,-+} \\ r_{j,+-} & r_{j,--} \end{pmatrix}. \tag{3.73b}$$

Using the above expressions for the elements of these matrices, we also see that $S_{j,t} = I + S_{j,r}$ holds (I is a 2×2 identity matrix). This, in turn, allows to write the transfer matrix in terms of a single parameter $\beta_j = -S_{j,t}^{-1} S_{j,r}$.

As for the calculations using the continuum model in section 3.3.1, we will also use $\omega_{b_+c} = \omega_{b_-c}$ and $\Omega_+ = \Omega_- = \Omega_0/2$ in the discrete model. This implies that $r_{j,+-} = r_{j,-+}$, and hence that the matrices $S_{j,kl}$ are symmetric, i.e. $S_{j,kl} = S_{j,kl}^{\mathrm{T}}$, where $S_{j,kl}^{\mathrm{T}}$ is the transpose of $S_{j,kl}$. Since the product of commuting symmetric matrices is symmetric, it also follows that β_j is symmetric.

3.4.3 Multi-mode transfer matrix formalism

Now we describe the multi-mode transfer matrix formalism that we use in the discrete model. The approach is very similar to the transfer matrix theory used in elastostatics [78]. This is a more general version of the single-mode transfer matrix formalism [79] that is commonly used for calculating electric fields in one-dimensional systems.

In the transfer matrix formalism, the electric field at the position z is represented by the vector

$$\mathbf{E}(z) = \begin{pmatrix} \mathbf{E}_+(z) \\ \mathbf{E}_-(z) \end{pmatrix}. \tag{3.74}$$

The two parts $\mathbf{E}_\pm(z)$ (right-moving and left-moving fields) are, in general, vectors with n_{m} elements—one for each of n_{m} different modes of the electric field. For the Λ-type scheme (see figure 3.1(b)), only a single polarization mode of the field is necessary, so that we have $n_{\mathrm{m}} = 1$, and $E_\pm(z)$ are scalars (omitting the bold script). In terms of the definitions of the fields for the continuum model we have

$$E_\pm(z) = \mathcal{E}_\pm(z) e^{\pm i k_0 z}, \tag{3.75}$$

i.e. contrary to $\mathcal{E}_\pm$, these fields are not slowly-varying in space. For the dual-V scheme (see figure 3.1(a)), we have $n_{\mathrm{m}} = 2$ (for the σ_+ and σ_- polarization modes), and the vectors are similarly related to the continuum model definitions by

$$\mathbf{E}_\pm(z) = \begin{pmatrix} \mathcal{E}_{\sigma_+,\pm}(z) \\ \mathcal{E}_{\sigma_-,\pm}(z) \end{pmatrix} e^{\pm i k_0 z}. \tag{3.76}$$

When one solves the scattering problem for an atom j with position z_j, the result is the scattering matrix (see sections 3.4.1 and 3.4.2 above). In terms of the right-moving and left-moving parts of the electric field vector defined by equation (3.74), the relation is of the form

$$\begin{pmatrix} \mathbf{E}_+(z_j^+) \\ \mathbf{E}_-(z_j^-) \end{pmatrix} = \begin{pmatrix} S_{j,11} & S_{j,12} \\ S_{j,21} & S_{j,22} \end{pmatrix} \begin{pmatrix} \mathbf{E}_+(z_j^-) \\ \mathbf{E}_-(z_j^+) \end{pmatrix}, \tag{3.77}$$

where the blocks $S_{j,kl}$ are in general $n_\mathrm{m} \times n_\mathrm{m}$ matrices. The scattering matrix thus relates output fields on both sides of the scatterer to the inputs.

A transfer matrix for the atom

$$T_{\mathrm{a},j} = \begin{pmatrix} T_{\mathrm{a},j,11} & T_{\mathrm{a},j,12} \\ T_{\mathrm{a},j,21} & T_{\mathrm{a},j,22} \end{pmatrix} \tag{3.78}$$

is a relation of the form

$$\begin{pmatrix} \mathbf{E}_+(z_j^+) \\ \mathbf{E}_-(z_j^+) \end{pmatrix} = T_{\mathrm{a},j} \begin{pmatrix} \mathbf{E}_+(z_j^-) \\ \mathbf{E}_-(z_j^-) \end{pmatrix}, \tag{3.79}$$

i.e. it relates the fields on one side of the atom to the fields on the other side. By rearranging equation (3.77) into the form of equation (3.79) one can show that

$$T_{\mathrm{a},j,11} = S_{j,11} - S_{j,12}S_{j,22}^{-1}S_{j,21}, \tag{3.80a}$$
$$T_{\mathrm{a},j,12} = S_{j,12}S_{j,22}^{-1}, \tag{3.80b}$$
$$T_{\mathrm{a},j,21} = -S_{j,22}^{-1}S_{j,21}, \tag{3.80c}$$
$$T_{\mathrm{a},j,22} = S_{j,22}^{-1}. \tag{3.80d}$$

In section 3.4.1 and section 3.4.2 we have shown that the blocks of the scattering matrix for the Λ-type and dual-V atoms fulfill

$$S_{j,11} = S_{j,22} = S_{j,t}, \tag{3.81a}$$
$$S_{j,12} = S_{j,21} = S_{j,r}, \tag{3.81b}$$

where the matrices $S_{j,r}$ and $S_{j,t}$ are related by

$$S_{j,t} = I + S_{j,r}, \tag{3.82}$$

with I being the $n_\mathrm{m} \times n_\mathrm{m}$ identity matrix. From equation (3.82) we see that the matrices $S_{j,r}$ and $S_{j,t}$ commute. By writing

$$S_{j,r}S_{j,t} = S_{j,t}S_{j,r} \tag{3.83}$$

and multiplying both sides by $S_{j,t}^{-1}$ from right and left, we get

$$S_{j,t}^{-1}S_{j,r} = S_{j,r}S_{j,t}^{-1}, \tag{3.84}$$

which implies that $S_{j,r}$ and $S_{j,t}^{-1}$ commute. This allows us to write equations (3.80) in terms of a single matrix

$$\beta_j = -S_{j,t}^{-1} S_{j,r}. \tag{3.85}$$

We obtain

$$T_{\mathrm{a},j,11} = S_{j,t} - S_{j,t}^{-1} S_{j,r}^2 = I - \beta_j, \tag{3.86a}$$
$$T_{\mathrm{a},j,12} = S_{j,t}^{-1} S_{j,r} = -\beta_j, \tag{3.86b}$$
$$T_{\mathrm{a},j,21} = -S_{j,t}^{-1} S_{j,r} = \beta_j, \tag{3.86c}$$
$$T_{\mathrm{a},j,22} = S_{j,t}^{-1} = I + \beta_j. \tag{3.86d}$$

For the Λ-type atoms and dual-V atoms with $\Omega_+ = \Omega_-$ and $\omega_{b_+c} = \omega_{b_-c}$, β_j is a symmetric matrix or a scalar (see sections 3.4.1 and 3.4.2). Using this fact we also see that the transfer matrix $T_{\mathrm{a},j}$ is symplectic. This means that if we define a matrix

$$J = \begin{pmatrix} 0 & I \\ -I & 0 \end{pmatrix}, \tag{3.87}$$

where zeros mean $n_\mathrm{m} \times n_\mathrm{m}$ matrices with all elements equal to zero, then it holds that

$$T_{\mathrm{a},j}^{\mathrm{T}} J T_{\mathrm{a},j} = J. \tag{3.88}$$

This can be seen from the fact that if β_j is symmetric, then so is $I \pm \beta_j$, and equation (3.88) can be shown by writing out the left hand side using equations (3.86).

Free propagation of the electric field with the wave vector k_0 for a distance d has the transfer matrix

$$T_\mathrm{f} = \begin{pmatrix} e^{ik_0 d} I & 0 \\ 0 & e^{-ik_0 d} I \end{pmatrix}. \tag{3.89}$$

The free propagation matrix $T_{\mathrm{f},j}$ between atoms j and $j+1$ at positions z_j and z_{j+1} fulfills $\mathbf{E}(z_{j+1}^-) = T_{\mathrm{f},j}\mathbf{E}(z_j^+)$ and is given by equation (3.89) with $d = z_{j+1} - z_j$. For the last transfer matrix $T_{\mathrm{f},N}$, we define $\mathbf{E}(z_{N+1}^-) = \mathbf{E}(L)$, where N is the total number of atoms, and L is the total length of the ensemble.

The free propagation transfer matrices $T_{\mathrm{f},j}$ are always symplectic. Therefore, the transfer matrix of a unit cell (or the whole ensemble), which is a product of the matrices $T_{\mathrm{a},j}$ and $T_{\mathrm{f},j}$, is symplectic if $T_{\mathrm{a},j}$ is symplectic for all j. This can be seen by considering a product of two symplectic transfer matrices, T_1 and T_2. It holds that

$$(T_1 T_2)^{\mathrm{T}} J (T_1 T_2) = T_2^{\mathrm{T}} T_1^{\mathrm{T}} J T_1 T_2 = T_2^{\mathrm{T}} J T_2 = J, \tag{3.90}$$

hence the matrix $T_1 T_2$ is symplectic.

The transfer matrix of the whole ensemble is the product of the transfer matrices of each atom in the ensemble and the free propagation between them. We will consider two types of placement of the atoms: periodic with respect to the classical drives and completely random. The former will allow us to tailor the properties of the stationary light, and the latter is used to reproduce the results of the continuum model investigated above. If the arrangement of the atoms is periodic, then studying the repeated unit cell is sufficient to obtain full information about the system. If the arrangement of the atoms is random, then we need to do statistical averaging over placement of the atoms inside a single period of the classical drives.

For the random placement of the atoms, the starting point is the observation (shown in sections 3.4.1 and 3.4.2) that the scattering matrix for both the Λ-type and dual-V atoms with applied counter-propagating classical drives is invariant under shift of the atomic position by π/k_0 (assuming $k_c \approx k_0$) and not $2\pi/k_0$, which is the periodicity of each of the classical drives. For the Λ-type atoms, this is due to the fact that the two classical drives form a standing wave, which has half the period of the individual running waves. For the dual-V atoms, it is also true, even though there is no obvious standing wave pattern due to the two classical drives.

Having identified π/k_0 as the period of the effective potential due to the two classical drives, we can now explain the statistical averaging procedure. The basic idea is to take an integer number of periods as the length L_u of the unit cell and randomly place N_u atoms within this unit cell with a uniform distribution. Then this unit cell is used to find the dispersion relation in the same way as the unit cells for the periodic placement of the atoms (with one technical difference as discussed below). To obtain a better statistical averaging, we increase the number of periods in L_u, while simultaneously increasing the number of atoms N_u, such that the density $n_0 = N_u/L_u$ is held fixed.

In the transfer matrix theory, Bloch's theorem is a statement about the eigenvalues and eigenvectors of the transfer matrix for the unit cell T_{cell}. Assuming that the unit cell has length L_u and starts at $z = 0$, we have the relation

$$\begin{pmatrix} \mathbf{E}_+(L_u^+) \\ \mathbf{E}_-(L_u^+) \end{pmatrix} = T_{cell} \begin{pmatrix} \mathbf{E}_+(0^-) \\ \mathbf{E}_-(0^-) \end{pmatrix}. \tag{3.91}$$

If $\mathbf{E}_\lambda$ is an eigenvector of T_{cell} with the eigenvalue λ, then $\mathbf{E}_\lambda$ is the periodic part of the Bloch wave (that spatially varies in discrete steps by successively applying transfer matrices whose product is equal to T_{cell}), and the eigenvalue λ is related to the Bloch vector. One natural relation is

$$\lambda = \exp(i\tilde{q}L_u), \tag{3.92}$$

where we denote the Bloch vector with $\tilde{q}$ to make it distinct from the Bloch vector q that we used in the continuum model. The difference is entirely due to defining the electric fields either slowly varying in space (continuum model) or not (discrete model).

For consistency with the continuum model, we will also use a slightly modified relation. Since the elements of the electric field vectors (equations (3.75) and (3.76)) are

defined not to be slowly varying in space, the length of the unit cell $L_\mathrm{u} = n_\mathrm{u}\pi/k_0$ with integer n_u results in free propagation factors $e^{\pm ik_0 L_\mathrm{u}} = (-1)^{n_\mathrm{u}}$ being multiplied onto the vectors. Therefore, we take the relation between the eigenvalue and the Bloch vector to be

$$\lambda = (-1)^{n_\mathrm{u}} \exp(iqL_\mathrm{u})\,. \tag{3.93}$$

which is equivalent to a constant shift of q compared to $\tilde{q}$.

As discussed above, for the Λ-type atoms and dual-V atoms with $\Omega_+ = \Omega_-$ and $\omega_{b_+c} = \omega_{b_-c}$, T_cell is symplectic. Using the eigenvalue relation

$$T_\mathrm{cell}\mathbf{E}_\lambda = \lambda\mathbf{E}_\lambda. \tag{3.94}$$

and the symplectic property $T_\mathrm{cell}^\mathrm{T} J T_\mathrm{cell} = J$ we have

$$T_\mathrm{cell}^\mathrm{T}(J\mathbf{E}_\lambda) = T_\mathrm{cell}^\mathrm{T} J T_\mathrm{cell}(1/\lambda)\mathbf{E}_\lambda = (1/\lambda)(J\mathbf{E}_\lambda). \tag{3.95}$$

Therefore, $J\mathbf{E}_\lambda$ is an eigenvector of $T_\mathrm{cell}^\mathrm{T}$ with the eigenvalue $1/\lambda$. Since T_cell and $T_\mathrm{cell}^\mathrm{T}$ have the same set of eigenvalues, $1/\lambda$ is also an eigenvalue of T_cell. Hence, if q is a Bloch vector, then $-q$ is also a Bloch vector.

Inverting equation (3.93), we can find the Bloch vector from the eigenvalue through

$$\frac{q}{n_0} = -\frac{i}{N_\mathrm{u}}\mathrm{Log}\big((-1)^{n_\mathrm{u}}\lambda\big)\,, \tag{3.96}$$

where Log is the complex logarithm.

When using equation (3.96) to determine the Bloch vector, care is required in selecting the right branch of the complex logarithm, when q is calculated as a function of δ. If the principal branch of the complex logarithm is always used, then $\mathrm{Im}[\mathrm{Log}(\lambda)]$ is constrained to the interval $(-\pi, \pi]$, so that equation (3.96) will result in $\mathrm{Re}[q]/n_0$ being constrained to the interval $(-\pi/N_\mathrm{u}, \pi/N_\mathrm{u}]$. As we let N_u go to infinity to obtain good statistical averaging, this interval becomes arbitrarily small. In practice, this means that as δ is increased, and if $\mathrm{Re}[q]/n_0$ increases and reaches π/N_u, all the subsequent values of $\mathrm{Re}[q]/n_0$ will be shifted by $-2\pi/N_\mathrm{u}$. In the numerical evaluation of the dispersion relations with statistical averaging we thus need to undo these shifts, which is equivalent to selecting different branches of the complex logarithm.

3.4.4 Dispersion relations for cold dual-V atoms

We first use the transfer matrix formalism to find the dispersion relations for ensembles of randomly and regularly placed dual-V atoms. In figure 3.3 we plot the dispersion relations for the randomly placed atoms. The dashed yellow curve is the linear dispersion relation and the dashed green curve is the quadratic dispersion relation. They have an excellent agreement with the analytical solutions given by equations (3.19) and (3.23), which are shown by the solid cyan and red curves respectively. The curves showing the linear dispersion relation for the dual-V scheme have a non-zero $\mathrm{Re}[q]$ for $\delta = 0$ (see equation (3.19)), and hence look vertical for small δ/Γ on the log-log plot.

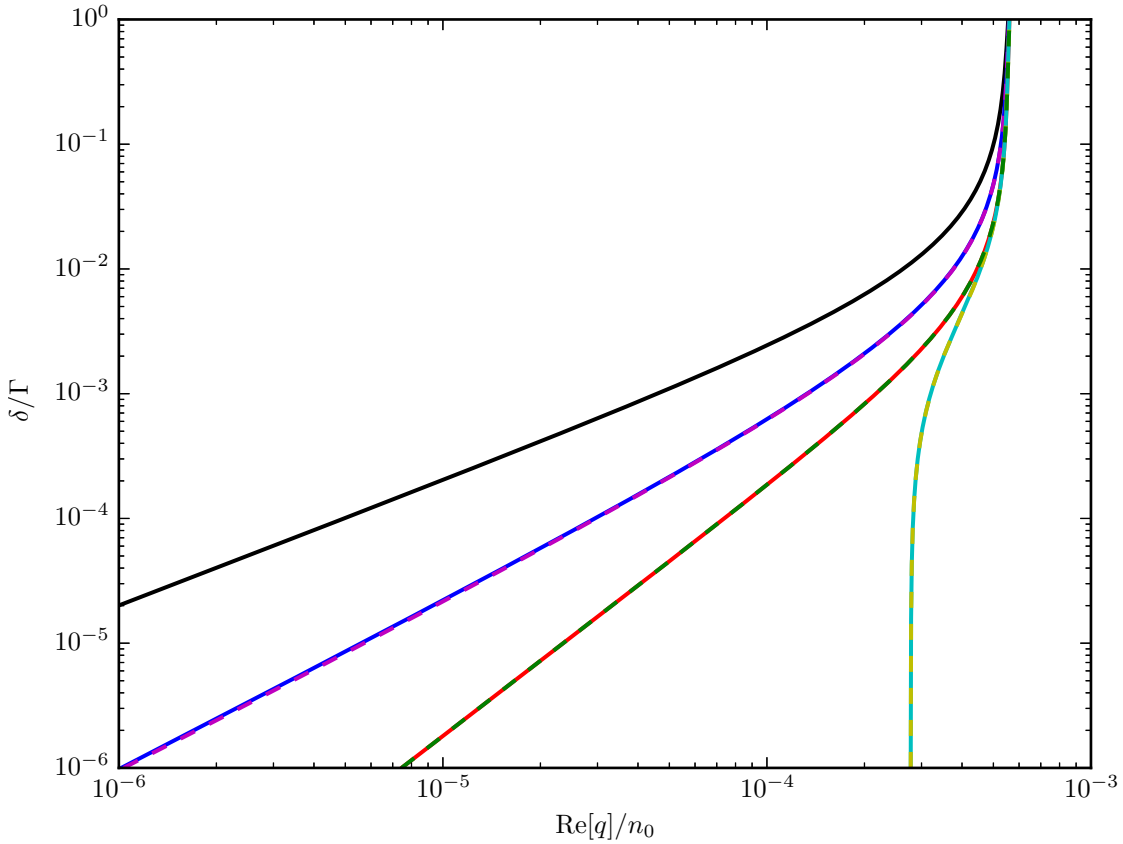

Figure 3.3: Log-log plot of the dispersion relations calculated analytically with the continuum model and numerically with the discrete model for randomly placed atoms. The solid black (upper), red (lower) and blue (in between) curves are as in figure 3.2 and are shown for reference. The middle dashed magenta curve is for Λ-type scheme computed numerically with the discrete model. It overlaps with the solid blue curve (the same dispersion relation computed analytically), so that the difference is not visible. The lower dashed green curve is the quadratic dispersion relation for the dual-V scheme found numerically with the discrete model. The solid cyan and dashed yellow curves that are almost vertical for small δ/Γ show the linear dispersion relation for the dual-V scheme. The solid cyan curve is the analytical result given by equation (3.19), while the dashed yellow curve is computed numerically with the discrete model. Both the numerical curves for the two dispersion relations for the dual-V scheme (linear and quadratic) overlap with the respective analytical solutions, so that the difference in not visible. The common parameters are: $\Gamma_{1D}/\Gamma = 0.1$, $\Delta_c/\Gamma = -90$, $\Omega_0/\Gamma = 1$, $k_0/n_0 = \pi/2$ and $N_u = 10^4$ (i.e. $L_u = (10^4/2)\pi/k_0$).

If the dual-V atoms are placed regularly, the only noticeable difference we have found between the continuum and discrete theory is when the atoms in the discrete model are spaced with either $d = \pi/k_0$ or $d = \pi/(2k_0)$. The former is equivalent to the atomic mirror [21], and since we neglect the vacuum dispersion relation, for $d = \pi/k_0$ we find the constant Bloch vector q independent of δ. The latter, $d = \pi/(2k_0)$, changes the linear dispersion relation (3.19). The reason for this is that in the derivation of equation (3.19), we have neglected the terms with $e^{\pm 2ik_0 z}$ and $e^{\pm 4ik_0 z}$. For discrete positions $z = jd = j\pi/(2k_0)$ (j is an integer), these factors are $e^{\pm 2ik_0 z} = e^{\pm i\pi j}$ and $e^{\pm 4ik_0 z} = 1$. We see that for discrete atoms with spacing $d = \pi/(2k_0)$, the factors $e^{\pm 4ik_0 z} = 1$ should not be neglected, since they are constant and not rapidly varying. With this correction, equations (3.18b) become

$$\mp\frac{q}{n_0}\mathcal{E}_{\sigma_\pm,\mp} = -\frac{\Gamma_{1D}}{2\tilde{\Delta}}\left[\frac{\delta-\delta_S/2}{\delta-\delta_S}\mathcal{E}_{\sigma_\pm,\mp} + \frac{\delta_S/2}{\delta-\delta_S}\mathcal{E}_{\sigma_\mp,\pm}\right], \tag{3.97}$$

which makes them of exactly the same coupled form as equations (3.18a) and therefore results in the same quadratic dispersion relation (3.23) instead of a linear one. This behavior is reproduced by the numerical calculations with the discrete model.

3.4.5 Dispersion relations for cold Λ-type atoms

As for the dual-V atoms above, we can calculate the dispersion relation of an ensemble with randomly placed Λ-type atoms. As shown in figure 3.3, the dispersion relation obtained in this way (dashed magenta) matches the one that was found analytically for the continuum model (solid blue).

For the regularly placed Λ-type atoms, we can also obtain dispersion relations, which are different from the predictions of the continuum model. To this end we consider the ensembles shown in figure 3.4. The atoms are spaced with a distance $d = \pi/(N_u k_0)$, where we only take even N_u for simplicity. (As explained above, adding integer multiples of π/k_0 to d does not change the results.) A unit cell consists of $N_u - 1$ atoms, which experience a non-zero classical drive, and one atom, which is placed such that the classical drive is zero, i.e. on the node of the standing wave of the classical drive. For such a setup, we show in appendix C that the dispersion relation for two-photon detunings fulfilling

$$\delta \ll 2|\delta_S|\cos^2\left(\frac{\pi}{2}-\frac{\pi}{N_u}\right) \approx 2|\delta_S|\left(\frac{\pi}{N_u}\right)^2 \tag{3.98}$$

(i.e. if frequency is within the smallest EIT window of the atoms that are not placed on the node) is given by

$$\delta \approx \frac{1}{2m}\left(\frac{q}{n_0}\right)^2, \tag{3.99}$$

where $n_0 = 1/d$, and

$$m = -\frac{(N_u-1)\Gamma_{1D}^2}{2N_u^2(\Delta_c + i\Gamma'/2)|\Omega_0|^2} \tag{3.100}$$

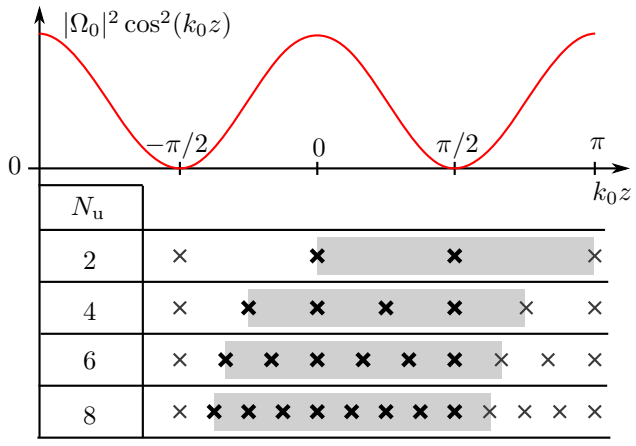

Figure 3.4: Placement of atoms for periodic ensembles. At the top, the standing wave of the classical drive is plotted. In the table below, the crosses indicate the positions of the atoms in the standing wave of the classical drive for different values of the number of atoms per unit cell N_u. The thick crosses are the atoms in the chosen unit cell, and the thin crosses are the other atoms in the ensemble. The particular choice of the unit cell (gray) is such that the atoms with the non-zero classical drive are taken first (when propagating from the left), and the last atom is placed on the node of the classical drive (at $k_0 z = \pi/2$) which effectively makes it a two-level atom.

is the effective mass. Note that the quadratic dispersion relation in equation (3.99) is of the same form as equation (3.24), but with the effective mass in equation (3.100) differing by a factor $2(N_\mathrm{u}-1)/N_\mathrm{u}^2$ from the one in equation (3.25).

The above quadratic dispersion relation is obtained by placing the atoms such that one of them coincides exactly with the node of the standing wave of the classical drive. The dispersion relation can be completely changed, however, by shifting the position of the atoms relative to the drive. This can be achieved if the classical drive is given by $\Omega(z) = \Omega_0 \cos(k_0 z + \varphi)$ (with the situation above corresponding to $\varphi = 0$). By choosing $\varphi = k_0 d/2 = \pi/(2N_\mathrm{u})$, the node of the standing wave is placed exactly in the middle of the free-space separation between two atoms.

We show the numerically calculated dispersion relation for $\varphi = 0$ and $\varphi = k_0 d/2$ in figure 3.5. For $\varphi = 0$ (dashed green curves), the dispersion relation becomes quadratic for small $\mathrm{Re}[q]/n_0$ as given by equation (3.99). The range of validity of the quadratic approximation becomes smaller for increasing N_u, as predicted by the condition in equation (3.98). For $\varphi = k_0 d/2$ (dash-dotted magenta curves), the dispersion relation becomes linear (parallel to the EIT dispersion relation) instead of quadratic for small $\mathrm{Re}[q]/n_0$. As N_u increases, both for $\varphi = 0$ and $\varphi = k_0 d/2$, the dispersion relation approaches the one for an ensemble of cold randomly placed Λ-type atoms (solid blue). The two choices of the phase, $\varphi = 0$ and $\varphi = k_0 d/2$, are thus similar to respectively the odd and even n truncations in figure 3.2. In essence, having a finite number of atoms per unit cell gives a truncation because a finite number of atoms can only support a finite number of Fourier components of σ_{ab} and σ_{ac}.

The two situations, $\varphi = 0$ and $\varphi = k_0 d/2$, considered in figure 3.5, represent the two extreme cases with the node of the classical drive either coinciding with an atom or being placed as far away from the atoms as possible. In between these extremes there is a whole continuum of possibilities. In general, if no atoms are placed at the nodes, all atoms will have a finite EIT window and hence the dispersion relation will be linear for sufficiently small δ. This also implies that with a finite number of randomly placed stationary Λ-type atoms, it is impossible to realize a $\delta \propto |q|^{4/3}$ dispersion in the limit $\delta \to 0$, as there is formally zero probability for the point-like atoms to sit exactly at the nodes, and hence the dispersion relation will eventually cross over to the linear one.

3.5 Scattering properties

3.5.1 Methods

A different way to compare the ensembles with regularly and randomly placed Λ-type atoms is to look at the scattering properties (transmission and reflection coefficients) of the whole ensemble. Contrary to the dispersion relation, which, in principle, is only valid for an infinite ensemble, the total number of atoms does matter for the scattering properties. If the number of the atoms is sufficiently large, the dispersion relation is still reflected in the behavior of the transmission and reflection coefficients. Hence, the scattering properties can also be used to characterize the dispersion relation.

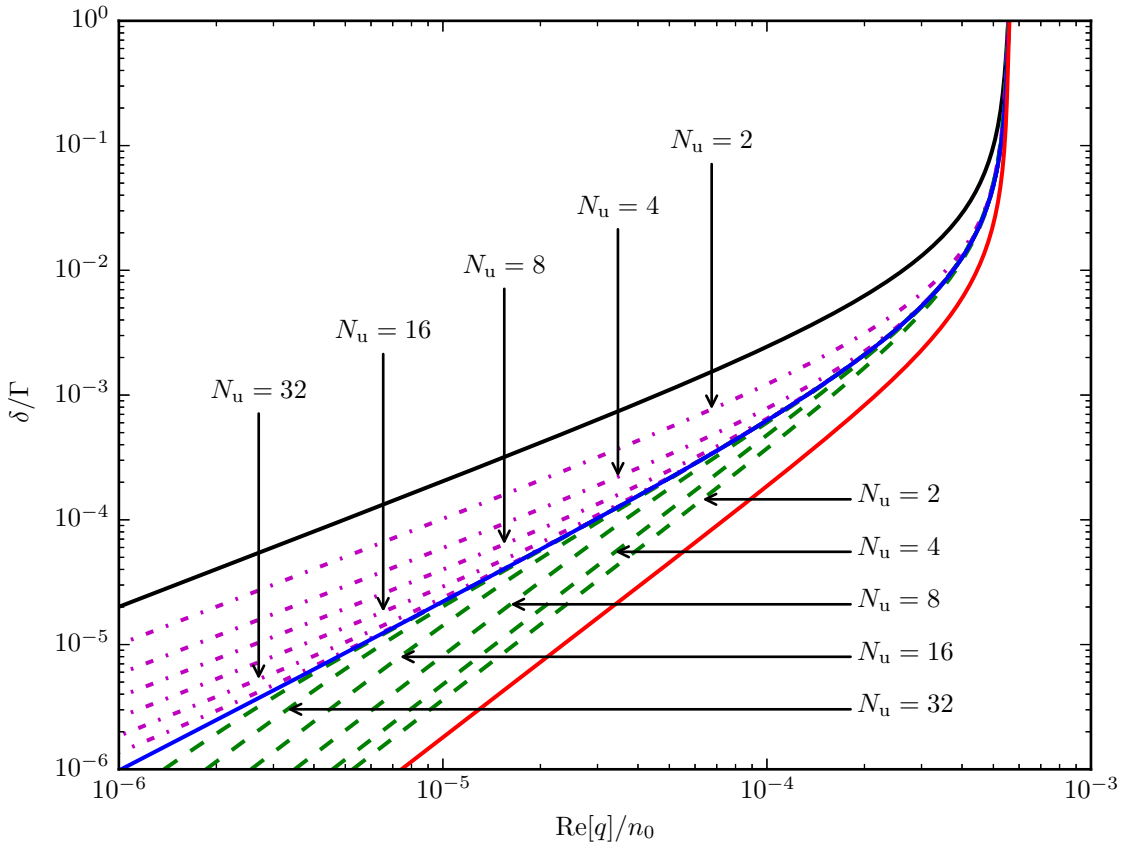

Figure 3.5: Log-log plot of the dispersion relations for Λ-type atoms with different placement of the atoms within the unit cell. The solid black (upper), red (lower) and blue (in between) curves are as in figure 3.2 and are shown for reference. The dashed green curves are for ensembles with regularly placed atoms (see figure 3.4) for the period lengths $N_\mathrm{u} = 2, 4, 8, 16, 32$. The dash-dotted magenta curves are for the same setups, but with a shifted standing wave of the classical drive: $\Omega(z) = \Omega_0 \cos(k_0 z + \varphi)$ with $\varphi = \pi/(2N_\mathrm{u})$. The common parameters are: $\Gamma_{1\mathrm{D}}/\Gamma = 0.1$, $\Delta_\mathrm{c}/\Gamma = -90$, $\Omega_0/\Gamma = 1$. The density of the atoms n_0 is related to the spacing between the atoms d by $n_0 = 1/d$. The distance d depends on the desired period length and is given by $d = \pi/(N_\mathrm{u} k_0)$ (plus any integer multiple of π/k_0).

Below, the transmission coefficients t and reflection coefficients r will be obtained numerically by multiplying the transfer matrices for the atoms and free propagation to obtain the transfer matrix for the whole ensemble T_e and afterwards extracting the scattering coefficients from T_e. Assuming that the ensemble has length L and starts at $z = 0$, we have the relation

$$\begin{pmatrix} \mathbf{E}_+(L^+) \\ \mathbf{E}_-(L^+) \end{pmatrix} = \begin{pmatrix} T_{\mathrm{e},11} & T_{\mathrm{e},12} \\ T_{\mathrm{e},21} & T_{\mathrm{e},22} \end{pmatrix} \begin{pmatrix} \mathbf{E}_+(0^-) \\ \mathbf{E}_-(0^-) \end{pmatrix}. \tag{3.101}$$

For concreteness, we assume a two-mode transfer matrix as is relevant for the dual-V scheme. Hence, the vectors $\mathbf{E}_\pm$ have two elements. We adopt the convention that the first element is a σ_+ component, and the second element is the σ_- component of the field (the same definition as in equation (3.76)). As an example, consider a scattering problem with the incoming fields

$$\mathbf{E}_+(0^-) = \begin{pmatrix} 1 \\ 0 \end{pmatrix}, \quad \mathbf{E}_-(L^+) = \begin{pmatrix} 0 \\ 0 \end{pmatrix}, \tag{3.102}$$

i.e. there is only a σ_+ input field from the left. We want to find the outgoing fields: $\mathbf{E}_+(L^+)$ (the transmitted field) and $\mathbf{E}_-(0^-)$ (the reflected field).

After insertion of equations (3.102) into equation (3.101) we find

$$\mathbf{E}_-(0^-) = -T_{\mathrm{e},22}^{-1} T_{\mathrm{e},12} \mathbf{E}_+(0^-), \tag{3.103a}$$

$$\mathbf{E}_+(L^+) = (T_{\mathrm{e},11} - T_{\mathrm{e},12} T_{\mathrm{e},22}^{-1} T_{\mathrm{e},21}) \mathbf{E}_+(0^-). \tag{3.103b}$$

For the single-mode transfer matrices, $T_{\mathrm{e},kl}$ are scalars. Furthermore, from equations (3.86) and (3.89) we see that the transfer matrices for atoms and free propagation have determinants equal to unity. Using the fact that $\det(T_1 T_2) = \det(T_1)\det(T_2)$ for any two square matrices T_1 and T_2, we have $T_{\mathrm{e},11} T_{\mathrm{e},22} - T_{\mathrm{e},12} T_{\mathrm{e},21} = \det(T_\mathrm{e}) = 1$. This leads to a simplification of equations (3.103), so that they become

$$E_-(0^-) = -(T_{\mathrm{e},12}/T_{\mathrm{e},22}) E_+(0^-), \tag{3.104a}$$

$$E_+(L^+) = (1/T_{\mathrm{e},22}) E_+(0^-). \tag{3.104b}$$

For regularly placed discrete atoms and the continuum model, one can derive closed-form expressions for the T_e. The assumption is that the ensemble either consists of n_e copies of the same unit cell with the transfer matrix

$$T_\mathrm{cell} = \begin{pmatrix} T_{11} & T_{12} \\ T_{21} & T_{22} \end{pmatrix} \tag{3.105}$$

in the discrete case, or is governed by the equations of the form

$$\frac{\partial}{\partial z} \begin{pmatrix} \mathcal{E}_+ \\ \mathcal{E}_- \end{pmatrix} = i n_0 \begin{pmatrix} -\alpha_1 & -\alpha_2 \\ \alpha_2 & \alpha_1 \end{pmatrix} \begin{pmatrix} \mathcal{E}_+ \\ \mathcal{E}_- \end{pmatrix} \tag{3.106}$$

in the continuum case. For the continuum case, we note that equations (3.14a) for the dual-V scheme and the equivalent equations for the Λ-type scheme can be written in the form above (neglecting the vacuum dispersion relation) with α_1 and α_2 being given by either equations (3.22) or equations (3.47), depending on the scheme.

The starting point of the derivation is diagonalizing either the transfer matrix in equation (3.105) or the matrix in equation (3.106). This gives

$$\begin{pmatrix} T_{11} & T_{12} \\ T_{21} & T_{22} \end{pmatrix} = V_{\text{cell}} D_{\text{cell}} V_{\text{cell}}^{-1}, \tag{3.107}$$

$$\begin{pmatrix} -\alpha_1 & -\alpha_2 \\ \alpha_2 & \alpha_1 \end{pmatrix} = V_\alpha D_\alpha V_\alpha^{-1}, \tag{3.108}$$

where the diagonal matrix D_{cell} has elements (eigenvalues) $\exp(\pm i\tilde{q}L_{\text{u}})$, and the diagonal matrix D_α has elements $\pm q/n_0$. Here we use the relation (3.92) between the Bloch vector and the elements of D_{cell} for brevity. The eigenvector matrices are

$$V_{\text{cell}} = \begin{pmatrix} 1 & 1 \\ (e^{i\tilde{q}L_{\text{u}}} - T_{11})/T_{12} & (e^{-i\tilde{q}L_{\text{u}}} - T_{11})/T_{12} \end{pmatrix}, \tag{3.109}$$

$$V_\alpha = \begin{pmatrix} 1 & 1 \\ -(q/n_0 + \alpha_1)/\alpha_2 & -(-q/n_0 + \alpha_1)/\alpha_2 \end{pmatrix}. \tag{3.110}$$

In the discrete case, the transfer matrix for the whole ensemble is $T_{\text{e}} = T_{\text{cell}}^{n_{\text{e}}}$, where $n_{\text{e}} = L/L_{\text{u}}$ is an integer. This expression can be written as

$$\begin{aligned} T_{\text{e}} &= V_{\text{cell}} D_{\text{cell}}^{n_{\text{e}}} V_{\text{cell}}^{-1} \\ &= V_{\text{cell}} \left(\cos(\tilde{q}L) I + i \sin(\tilde{q}L)\sigma_z\right) V_{\text{cell}}^{-1} \\ &= \cos(\tilde{q}L) I + i \sin(\tilde{q}L) V_{\text{cell}} \sigma_z V_{\text{cell}}^{-1}, \end{aligned} \tag{3.111}$$

where I is the identity matrix and

$$\sigma_z = \begin{pmatrix} 1 & 0 \\ 0 & -1 \end{pmatrix}. \tag{3.112}$$

By doing the matrix multiplications and using $2\cos(\tilde{q}L_{\text{u}}) = \text{tr}(T_{\text{cell}}) = T_{11} + T_{12}$ and $\det(T_{\text{cell}}) = 1$, we find

$$V_{\text{cell}} \sigma_z V_{\text{cell}}^{-1} = \frac{1}{\sin(\tilde{q}L_{\text{u}})} \begin{pmatrix} \frac{i}{2}(T_{22} - T_{11}) & -iT_{12} \\ -iT_{21} & -\frac{i}{2}(T_{22} - T_{11}) \end{pmatrix}. \tag{3.113}$$

In the continuum case, the transfer matrix for the whole ensemble is

$$\begin{aligned} T_{\text{e}} &= \exp\left(i n_0 \begin{pmatrix} -\alpha_1 & -\alpha_2 \\ \alpha_2 & \alpha_1 \end{pmatrix} L \right) \\ &= \cos(qL) I + i \sin(qL) V_\alpha \sigma_z V_\alpha^{-1}, \end{aligned} \tag{3.114}$$

where (using $\alpha_1^2 - (q/n_0)^2 - \alpha_2^2 = 0$)

$$V_\alpha \sigma_z V_\alpha^{-1} = \frac{1}{q/n_0} \begin{pmatrix} -\alpha_1 & -\alpha_2 \\ \alpha_2 & \alpha_1 \end{pmatrix}. \tag{3.115}$$

3.5.2 Results

In figures 3.6 and 3.7(a), we plot transmittance $|t|^2$ and reflectance $|r|^2$ for ensembles with regular ($N_\mathrm{u} = 2$) and random (average of 100 ensemble realizations) placement of Λ-type atoms. As discussed above, the latter case can also be calculated using the continuum model. The main visible difference between the discrete model with random placement and the continuum model is that the former has noise in the region $-0.01 \lesssim \delta/\Gamma \leq 0$ due to finite number of ensemble realizations. In figure 3.7(a) we additionally show the reflection coefficient for randomly placed dual-V atoms (single ensemble realization) with σ_+ input incident from the left and finding the left-moving σ_- field to the left of the ensemble (such that the quadratic dispersion relation is valid). The reflection coefficient of the dual-V scheme overlaps completely with the reflection coefficient of the regularly placed Λ-type scheme, because we have increased the classical drive strength Ω_0 of the dual-V scheme by a factor of $\sqrt{2}$ to make the masses in equation (3.25) and equation (3.100) equal.

The plots and the chosen parameters are similar to the ones in Ref. [22]. As opposed to Ref. [22], however, we do not make the secular approximation for the Λ-type scheme, and this leads to very different results, which depend on how the atoms are placed (and whether we use the dual-V scheme instead). For the regularly placed Λ-type atoms, we see a clear signature of a photonic band gap in the region $-0.01 \lesssim \delta/\Gamma \leq 0$, where there is a near unit reflectance and negligible transmittance. For the randomly placed Λ-type atoms, the situation is more complex with a similar negligible transmittance but a rather limited reflectance. For $\delta > 0$, the position of the resonances with low reflection and high transmission corresponds to the condition $\sin\big(\mathrm{Re}[q]L\big) = 0$, i.e. there is a standing wave of the Bloch vectors inside the ensemble. Specifically, the high transmission resonance occurs each time $\mathrm{Re}[q]/n_0$ crosses a multiple of π/N, as can be seen in figure 3.7(b). This behavior can also be seen from the closed-form expressions in section 3.5.1. Due to non-zero incoherent decay rate Γ', the sum $|t|^2 + |r|^2$ is in general not equal to unity.

As we have shown above, the regularly and randomly placed Λ-type atoms have very different dispersion relations, and this translates into very different positions of the high transmission resonances in figures 3.6 and 3.7(a). For the randomly placed Λ-type scheme, there additionally occurs a high transmission resonance at $\delta = 0$, since no atoms are placed exactly at the node of the standing wave of the classical drive, and hence all the atoms are transmissive due to EIT. For the regularly placed setup with $N_\mathrm{u} = 2$, half of the atoms are placed on the nodes and therefore behave as effective two-level atoms. For $\delta = 0$, the other half of the atoms becomes transparent, and the whole ensemble is exactly equivalent to the atomic mirror [21]. For the dual-V atoms, as shown in section 3.4.2 the reflection coefficients of a single atom do not become zero for $\delta = 0$, regardless of how the individual atoms are placed.

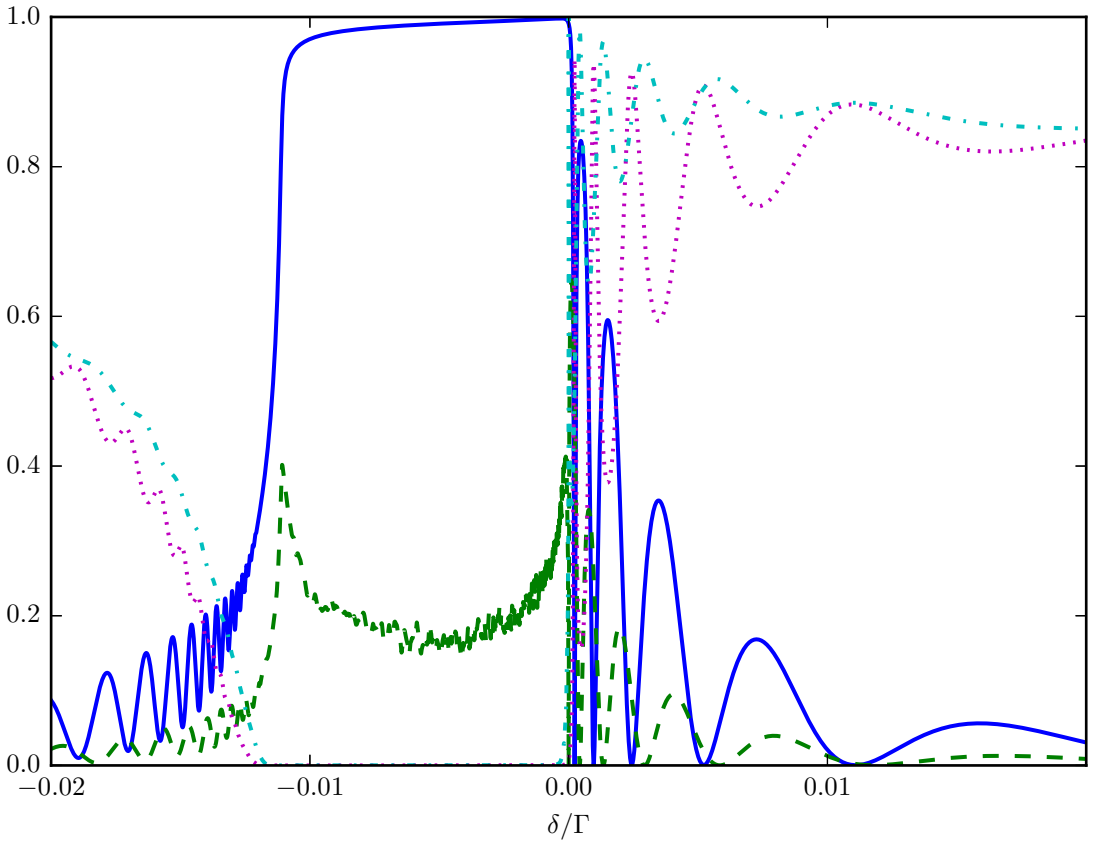

Figure 3.6: Plot of transmittance $|t|^2$ and reflectance $|r|^2$ of ensembles with $N = 4 \cdot 10^4$ atoms. The dotted magenta and solid blue curves are respectively the transmittance and reflectance of an ensemble with regularly placed Λ-type atoms and $N_\mathrm{u} = 2$ (with the placement shown in figure 3.4). The dash-dotted cyan and dashed green curves are respectively the transmittance and reflectance of an ensemble with randomly placed Λ-type atoms and is averaged over 100 ensemble realizations. The other parameters are: $\Gamma_{1\mathrm{D}}/\Gamma = 0.1$, $\Delta_\mathrm{c}/\Gamma = -90$, $\Omega_0/\Gamma = 1$, $k_0/n_0 = \pi/2$. The interval around $\delta = 0$ is shown in more detail in figure 3.7(a).

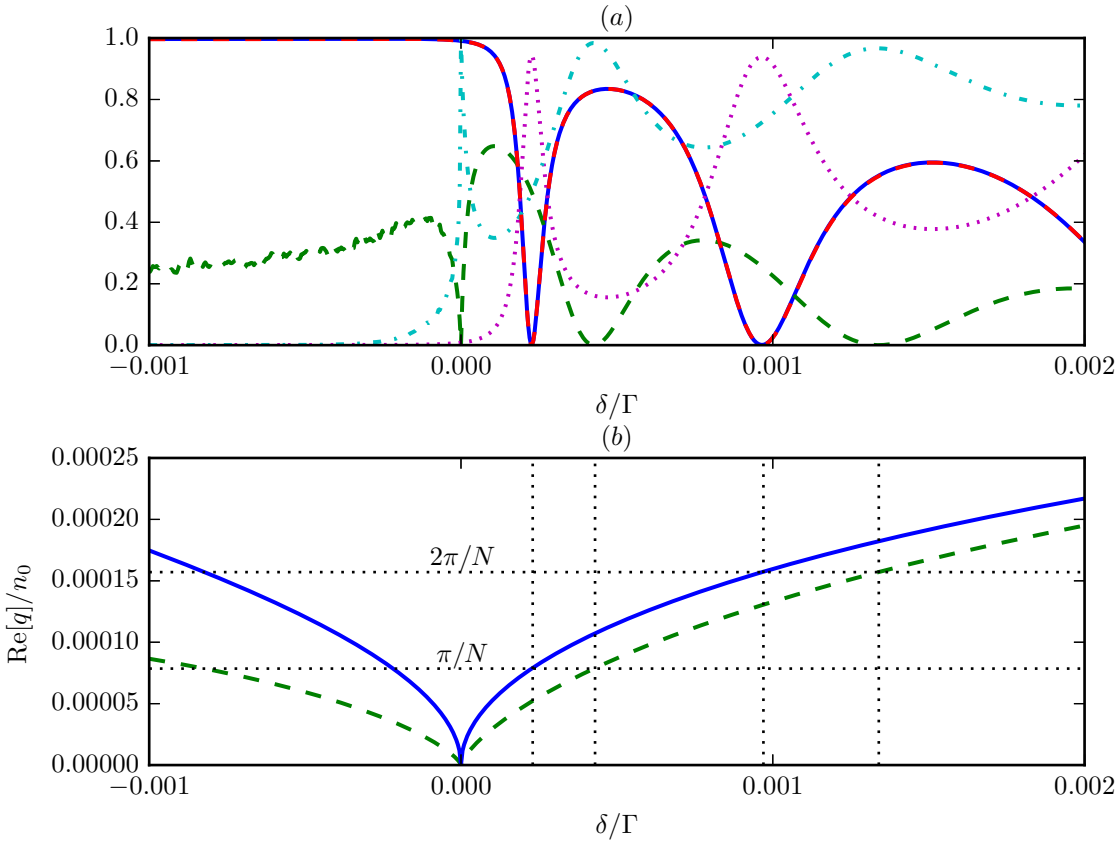

Figure 3.7: (a) Same as figure 3.6, but zoomed in around $\delta = 0$. Additionally, the reflectance for an ensemble with randomly placed dual-V atoms is plotted (dashed red), and it completely overlaps the reflectance for the regularly placed Λ-type scheme. The dual-V scheme has the same parameters except that Ω_0 is multiplied by $\sqrt{2}$ to make the dispersion relation equal to the one of the regularly placed Λ-type scheme. (b) Dispersion relations for Λ-type scheme: regularly placed (solid blue) and randomly placed (dashed green). The dispersion relation was calculated numerically with the transfer matrix formalism for the regularly placed ensemble, and using equation (3.48) for the randomly placed ensemble. The two horizontal dotted lines at $\mathrm{Re}[q]/n_0 = \pi/N$ and $\mathrm{Re}[q]/n_0 = 2\pi/N$, give the condition for the first and the second high transmission resonance. At each intersection (for $\delta > 0$) of these horizontal lines with the dispersion relation curves, vertical dotted lines are drawn, which can be seen to coincide with the high transmission resonances in (a).

Chapter 4

Controlled-phase gate

4.1 Acknowledgements

This chapter is based on the material in Ref. [5]. The application of the proposed controlled-phase gate to quantum repeaters was done by Johannes Borregaard. Experimental parameters of Ref. [3] are used in the discussion.

4.1.1 Introduction

In this chapter, we build upon the understanding of the linear properties of stationary light in chapter 3 to make a controlled-phase for photons. First, we do a short description of the gate, omitting some technical details, which can then be found the later sections of this chapter.

4.2 Short description

4.2.1 Overview

We consider two different level schemes for the atoms in the ensemble: Λ-type and dual-V (figures 4.1(a) and 4.1(b), respectively). The linear properties of these two schemes are described in detail in chapter 3. For the Λ-type scheme, we assume that the atoms are placed at positions $z_j = j\pi/(2k_0)$ with $0 \leq j \leq N-1$. (In other words, atoms are assumed to be placed a quarter of a wavelength $\lambda = 2\pi/k_0$ from each other, but any odd number of quarter wave lengths will produce the same results.) This is the setup from section (3.4.5) with $N_{\mathrm{u}} = 2$ and $\phi = 0$, where every other atom is placed on the node of the standing wave of the classical drive. This setup is chosen since the effective mass is the biggest, which translates in the lowest possible group velocity. Due to regular placement of the atoms, this scheme is easier to analyze, and all our analytical results in this chapter are obtained for this scheme. To produce an optical nonlinearity, the Λ-type level scheme is extended by two additional levels $|d\rangle$ and $|e\rangle$, which can separately function as a two-level atom. This two-level atom is always assumed to be resonant with the incident single photon (probe field).

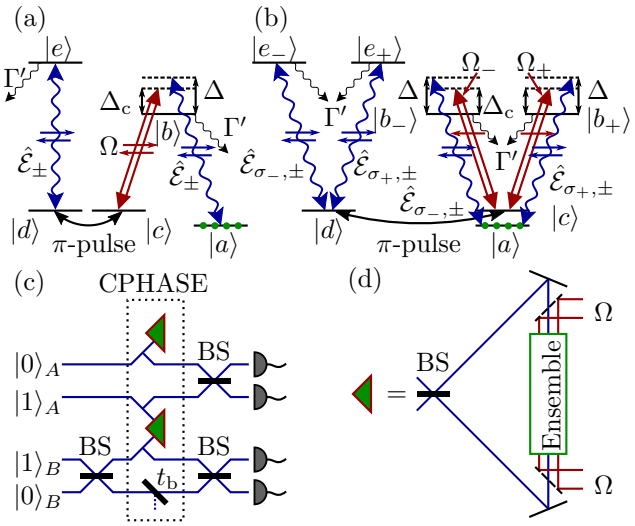

Figure 4.1: (a) Level diagram of a Λ-type atom (levels $|a\rangle$, $|b\rangle$, and $|c\rangle$), which can be switched to a two-level atom (levels $|d\rangle$ and $|e\rangle$) by the storage of a photon followed by a π-pulse. The green dots indicate the initial state of the atoms. (b) Level diagram of a dual-V atom which can be switched to a V-type atom. (c) A dual-rail Bell-state measurement setup with the controlled-phase gate (labeled by CPHASE) as a part of it. An ensemble of atoms is placed inside a Sagnac interferometer, shown as a triangle in (c) and defined by (d). In the rail corresponding to state $|0\rangle_B$, a beam splitter is added with transmission coefficient t_b. All the other beam splitters (BS) are 50:50.

As discussed in chapter 3, the dual-V scheme with appropriately chosen combination of polarization and propagation directions always has a quadratic dispersion relation regardless of positioning of the atoms. To produce an optical nonlinearity, the dual-V scheme is extended by three additional states $|d\rangle$, $|e_+\rangle$ and $|e_-\rangle$, which can function as a V-type atom. For the dual-V scheme, we only verify numerically that the gate errors have the same scaling as for the Λ-type scheme.

The coupling of the atoms to the waveguide is characterized by the parameter $\Gamma_{1\mathrm{D}}/\Gamma$ (half of the resonant optical depth per atom), where $\Gamma_{1\mathrm{D}}$ is the decay rate from each of the states $|b\rangle$ and $|e\rangle$ for the Λ-type scheme into both right-moving and left-moving guided modes (assumed to be equal), Γ' is the decay rate into all the other modes, and $\Gamma = \Gamma_{1\mathrm{D}} + \Gamma'$ is the total decay rate. For the dual-V scheme, $\Gamma_{1\mathrm{D}}$ is the decay rate from each of the states $|b_\pm\rangle$ and $|e_\pm\rangle$. In the dual-rail encoding of photonic qubits shown in figure 4.1(c), two identical atomic ensembles are required, where the upper one only functions as a memory. Alternatively, the single-rail encoding can also be implemented with one atomic ensemble [1], but the dual-rail encoding allows heralded operation, which has better fidelity. Each ensemble is placed inside a Sagnac interferometer (figure 4.1(d)).

The operation of the CP gate is sequential. First, photon A is stored either in the upper ($|0\rangle_A$) or the lower ($|1\rangle_A$) ensemble using electromagnetically induced transparency

(EIT) [55]. Then photon B is scattered from the lower ensemble under conditions of stationary light ($|1\rangle_B$) or passes through a beam splitter with transmission coefficient t_b ($|0\rangle_B$). The role of this beam splitter will be explained below. The Sagnac interferometer can be set up such that most of the incident power in each of its two input ports is reflected back through the same port, regardless of whether the ensemble is reflective or transmissive [80, 81] (see section 4.4 below). Reflection or transmission of the ensemble instead controls the phase of the reflected field. The scattering of photon B can be arranged such that if there is no stored photon in the lower ensemble (photon A is in the state $|0\rangle_A$), the atomic ensemble is completely transmissive in the ideal case, and photon B is reflected from the Sagnac interferometer with no additional phase. If there is a stored photon (photon A is in state $|1\rangle_A$), photon B is reflected from the interferometer with a π phase shift. The latter case performs the desired controlled-phase gate operation $|11\rangle_{AB} \rightarrow -|11\rangle_{AB}$, while the rest of the basis states are unchanged. Finally, photon A is retrieved using EIT.

For the dual-V scheme, it is in principle possible to store the photon such that it is incident only from one side instead of symmetrically from both sides, as required for the Λ-type scheme (explained below). If one-sided storage is desired, a different setup can be used, where the photons are incident on the ensemble directly (without placing the ensemble inside a Sagnac interferometer). To convert between conditional reflection or transmission and conditional phase shift, a mirror behind the ensemble can be used. This setup may require less stabilization of path lengths than a Sagnac interferometer. The unconditional fidelity in this setup is found to be approximately the same, but the conditional fidelity has a worse scaling. The latter is because in equations (4.3) and (4.4) below, the terms linear in $(\tilde{z} - 1/2)$ do not cancel as in the symmetric case (also see the fidelity derivations in section 4.6 below). Therefore, we focus only on two-sided storage below.

4.2.2 Storage and retrieval

Under EIT storage and retrieval, the incident photon is assumed resonant with the classical drive (i.e. the two-photon detuning δ is zero), and the classical drive is incident from one side and is assumed to be resonant with its transition for simplicity ($\Delta_\mathrm{c} = 0$). Hence, for storage and retrieval, the Λ-type scheme and the dual-V scheme behave in exactly the same way. After entering the Sagnac interferometer, photon A will be split into two halves by the 50:50 beam-splitter (see figure 4.1(d)), which upon reaching the ensemble from the opposite sides will have opposite spatial phase factors $e^{ik_0 z}$ and $e^{-ik_0 z}$ and interfere inside the ensemble resulting in a spatially modulated $\cos(k_0 z)$ stored spin wave. Such storage procedure is necessary for the Λ-type scheme, since the part of the excitation that is stored on the nodes of the standing wave of the classical drive (that is applied during scattering of photon B) does not change the scattering properties of the ensemble. Before the EIT storage, all atoms are initialized in state $|a\rangle$, and after storage, the incident photon is mapped onto an atom being in state $|c\rangle$. To produce an optical nonlinearity, we assume that state $|c\rangle$ is subsequently transferred to state $|d\rangle$ using a π-pulse.

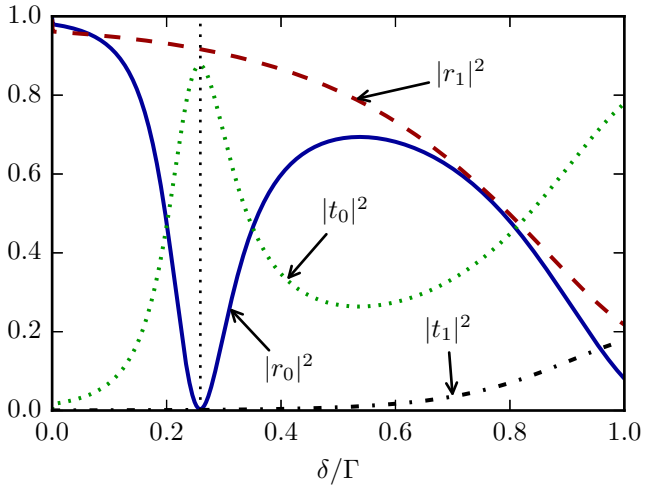

Figure 4.2: Reflectances ($|r_0|^2$, $|r_1|^2$) and transmittances ($|t_0|^2$, $|t_1|^2$) of an ensemble of Λ-type atoms without ($|r_0|^2$, $|t_0|^2$) and with ($|r_1|^2$, $|t_1|^2$) a stored photon for different frequencies (two-photon detunings) δ in units of the total linewidth Γ. The vertical dotted line marks the operation point. The parameters are: number of atoms $N = 1000$, $\Gamma_{1D}/\Gamma = 0.5$, $\Delta_c/\Gamma = -16$, and $\Omega_0/\Gamma = 10$.

4.2.3 Reflection and transmission

We use the (multi-mode) transfer matrix formalism (see sections 3.4.3 and 3.5.1 above) to model the scattering process. To illustrate the scattering behavior, we assume that photon A was stored in the center of an atomic ensemble of Λ-type atoms at an anti-node of the classical drive. The reflectances and transmittances of the ensemble are plotted in figure 4.2(a) as functions of the two-photon detuning $\delta = \Delta - \Delta_c$, where Δ (Δ_c) is the detuning of the probe field (classical drive). The reflectance $|r_0|^2$ ($|r_1|^2$) and transmittance $|t_0|^2$ ($|t_1|^2$) are for an ensemble without (with) a stored photon. The ensemble is seen to have transmittance resonances with a large transmittance and a small reflectance, similar to the transmission of a cavity. These resonances occur when the standing wave condition is fulfilled, i.e. $\sin(qL) = 0$, where q is the Bloch vector of the stationary light polaritons and L is the length of the ensemble (see section 3.5 above). When a photon is stored in the ensemble, an atom changes from state $|a\rangle$ to $|d\rangle$. In state $|d\rangle$, the atom acts as a two-level atom that is resonant with the incident photon (see figure 4.1(a)). Since the effective interaction is enhanced by the cavity-like behavior of the ensemble, this single two-level atom can have a strong effect of an incident photon, even though the atom in itself has a limited coupling.

We focus on the behavior at the resonance nearest $\delta = 0$ (vertical dotted line in figure 4.2(a)). In the limit of large atom number N and for $|\Delta_c| \neq 0$, this resonance is at a two-photon detuning $\delta_{res} \approx -4\Delta_c\pi^2|\Omega_0|^2/(\Gamma_{1D}^2 N^2)$, for which we obtain (see section 4.3

below)

$$r_0 \approx \frac{\Gamma_{1D}\Gamma' N}{16\Delta_c^2} + \frac{\Gamma'|\Omega_0|^2\pi^2}{2\Delta_c^2\Gamma_{1D}N}, \tag{4.1}$$

$$t_0 \approx 1 - r_0, \tag{4.2}$$

$$\begin{aligned} r_1(\tilde{z}) \approx 1 &- \frac{4\pi^2\Gamma'\Delta_c^2}{\Gamma_{1D}^3N^2} + \frac{32\pi^4\Delta_c^2\Gamma'|\Omega_0|^2}{\Gamma_{1D}^5N^4} - \frac{4i\pi^2\Delta_c}{\Gamma_{1D}N}\left(\tilde{z}-\frac{1}{2}\right) \\ &- \frac{4\pi^4\Delta_c^2(2\Gamma_{1D}+\Gamma')}{\Gamma_{1D}^3N^2}\left(\tilde{z}-\frac{1}{2}\right)^2, \end{aligned} \tag{4.3}$$

$$t_1(\tilde{z}) \approx \frac{4\pi^2\Delta_c^2\Gamma'}{\Gamma_{1D}^3N^2} - \frac{32\pi^4\Delta_c^2\Gamma'|\Omega_0|^2}{\Gamma_{1D}^5N^4} + \frac{8\pi^4\Delta_c^2\Gamma'}{\Gamma_{1D}^3N^3}\left(\tilde{z}-\frac{1}{2}\right) + \frac{4\pi^4\Delta_c^2\Gamma'}{\Gamma_{1D}^3N^2}\left(\tilde{z}-\frac{1}{2}\right)^2. \tag{4.4}$$

Here, t_1 and r_1, were obtained by solving the discrete problem, where a photon is stored in a single discrete atom and then taking the continuum limit such that the index of the atom is replaced by its position inside the ensemble $\tilde{z} = z/L$. The Ω_0 dependent terms are only relevant for determining the gate time and will be ignored for now. By aligning the interferometer, the reflection coefficients of the combined interferometer-ensemble system are given by $R_0 = -(r_0 - t_0)$ and $R_1(\tilde{z}) = -(r_1(\tilde{z}) - t_1(\tilde{z}))$ (see section 4.4 below). If we take $\tilde{z} = 1/2$ and a detuning $|\Delta_c| \sim \Gamma_{1D}N^{3/4}$, we have $r_0, t_1 \sim \Gamma'/(\Gamma_{1D}\sqrt{N})$, $r_1 \approx 1 - t_1$, and $t_0 \approx 1 - r_0$. Hence, regardless of the value of Γ'/Γ_{1D} we can achieve an ideal CP gate $R_0 = 1$, $R_1 = -1$ with sufficiently many atoms.

4.2.4 Fidelity

To quantify the errors of the gate, we calculate the Choi-Jamiolkowski (CJ) fidelity (see chapter 2). The EIT storage is described using the storage K_s and retrieval K_r kernels derived in Ref. [55] (suitably modified to take into account storage from both directions as shown in section 4.5 below). When photon A is stored and retrieved without a scattering taking place, its wave function is $\phi_{A,\text{out},0}(t) = \int\int K_r(\tilde{z},t)K_s(\tilde{z},t')\phi_{A,\text{in}}(t')\,\mathrm{d}t'\,\mathrm{d}\tilde{z}$, where $\phi_{A,\text{in}}$ is the wave function of the input photon A. Here, we use a continuum approximation of the kernels, which is relevant for the analytical calculations. For the numerical calculations, discrete definitions of the kernels are used (see e.g. equations (2.92) and (2.93)). The efficiency of the storage and retrieval is then $\eta_{\text{EIT}} = \int |\phi_{A,\text{out},0}(t)|^2\,\mathrm{d}t$. If photon B was reflected from the interferometer, while photon A was stored in the ensemble (computational basis state $|11\rangle_{AB}$), the wave function of the retrieved photon A is instead $\phi_{A,\text{out},1}(t) = \int\int K_r(\tilde{z},t)R_1(\tilde{z})K_s(\tilde{z},t')\phi_{A,\text{in}}(t')\,\mathrm{d}t'\,\mathrm{d}z$. Neglecting bandwidth effects of photon B, we obtain the CJ fidelity (equation (2.94) with $|\phi_B(\omega_B)|^2 = \delta(\omega_B - \delta_{\text{res}})$ if we assume that the frequency ω_B means two-photon detuning)

$$F_{\text{CJ}} = \frac{\eta_{\text{EIT}}}{16}\left|2t_b + R_0 - R_{1,1}\right|^2, \tag{4.5}$$

where $R_{1,1} = (1/\eta_{\mathrm{EIT}}) \int \phi^*_{A,\mathrm{out},0}(t)\phi_{A,\mathrm{out},1}(t)\,\mathrm{d}t$. If the gate is conditioned on the presence of two photons after the gate operation, we find that the success probability is (equation (2.95) with $|\phi_B(\omega_B)|^2 = \delta(\omega_B - \delta_{\mathrm{res}})$)

$$P_{\mathrm{suc}} = \frac{\eta_{\mathrm{EIT}}}{4}\left(2|t_{\mathrm{b}}|^2 + |R_0|^2 + R_{1,2}\right), \tag{4.6}$$

with $R_{1,2} = (1/\eta_{\mathrm{EIT}}) \int |\phi_{A,\mathrm{out},1}(t)|^2\,\mathrm{d}t$, and the conditional CJ fidelity is

$$F_{\mathrm{CJ,cond}} = F_{\mathrm{CJ}}/P_{\mathrm{suc}}. \tag{4.7}$$

To optimize the performance of the gate, we set $t_{\mathrm{b}} = 1$ and optimize Δ_{c} and the width of the stored spin wave $\tilde{\sigma} = \sigma/L$ such that F_{CJ} is maximal. Afterwards, for fixed optimal Δ_{c} and $\tilde{\sigma}$ we explore the effect of $t_{\mathrm{b}} < 1$. As shown below, $F_{\mathrm{CJ,cond}}$ can be substantially improved by choosing a particular $t_{\mathrm{b}} < 1$ at the cost of increasing $1 - P_{\mathrm{suc}}$ by a constant factor. Whether this is a desirable trade off, depends on the particular application. In figure 4.3(a) we plot the numerically calculated $F_{\mathrm{CJ}} \approx P_{\mathrm{suc}}$ and $F_{\mathrm{CJ,cond}}$ for the Λ-type scheme, where photon A was chosen to have a Gaussian temporal profile, and photon B is centered on $\delta = \delta_{\mathrm{res}}$ and assumed to be narrow in frequency compared to the resonance width. As seen in the figure, both F_{CJ} and $F_{\mathrm{CJ,cond}}$ approach their ideal value of unity for large N, but $F_{\mathrm{CJ,cond}}$ approaches it much faster.

For large N, we can find analytical expressions for the curves in figure 4.3(a). The stored spin wave will be approximately Gaussian so that it has the form

$$S(\tilde{z}) = (2\pi\tilde{\sigma}^2)^{-1/4} \exp\!\left(-(\tilde{z} - 1/2)^2/(4\tilde{\sigma}^2)\right). \tag{4.8}$$

Consequently, $\eta_{\mathrm{EIT}} \approx 1 - \Gamma'/(2N\Gamma_{1\mathrm{D}}\tilde{\sigma}^2)$ (see section 4.5.2 below). Neglecting distortions of photon A under storage and retrieval, but still accounting for errors due to the spatial extent of the stored excitation, we approximate $R_{1,1} \approx \int R_{1,\mathrm{s}}(\tilde{z})|S(\tilde{z})|^2\,\mathrm{d}\tilde{z}$ and $R_{1,2} \approx \int |R_{1,\mathrm{s}}(\tilde{z})|^2|S(\tilde{z})|^2\,\mathrm{d}\tilde{z}$. Here, $R_{1,\mathrm{s}}(\tilde{z}) = (R_1(\tilde{z}) + R_1(1-\tilde{z}))/2$ is a symmetrized version of R_1, which accounts for storage and scattering from both sides of the ensemble due to the Sagnac interferometer.

For fixed $\Gamma_{1\mathrm{D}}$ and large N, after choosing $\tilde{\sigma}^2 = 1/(\pi^{3/2}N^{1/4})\sqrt{\Gamma'/(\Gamma_{1\mathrm{D}} + \Gamma')}$, $\Delta_{\mathrm{c}}^2 = (\Gamma_{1\mathrm{D}}^2 N^{3/2})/(8\pi)$, and $t_{\mathrm{b}} = 1$, such that F_{CJ} is maximal, we get (see section 4.6 below)

$$F_{\mathrm{CJ},t_{\mathrm{b}}=1} \approx P_{\mathrm{suc},t_{\mathrm{b}}=1} \approx 1 - \frac{\pi\Gamma'}{\Gamma_{1\mathrm{D}}\sqrt{N}}, \tag{4.9}$$

$$F_{\mathrm{CJ,cond},t_{\mathrm{b}}=1} \approx 1 - \frac{\pi^2\Gamma'^2}{4\Gamma_{1\mathrm{D}}^2 N}. \tag{4.10}$$

If $t_{\mathrm{b}} = R_0$, $F_{\mathrm{CJ,cond}}$ is maximal, and we get

$$F_{\mathrm{CJ},t_{\mathrm{b}}=R_0} \approx P_{\mathrm{suc},t_{\mathrm{b}}=R_0} \approx 1 - \frac{2\pi\Gamma'}{\Gamma_{1\mathrm{D}}\sqrt{N}}, \tag{4.11}$$

$$F_{\mathrm{CJ,cond},t_{\mathrm{b}}=R_0} \approx 1 - \frac{11\pi^3\left(\Gamma_{1\mathrm{D}} + \Gamma'\right)\Gamma'}{16\Gamma_{1\mathrm{D}}^2 N^{3/2}}. \tag{4.12}$$

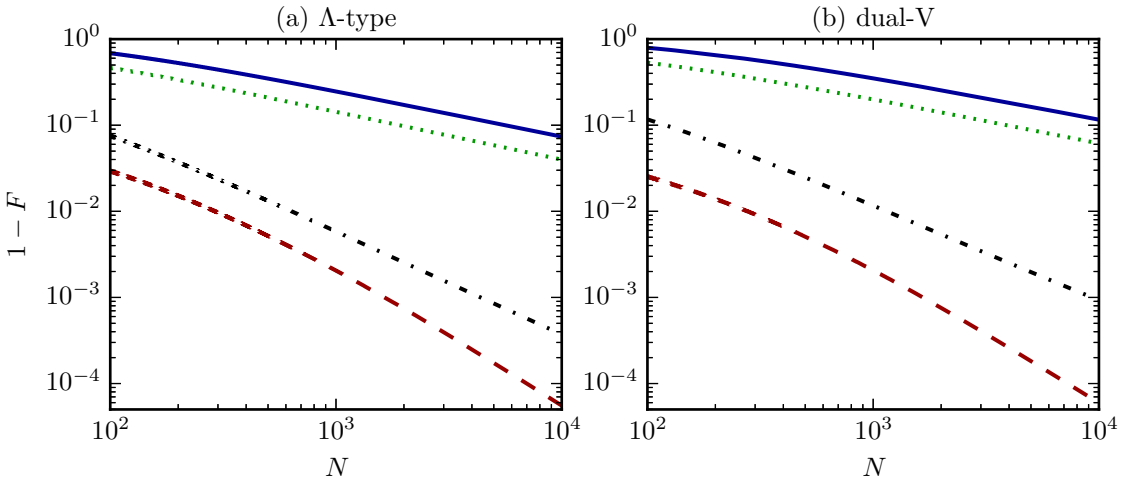

Figure 4.3: (a) Numerically calculated fidelities for the Λ-type scheme. For $t_\mathrm{b} = 1$, $F_\mathrm{CJ} \approx P_\mathrm{suc}$ and $F_\mathrm{CJ,cond}$ are shown by dotted green and dash-dotted black curves respectively. For $t_\mathrm{b} < 1$ chosen such that $F_\mathrm{CJ,cond}$ is maximal, $F_\mathrm{CJ} \approx P_\mathrm{suc}$ and $F_\mathrm{CJ,cond}$ are shown by solid blue and dashed red lines respectively. (b) The same as in (a), but using the dual-V instead and interatomic spacing $d = 0.266\pi/k_0$. The common parameters are $\Gamma_\mathrm{1D}/\Gamma = 0.5$, and $\Omega_0/\Gamma = 1$. Under EIT (storage and retrieval), $\Omega(z) = \Omega_0$. Under stationary light (scattering), $\Omega(z) = \Omega_0 \cos(k_0 z)$ and $\Omega_\pm(z) = \Omega_0 e^{\pm i k_0 z}$ for Λ-type and dual-V respectively.

These expressions confirm that the gate fidelity improves with N and that the conditional fidelities have better scaling.

In figure 4.3(b) we plot the numerically calculated fidelities F_CJ and $F_\mathrm{CJ,cond}$ for the dual-V scheme. In the simulation, the distance between the atoms was set to be incommensurate with the wavelength of the classical drive $d = 0.266\pi/k_0$. The results are, however, almost independent of d, and the gate can function even with completely random placement of the atoms (see section 4.7 below). The dual-V scheme is seen to have a very similar behavior to the Λ-type scheme.

4.2.5 Gate time

The gate time will be set both by the storage and retrieval time of photon A and the necessity of the scattered photon B to be narrow in frequency. The EIT storage and retrieval time is limited by $1/(\Gamma_\mathrm{1D} N)$ [55] and decreases with larger N. We therefore focus on the scattering of photon B.

Due to non-zero bandwidth of photon B, the reflection coefficient R_0 (at $\delta = \delta_\mathrm{res}$) in equation (4.5) should be replaced by $\int R_0(\delta)|\phi_B(\delta)|^2 \,\mathrm{d}\delta$ (see section 4.6 below), where ϕ_B is the frequency distribution of photon B. Since r_1 and t_1 vary much slower than r_0 and t_0 around $\delta = \delta_\mathrm{res}$ (vertical dotted line in figure 4.2(a)), we ignore a similar

modification to $R_{1,1}$ in equation (4.5).

We first expand the reflection coefficient r_0 around $\delta_{\rm res}$. We thereby obtain

$$r_0(\delta) \approx (2/w^2)(\delta - \delta_{\rm res})^2 + r_0(\delta_{\rm res}) \tag{4.13}$$

with

$$w = (32\sqrt{2}\Delta_{\rm c}^2|\Omega_0|^2\pi^2)/(\Gamma_{\rm 1D}^3 N^3) \tag{4.14}$$

being the resonance width. Defining the spectral width of photon B by

$$\sigma_B = \int (\delta - \delta_{\rm res})^2 |\phi_B(\delta)|^2 \,{\rm d}\delta, \tag{4.15}$$

we get $\int R_0(\delta)|\phi_B(\delta)|^2 \,{\rm d}\delta \approx R_0(\delta_{\rm res}) - (4/w^2)\sigma_B^2$. We now include the Ω_0 dependent terms in equations (4.1) and (4.2). For optimal $|\Omega_0|^2 = (\Gamma_{\rm 1D}^{5/3} N^{11/6} \sigma_B^{2/3})/(2^{5/3}\pi^{5/3}\Gamma'^{1/3})$, we get

$$F_{{\rm CJ},t_{\rm b}=1,\sigma_B} \approx F_{{\rm CJ},t_{\rm b}=1} - \frac{3\pi^{4/3}\Gamma'^{2/3}\sigma_B^{2/3}}{2^{2/3}\Gamma_{\rm 1D}^{4/3}N^{2/3}}. \tag{4.16}$$

Requiring the error from finite bandwidth to be proportional to the error in equation (4.9), we find that the required time is

$$1/\sigma_B \sim 1/(\sqrt{\Gamma_{\rm 1D}\Gamma'}N^{1/4}). \tag{4.17}$$

Hence, the gate time decreases with N.

4.2.6 Repeater secret key rate

As a direct application of the proposed CP gate, we consider quantum repeaters based on atomic ensembles [42, 43]. We modify one of the fastest known repeater protocols for atomic ensembles [82] by implementing the proposed CP gate instead of linear optics for entanglement swapping using the setup in figure 4.1(c). The secret key rate per repeater station is calculated as described in Ref. [83] and compared to the results of the original protocol (see figure 4.2(b)). This analysis is similar to the CP gate in Ref. [1] with the difference that we also consider the possibility of generating the initial entanglement using the CP gate. For a fair comparison, we consider equal storage and retrieval efficiencies for both protocols. As seen in figure 4.2(b) for $\Gamma_{\rm 1D}/\Gamma = 0.5$, the proposed gate allows improving the rate of quantum repeaters if $N \gtrsim 1000$.

4.3 Scattering coefficients for the ensemble

4.3.1 Reflection and transmission for the Λ-type scheme

4.3.1.1 Without a stored photon

Here, we derive the scattering coefficients r_0 and t_0 given by equations (4.1) and (4.2). For the Λ-type atoms, we use single-mode transfer matrices, and hence the parameter β_j

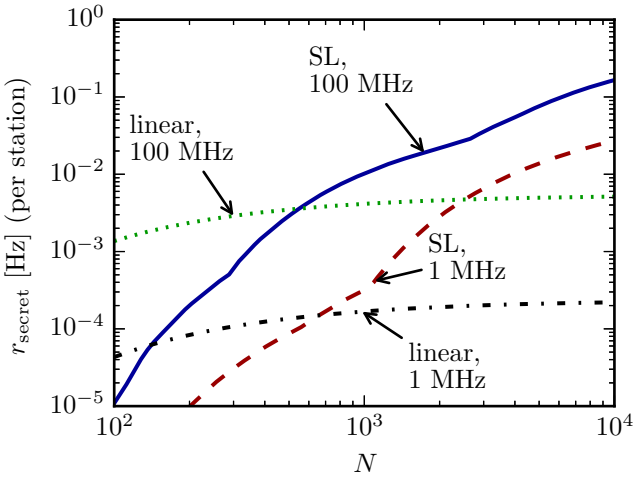

Figure 4.4: Secret key rate r_{secret} per repeater station as a function of the number of atoms N with fixed $\Gamma_{1\text{D}}/\Gamma = 0.5$ for dual-V atoms and a communication distance of 1000 km. We compare the protocol of Ref. [82] ("linear") with a modified protocol where the entanglement swapping (and also initial entanglement generation if it improves r_{secret}) is performed with the proposed stationary light CP gate ("SL"). We consider two different source repetition rates: 100 MHz and 1 MHz. We assume an attenuation length of 22 km in the fibers and an optical signal speed of 2×10^5 km/s. The ensemble storage and retrieval efficiency increases with N and is set to the same value in the original protocol as for the modified one. The photodetector efficiency is assumed to be 90%. The steps in the curves occur when the fidelity of the CP gate allows additional swap levels.

in the elements of the transfer matrices $T_{\text{a},j}$ describing the atoms with elements (3.86) is a scalar. For the Λ-type scheme, the atoms are regularly placed with distance $\pi/(2k_0)$, as shown in figure 4.5. Hence, the ensemble consists of repeated unit cells, and one can instead exponentiate the transfer matrix for a single unit cell to find the transfer matrix for the whole ensemble. We consider a unit cell that consists of two atoms and two lengths of free propagation (see figure 4.5). One of the atoms is placed on the anti-node of the standing wave of the classical drive, and the other is placed on the node. The scattering from the former ($j = 1$) is described by the parameter (3.62) with $\Omega(z_j) = \Omega_0$, i.e.

$$\beta_1 = \frac{\Gamma_{1\text{D}}\delta}{(\Gamma' - 2i\Delta)\delta + 2i|\Omega_0|^2}, \tag{4.18}$$

while the scattering for the latter ($j = 2$, an effective two-level atom) is described by the parameter (3.62) with $\Omega(z_j) = 0$, i.e.

$$\beta_2 = \frac{\Gamma_{1\text{D}}}{\Gamma' - 2i\Delta}. \tag{4.19}$$

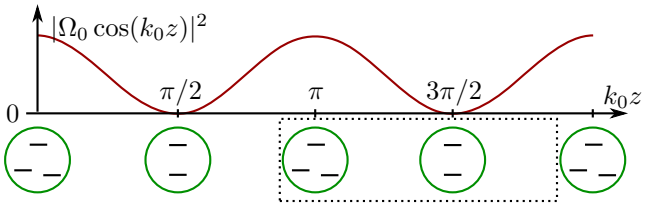

Figure 4.5: Standing wave of the Rabi frequency of classical drive for the Λ-type scheme. The circles with 2 or 3 energy levels below the plot represent how the atoms will effectively behave in the different positions, i.e. either as two-level atoms on the nodes or as Λ-type atoms on the anti-nodes. The unit cell is shown by the dotted rectangle.

The transfer matrices for the atoms $T_{\mathrm{a},j}$ have elements given by equations (3.86). The transfer matrices of free propagation T_{f} are given by equation (3.89) with $k_0 d = \pi/2$. The transfer matrix for the unit cell is then

$$T_{\mathrm{cell}} = T_{\mathrm{f}} T_{\mathrm{a},2} T_{\mathrm{f}} T_{\mathrm{a},1}. \tag{4.20}$$

Carrying out the above matrix multiplications results in

$$T_{\mathrm{cell}} = \begin{pmatrix} -(1-\beta_2)(1-\beta_1) - \beta_2\beta_1 & \beta_1(1-\beta_2) - \beta_2(1+\beta_1) \\ \beta_2(1-\beta_1) - \beta_1(1+\beta_2) & -\beta_2\beta_1 - (1+\beta_2)(1+\beta_1) \end{pmatrix}. \tag{4.21}$$

From equations (3.111) and (3.113), we then have

$$T_{\mathrm{e}} = T_{\mathrm{cell}}^{n_{\mathrm{e}}} = \cos(n_{\mathrm{e}}\theta) \begin{pmatrix} 1 & 0 \\ 0 & 1 \end{pmatrix} + \frac{\sin(n_{\mathrm{e}}\theta)}{\sin(\theta)} \begin{pmatrix} \beta_2 + \beta_1 & -\beta_2 + \beta_1 - 2\beta_2\beta_1 \\ \beta_2 - \beta_1 - 2\beta_2\beta_1 & -\beta_2 - \beta_1 \end{pmatrix} \tag{4.22}$$

with $\theta = \tilde{q} L_{\mathrm{u}}$ given by $\cos(\theta) = \mathrm{tr}(T_{\mathrm{cell}})/2 = -1 - 2\beta_2\beta_1$. From this matrix, we obtain the reflection and transmission coefficients

$$r_0 = -\frac{T_{\mathrm{e},21}}{T_{\mathrm{e},22}} = \frac{-\beta_2 + \beta_1 + 2\beta_2\beta_1}{\frac{\cos(n_{\mathrm{e}}\theta)}{\sin(n_{\mathrm{e}}\theta)} \sin(\theta) - (\beta_2 + \beta_1)}, \tag{4.23}$$

$$t_0 = \frac{1}{T_{\mathrm{e},22}} = \frac{1}{\cos(n_{\mathrm{e}}\theta) - \frac{\sin(n_{\mathrm{e}}\theta)}{\sin(\theta)}(\beta_2 + \beta_1)}. \tag{4.24}$$

The minima of r_0 and maxima of t_0 (see figure 4.2) occur when $\sin(n_{\mathrm{e}}\theta)$ in equation (4.22) is approximately equal to zero. However, exact equality is never satisfied, since θ is complex (a consequence of $\Gamma' > 0$). In the regime, where losses are small ($\mathrm{Im}[\mathrm{tr}(T_{\mathrm{cell}})] \ll 1$), the approximate resonance condition is

$$\sin\big(n_{\mathrm{e}} \arccos(\mathrm{Re}[\mathrm{tr}(T_{\mathrm{cell}})]/2)\big) = 0. \tag{4.25}$$

In the coefficients (4.23) and (4.24) we can approximate

$$\begin{aligned}\theta &= \arccos(\mathrm{tr}(T_{\mathrm{cell}})/2) \\ &\approx \arccos(\mathrm{Re}[\mathrm{tr}(T_{\mathrm{cell}})]/2) - \frac{i\,\mathrm{Im}[\mathrm{tr}(T_{\mathrm{cell}})]/2}{\sqrt{(1-\mathrm{Re}[\mathrm{tr}(T_{\mathrm{cell}})]/2)(1+\mathrm{Re}[\mathrm{tr}(T_{\mathrm{cell}})]/2)}}.\end{aligned} \tag{4.26}$$

From equation (4.25) we have

$$n_{\mathrm{e}}\arccos(\mathrm{Re}[\mathrm{tr}(T_{\mathrm{cell}})]/2) = \pi k \tag{4.27}$$

for some integer k. Since the are interested in the first reflection minimum closest to $\delta = 0$, we choose $k = n_{\mathrm{e}} - 1$. For large n, we have

$$\mathrm{Re}[\mathrm{tr}(T_{\mathrm{cell}})]/2 = \cos(\pi(n_{\mathrm{e}}-1)/n_{\mathrm{e}}) \approx -1 + \pi^2/(2n_{\mathrm{e}}^2). \tag{4.28}$$

Hence, equation (4.26) can be approximated as

$$\theta \approx \pi(n_{\mathrm{e}}-1)/n_{\mathrm{e}} - in_{\mathrm{e}}\,\mathrm{Im}[\mathrm{tr}(T_{\mathrm{cell}})]/(2\pi), \tag{4.29}$$

and we also obtain the approximate expressions:

$$\sin(n_{\mathrm{e}}\theta) \approx (-1)^{n_{\mathrm{e}}-1}\left(-in_{\mathrm{e}}^2\,\mathrm{Im}[\mathrm{tr}(T_{\mathrm{cell}})]/(2\pi)\right), \tag{4.30}$$

$$\cos(n_{\mathrm{e}}\theta) \approx (-1)^{n_{\mathrm{e}}-1}, \tag{4.31}$$

$$\sin(\theta) \approx \pi/n_{\mathrm{e}}. \tag{4.32}$$

With these approximations and using the fact that $\mathrm{Im}[\mathrm{tr}(T_{\mathrm{cell}})] = -4\,\mathrm{Im}[\beta_2\beta_1]$, equations (4.23) and (4.24) become

$$r_0 \approx \frac{-\beta_2+\beta_1+2\beta_2\beta_1}{-\frac{i\pi^2}{2n_{\mathrm{e}}^3\,\mathrm{Im}[\beta_2\beta_1]}-\beta_2-\beta_1}, \tag{4.33}$$

$$t_0 \approx \frac{(-1)^{n_{\mathrm{e}}-1}}{1-\frac{2in_{\mathrm{e}}^3\,\mathrm{Im}[\beta_2\beta_1]}{i\pi^2}(\beta_2+\beta_1)}. \tag{4.34}$$

To determine the dominant terms in equations (4.33) and (4.34), we write the approximate expressions for equations (4.18) and (4.19) in the limit, where δ is small, and $|\Delta_{\mathrm{c}}|$ is large ($\Delta = \Delta_{\mathrm{c}} + \delta$). We thereby get

$$\beta_1 \approx -i\frac{\Gamma_{1\mathrm{D}}\delta}{2|\Omega_0|^2}, \tag{4.35}$$

$$\beta_2 \approx i\frac{\Gamma_{1\mathrm{D}}}{2\Delta} + \frac{\Gamma_{1\mathrm{D}}\Gamma'}{4\Delta^2}. \tag{4.36}$$

The second term on the right hand side of equation (4.36) is included for the sole purpose of finding an approximation for $\mathrm{Im}[\beta_2\beta_1] \approx \mathrm{Re}[\beta_2]\,\mathrm{Im}[\beta_1]$. An expression for the

detuning δ can be found using equation (4.28). Expanding its left hand side in δ around 0 to second order results in

$$\frac{\Gamma_{1D}^2}{2\Delta_c|\Omega_0|^2}\delta - \frac{\Gamma_{1D}^2(|\Omega_0|^2-\Delta_c^2)}{2\Delta_c^2|\Omega_0|^4}\delta^2 + \frac{\pi^2}{2n_e^2} = 0. \tag{4.37}$$

We choose the solution, where δ and Δ_c have opposite signs (we assume $\delta > 0$ and $\Delta_c < 0$, but the opposite case should also work). Hence,

$$\frac{\delta}{|\Omega_0|^2} = \frac{\Delta_c\left(-\Gamma_{1D} + \sqrt{\Gamma_{1D} - 4(\Delta_c^2 - |\Omega_0|^2)\pi^2/n_e^2}\right)}{2\Gamma_{1D}(\Delta_c^2 - |\Omega_0|^2)} \tag{4.38}$$

Expanding this around the limit of large n we find

$$\frac{\delta}{|\Omega_0|^2} \approx -\frac{\Delta_c\pi^2}{\Gamma_{1D}^2 n_e^2} - \frac{\Delta_c^3\pi^4}{\Gamma_{1D}^4 n_e^4} + \frac{\Delta_c|\Omega_0|^2\pi^4}{\Gamma_{1D}^4 n_e^4}. \tag{4.39}$$

The first term on the right hand side of equation (4.39) could also be derived from the dispersion relation (3.99) (with $N_u = 2$), and setting $\mathrm{Re}[q]/n_0 = \pi/N$, as discussed in section 3.5.2, but the other two terms in equation (4.39) result from higher order corrections to the quadratic approximation.

When we calculate the fidelity F_{CJ} in section 4.6 below, we find that it is maximal for a detuning

$$|\Delta_c| \propto \Gamma_{1D} n_e^{3/4}. \tag{4.40}$$

If we insert this expression into (4.39), we find that the first term on the right hand side is proportional to $n_e^{-5/4}$, and the second one is proportional to $n_e^{-7/4}$. Hence, the second one is smaller for large n_e and can be neglected. We keep the third term, since it depends on Ω_0 and will be important when accounting for the non-zero bandwidth of the scattered photon.

Using only the first term in equation (4.39) and inserting it into the first term of equation (4.36), we find

$$\beta_2 \approx i\frac{\Gamma_{1D}}{2\Delta_c\left(1-(\pi^2|\Omega_0|^2)/(\Gamma_{1D}^2 n_e^2)\right)} \approx i\frac{\Gamma_{1D}}{2\Delta_c} + i\frac{|\Omega_0|^2\pi^2}{2\Delta_c\Gamma_{1D}n_e^2}. \tag{4.41}$$

Inserting into the second term of equation (4.36) gives

$$\mathrm{Re}[\beta_2] \approx \frac{\Gamma_{1D}\Gamma'}{4\Delta_c^2\left(1-(\pi^2|\Omega_0|^2)/(\Gamma_{1D}^2 n_e^2)\right)^2} \approx \frac{\Gamma_{1D}\Gamma'}{4\Delta_c^2} + \frac{|\Omega_0|^2\pi^2\Gamma'}{2\Delta_c^2\Gamma_{1D}n_e^2}. \tag{4.42}$$

Using the first and the third terms of equation (4.39) and inserting them into equation (4.35), we find

$$\beta_1 \approx -i\frac{\Gamma_{1D}}{2}\left(-\frac{\Delta_c\pi^2}{\Gamma_{1D}^2 n_e^2} + \frac{\Delta_c|\Omega_0|^2\pi^4}{\Gamma_{1D}^4 n_e^4}\right) \approx i\frac{\Delta_c\pi^2}{2\Gamma_{1D}n_e^2} - i\frac{\Delta_c|\Omega_0|^2\pi^4}{2\Gamma_{1D}^3 n_e^4}. \tag{4.43}$$

Combining equations (4.42) and (4.43) and neglecting a term of order n_e^{-6} results in

$$\mathrm{Im}[\beta_2\beta_1] \approx \mathrm{Re}[\beta_2]\,\mathrm{Im}[\beta_1] \approx \frac{\pi^2\Gamma'}{8\Delta_c n_e^2} + \frac{|\Omega_0|^2\pi^4\Gamma'}{8\Delta_c\Gamma_{1D}^2 n_e^4}. \tag{4.44}$$

Invoking equation (4.40) again and neglecting the Ω_0 dependent terms for a moment, we see that $\beta_2 \propto n_e^{-3/4}$, $\beta_1 \propto n_e^{-5/4}$ and $n_e^3\,\mathrm{Im}[\beta_2\beta_1] \propto n_e^{1/4}$. Hence, $\beta_1 \ll \beta_2$; $\beta_2, \beta_1 \ll (n_e^3\,\mathrm{Im}[\beta_2\beta_1])^{-1}$, and we can approximate equations (4.33) and (4.34) (now including the Ω_0 dependent terms) by

$$r_0 \approx -i\frac{2n_e^3}{\pi^2}\beta_2\,\mathrm{Im}[\beta_2\beta_1] \approx \frac{\Gamma_{1D}\Gamma' n_e}{8\Delta_c^2} + \frac{|\Omega_0|^2\pi^2\Gamma'}{4\Delta_c^2\Gamma_{1D} n_e}, \tag{4.45}$$

$$t_0 \approx (-1)^{n_e-1}\left(1 + i\frac{2n_e^3}{\pi^2}\beta_2\,\mathrm{Im}[\beta_2\beta_1]\right) \approx (-1)^{n_e-1}\left(1 - \frac{\Gamma_{1D}\Gamma' n_e}{8\Delta_c^2} - \frac{|\Omega_0|^2\pi^2\Gamma'}{4\Delta_c^2\Gamma_{1D} n_e}\right). \tag{4.46}$$

Since the number of atoms is $N = 2n_e$, the above expressions correspond to equations (4.1) and (4.2), except for the removal of the overall phase factor $(-1)^{n_e-1}$ for the transmission coefficient t_0 (discussed in section 4.4 below). In figure 4.6(a) we plot $|t_0|^2$ as a function of Ω_0 and show that the analytical expression in equation (4.46) matches the full expression in equation (4.24) evaluated at the resonance frequency.

To account for the non-zero bandwidth of the scattered photon, we also need the width of the resonance. After expanding the reflection coefficient r_0 around δ_{res}, we get

$$r_0(\delta) \approx (2/w^2)(\delta - \delta_{res})^2 + r_0(\delta_{res}), \tag{4.47}$$

where $r_0(\delta_{res})$ is given by equation (4.45) and

$$w = \frac{32\sqrt{2}\Delta_c^2|\Omega_0|^2\pi^2}{\Gamma_{1D}^3 N^3}, \tag{4.48}$$

is the width. Since we approximately have that $t_0 \approx 1 - r_0$, the width of the transmission resonance is w. In figure 4.6(b) we compare equation (4.48) with the numerically computed width.

4.3.1.2 With a stored photon

Here, we derive the scattering coefficients r_1 and t_1 given by equations (4.3) and (4.4). The starting point is the assumption that the photon has been stored in a single atom that is placed at the anti-node of the standing wave of the classical drive (storing in an atom that is on the node will have a negligible change in the scattering properties, unless Γ_{1D}/Γ is close to unity). The storage of a photon in the atom transfers it from state $|a\rangle$ to state $|d\rangle$, such that it behaves like a resonant two-level atom (given by the

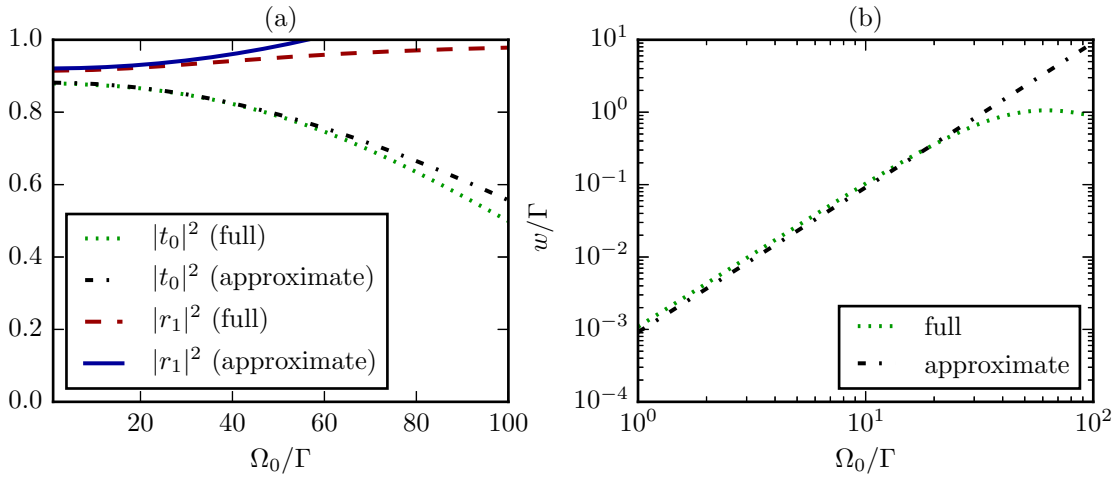

Figure 4.6: (a) Reflectance with a stored photon $|r_1|^2$ and transmittance without a stored photon $|t_0|^2$ of an ensemble of Λ-type atoms plotted as functions of the Rabi frequency of the classical drive Ω_0 and evaluated at the transmission resonance closest to $\delta = 0$ (see figure 4.2), i.e. at $\delta = \delta_{\text{res}} \approx -4\Delta_c\pi^2|\Omega_0|^2/(\Gamma_{1D}^2 N^2)$. Both t_0 and r_1 are calculated either directly from the transfer matrix with no approximations ("full"), which for t_0 is given by equation (4.24), or from the approximate expressions in equations (4.46) and (4.58) respectively ("approximate"). (b) The width of the transmission resonance calculated either from the full expression as $w = \text{Re}\left[\sqrt{4/\partial_\delta^2 t_0(\delta)}\right]\Big|_{\delta=\delta_{\text{res}}}$ or using the approximate expression (4.48) (dash-dotted black). The parameters for both (a) and (b) are: number of atoms $N = 1000$, $\Gamma_{1D}/\Gamma = 0.5$, and $\Delta_c/\Gamma = -16$. (The same as in figure 4.2 except for Ω_0, which is varied here.)

$|d\rangle \leftrightarrow |e\rangle$ transition). Therefore, the transfer matrix for the first atom in the unit cell $T_{a,1}$ with β_1 given by equation (4.18) is replaced by the transfer matrix $T_{a,1,de}$ with

$$\beta_{1,de} = \frac{\Gamma_{1D}}{\Gamma'}. \tag{4.49}$$

Hence, the transfer matrix for the unit cell containing the stored photon will be given by

$$T_{\text{cell,ph}} = T_f T_{a,2} T_f T_{a,1,de}. \tag{4.50}$$

instead of equation (4.20). If we assume that the photon is stored in the unit cell with index n_{ph}, the transfer matrix for the whole ensemble $T_{e,n_{\text{ph}}}$ is given by

$$T_{e,n_{\text{ph}}} = T_{\text{cell}}^{n_e - n_{\text{ph}}} T_{\text{cell,ph}} T_{\text{cell}}^{n_{\text{ph}}-1}. \tag{4.51}$$

From equation (4.51) we can find the scattering coefficients using

$$r_{1,n_{\mathrm{ph}}} = -\frac{T_{\mathrm{e},n_{\mathrm{ph}},21}}{T_{\mathrm{e},n_{\mathrm{ph}},22}}, \tag{4.52}$$

$$t_{1,n_{\mathrm{ph}}} = \frac{1}{T_{\mathrm{e},n_{\mathrm{ph}},22}}, \tag{4.53}$$

where $T_{\mathrm{e},n_{\mathrm{ph}},xx'}$ are the elements of the matrix $T_{\mathrm{e},n_{\mathrm{ph}}}$ similar to the definition (3.101) of the elements of the matrix T_{e}. For the numerical calculations, equations (4.52) and (4.53) are used directly.

For the analytical calculations, we can find approximate expressions for the scattering coefficients, but the procedure is rather involved. We shall therefore restrict ourselves to a brief discussion of the main steps. We do several simplifications on the (very complicated) expressions resulting from equations (4.52) and (4.53). We use the fact that $\beta_2\beta_1 = (-1-\cos(\theta))/2$ and the approximate expression $\theta \approx \pi(n_{\mathrm{e}}-1)/n_{\mathrm{e}}$. Also, while expanding the numerator and denominator around large n_{e}, we use that $\beta_2 \propto n_{\mathrm{e}}^{-3/4}$ (a consequence of equations (4.19) and (4.40)) to determine which terms can be neglected. Then we replace the index of the unit cell with the stored photon n_{ph} by $n_{\mathrm{e}}\tilde{z}$, where $\tilde{z} = z/L$ is the rescaled position coordinate. After further approximating $1/n_{\mathrm{e}} \approx 0$ and $n_{\mathrm{e}} \pm 1 \approx n_{\mathrm{e}}$, we get

$$r_1(\tilde{z}) = -\frac{\beta_{2,de}(\pi\cos(\pi\tilde{z}) - 2\beta_2 n_{\mathrm{e}}\sin(\pi\tilde{z}))^2}{\sin^2(\pi\tilde{z})\left(\pi^2 - 4\beta_2^2\beta_{2,de}n_{\mathrm{e}}^2\right) - 2\pi\beta_2^2\beta_{2,de}n_{\mathrm{e}}\sin(2\pi\tilde{z}) + \pi^2(\beta_{2,de}+1)\cos^2(\pi\tilde{z})}, \tag{4.54}$$

$$t_1(\tilde{z}) = \frac{(-1)^{n_{\mathrm{e}}-1}\pi^2}{\sin^2(\pi\tilde{z})\left(\pi^2 - 4\beta_2^2\beta_{2,de}n_{\mathrm{e}}^2\right) - 2\pi\beta_2^2\beta_{2,de}n_{\mathrm{e}}\sin(2\pi\tilde{z}) + \pi^2(\beta_{2,de}+1)\cos^2(\pi\tilde{z})}. \tag{4.55}$$

Next, we insert the expressions for β_2 and $\beta_{2,de}$ with the approximation $\Delta \approx \Delta_{\mathrm{c}}$, expand around $\tilde{z} = 1/2$, and use $|\Delta_{\mathrm{c}}| \propto \Gamma_{1\mathrm{D}} n_{\mathrm{e}}^{3/4}$ to identify which terms are dominant for large n_{e}. This results in

$$r_1(\tilde{z}) \approx 1 - \frac{\pi^2\Gamma'\Delta_{\mathrm{c}}^2}{\Gamma_{1\mathrm{D}}^3 n_{\mathrm{e}}^2} - \frac{2i\pi^2\Delta_{\mathrm{c}}}{\Gamma_{1\mathrm{D}}n_{\mathrm{e}}}\left(\tilde{z}-\frac{1}{2}\right) - \frac{\pi^4\Delta_{\mathrm{c}}^2(2\Gamma_{1\mathrm{D}}+\Gamma')}{\Gamma_{1\mathrm{D}}^3 n_{\mathrm{e}}^2}\left(\tilde{z}-\frac{1}{2}\right)^2, \tag{4.56}$$

$$t_1(\tilde{z}) \approx (-1)^{n_{\mathrm{e}}-1}\left(\frac{\pi^2\Delta_{\mathrm{c}}^2\Gamma'}{\Gamma_{1\mathrm{D}}^3 n_{\mathrm{e}}^2} + \frac{\pi^4\Delta_{\mathrm{c}}^2\Gamma'}{\Gamma_{1\mathrm{D}}^3 n_{\mathrm{e}}^3}\left(\tilde{z}-\frac{1}{2}\right) + \frac{\pi^4\Delta_{\mathrm{c}}^2\Gamma'}{\Gamma_{1\mathrm{D}}^3 n_{\mathrm{e}}^2}\left(\tilde{z}-\frac{1}{2}\right)^2\right). \tag{4.57}$$

We see that the resulting expressions do not depend on Ω_0. This is a consequence of approximating $\Delta \approx \Delta_{\mathrm{c}}$. If we use $\Delta = \Delta_{\mathrm{c}} + \delta$ together with equation (4.39), we find corrections from the dependence on Ω_0. We only need the first term in equation (4.39) to find the lowest order correction due to Ω_0. At $\tilde{z} = 1/2$, and expanding around large

n_e, we have

$$r_1 \approx 1 - \frac{\pi^2 \Delta_c^2 \Gamma'}{\Gamma_{1D}^3 n_e^2} + \frac{2\pi^4 \Delta_c^2 \Gamma' |\Omega_0|^2}{\Gamma_{1D}^5 n_e^4}, \tag{4.58}$$

$$t_1 \approx (-1)^{n_e - 1} \left(\frac{\Delta_c^2 \pi^2 \Gamma'}{\Gamma_{1D}^3 n_e^2} - \frac{2\pi^4 \Delta_c^2 \Gamma' |\Omega_0|^2}{\Gamma_{1D}^5 n_e^4} \right). \tag{4.59}$$

In figure 4.6(a), we plot $|r_1|^2$ as a function of Ω_0 and show that the analytical expression in equation (4.58) matches the full expression calculated using equation (4.52) (evaluated at the resonance frequency) without doing any approximations. In equation (4.3), we include all error terms of equation (4.56) and also add the Ω_0 dependent error term from equation (4.58). Likewise, in equation (4.4), we include all error terms of equation (4.57) and also add the Ω_0 dependent error term from equation (4.59).

4.3.2 Reflection and transmission for the dual-V scheme

For the dual-V scheme, we need two-mode (4×4) transfer matrices to describe the σ_+ and σ_- polarized modes. The transfer matrices can be calculated using sections 3.4.2 and 3.4.3. To recap, the four blocks of the transfer matrices for the atoms are given by equation (3.86), where

$$\beta_j = -(I + S_{j,r})^{-1} S_{j,r}, \tag{4.60}$$

and

$$S_{j,r} = \begin{pmatrix} r_{j,++} & r_{j,-+} \\ r_{j,+-} & r_{j,--} \end{pmatrix}. \tag{4.61}$$

If the atom is in state $|a\rangle$ (without a stored photon), we use the expressions for the elements of $S_{j,r}$ are given by equations (3.69) and (3.72). Under the assumptions $\omega_{b_+c} = \omega_{b_-c}$ and $\Omega_+ = \Omega_- = \Omega_0$, we have $\tilde{\Delta}_{tot}^{(+)} = \tilde{\Delta}_{tot}^{(-)} = \tilde{\Delta}_{tot}$, and the elements of $S_{j,r}$ become

$$r_{j,--} = r_{j,++} = -\frac{i(\Gamma_{1D}/2)\left(\tilde{\Delta}_{tot}\delta - |\Omega_0|^2\right)}{\tilde{\Delta}_{tot}^2 \delta - 2\tilde{\Delta}_{tot}|\Omega_0|^2}, \tag{4.62}$$

$$r_{j,-+} = -\frac{i(\Gamma_{1D}/2)|\Omega_0|^2}{\tilde{\Delta}_{tot}^2 \delta - 2\tilde{\Delta}_{tot}|\Omega_0|^2} e^{2ik_0 z_j}, \tag{4.63}$$

$$r_{j,+-} = -\frac{i(\Gamma_{1D}/2)|\Omega_0|^2}{\tilde{\Delta}_{tot}^2 \delta - 2\tilde{\Delta}_{tot}|\Omega_0|^2} e^{-2ik_0 z_j}. \tag{4.64}$$

If the atom is in state $|d\rangle$ (with a stored photon), it acts as a resonant V-type atoms, and hence the elements of $S_{j,r}$ are given by

$$r_{j,--} = r_{j,++} = -\frac{\Gamma_{1D}}{\Gamma}, \tag{4.65}$$

$$r_{j,-+} = r_{j,+-} = 0. \tag{4.66}$$

We will only calculate the reflection and transmission of ensembles of dual-V atoms numerically.

4.4 Sagnac interferometer and adjustment of the phases

Here, we calculate the result of scattering from the Sagnac interferometer shown in figure 4.1(d). The sequential picture of the scattering is that the incident field on one of the ports is split by the 50:50 beam splitter, gets scattered by the ensemble, and then the transmitted and reflected parts will again interfere on the same beam splitter. Thus the matrix that relates the outputs to the inputs can be written

$$M_{\text{Sagnac}} = HSH, \tag{4.67}$$

where the matrix H describes the beam splitter, and the matrix S describes the ensemble. We choose the phases of the beam splitter, such that it performs the Hadamard operation on the field, i.e.

$$H = \frac{1}{\sqrt{2}} \begin{pmatrix} 1 & 1 \\ 1 & -1 \end{pmatrix}, \tag{4.68}$$

The ensemble can, in general, have different transmission and reflection coefficients depending on, whether the field is incident from the left or right. Therefore, we write

$$S = \begin{pmatrix} r_+ & t_+ \\ t_- & r_- \end{pmatrix}, \tag{4.69}$$

where r_+ and t_+ are respectively the reflection and transmission coefficients when the field is incident from the left (propagating in the positive direction), and r_- and t_- are respectively the reflection and transmission coefficients when the field is incident from the right (propagating in the negative direction).

Multiplying the matrices, we get

$$M_{\text{Sagnac}} = \frac{1}{2} \begin{pmatrix} r_+ + t_+ + (r_- + t_-) & r_+ - t_+ - (r_- - t_-) \\ r_+ + t_+ - (r_- + t_-) & r_+ - t_+ + (r_- - t_-) \end{pmatrix}. \tag{4.70}$$

For a standard (non-rotating) Sagnac interferometer where $r_+ = r_-$ and $t_+ = t_-$, we recover the well known result, that light always leaves the port in which it is incident [80, 81]. Because the equality $r_+ = r_-$ need not be true, the off-diagonal entries of M_{Sagnac} are, in general, not zero and describe the leakage of the incident power to the other port of the Sagnac interferometer. However, due to the sequential operation of the gate, this leakage does not introduce any logic errors. Since scattering of photon B happens, while photon A is stored inside the ensemble, leakage of photon B into the rail that encodes state $|1\rangle_A$ (see figure 4.1(c)) is separated in time from the subsequent retrieval of photon A and hence can be either absorbed or rerouted along a different path.

Even though the off-diagonal entries of M_{Sagnac} are non-zero in general, they are strongly suppressed in the ideal limit, since e.g. both r_+ and r_- approach the same value (either 1 or 0 depending on, whether a photon was stored in the ensemble or not). As a concrete example, for the Λ-type scheme, we can use equation (4.22) and find

$$r_{0+} = -\frac{T_{\text{e},21}}{T_{\text{e},22}} = \frac{-\beta_2 + \beta_3 + 2\beta_2\beta_3}{\frac{\cos(n_\text{e}\theta)}{\sin(n_\text{e}\theta)}\sin(\theta) - (\beta_2 + \beta_3)}, \tag{4.71}$$

$$r_{0-} = \frac{T_{\text{e},12}}{T_{\text{e},22}} = \frac{-\beta_2 + \beta_3 - 2\beta_2\beta_3}{\frac{\cos(n_\text{e}\theta)}{\sin(n_\text{e}\theta)}\sin(\theta) - (\beta_2 + \beta_3)}, \tag{4.72}$$

where r_{0+} is the same as r_0 (4.23), and r_{0-} is the reflection coefficient where the field is incident from the right instead of the left. The difference between equations (4.71) and (4.72) is only in the sign of the term $2\beta_2\beta_3$ in the numerator. As discussed above equation (4.45), this term is much smaller than β_2 in the limit of large number of atoms and has therefore been neglected in equation (4.45). Hence, equation (4.45) can serve as an approximate expression for both r_{0+} and r_{0-}. We also note that it can be shown that the transmission coefficient for any 2×2 transfer matrix is independent of whether the field is incident from one side or the other (given by equation (4.24) for t_0). However, we still account for the possible difference in the scattering coefficients in the numerical calculations (both for 2×2 and 4×4 transfer matrices) by defining the scattering coefficients R_0 and R_1 in equations (2.93) and (2.94) as

$$R_0 = -(r_{0+} + r_{0-} - (t_{0+} + t_{0-}))/2, \tag{4.73}$$

$$R_1 = -(r_{1+} + r_{1-} - (t_{1+} + t_{1-}))/2, \tag{4.74}$$

where the scattering coefficients with "+" in the subscript assume incident photon from the left of the ensemble and the scattering coefficients with "−" in the subscript assume incident photon from the right of the ensemble. Similar definitions are made for the scattering coefficients $R_{0,n}$ and $R_{1,n}$ in equations (2.79) and (2.81).

We also need to discuss the choice of the phases in the interferometer. In equation (4.67) there is an implicit assumption that the lengths of free propagation in the interferometer are chosen such that the distance from the beam splitter to either end of the ensemble is a multiple of the wavelength $\lambda = 2\pi/k_0$. Hence, the phase of free propagation is equal to unity for these parts. What we call "ensemble" may also contain some length of free propagation to the right of the ensemble to adjust the phases of its scattering coefficients.

To illustrate the necessity of phase adjustment, note that there is an overall phase factor $(-1)^{n_\text{e}-1}$ in equations (4.46), (4.57), and (4.59) compared with equations (4.2) and (4.4). When $r_{0\pm} \approx 0$ and $|t_{0\pm}| \approx 1$, the factor $(-1)^{n_\text{e}-1}$ directly appears as the overall phase of R_0. Hence, the ideal value $R_0 = 1$ can only be obtained for odd n_e. There are similar phase factor considerations for R_1 due to the phase factor of the reflection coefficient r_{0-} (r_{0+} is assumed to be at $z = 0$ and hence does not acquire phase factors with changing ensemble length). If the overall phase of the transmission coefficients

is adjusted, the correct phase of R_0 and R_1 is obtained and the controlled-phase gate operation can approach the ideal limit as the number of the atoms is increased.

For the dual-V scheme, we can choose any inter-atomic spacing d, which is not a multiple of $\pi/(2k_0)$ (see figure 4.11 below). For this general case, we expect that instead of the overall phase factor $(-1)^{n_e-1}$, the transmission coefficients have the phase factor $\exp(ik_0L+\pi)$, which we likewise remove by adding a distance of free propagation d_{extra} to the right of the ensemble chosen such that $\exp(ik_0d_{\text{extra}}) = \exp(-ik_0L-\pi)$. Multiplying this extra matrix of free propagation modifies the scattering coefficients according to

$$\begin{aligned} r_{0+} &\to r_{0+}, \\ r_{0-} &\to r_{0-}\exp(2ik_0d_{\text{extra}}) \\ t_{0\pm} &\to t_{0\pm}\exp(ik_0d_{\text{extra}}). \end{aligned} \tag{4.75}$$

The physical interpretation of this mathematical result is that, since the free propagation was added on the right of the ensemble, then reflection for the field incident from the left (r_{0+}) is unaffected, while the reflection coefficient for fields incident from the right (r_{0-}) acquires twice the propagation phase. The transmission coefficients only acquire the propagation phase once.

The phase adjustments above effectively force the interferometer round trip length to be equal to an odd multiple of half wavelengths ($\exp(ik_0(L + d_{\text{extra}})) = -1$). Hence, the phase adjustment can be made independent of the number of atoms.

4.5 EIT storage and retrieval

4.5.1 Overview

We will model the EIT storage and retrieval process in three different ways:

1. Using the dispersion relation (see for instance Ref. [65] and section 4.5.2 below).
2. Using the fully discrete theory (see Ref. [84] and section 4.5.3 below).
3. Using the storage and retrieval kernels (see Ref. [55] and section 4.5.4 below).

We will consider the so-called adiabatic EIT storage [55], where a single-photon wave packet is incident on the ensemble and is mapped onto a spin wave (a superposition of states, where a single atom is in state $|c\rangle$ and the rest are in state $|a\rangle$). We assume a constant Rabi frequency of the classical drive $\Omega(z,t) = \Omega_0$, but choosing a co-propagating classical drive with Rabi frequency $\Omega(z,t) = \Omega_0 e^{\pm ik_0 z}$ will only change the spatially-dependent phase factor of the stored spin wave. In the limit of high storage efficiency, the temporal profile of the photon and the spatial profile of the stored spin wave will approximately have the same form. E.g. if a photon with Gaussian temporal wave packet is stored, the resulting spin wave will have a Gaussian spatial profile. This is a consequence of the time-independent Rabi frequency of the classical drive and allows us to use the EIT dispersion relation to describe the storage and retrieval.

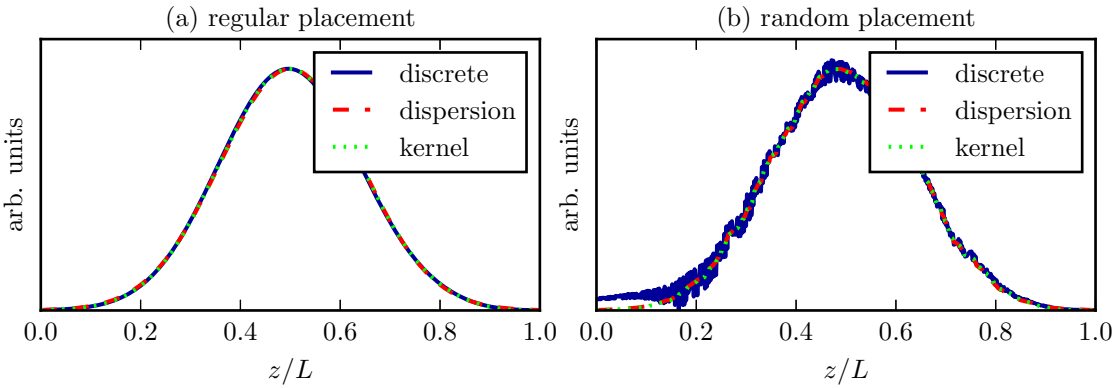

Figure 4.7: The stored Gaussian spin wave computed using three different models for EIT storage: the dispersion relation of section 4.5.2 ("dispersion"), the fully discrete theory of section 4.5.3 ("discrete"), and the storage kernel of section 4.5.4 ("kernel"). Contrary to the fidelity calculations, here we assume EIT storage from one side (left) only, to show the influence of random placement of the atoms more clearly. The common parameters for the two subplots are $\Gamma_{1D}/\Gamma = 0.5$, $N = 1000$, $\Omega_0/\Gamma = 1$, $\sigma/L = 0.1$ (width of the stored Gaussian spin wave). (a) Regularly placed atoms are assumed with inter-atomic distance $d = 0.266\pi/k_0$. All three curves are nearly indistinguishable from each other. (b) Randomly placed atoms, where the position of each atom is chosen from a uniform distribution over the whole ensemble. The average density is the same as in (a). The curve for the fully discrete storage is clearly distinct from the two others and exhibits rapid variation with position.

The EIT dispersion relation is used to gain intuition about the storage and retrieval process and also for the analytical calculations. In the numerical calculations of the fidelities and success probability, the atoms are always modeled as being discrete. Using the fully discrete EIT storage and retrieval model (section 4.5.3) becomes very costly as the number of atoms increases. Therefore, to be able to calculate fidelities with a large number of atoms, we instead use the less computationally demanding storage and retrieval kernels derived in the continuum model and suitably discretized (section 4.5.4). In figure 4.7, we show that the three models agree very well for the case of regularly placed ensembles with large optical depth $d_{\text{opt}} = 2N\Gamma_{1D}/\Gamma = 1000$. For randomly placed atoms, the fully discrete theory gives noticeably different results compared to using the discretized continuum theories (dispersion relation or storage kernel). Since we assume regular placement for the curves in figure 4.3, the discretized storage and retrieval kernels are sufficient. We also verify this in figure 4.8 below for the Λ-type scheme, and the same conclusion holds for the dual-V scheme. In figure 4.12 below, where we show fidelities for randomly placed atoms, we only use the fully discrete model for storage and retrieval, even though it limits the maximal number of atoms that can be used in the calculations.

4.5.2 Using the dispersion relation

The adiabatic EIT storage and retrieval can be modeled in a particularly simple way if the influence of the interface between the atomic medium and vacuum is ignored. To use the EIT dispersion relation, we need to assume that the ensemble is of an infinite extent. However, to compute the the storage and retrieval efficiency, we need to assume propagation through a finite ensemble. In the calculations below, this is reflected in infinite bounds for the integration but a finite propagation length. The only processes that happen in this model is that the stored photon wave packet broadens in space as it propagates, and its norm decays due to spontaneous emission. The EIT storage and retrieval efficiency will then be the norm of the wave packet that has propagated for the full length of the ensemble L (with a stop at $L/2$ to allow for the second photon to be scattered off the ensemble).

The EIT dispersion relation is [65]

$$\delta_k \approx v_{\rm g}(k-k_0) + \frac{1}{2}\alpha(k-k_0)^2 \tag{4.76}$$

with

$$v_{\rm g} = \frac{2L|\Omega_0|^2}{N\Gamma_{\rm 1D}}, \quad \alpha = -i\frac{4L^2|\Omega_0|^2\Gamma'}{N^2\Gamma_{\rm 1D}^2}. \tag{4.77}$$

In rescaled coordinates $\tilde{z} = z/L$ and wave vectors $\tilde{k} = kL$ the dispersion can be written

$$\delta_{\tilde{k}} \approx \tilde{v}_{\rm g}(\tilde{k}-\tilde{k}_0) + \frac{1}{2}\tilde{\alpha}(\tilde{k}-\tilde{k}_0)^2 \tag{4.78}$$

with

$$\tilde{v}_{\rm g} = \frac{v_{\rm g}}{L} = \frac{2|\Omega_0|^2}{N\Gamma_{\rm 1D}}, \quad \tilde{\alpha} = \frac{\alpha}{L^2} = -i\frac{4|\Omega_0|^2\Gamma'}{N^2\Gamma_{\rm 1D}^2}. \tag{4.79}$$

We only consider incident photons where the temporal profile is Gaussian. When such a photon is mapped onto a stored excitation, this results in an approximately Gaussian spatial profile of the form

$$S(\tilde{z}) = \frac{1}{(2\pi\tilde{\sigma}^2)^{1/4}}\exp\left(-\frac{(\tilde{z}-\tilde{\mu})^2}{4\tilde{\sigma}^2}\right)e^{i\tilde{k}_0\tilde{z}}, \tag{4.80}$$

where the rescaled quantities are $\tilde{\sigma} = \sigma/L$, $\tilde{\mu} = \mu/L$, $\tilde{k}_0 = \tilde{k}_0 L$. By Fourier transforming this wave function to get $\tilde{S}(\tilde{k})$, multiplying the Fourier transform by $\exp(-i\delta_{\tilde{k}}t)$ and Fourier transforming back we find

$$S(\tilde{z},t) = \frac{1}{(2\pi\tilde{\sigma}^2)^{1/4}}\sqrt{\frac{1}{1+i\tilde{\alpha}t/(2\tilde{\sigma}^2)}}\exp\left(-\frac{(\tilde{z}-\tilde{\mu}-\tilde{v}_{\rm g}t)^2}{4\tilde{\sigma}^2\left(1+i\tilde{\alpha}t/(2\tilde{\sigma}^2)\right)}\right)e^{i\tilde{k}_0\tilde{z}}. \tag{4.81}$$

The norm squared of the wave packet at time $t \geq 0$ is given by

$$\mathcal{N}_S^2(t) = \int_{-\infty}^{\infty} |f(z,t)|^2 dz = \frac{1}{\sqrt{1 + i\tilde{\alpha}t/(2\tilde{\sigma}^2)}}. \tag{4.82}$$

The combined storage and retrieval efficiency is given by equation (4.82) with $t = 1/\tilde{v}_\mathrm{g} = L/v_\mathrm{g}$, i.e. the time required to pass the whole ensemble. We thereby get

$$\eta_\mathrm{EIT} = \mathcal{N}_S^2(t = 1/\tilde{v}_\mathrm{g}) = \frac{1}{\sqrt{1 + \frac{\Gamma'}{N\Gamma_\mathrm{1D}\tilde{\sigma}^2}}} \approx 1 - \frac{1}{2}\frac{\Gamma'}{N\Gamma_\mathrm{1D}\tilde{\sigma}^2}. \tag{4.83}$$

4.5.3 Using the fully discrete theory

Using the intuition about EIT from section 4.5.2, one can implement the numerical simulations of EIT storage and retrieval accounting for the discrete nature of atoms. This approach is very similar to the "electric field elimination" approach of Ref. [84]. The main difference is that, since storage and retrieval of a single photon only requires calculating the dynamics in the atomic single-excitation manifold, we can eliminate the electric field directly in the Schrödinger picture instead of the Heisenberg picture like in Ref. [84].

The Hamiltonian for the ensemble of Λ-type atoms coupled to the electric field is given by equations (3.26), where the atomic operators are given by equation (3.1) and preserve the discrete nature of the atoms. For EIT storage and retrieval we assume that the detuning Δ_0 is always set to zero during storage and retrieval (this was also assumed in section 4.5.2 above). However, if desired, off-resonant ($\Delta_0 \neq 0$) EIT storage and retrieval is also possible [55], and hence we keep the Δ_0 term in the equations of motion below. On the other hand, we set $\Omega(z) = \Omega_0$ from the beginning.

Compared to chapter 3, where we have calculated the dynamics using Heisenberg equations of motion and subsequently reinterpreted operators as complex-valued functions, we will use the Schrödinger picture here to be more explicit about the states of the atoms and the field. These two ways are entirely equivalent. On the single-excitation manifold, the state can be written

$$\begin{aligned} |\psi(t)\rangle = &\sum_j \left(P_j(t)\hat{\sigma}_{ba,j} + S_j(t)\hat{\sigma}_{ca,j}\right)|a\rangle^N|\mathrm{vac}\rangle \\ &+ \left(\int \frac{\Phi_+(z,t)}{\sqrt{c}}\hat{\mathcal{E}}_+^\dagger(z)|\mathrm{vac}\rangle\,\mathrm{d}z + \int \frac{\Phi_-(z,t)}{\sqrt{c}}\hat{\mathcal{E}}_-^\dagger(z)|\mathrm{vac}\rangle\,\mathrm{d}z\right)|a\rangle^N. \end{aligned} \tag{4.84}$$

From the Schrödinger equation, we get the equations of motion for the atomic coefficients

$$\frac{\partial P_j}{\partial t} = i\left(\Delta_0 + i\frac{\Gamma'}{2}\right)P_j + i\Omega_0 S_j + i\sqrt{\frac{\Gamma_\mathrm{1D}}{2}}\left(\Phi_+(z_j,t)e^{ik_0 z_j} + \Phi_-(z_j,t)e^{-ik_0 z_j}\right), \tag{4.85}$$

$$\frac{\partial S_j}{\partial t} = i\delta_0 S_j + i\Omega_0^* P_j, \tag{4.86}$$

where $\Gamma_{1D} = 4\pi g^2/c$. For the electric field coefficients $\Phi_\pm$ we have the equations

$$\left(\frac{\partial}{\partial t} \pm c\,\frac{\partial}{\partial z}\right)\Phi_\pm(z,t) = ic\sqrt{\frac{\Gamma_{1D}}{2}}\sum_j \delta(z-z_j)P_j e^{\mp ik_0 z_j}. \tag{4.87}$$

These equations can be formally solved, so that we obtain

$$\Phi_\pm(z,t) = \Phi_{\pm,\mathrm{in}}(z \mp ct) + i\sqrt{\frac{\Gamma_{1D}}{2}}\sum_j \theta\big(\pm(z-z_j)\big)\,P_j\left(t \mp \frac{z-z_j}{c}\right)e^{\mp ik_0 z_j}, \tag{4.88}$$

where $\Phi_{\pm,\mathrm{in}}(z \pm ct)$ are the input fields, and θ is the Heaviside theta function. Inserting these solutions into equation (4.85) and approximating $P_j\big(t-|z-z_j|/c\big) \approx P_j(t)$ [84], we find

$$\begin{aligned}\frac{\partial P_j}{\partial t} = i\left(\Delta_0 + i\frac{\Gamma'}{2}\right)P_j + i\Omega_0 S_j + \frac{\Gamma_{1D}}{2}\sum_{j'} P_{j'}e^{ik_0|z_j-z_{j'}|} \\ + i\sqrt{\frac{\Gamma_{1D}}{2}}\left(\Phi_{+,\mathrm{in}}(z_j-ct)e^{ik_0 z_j} + \Phi_{-,\mathrm{in}}(z_j+ct)e^{-ik_0 z_j}\right).\end{aligned} \tag{4.89}$$

The fidelity calculations in chapter 2 are formulated in terms of $\phi_{A,\mathrm{in}}(t)$ and $\phi_{A,\mathrm{out}}(t)$, which are respectively the input field to be stored and the retrieved output field. In that chapter, several kinds of retrieved output fields are defined, but for the general discussion of storage and retrieval, the difference between them is not important. We need to account for the beam splitter in the Sagnac interferometer. Hence, the relations between the fields in this section and chapter 2 are

$$\Phi_{+,\mathrm{in}}(z_j-ct) = \frac{1}{\sqrt{2}}\phi_{A,\mathrm{in}}(t-z_j/c), \tag{4.90}$$

$$\Phi_{-,\mathrm{in}}(z_j+ct) = \frac{1}{\sqrt{2}}\phi_{A,\mathrm{in}}(t-(L-z_j)/c), \tag{4.91}$$

$$\phi_{A,\mathrm{out}}(t) = \frac{1}{\sqrt{2}}\left(\Phi_+(L,t) + \Phi_-(0,t)\right). \tag{4.92}$$

Note that storage is done from two directions in order to ensure that no excitations are stored on atoms at the nodes of the standing wave of the classical drive applied during the scattering for the Λ-type scheme. The conditions for this may not necessarily be the same as the conditions derived for scattering from the Sagnac interferometer (see section 4.4). If this is an issue, it can be compensated by adjusting the position of the atoms between storage and scattering, e.g., by adjusting the phases of the trapping lasers or of the classical drives. For the dual-V scheme, there is no phase requirement during storage and this is not a concern.

As the input wave function, we assume

$$\phi_{A,\mathrm{in}}(t) = \frac{1}{(2\pi\sigma_{\mathrm{in}}^2)^{1/4}}\exp\left(-\frac{(t-\mu_{\mathrm{in}}/c)^2}{4\sigma_{\mathrm{in}}^2}\right) \tag{4.93}$$

where the width and central time

$$\sigma_{\text{in}} = \sigma / \left(v_{\text{g}} \sqrt{1 + i\alpha L/(4\sigma^2 v_{\text{g}})} \right), \tag{4.94}$$

$$\mu_{\text{in}} = 4\sigma_{\text{in}}, \tag{4.95}$$

are defined in terms of the EIT group velocity (4.77). The factor $\sqrt{1 + i\alpha L/(4\sigma^2 v_{\text{g}})}$ (a real number, since α is imaginary) in the definition of σ_{in} is introduced to compensate for the spin wave becoming wider as it propagates inside the ensemble (see equation (4.81)). This particular factor is chosen such that the stored Gaussian spin wave (centered at the position $L/2$) has width σ. In the end, since we optimize over σ, this adjustment has no effect on the final values of the numerically calculated fidelities and success probability. However, it ensures that the optimal σ in the numerical calculations is similar to the optimal value found by neglecting broadening of the spin wave under propagation.

In the fully discrete model, we do not explicitly calculate the storage and retrieval kernels that appear in equations (2.71), (2.80), (2.81), (2.92) and (2.93). Instead, we calculate the action of these kernels on respectively a specific $\phi_{A,\text{in}}(t)$ or a spin wave given by the coefficients S_j. For storage, this amounts to numerically solving equations (4.86) and (4.89) for a given $\phi_{A,\text{in}}(t)$ and the initial condition $P_j = S_j = 0$ at $t = 0$. We take the stored spin wave to be the coefficients S_j at $t = \mu_{\text{in}}/c + L/(2v_{\text{g}})$. This final time is the sum of the time for propagation through vacuum and (half of) the EIT medium. For retrieval, equations (4.86) and (4.89) are solved with $\phi_{A,\text{in}}(t) = 0$ under the initial conditions that at $t = 0$ the coefficients $S_j(t = 0)$ are set to the spin wave that is to be retrieved, and $P_j(t = 0) = 0$. At each time step, we calculate $\phi_{A,\text{out}}(t)$ using equations (4.88) with $P_j\big(t \mp (z - z_j)/c\big) \approx P_j(t)$ along with equation (4.92). We assume that the retrieval happens until $t = L/v_{\text{g}}$, i.e. the time that it takes for the EIT polaritons to move through the whole ensemble.

4.5.4 Using the storage and retrieval kernels

As an approximation to the fully discrete theory of section 4.5.3, one can use the continuum theory of Ref. [55]. The continuum approximation allows the derivation of explicit expressions for the linear maps (given in terms of integration with a particular kernel) describing storage and retrieval.

To make the continuum approximation, we use the Hamiltonian in the form (3.26) (with $\Omega(z) = \Omega_0$). Instead of the state (4.84), we use

$$\begin{aligned} |\psi(t)\rangle = & \int \left(\frac{\sqrt{N}}{L} P(z,t)\hat{\sigma}_{ba}(z) + \frac{\sqrt{N}}{L} S(z,t)\hat{\sigma}_{ca}(z) \right) |a\rangle^N |\text{vac}\rangle \, \mathrm{d}z \\ & + \left(\int \frac{\Phi_+(z,t)}{\sqrt{c}} \hat{\mathcal{E}}_+^\dagger(z)|\text{vac}\rangle \, \mathrm{d}z + \int \frac{\Phi_-(z,t)}{\sqrt{c}} \hat{\mathcal{E}}_-^\dagger(z)|\text{vac}\rangle \, \mathrm{d}z \right) |a\rangle^N. \end{aligned} \tag{4.96}$$

Note that if, for example, the excitation is entirely in the metastable states at a time t,

we have

$$1 = \langle\psi(t)|\psi(t)\rangle = \frac{N}{L^2}\int\int S^*(z,t)S(z',t)[\hat{\sigma}_{ab}(z),\hat{\sigma}_{ba}(z')]\,\mathrm{d}z = \frac{1}{L}\int\int |S(z,t)|^2\,\mathrm{d}z, \tag{4.97}$$

where we have used the continuum approximation $\sum_j \delta(z-z_j) \approx n_0$ (as discussed in section 3.3.1 for the Heisenberg picture) together with the low excitation approximation $\sigma_{aa,j} \approx 1$ to get $\sigma_{aa}(z) \approx 1$ and $\sigma_{bb} \approx 0$. Equation (4.97) also gives the normalization condition for S in the continuum model (and similarly for P).

The equations for the coefficients are

$$\left(\frac{\partial}{\partial t} \pm c\,\frac{\partial}{\partial z}\right)\Phi_\pm(z,t) = ic\sqrt{\frac{\Gamma_{1\mathrm{D}}N}{2}}\frac{1}{L}P(z,t), \tag{4.98}$$

$$\begin{aligned}\frac{\partial}{\partial t}P(z,t) = i\left(\Delta_0 + i\frac{\Gamma'}{2}\right)P(z,t) + i\Omega_0 S(z,t)\\ + i\sqrt{\frac{\Gamma_{1\mathrm{D}}N}{2}}\left(\Phi_+(z,t)e^{ik_0z} + \Phi_-(z,t)e^{-ik_0z}\right),\end{aligned} \tag{4.99}$$

$$\frac{\partial}{\partial t}S(z,t) = i\delta_0 S(z,t) + i\Omega_0^* P(z,t). \tag{4.100}$$

As an extension to the theory of Ref. [55], we want to consider an input field which is, in general, incident from both sides instead of only one. The approach that we use is to consider the parts of the single photon excitation incident from both sides as being stored separately from each other. When doing this we ignore the fact that the two parts have opposite spatial phases $e^{\pm ik_0z}$, which interfere inside the ensemble to produce a spatially modulated spin wave with amplitude proportional to $\cos(k_0z)$.

This spatial modulation of the stored spin wave is very important for the Λ-scheme, since the part of the excitation that is stored on the nodes of the standing wave of the classical drive does not significantly change the scattering properties of the ensemble (see section 4.3.1.2). Expressed in terms of the notation introduced in the fidelity calculations (see equations (2.93) and (2.94)) we have $R_{1,j}(\omega_B) \approx R_0(\omega_B)$ for odd j with atoms placed at positions $z_j = j\pi/(2k_0)$ $(0 \le j \le N-1)$, i.e. k_0z_j being an odd multiple of $\pi/2$. With the photon incident from both sides, we ensure that there is no amplitude on these atoms, since $S(z_j) \propto \cos(k_0z_j) = 0$ for odd j. This is correctly reproduced by the fully discrete model of section 4.5.3, since it always accounts for the phases of free propagation. On the other hand, due to the removal of the rapidly varying spatial phases in the continuum theory, this factor $\cos(k_0z_j)$ is not present in the two separate parts of the stored spin wave. To compensate for this, we set $R_{1,j}(\omega_B) = R_{1,j-1}(\omega_B)$ for odd j. As we show in figure 4.8, this phenomenological adjustment of the reflection coefficient gives results that are essentially indistinguishable from the results produced by the fully discrete model of section 4.5.3. For the dual-V scheme, no such adjustment of the reflection coefficients is needed neither in the continuum nor the discrete model, which also produce indistinguishable results.

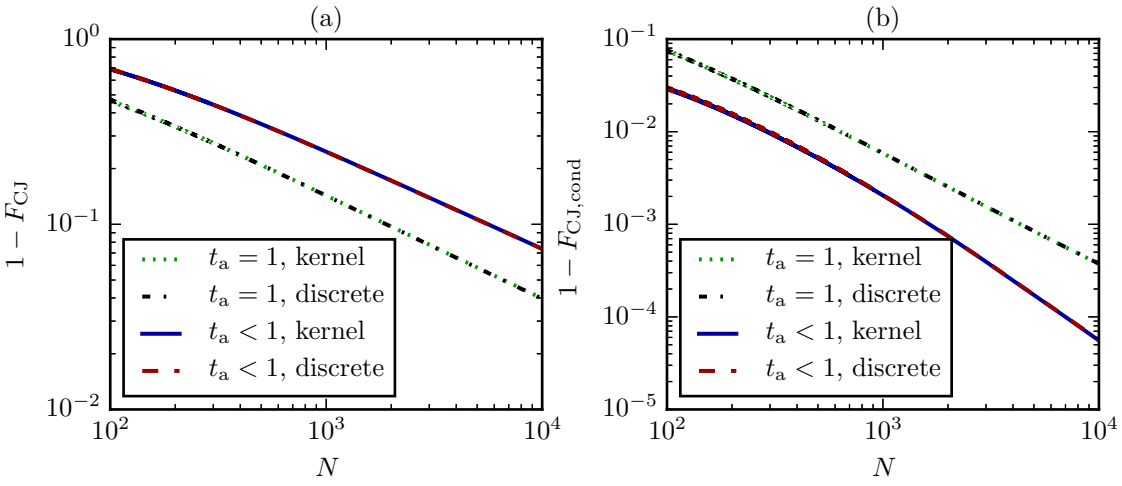

Figure 4.8: Comparison of (a) unconditional and (b) conditional Choi-Jamiolkowski fidelities for the Λ-type scheme with different models used for EIT storage and retrieval plotted as functions of the number of atoms N with fixed $\Gamma_{1\mathrm{D}}/\Gamma = 0.5$. The "discrete" plots use the fully discrete theory of section 4.5.3, and the "kernel" plots use the discretized storage and retrieval kernels derived in section 4.5.4. In both cases, the optimal Δ_{c} and $\tilde{\sigma}$ (width of the stored Gaussian spin wave) are found by doing numerical optimization using the discretized storage and retrieval kernels, since the fully discrete model is much more computationally demanding.

The photons incident from the left and right couple to different components of the atomic coefficients, which can be written

$$P(z,t) = P_+(z,t)e^{ik_0 z} + P_-(z,t)e^{-ik_0 z}, \tag{4.101}$$

$$S(z,t) = S_+(z,t)e^{ik_0 z} + S_-(z,t)e^{-ik_0 z}. \tag{4.102}$$

After inserting these definitions into equations (4.98), (4.99) and (4.100) and separating the components, we get

$$\left(\frac{\partial}{\partial t} \pm c\,\frac{\partial}{\partial z}\right)\Phi_\pm(z,t) = ic\sqrt{\frac{\Gamma_{1\mathrm{D}}N}{2}}\frac{1}{L}P_\pm(z,t), \tag{4.103}$$

$$\frac{\partial}{\partial t}P_\pm(z,t) = i\left(\Delta_0 + i\frac{\Gamma'}{2}\right)P_\pm(z,t) + i\Omega_0 S_\pm(z,t) + i\sqrt{\frac{\Gamma_{1\mathrm{D}}N}{2}}\Phi_\pm(z,t), \tag{4.104}$$

$$\frac{\partial}{\partial t}S_\pm(z,t) = i\delta_0 S_\pm(z,t) + i\Omega_0^* P_\pm(z,t), \tag{4.105}$$

To solve for Φ_+, P_+ and S_+, the approach in Ref. [55] can be directly used. It consists of transforming into the coordinates $\tilde{z} = z/L$ and $\tilde{t} = t - z/c$, Laplace transforming in space, solving the algebraic equations of the Laplace transforms (under the adiabatic

approximation $\frac{\partial}{\partial t}P_+ \approx 0$) and then Laplace transforming back. As a minor modification, we also transform back from the co-propagating time coordinate $\tilde{t} = t - z/c$ to the original t (by replacing all $\tilde{t}$ by t in the final expressions). Solving for Φ_-, P_- and S_- is simply a spatial reflection of the original problem around $\tilde{z} = 1/2$. We find that the stored spin wave is

$$S_+(\tilde{z},t) = \int_0^t K_\mathrm{s}(\tilde{z}, t-t')\Phi_+(\tilde{z}=0,t')\,\mathrm{d}t', \tag{4.106}$$

$$S_-(\tilde{z},t) = \int_0^t K_\mathrm{s}(1-\tilde{z}, t-t')\Phi_-(\tilde{z}=1,t')\,\mathrm{d}t', \tag{4.107}$$

where the storage kernel (in the adiabatic approximation) is

$$K_\mathrm{s}(\tilde{z},t) \approx -\frac{\sqrt{b}\Omega_0^* e^{i\delta_0 t}}{(\Gamma'/2) - i\Delta_0} I_0\left(2\frac{\sqrt{|\Omega_0|^2 tb\tilde{z}}}{(\Gamma'/2)-i\Delta_0}\right)\exp\left(-\frac{|\Omega_0|^2 t + b\tilde{z}}{(\Gamma'/2)-i\Delta_0}\right), \tag{4.108}$$

written in terms of $b = (N\Gamma_{1\mathrm{D}})/2$ (related to the resonant optical depth by $d_\mathrm{opt} = 4b/\Gamma$) and the modified Bessel function of the first kind I_0. The retrieved field is

$$\Phi_+(\tilde{z}=1,t) = \int_0^1 K_\mathrm{r}(\tilde{z},t)S_+(\tilde{z},t=0)\,\mathrm{d}\tilde{z}, \tag{4.109}$$

$$\Phi_-(\tilde{z}=0,t) = \int_0^1 K_\mathrm{r}(1-\tilde{z},t)S_-(\tilde{z},t=0)\,\mathrm{d}\tilde{z}, \tag{4.110}$$

where the retrieval kernel is

$$K_\mathrm{r}(\tilde{z},t) \approx -\frac{\sqrt{b}\Omega_0 e^{i\delta_0 t}}{(\Gamma'/2) - i\Delta_0} I_0\left(2\frac{\sqrt{|\Omega_0|^2 tb(1-\tilde{z})}}{(\Gamma'/2)-i\Delta_0}\right)\exp\left(-\frac{|\Omega_0|^2 t + b(1-\tilde{z})}{(\Gamma'/2)-i\Delta_0}\right). \tag{4.111}$$

The stored spin waves are chosen such that they are centered at $\tilde{z} = 1/2$ and become narrower in space for increasing optical depth (see the fidelity derivations in section 4.6 below). The input and output photon wave functions are centered around times $t \propto L/v_\mathrm{g} = N\Gamma_{1\mathrm{D}}/(2|\Omega_0|^2) = b/|\Omega_0|^2$. Inserting these mean values into equations (4.108) and (4.111), we see that the argument of I_0 becomes very big, since $\sqrt{|\Omega_0|^2 tb\tilde{z}} = \sqrt{|\Omega_0|^2 tb(1-\tilde{z})} \propto b$ and $\Delta_0 = 0$. This allows us to use the asymptotic expansion $I_0(x) \approx \exp(x)/\sqrt{2\pi x}$, which is valid for $|x| \gg 1$ and $\arg(x) < \pi/2$. In this limit, the kernels become

$$K_\mathrm{s}(\tilde{z},t) \approx -\frac{\sqrt{b}\Omega_0^* e^{i\delta t}}{2\sqrt{\pi}\sqrt{(\Gamma'/2)-i\Delta_0}} \frac{1}{\left(|\Omega_0|^2 tb\tilde{z}\right)^{1/4}} \exp\left(-\frac{\left(\sqrt{|\Omega_0|^2 t} - \sqrt{b\tilde{z}}\right)^2}{(\Gamma'/2)-i\Delta_0}\right), \tag{4.112}$$

$$K_\mathrm{r}(\tilde{z},t) \approx -\frac{\sqrt{b}\Omega_0 e^{i\delta t}}{2\sqrt{\pi}\sqrt{(\Gamma'/2)-i\Delta_0}} \frac{1}{\left(|\Omega_0|^2 tb(1-\tilde{z})\right)^{1/4}} \exp\left(-\frac{\left(\sqrt{|\Omega_0|^2 t} - \sqrt{b(1-\tilde{z})}\right)^2}{(\Gamma'/2)-i\Delta_0}\right). \tag{4.113}$$

These formulas have a better numerical behavior compared to equations (4.108) and (4.111), since one does not need to multiply the value of the I_0 (exponentially large) with an exponentially small factor. Hence, we always use equations (4.112) and (4.113) in the numerical calculations.

The relations between the fields in this section and chapter 2 are

$$\Phi_+(\tilde{z}=0,t) = \frac{1}{\sqrt{2}}\phi_{A,\mathrm{in}}(t), \tag{4.114}$$

$$\Phi_-(\tilde{z}=1,t) = \frac{1}{\sqrt{2}}\phi_{A,\mathrm{in}}(t), \tag{4.115}$$

$$\phi_{A,\mathrm{out}}(t) = \frac{1}{\sqrt{2}}\left(\Phi_+(\tilde{z}=1,t) + \Phi_-(\tilde{z}=0,t)\right). \tag{4.116}$$

The results of this section assume that the atoms can be modeled as a continuum, but the scattering coefficients in equations (2.81) and (2.93) are only given at the discrete atom positions. Hence, we need to sample the resulting continuum solutions at the discrete positions of the atoms. In the numerical calculations, the continuum solutions are always sampled as if the atoms were placed regularly independent of the actual placement. To justify regular sampling, we note that instead of the rescaled position coordinate $\tilde{z} = z/L$, one could use $\tilde{z} = \int_0^z (n_0(z')/N)\,\mathrm{d}z'$ [55], where $n_0(z)$ is the local density of the atoms. For an average density $n_0 = N/L$, this rescaled coordinate is equivalent to $\tilde{z} = z/L$. For the local density $n_0(z) = \sum_j \delta(z - z_j)$, the rescaled position becomes $\tilde{z} = \sum_j \theta(z - z_j)/N$, where θ is the the Heaviside theta function. With the convention $\theta(0) = 0$, each z_j is transformed into $\tilde{z} = (j-1)/N$ regardless of the actual value of z_j. As shown in figure 4.7(b) for random placement of the atoms, even though the continuum solutions seem to be able to reproduce the results of the fully discrete theory to some degree, there are still significant differences, which we believe to be caused by reflection of parts of the propagating excitation due to disorder, which are not accounted for in the continuum theory. Hence, with randomly placed atoms, the fully discrete model is required.

Having in mind both the separation of the spin waves into two independent parts and the sampling of the continuum solutions at regular intervals, we can define the storage and retrieval kernels that will be used in equations (2.92) and (2.93). (We use the fidelity expressions with a single realization of the atomic ensemble, since in the continuum approximation, there is no difference between regular and random placement of the atoms.) We define the vector representing the spin wave to have $2N$ elements—for two separately stored spin waves that have fields incident either from the left or from the right as the input. Using the same storage time $\mu_{\mathrm{in}}/c + L/(2v_{\mathrm{g}})$ as for the discrete model in section 4.5.3, the storage kernel is

$$K_{\mathrm{s},j}(t_A) = K_{\mathrm{s}}\big(\tilde{z} = j/N, t = \mu_{\mathrm{in}}/c + L/(2v_{\mathrm{g}}) - t_A\big)/\sqrt{N} \text{ for } 0 \le j \le N-1, \tag{4.117}$$

$$K_{\mathrm{s},j}(t_A) = K_{\mathrm{s}}\big(\tilde{z} = 1-(j-N)/N, t = \mu_{\mathrm{in}}/c + L/(2v_{\mathrm{g}}) - t_A\big)/\sqrt{N} \text{ for } N \le j \le 2N-1, \tag{4.118}$$

where we have assumed that the coefficients corresponding to S_+ are stored in the part of the vector with indices $0 \leq j \leq N-1$, and the coefficients corresponding to S_- are stored in the part of the vector with $N \leq j \leq 2N-1$. The retrieval kernel is

$$K_{\mathrm{r},j}(t_A) = K_{\mathrm{r}}(\tilde{z} = j/N, t = t_A)/\sqrt{N} \text{ for } 0 \leq j \leq N-1, \tag{4.119}$$

$$K_{\mathrm{r},j}(t_A) = K_{\mathrm{r}}(\tilde{z} = 1-(j-N)/N, t = t_A)/\sqrt{N} \text{ for } N \leq j \leq 2N-1. \tag{4.120}$$

As a consequence of having a spin wave vector with $2N$ elements, in equation (2.93) we define $R_{1,j}(\omega_B) = R_{1,j-N}(\omega_B)$ for $N \leq j \leq 2N-1$.

4.6 Analytical fidelity of the gate with Λ-type atoms

Here, we derive equations (4.9) to (4.12). We also derive the bandwidth dependent correction to equation (4.9), which is used in the discussion of the gate time.

From equations (4.1) to (4.4), we find the approximate reflection coefficients of the combined system of the atomic ensemble and the Sagnac interferometer. They are

$$R_0 = -(r_0 - t_0) \approx -\left(\frac{\Gamma_{1\mathrm{D}}\Gamma' N}{16\Delta_{\mathrm{c}}^2} - \left(1 - \frac{\Gamma_{1\mathrm{D}}\Gamma' N}{16\Delta_{\mathrm{c}}^2}\right)\right) = 1 - \frac{\Gamma_{1\mathrm{D}}\Gamma' N}{8\Delta_{\mathrm{c}}^2}, \tag{4.121}$$

$$\begin{aligned} R_{1,\mathrm{s}}(\tilde{z}) &= \frac{1}{2}(R_1(\tilde{z}) + R_1(1-\tilde{z})) = -\frac{1}{2}\Big(r_1(\tilde{z}) + r_1(1-\tilde{z}) - \big(t_1(\tilde{z}) + t_1(1-\tilde{z})\big)\Big) \\ &\approx -\left(1 - \frac{8\pi^2\Delta_{\mathrm{c}}^2\Gamma'}{\Gamma_{1\mathrm{D}}^3 N^2} - \frac{8\pi^4\Delta_{\mathrm{c}}^2(\Gamma_{1\mathrm{D}}+\Gamma')}{\Gamma_{1\mathrm{D}}^3 N^2}\left(\tilde{z} - \frac{1}{2}\right)^2\right). \end{aligned} \tag{4.122}$$

Note that in the symmetrized reflection coefficient $R_{1,\mathrm{s}}(\tilde{z})$, the linear terms proportional to $\pm(\tilde{z} - 1/2)$ (which are present in equations (4.3) and (4.4)) cancel each other. Using the expression for the spin wave given by equation (4.80) with $\tilde{\mu} = 1/2$ we get

$$R_{1,1} \approx \int R_{1,\mathrm{s}}(\tilde{z})|S(\tilde{z})|^2 \,\mathrm{d}\tilde{z} = -\left(1 - \frac{8\pi^2\Delta_{\mathrm{c}}^2\Gamma'}{\Gamma_{1\mathrm{D}}^3 N^2} - \frac{8\pi^4\Delta_{\mathrm{c}}^2(\Gamma_{1\mathrm{D}}+\Gamma')}{\Gamma_{1\mathrm{D}}^3 N^2}\tilde{\sigma}^2\right) \tag{4.123}$$

Using equation (4.5), an approximation for the unconditional CJ fidelity is

$$F_{\mathrm{CJ}} \approx 1 - \epsilon_{\mathrm{b}} - \frac{\Gamma_{1\mathrm{D}}\Gamma' N}{16\Delta_{\mathrm{c}}^2} - \frac{4\pi^2\Delta_{\mathrm{c}}^2\Gamma'}{\Gamma_{1\mathrm{D}}^3 N^2} - \frac{4\pi^4\Delta_{\mathrm{c}}^2(\Gamma_{1\mathrm{D}}+\Gamma')}{\Gamma_{1\mathrm{D}}^3 N^2}\tilde{\sigma}^2 - \frac{1}{2}\frac{\Gamma'}{N\Gamma_{1\mathrm{D}}}\frac{1}{\tilde{\sigma}^2}, \tag{4.124}$$

where $\epsilon_{\mathrm{b}} = 1 - t_{\mathrm{b}}$, and all the error terms (including ϵ_{b}) are assumed to be small.

In principle, if we want to optimize the above expression, we should optimize with respect to Δ_{c} and $\tilde{\sigma}$ simultaneously (we do this in the numerical calculations). Here, we use an approximate optimization procedure, which ignores the fact that one of the error terms depends on the product of Δ_{c} and $\tilde{\sigma}$. As we will see, however, this error term is smaller than the error terms, which only depend on Δ_{c} for fixed $\Gamma_{1\mathrm{D}}/\Gamma$ and large N.

Therefore, we first optimize F_{CJ} over Δ_{c} separately and then use the optimal value of Δ_{c} to optimize over $\tilde{\sigma}$. The optimal value of Δ_{c} is determined by the condition that the third and fourth error terms on the right hand side of equation (4.124) are equal, i.e.

$$\frac{\Gamma_{1\mathrm{D}}\Gamma' N}{16\Delta_{\mathrm{c}}^2} = \frac{4\pi^2\Delta_{\mathrm{c}}^2\Gamma'}{\Gamma_{1\mathrm{D}}^3 N^2}. \tag{4.125}$$

This results in

$$\Delta_{\mathrm{c}}^2 = \frac{\Gamma_{1\mathrm{D}}^2 N^{3/2}}{8\pi}. \tag{4.126}$$

Inserting this value of Δ_{c} into equation (4.124) we obtain

$$F_{\mathrm{CJ}} \approx 1 - \epsilon_{\mathrm{b}} - \frac{\pi\Gamma'}{\Gamma_{1\mathrm{D}}\sqrt{N}} - \frac{\pi^3(\Gamma_{1\mathrm{D}}+\Gamma')}{2\Gamma_{1\mathrm{D}}\sqrt{N}}\tilde{\sigma}^2 - \frac{1}{2}\frac{\Gamma'}{N\Gamma_{1\mathrm{D}}}\frac{1}{\tilde{\sigma}^2}. \tag{4.127}$$

We use this expression to optimize over $\tilde{\sigma}$. The optimal $\tilde{\sigma}$ is obtained when

$$\frac{\pi^3(\Gamma_{1\mathrm{D}}+\Gamma')}{2\Gamma_{1\mathrm{D}}\sqrt{N}}\tilde{\sigma}^2 = \frac{1}{2}\frac{\Gamma'}{N\Gamma_{1\mathrm{D}}}\frac{1}{\tilde{\sigma}^2}. \tag{4.128}$$

From this condition we get

$$\tilde{\sigma}^2 = \frac{1}{\pi^{3/2}N^{1/4}}\sqrt{\frac{\Gamma'}{\Gamma_{1\mathrm{D}}+\Gamma'}} \tag{4.129}$$

and with this value of $\tilde{\sigma}$, equation (4.127) becomes

$$F_{\mathrm{CJ}} \approx 1 - \epsilon_{\mathrm{b}} - \frac{\pi\Gamma'}{\Gamma_{1\mathrm{D}}\sqrt{N}} - \frac{\pi^{3/2}\sqrt{\Gamma_{1\mathrm{D}}+\Gamma'}\sqrt{\Gamma'}}{\Gamma_{1\mathrm{D}}N^{3/4}}. \tag{4.130}$$

We see that for $N \to \infty$, the last term in this expression approaches zero faster than the second one. Hence, in equations (4.9) and (4.11) we have omitted this term. The difference between equation (4.9) and equation (4.11) is whether we set respectively $\epsilon_{\mathrm{b}} = 0$ or $\epsilon_{\mathrm{b}} = 1 - R_0 = (\Gamma_{1\mathrm{D}}\Gamma' N)/(8\Delta_{\mathrm{c}}^2) = (\pi\Gamma')/(\Gamma_{1\mathrm{D}}\sqrt{N})$.

Next we calculate the conditional fidelity $F_{\mathrm{CJ,cond}}$. Since it is given by $F_{\mathrm{CJ,cond}} = F_{\mathrm{CJ}}/P_{\mathrm{suc}}$, the expansion of the ratio will contain higher order error terms than the expansion of the unconditional fidelity F_{CJ}. Hence, we need an expansion of F_{CJ} with more terms than in equation (4.124). Including the second order terms and dividing out η_{EIT} (since it gets canceled in $F_{\mathrm{CJ,cond}}$), we get

$$\frac{F_{\mathrm{CJ}}}{\eta_{\mathrm{EIT}}} \approx 1 - \epsilon_{\mathrm{b}} - \frac{\Gamma_{1\mathrm{D}}\Gamma' N}{16\Delta_{\mathrm{c}}^2} - \frac{4\pi^2\Delta_{\mathrm{c}}^2\Gamma'}{\Gamma_{1\mathrm{D}}^3 N^2} - \frac{4\pi^4\Delta_{\mathrm{c}}^2(\Gamma_{1\mathrm{D}}+\Gamma')}{\Gamma_{1\mathrm{D}}^3 N^2}\tilde{\sigma}^2 \tag{4.131}$$

$$+ \left(\frac{1}{2}\epsilon_{\mathrm{b}} + \frac{\Gamma_{1\mathrm{D}}\Gamma' N}{32\Delta_{\mathrm{c}}^2} + \frac{2\pi^2\Delta_{\mathrm{c}}^2\Gamma'}{\Gamma_{1\mathrm{D}}^3 N^2} + \frac{2\pi^4\Delta_{\mathrm{c}}^2(\Gamma_{1\mathrm{D}}+\Gamma')}{\Gamma_{1\mathrm{D}}^3 N^2}\tilde{\sigma}^2\right)^2 \tag{4.132}$$

Using equation (4.6), we also get the success probability

$$\frac{P_{\rm suc}}{\eta_{\rm EIT}} = \frac{1}{4}\left(2(1-\epsilon_{\rm b})^2 + \left(1 - \frac{\Gamma_{\rm 1D}\Gamma' N}{8\Delta_{\rm c}^2}\right)^2 + R_{1,2}\right), \tag{4.133}$$

where

$$\begin{aligned} R_{1,2} &\approx \int |R_{1,\rm s}(\tilde{z})|^2 |S(\tilde{z})|^2 \,\mathrm{d}\tilde{z} \\ &= 1 - \frac{16\pi^2\Delta_{\rm c}^2\Gamma'}{\Gamma_{\rm 1D}^3 N^2} - \frac{16\pi^4\Delta_{\rm c}^2(\Gamma_{\rm 1D}+\Gamma')}{\Gamma_{\rm 1D}^3 N^2}\tilde{\sigma}^2 + \left(\frac{8\pi^2\Delta_{\rm c}^2\Gamma'}{\Gamma_{\rm 1D}^3 N^2}\right)^2 \\ &\quad + \left(\frac{8\pi^4\Delta_{\rm c}^2(\Gamma_{\rm 1D}+\Gamma')}{\Gamma_{\rm 1D}^3 N^2}\right)\left(3\tilde{\sigma}^4\right) + 2\left(\frac{8\pi^2\Delta_{\rm c}^2\Gamma'}{\Gamma_{\rm 1D}^3 N^2}\right)\left(\frac{8\pi^4\Delta_{\rm c}^2(\Gamma_{\rm 1D}+\Gamma')}{\Gamma_{\rm 1D}^3 N^2}\right)\tilde{\sigma}^2. \end{aligned} \tag{4.134}$$

Using the above expressions, the conditional fidelity can be written

$$F_{\rm CJ,cond} \approx 1 - \epsilon_{\rm cond,1} - \epsilon_{\rm cond,2}, \tag{4.135}$$

where

$$\epsilon_{\rm cond,1} = \frac{1}{4}\left(2\epsilon_{\rm b}^2 + \left(\frac{\Gamma_{\rm 1D}\Gamma' N}{8\Delta_{\rm c}^2}\right)^2 + \left(\frac{8\pi^2\Delta_{\rm c}^2\Gamma'}{\Gamma_{\rm 1D}^3 N^2}\right)^2\right) - \frac{1}{16}\left(2\epsilon_{\rm b} + \frac{\Gamma_{\rm 1D}\Gamma' N}{8\Delta_{\rm c}^2} + \frac{8\pi^2\Delta_{\rm c}^2\Gamma'}{\Gamma_{\rm 1D}^3 N^2}\right)^2, \tag{4.136}$$

$$\epsilon_{\rm cond,2} = \frac{44\pi^8\Delta_{\rm c}^4(\Gamma_{\rm 1D}+\Gamma')^2}{\Gamma_{\rm 1D}^6 N^4}\tilde{\sigma}^4. \tag{4.137}$$

Using the $\Delta_{\rm c}$ from equation (4.126), we get

$$\epsilon_{\rm cond,1} = \frac{1}{2}\left(\epsilon_{\rm b}^2 + \left(\frac{\pi\Gamma'}{\Gamma_{\rm 1D}\sqrt{N}}\right)^2\right) - \frac{1}{4}\left(\epsilon_{\rm b} + \frac{\pi\Gamma'}{\Gamma_{\rm 1D}\sqrt{N}}\right)^2, \tag{4.138}$$

$$\epsilon_{\rm cond,2} = \frac{11\pi^6(\Gamma_{\rm 1D}+\Gamma')^2}{\Gamma_{\rm 1D}^2 N}\tilde{\sigma}^4. \tag{4.139}$$

If we choose $\epsilon_{\rm b} = 0$, $\epsilon_{\rm cond,1}$ is the dominant error term with the value

$$\epsilon_{\rm cond,1} = \frac{1}{4}\left(\frac{\pi\Gamma'}{\Gamma_{\rm 1D}\sqrt{N}}\right)^2, \tag{4.140}$$

in which case $\epsilon_{\rm cond,2}$ can be neglected. If we choose $\epsilon_{\rm b} = (\pi\Gamma')/(\Gamma_{\rm 1D}\sqrt{N})$, we get $\epsilon_{\rm cond,1} = 0$, and we need to keep $\epsilon_{\rm cond,2}$. The value of $\epsilon_{\rm cond,2}$ depends on the width of the stored Gaussian $\tilde{\sigma}$. For simplicity, we use the value of $\tilde{\sigma}$ given by equation (4.129), which

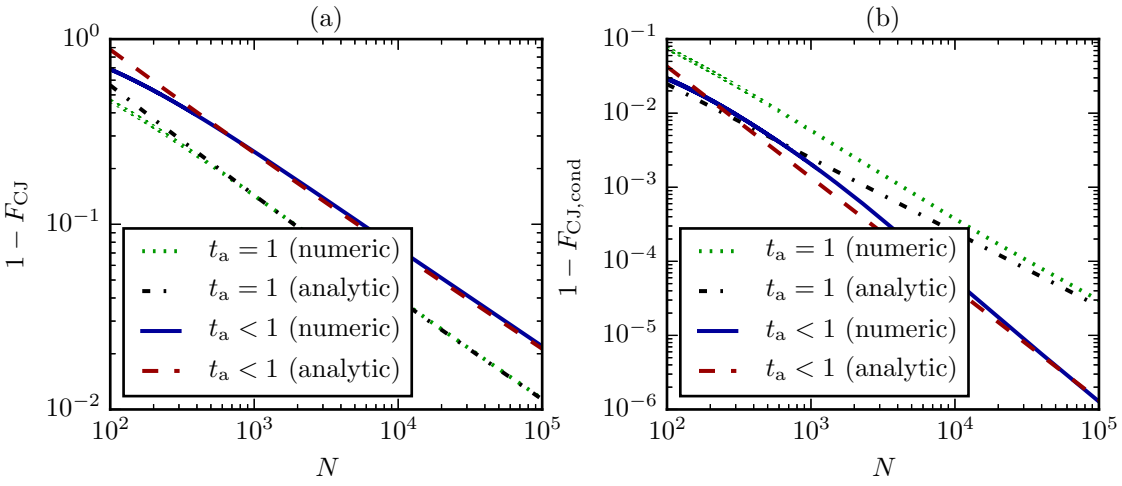

Figure 4.9: Comparison of (a) unconditional and (b) conditional Choi-Jamiolkowski fidelities for the Λ-type scheme plotted as functions of the number of atoms N with fixed $\Gamma_{1\mathrm{D}}/\Gamma = 0.5$. Dotted green curves are the numerically calculated fidelities with $t_{\mathrm{b}} = 1$. Dash-dotted black curves are the approximate analytical results given by equation (4.9) (unconditional) and equation (4.10) (conditional). Solid blue curves are the numerically calculated fidelities with t_{b} chosen such that the entanglement swap fidelity (which is approximately equal to the conditional Choi-Jamiolkowski fidelity as shown in figure 4.10) is maximal. The dashed red curves are the approximate analytical results given by equation (4.11) (unconditional) and equation (4.12) (conditional). For storage and retrieval in the numerical calculations, we use the discretized continuum theory described in section 4.5.4.

makes the unconditional fidelity maximal. With this choice, the conditional fidelity is given by equation (4.12). A comparison of the analytical formulas and the numerical results for F_{CJ} and $F_{\mathrm{CJ,cond}}$ is shown in figure 4.9.

As discussed in chapter 2, the abstract Choi-Jamiolkowski fidelity considered above can be related to more concrete figures of merit, such as entanglement swap fidelity and success probability in the setting of quantum repeaters. Furthermore, since F_{CJ} measures the probability for the photons to be in the right modes with the right phase, whereas P_{suc} measures whether the photons are coming out, it holds that $F_{\mathrm{CJ}} \leq P_{\mathrm{suc}}$. For our particular implementation of the controlled-phase gate, most of the error in F_{CJ} is caused by photon loss, and hence we have $F_{\mathrm{CJ}} \approx P_{\mathrm{suc}}$. At the same time, $F_{\mathrm{CJ,cond}}$ is a lower bound and an approximation for the entanglement swap fidelity F_{swap}. In figure 4.10, we illustrate the approximate equalities of F_{CJ} with P_{suc} and $F_{\mathrm{CJ,cond}}$ with F_{swap}.

Now we derive the correction to the unconditional fidelity due to non-zero bandwidth of the scattered photon B. The general expression for the fidelity is given by equation (2.94). As discussed in section 4.2 above, we ignore the non-zero bandwidth

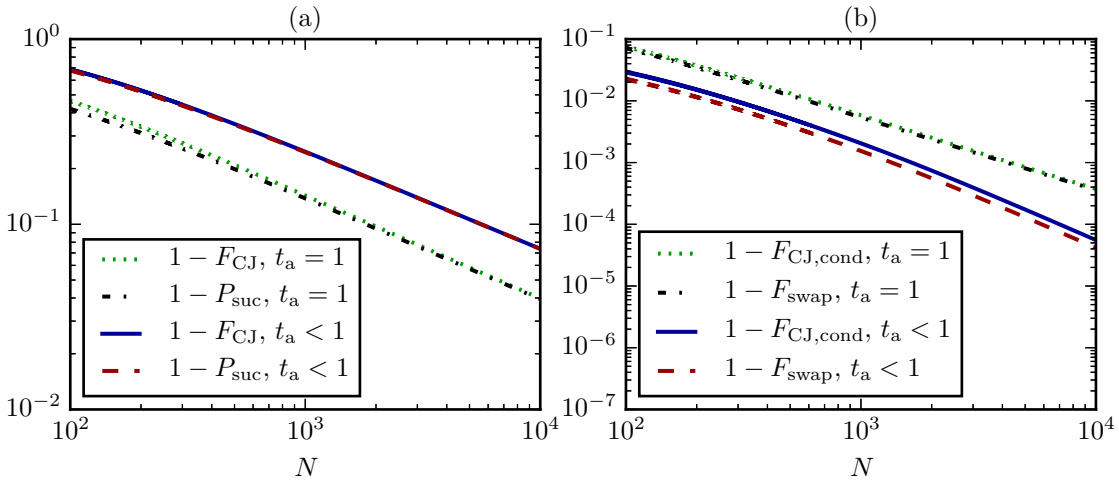

Figure 4.10: (a) Comparison of the Choi-Jamiolkowski fidelity F_{CJ} for deterministic operation of the controlled-phase gate with the success probability P_{suc} for heralded operation of the gate. (b) Comparison of the conditional Choi-Jamiolkowski fidelity $F_{\mathrm{CJ,cond}}$ with the entanglement swap fidelity F_{swap} for heralded operation of the gate. Both for (a) and (b), dotted green and dash-dotted black curves are calculated with $t_{\mathrm{b}} = 1$, while the solid blue and dashed red curves are calculated with t_{b} chosen such that the entanglement swap fidelity F_{swap} is maximal. All quantities are plotted as functions of the number of atoms N with fixed $\Gamma_{1\mathrm{D}}/\Gamma = 0.5$. For storage and retrieval, we use the continuum theory described in section 4.5.4.

in the last term since the variation of r_1 and t_1 with frequency around the resonance detuning δ_{res} is smaller than variation of r_0 and t_0. Hence, we approximate

$$\begin{aligned} &\frac{1}{\eta_{\mathrm{EIT}}} \int\int \phi^*_{A,\mathrm{out},0}(t_A)\phi_{A,\mathrm{out},1}(t_A,\omega_B)|\phi_B(\omega_B)|^2 \,\mathrm{d}t_A \,\mathrm{d}\omega_B \\ &\approx (1/\eta_{\mathrm{EIT}}) \int \phi^*_{A,\mathrm{out},0}(t)\phi_{A,\mathrm{out},1}(t) \,\mathrm{d}t = R_{1,1} \end{aligned} \tag{4.141}$$

such that the expression for the fidelity becomes

$$F_{\mathrm{CJ}} = \frac{\eta_{\mathrm{EIT}}}{16}\left|2t_{\mathrm{b}} + \int R_0(\omega_B)|\phi_B(\omega_B)|^2 \,\mathrm{d}\omega_B - R_{1,1}\right|^2. \tag{4.142}$$

Using equations (4.47) and (4.48) together with expressions $t_0 \approx 1 - r_0$ and $R_0 = -(r_0 - t_0)$ and defining the spectral width of photon B by $\sigma_B = \int(\delta - \delta_{\mathrm{res}})^2|\phi_B(\omega_B)|^2 \,\mathrm{d}\omega_B$, we get

$$\begin{aligned} \int R_0(\delta)|\phi_B(\omega_B)|^2 \,\mathrm{d}\omega_B &\approx R_0(\delta_{\mathrm{res}}) - (4/w^2)\sigma_B^2 \\ &\approx 1 - \frac{\Gamma_{1\mathrm{D}}\Gamma' N}{8\Delta_{\mathrm{c}}^2} - \frac{\Gamma'|\Omega_0|^2\pi^2}{\Delta_{\mathrm{c}}^2\Gamma_{1\mathrm{D}}N} - \frac{\Gamma_{1\mathrm{D}}^6 N^6}{512\Delta_{\mathrm{c}}^4|\Omega_0|^4\pi^4}\sigma_B^2. \end{aligned} \tag{4.143}$$

Using the optimal Δ_c from equation (4.126), this becomes

$$\int R_0(\delta)|\phi_B(\omega_B)|^2\,\mathrm{d}\omega_B \approx 1 - \frac{\pi\Gamma'}{\Gamma_{1D}\sqrt{N}} - \frac{8\Gamma'|\Omega_0|^2\pi^3}{\Gamma_{1D}^3 N^{5/2}} - \frac{\Gamma_{1D}^2 N^3}{8|\Omega_0|^4\pi^2}\sigma_B^2. \tag{4.144}$$

To minimize the sum of the two last error terms in this expression, we optimize over Ω_0 and get

$$\int R_0(\delta)|\phi_B(\omega_B)|^2\,\mathrm{d}\omega_B \approx 1 - \frac{\pi\Gamma'}{\Gamma_{1D}\sqrt{N}} - \frac{3\times 2^{1/3}\pi^{4/3}\Gamma'^{2/3}}{\Gamma_{1D}^{4/3}N^{2/3}}\sigma_B^{2/3} \tag{4.145}$$

for the optimal

$$|\Omega_0|^2 = \frac{\Gamma_{1D}^{5/3}N^{11/6}\sigma_B^{2/3}}{2^{5/3}\pi^{5/3}\Gamma'^{1/3}}. \tag{4.146}$$

Then the fidelity (4.142) is

$$F_{CJ} \approx 1 - \epsilon_b - \frac{\pi\Gamma'}{\Gamma_{1D}\sqrt{N}} - \frac{\pi^{3/2}\sqrt{\Gamma_{1D}+\Gamma'}\sqrt{\Gamma'}}{\Gamma_{1D}N^{3/4}} - \frac{3\pi^{4/3}\Gamma'^{2/3}}{2^{2/3}\Gamma_{1D}^{4/3}N^{2/3}}\sigma_B^{2/3}, \tag{4.147}$$

i.e. compared to equation (4.130), there is an extra error term that depends on σ_B.

4.7 Dependence on positions of the atoms

While the Λ-type scheme is highly sensitive to the exact placement of the atoms, the dual-V scheme is much less sensitive. To verify this, we numerically evaluate the gate performance for various placements of the atoms. First, we investigate the dependence for regularly placed dual-V atoms with different interatomic spacings d. In figure 4.11, we see that for $k_0 d$ different from multiples of $\pi/2$, both the conditional and unconditional fidelities are approximately constant.

Second, we consider randomly placed dual-V atoms. In figure 4.12, the fidelities with regular and random placement are seen to have qualitatively the same behavior, but the performance with random placement is slightly worse.

4.8 Relation to the atomic mirror

The controlled-phase gate proposed in this chapter is very demanding to experimental parameters. For example, the relevant parameters of the setup in Ref. [3] are $\Gamma_{1D}/\Gamma = 0.0051/2$ and $N = 1300$. With such parameters, realization of the controlled-phase gate discussed in chapter 4 is impossible. Therefore, the experiment of Ref. [3] had a simpler goal of making a so-called *atomic mirror* [21]. This effect can be observed with two-level atoms and is remarkable in itself, because it is very different to the behavior of atomic ensembles, where two-level atoms have random placement. For the latter case,

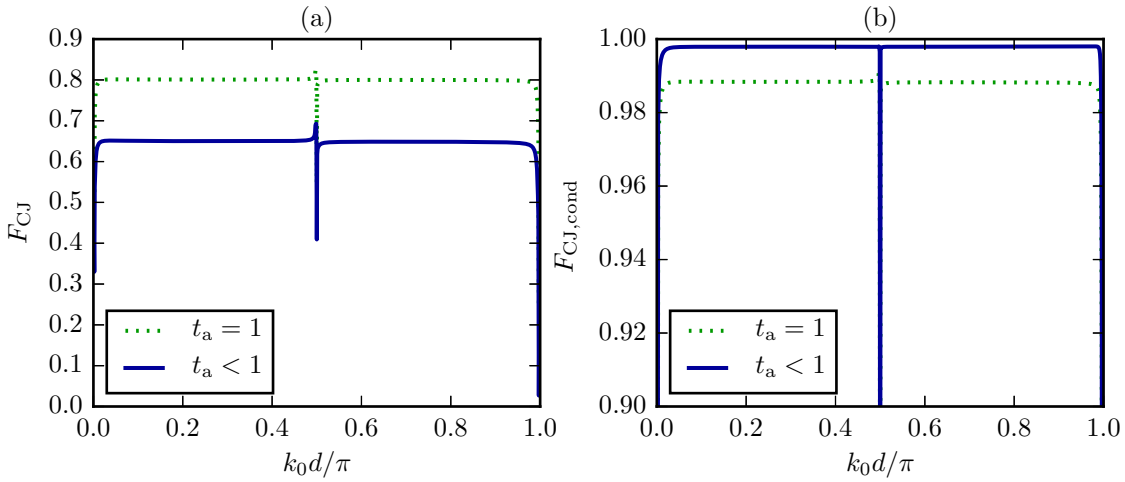

Figure 4.11: Comparison of (a) unconditional and (b) conditional Choi-Jamiolkowski fidelities for the dual-V scheme plotted as functions of the interatomic spacing d times the photon wave vector k_0 for fixed number of atoms $N = 1000$ and $\Gamma_{1\mathrm{D}}/\Gamma = 0.5$. For storage and retrieval, we use the discretized storage and retrieval kernels derived in section 4.5.4.

the Lambert-Beer law is valid, and the behavior of the probe pulse is such that the transmittance and reflectance on resonance are given by

$$|t|^2 = \exp(-2N\Gamma_{1\mathrm{D}}/\Gamma), \tag{4.148}$$

$$|r|^2 \approx 0, \tag{4.149}$$

where the factor $2N\Gamma_{1\mathrm{D}}/\Gamma$ is the resonant optical depth. The main message here is that with random placement, increasing the number of atoms just results in bigger losses of the transmitted signal and virtually nothing gets reflected. On the other hand, if the atoms are placed regularly with inter-atomic spacing of half of a wavelength, then the transmittance and reflectance on resonance are instead given by [21]

$$|r|^2 = \frac{(N\Gamma_{1\mathrm{D}})^2}{(\Gamma' + N\Gamma_{1\mathrm{D}})^2}, \tag{4.150}$$

$$|t|^2 = \frac{\Gamma'^2}{(\Gamma' + N\Gamma_{1\mathrm{D}})^2}. \tag{4.151}$$

With regular placement, we can arrange for almost perfect reflection of the signal for high optical depths. In contrast with the random placement, the signal does not experience losses in the ideal limit. Such kind of operation is necessary for coherent operation of light and is required for deterministic controlled-phase gates for photons. In fact, the controlled-phase gate for photons described in chapter 4 can be thought of as an extension of the atomic mirror concept by making it a conditional atomic mirror. The

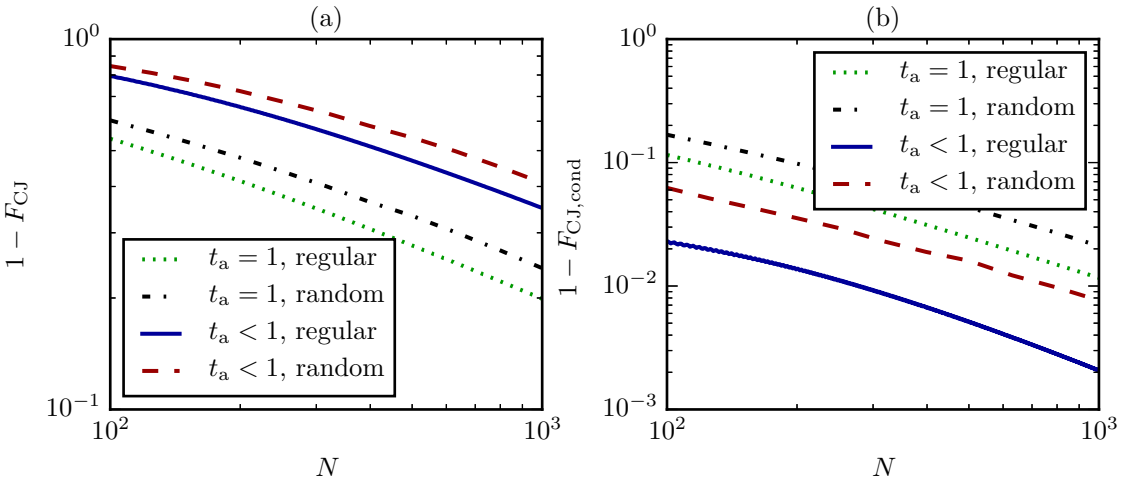

Figure 4.12: Comparison of (a) unconditional and (b) conditional Choi-Jamiolkowski fidelities for the dual-V scheme with different placement of the atoms (regular or random) plotted as functions of the number of atoms N with fixed $\Gamma_{1\mathrm{D}}/\Gamma = 0.5$. The regularly placed atoms have have positions $z_j = jd$ for $d = 0.266\pi/k_0$ and $0 \leq j \leq N-1$. The positions of the randomly placed atoms are chosen from the uniform distribution over the whole ensemble and then sorted in increasing order. For random placement, we average over 1000 ensemble realizations. For storage and retrieval, the fully discrete model of section 4.5.3 is used. For regular placement, it gives the same results as the discretized storage and retrieval kernels derived in section 4.5.4, but for random placement, the fully discrete model has significant deviations from the discretized storage and retrieval kernels as shown in figure 4.7. The optimal Δ_c and $\tilde{\sigma}$ (width of the stored Gaussian spin wave) are found by doing numerical optimization using the discretized storage and retrieval kernels, since the fully discrete model is much more computationally demanding.

analogy is most apparent for the Λ-type scheme of the controlled-phase gate, where we simply insert Λ-type atoms between the two-level atoms of the atomic mirror.

Chapter 5

Conclusion and outlook

The contributions of this thesis consist of three major parts. The first part is development of the theory to characterize the performance of two-qubit (controlled-phase) gates for photons with attention to specifics of the considered implementations. One of those specific things is that errors are mostly limited by photon loss, which motivated a heavy focus on conditional fidelities instead of unconditional ones. Even if, in general, it is not clear how to postselect photon loss efficiently, for at least one application, such postselection comes naturally. This application is quantum repeaters, where the entanglement swap operation is conditioned on measurement of qubits in the computational basis. Due to use of the dual-rail encoding of the photonic qubits, it is possible to discriminate between measuring one of the four states of the computational basis (each including two photons) and measuring vacuum (less than two clicks on the detectors), which indicates that an error has occurred.

The second part of the thesis is focusing on the physics of stationary light. The enhancement of light-matter interactions using stationary light can be explained in (at least) two ways. One explanation is that the coupled light-matter excitations under stationary light can have a small or even vanishing group velocity while maintaining a large photonic component. Since small group velocity implies bigger interaction time of the photons, this can give an increase in the effective photon-photon interaction strength. A different explanation is that under stationary light, the ensemble behaves similar to an optical cavity, which is often used to enhance light-matter and photon-photon interaction strengths in conventional cavity QED. The main goal of this part was to understand the behavior of each of different ways one can implement stationary light such that the best one can be selected for a given purpose.

The third part of the thesis is about applying the theory and understanding of the first two parts to propose a controlled-phase gate for photons. This gate uses additional level in the atoms to add optical nonlinearity in the system and stationary light to enhance it. Effectively the setup resembles a single two-level atom in a conventional optical cavity. The quality of the effective stationary light induced cavity is determined by the total number of the atoms in the ensemble and the single-atom coupling strength. In particular, this implies that nonlinear interactions can be enhanced by the total number

of atoms in the ensemble, which is often not the case. By a particular choice of the linear optics elements coupled to the ensemble we also ensure that the fidelity conditioned on presence of two photons after the gate operation, converges much more rapidly towards unity than the unconditional fidelity. This is very important for quantum repeaters, where extremely high conditional fidelities are required for achieving good secret key rates. We thus investigate, how good the parameters of the gate have to be able to compete with linear optics for this application.

Moving on to the discussion of possible extensions of the presented results, one specific thing which seems interesting is the combination of stationary light and Rydberg blockade. In the systems that we have considered for the stationary light gate in chapter 4, the moderate coupling strength of a single atom to light is accomplished by having a dielectric medium close to the atom (e.g. a tapered optical fiber). This precludes usage of Rydberg levels, since they will be disturbed by the dielectric medium close by. On the other hand, if the atomic ensemble is in free space, the single-atom coupling strength is so small that enhancing it by stationary light is virtually impossible. The hope is that for these systems, one can use Rydberg blockade such that it is not the coupling strength of a single atom that matters but the blockaded optical depth.

On a higher level, we see that there have been several proposals for deterministic controlled-phase gates recently, including the one discussed in this thesis. Even though many of them promise perfect deterministic operation in some limit of the experimental parameters, attaining those parameters is still extremely challenging. At the same time, we found that for quantum repeaters, deterministic operation of the controlled-phase gate in chapter 4 was unable to compete with linear optics for any realistic parameters. It is only when heralded operation of the stationary light gate was considered that improvement over linear optics for reasonable (but still challenging) parameters could be achieved. The intuitive reason is that linear optics can do the entanglement swapping operation with 50% probability but with unit conditional fidelity. The stationary light controlled-phase gate always has fidelity (conditional or unconditional) less than unity and after few swap levels the errors grow even more. Here, it helps tremendously that the proposed controlled-phase gate can operate in a heralded fashion with conditional fidelity that is much closer to unity than the unconditional one. The same analysis applies to the Rydberg blockade gate in Ref. [1].

If this is seen to be a general trend for the recently proposed controlled-phase gates for photons, then the focus would need to shift to heralded operation of those gates, even though they can operate deterministically in principle. Therefore, it would become a search not for a completely deterministic controlled-phase gate for photons but a heralded gate, which is better than linear optics for the given application. Ideally, the applications of the controlled-phase gates for photons will not limited to quantum repeaters. The linear optics was shown to be enough to realize universal quantum computation [40, 41], but has prohibitively high resource requirements (in terms of the number of photon detectors) [58]. It would be an interesting to find out, whether the stationary light controlled-phase gate of chapter 4 (or any of the others in the literature) can bring down the resource costs significantly, and how good it has to be for this to happen.

Appendix A

Derivation of the fidelity expressions

A.1 Introduction

Here, we derive the expressions in section 2.8.

A.2 Fidelity of creation of a Bell state

We start with the fidelity of creation of a Bell state. To account for possibility of many different realizations of the atomic ensemble, we use equation (2.20) together with equation (2.77) to get

$$F_{\text{Bell}} = \frac{1}{N_{\text{r}}} \sum_{n=1}^{N_{\text{r}}} \left(\left| \langle \psi_{\text{in}} | U_{AB}^{\dagger} V_{n,AB} | \psi_{\text{in}} \rangle \right|^2 + \langle \psi_{\text{in}} | U_{AB}^{\dagger} \mathcal{J}_{n,AB} \left(|\psi_{\text{in}}\rangle\langle\psi_{\text{in}}| \right) U_{AB} | \psi_{\text{in}} \rangle \right). \quad \text{(A.1)}$$

This expression reduces to equation (2.29) in the case of a single ensemble realization. Due to the assumption (2.78), the term involving $\mathcal{J}_{n,AB}$ in equation (A.1) vanishes. Using the definition (2.22) of the input state $|\psi_{\text{in}}\rangle$, the non-zero term can be written

$$\left| \langle \psi_{\text{in}} | U_{AB}^{\dagger} V_{n,AB} | \psi_{\text{in}} \rangle \right|^2 = \frac{1}{16} \left| \sum_{x,x'=0}^{1} \sum_{y,y'=0}^{1} \langle xx' |_{AB} U_{AB}^{\dagger} V_{n,AB} | yy' \rangle_{AB} \right|^2 . \quad \text{(A.2)}$$

Since the operators for the ideal and real evolution of the controlled-phase gate given by equations (2.76) and (2.79) are diagonal in the computational basis states, the cross terms ($x \neq y$ and $x' \neq y'$) in equation (A.2) vanish, and we get fidelity (2.86)

To find the success probability, we start with equation (2.32). Using equations (2.77)

and (2.82), we get

$$P_{\text{suc,Bell}} = \frac{1}{N_\text{r}} \sum_{n=1}^{N_\text{r}} \sum_{x,x'=0}^{1} \int\int \Big(\Big| \langle x_{t_A} x'_{\omega_B} | V_{n,AB} | \psi_\text{in} \rangle \Big|^2 + \langle x_{t_A} x'_{\omega_B} | \mathcal{J}_{n,AB} \big(|\psi_\text{in}\rangle\langle\psi_\text{in}| \big) \, | x_{t_A} x'_{\omega_B} \rangle \Big) \, \mathrm{d}t_A \, \mathrm{d}\omega_B. \tag{A.3}$$

Again, due to the assumption (2.78), the term involving $\mathcal{J}_{n,AB}$ vanishes. Rewriting the non-zero term, we get

$$P_{\text{suc,Bell}} = \frac{1}{4N_\text{r}} \sum_{x,x'=0}^{1} \sum_{y,y'=0}^{1} \int\int \Big| \langle x_{t_A} x'_{\omega_B} | V_{n,AB} | y y' \rangle_{AB} \Big|^2 \, \mathrm{d}t_A \, \mathrm{d}\omega_B. \tag{A.4}$$

Using equations (2.79), we thus get the success probability (2.87).

A.3 Choi-Jamiolkowski fidelity

For the Choi-Jamiolkowski fidelity, using equations (2.20) and (2.77), we get

$$F_\text{CJ} = \frac{1}{N_\text{r}} \sum_{n=1}^{N_\text{r}} \Big(\Big| \langle \Phi | (I_{A'B'} \otimes U_{AB}^\dagger V_{n,AB}) | \Phi \rangle \Big|^2 + \langle \Phi | (I_{A'B'} \otimes U_{AB}^\dagger) [\mathcal{I}_{A'B'} \otimes \mathcal{J}_{n,AB}] \big(|\Phi\rangle\langle\Phi| \big) \, (I_{A'B'} \otimes U_{AB}) | \Phi \rangle \Big). \tag{A.5}$$

The expression above is a generalization of equation (2.45) for many different realizations of the atomic ensemble. The term, involving $\mathcal{J}_{n,AB}$ can be rewritten to show more clearly that it vanishes due to the assumption (2.78). Since U_{AB} (ideal evolution operator) maps basis states onto basis states, it suffices to show that for all

$$x_1, x_2, y_1, y_2, x'_1, x'_2, y'_1, y'_2 \in \{0, 1\}, \tag{A.6}$$

it holds that

$$\langle x'_1 x'_2 |_{A'B'} \langle x_1 x_2 |_{AB} [\mathcal{I}_{A'B'} \otimes \mathcal{J}_{n,AB}] \big(|\Phi\rangle\langle\Phi| \big) \, | y'_1 y'_2 \rangle_{A'B'} | y_1 y_2 \rangle_{AB} = 0. \tag{A.7}$$

Using the definition (2.47) of the input state $|\Phi\rangle$, we have

$$\begin{aligned} &[\mathcal{I}_{A'B'} \otimes \mathcal{J}_{n,AB}] \big(|\Phi\rangle\langle\Phi| \big) \\ &= \frac{1}{4} \sum_{x_3,x_4=0}^{1} \sum_{y_3,y_4=0}^{1} [\mathcal{I}_{A'B'} \otimes \mathcal{J}_{n,AB}] \big(|x_3 x_4\rangle_{A'B'} | x_3 x_4 \rangle_{AB} \langle y_3 y_4 |_{A'B'} \langle y_3 y_4 |_{AB} \big) \\ &= \frac{1}{4} \sum_{x_3,x_4=0}^{1} \sum_{y_3,y_4=0}^{1} \mathcal{I}_{A'B'} \big(|x_3 x_4\rangle_{A'B'} \langle y_3 y_4 |_{A'B'} \big) \otimes \mathcal{J}_{n,AB} \big(|x_3 x_4\rangle_{AB} \langle y_3 y_4 |_{AB} \big) \\ &= \frac{1}{4} \sum_{x_3,x_4=0}^{1} \sum_{y_3,y_4=0}^{1} |x_3 x_4\rangle_{A'B'} \langle y_3 y_4 |_{A'B'} \otimes \mathcal{J}_{n,AB} \big(|x_3 x_4\rangle_{AB} \langle y_3 y_4 |_{AB} \big), \end{aligned} \tag{A.8}$$

we see that equation (A.7) holds because of the assumption (2.78), which implies that

$$\langle x_1 x_2|_{AB} \mathcal{J}_{n,AB}\big(|x_3 x_4\rangle_{AB}\langle y_3 y_4|_{AB}\big)\,|y_1 y_2\rangle_{AB} = 0. \tag{A.9}$$

The non-zero term in equation (A.5) can also be rewritten. For all $x, x', y, y' \in \{0,1\}$, we have

$$\begin{aligned}
&\Big|\langle\Phi|(I_{A'B'}\otimes U_{AB}^\dagger V_{n,AB})|\Phi\rangle\Big|^2 \\
&= \frac{1}{16}\left|\sum_{x,x'=0}^{1}\sum_{y,y'=0}^{1}\langle xx'|_{A'B'}\langle xx'|_{AB}(I_{A'B'}\otimes U_{AB}^\dagger V_{n,AB})|yy'\rangle_{A'B'}|yy'\rangle_{AB}\right|^2 \\
&= \frac{1}{16}\left|\sum_{x,x'=0}^{1}\sum_{y,y'=0}^{1}\langle xx'|yy'\rangle_{A'B'}\langle xx'|_{AB}U_{AB}^\dagger V_{n,AB}|yy'\rangle_{AB}\right|^2 \\
&= \frac{1}{16}\left|\sum_{x,x'=0}^{1}\langle xx'|_{AB}U_{AB}^\dagger V_{n,AB}|xx'\rangle_{AB}\right|^2 .
\end{aligned} \tag{A.10}$$

This is the same as equation (A.2), except for the cross terms ($x \neq y$ and $x' \neq y'$ in equation (A.2)). Since both the ideal and real evolution of the controlled-phase gate given by equations (2.76) and (2.79) is diagonal in the computational basis, the cross terms vanish, and hence equations (A.10) and (A.2) are the same. The conclusion is that Choi-Jamiolkowski fidelity is the same as the fidelity of creation of a Bell state,

$$F_{\mathrm{CJ}} = F_{\mathrm{Bell}}. \tag{A.11}$$

To find the conditional Choi-Jamiolkowski fidelity, we need to calculate the success probability (2.46). We can write it

$$\begin{aligned}
&P_{\mathrm{suc,CJ}} \\
&= \mathrm{tr}_{A'B'AB}\Big((I_{A'B'}\otimes P_{AB})\rho_{\mathcal{V}}(I_{A'B'}\otimes P_{AB})^\dagger\Big) \\
&= \mathrm{tr}_{A'B'AB}\Big((I_{A'B'}\otimes P_{AB})[\mathcal{I}_{A'B'}\otimes\mathcal{V}_{AB}]\big(|\Phi\rangle\langle\Phi|\big)\,(I_{A'B'}\otimes P_{AB})^\dagger\Big) \\
&= \frac{1}{4}\sum_{x,x'=0}^{1}\sum_{y,y'=0}^{1}\mathrm{tr}_{A'B'}\big(|xx'\rangle_{A'B'}\langle yy'|_{A'B'}\big)\,\mathrm{tr}_{AB}\Big(P_{AB}\mathcal{V}_{AB}\big(|xx'\rangle_{AB}\langle yy'|_{AB}\big)\,P_{AB}^\dagger\Big) \\
&= \frac{1}{4}\sum_{x,x'=0}^{1}\mathrm{tr}_{AB}\Big(P_{AB}\mathcal{V}_{AB}\big(|xx'\rangle_{AB}\langle xx'|_{AB}\big)\,P_{AB}^\dagger\Big).
\end{aligned} \tag{A.12}$$

Using equation (2.77), and the assumption (2.78) the above becomes the same as equation (A.4). Hence, the success probabilities for heralded operation of the gate are the

same both for the fidelity of creation of a Bell state and the Choi-Jamiolkowski fidelity, i.e.

$$P_{\text{suc,CJ}} = P_{\text{suc,Bell}}. \tag{A.13}$$

We also want to show that Choi-Jamiolkowski fidelity of the full circuit in figure 2.5 has the same fidelity. We assume that Hadamard operators are lossless and hence unitary. In general, any unitary operator acting after the controlled-phase gate has no effect, since fidelity is invariant unitary transformations. What is left to show is that any unitary acting before the controlled-phase gate has no effect on Choi-Jamiolkowski fidelity.

We can show it in the general case, assuming that a unitary O_{AB} acts before the controlled-phase gate. In our specific case,

$$O_{AB} = (I_A \otimes H_B). \tag{A.14}$$

Then we can choose to use a different basis for writing the initial state $|\Phi\rangle$. We choose a transformed computational basis, where

$$|\Phi\rangle = \frac{1}{2} \sum_{x,x'=0}^{1} (O^{\dagger}_{A'B'} \otimes O^{\dagger}_{AB})|xx'\rangle_{A'B'}|xx'\rangle_{AB}. \tag{A.15}$$

We denote the superoperators for ideal and real operation of the whole circuit for entanglement swap by respectively $\tilde{\mathcal{U}}$ and $\tilde{\mathcal{V}}$. The relation to the superoperators for the ideal and real operation of the controlled-phase gate itself is

$$\tilde{\mathcal{U}}_{AB}(\rho_{AB}) = (H_A \otimes H_B)\mathcal{U}\big((I_A \otimes H_B)\rho_{AB}(I_A \otimes H_B)\big)\,(H_A \otimes H_B), \tag{A.16}$$

$$\tilde{\mathcal{V}}_{AB}(\rho_{AB}) = (H_A \otimes H_B)\mathcal{V}\big((I_A \otimes H_B)\rho_{AB}(I_A \otimes H_B)\big)\,(H_A \otimes H_B). \tag{A.17}$$

In terms of the operators $\tilde{U}_{AB}$ and $\tilde{V}_{n,AB}$ that correspond to the superoperators $\tilde{\mathcal{U}}_{AB}$ and $\tilde{\mathcal{V}}_{AB}$, we have

$$\tilde{U}_{AB} = (H_A \otimes H_B)U_{AB}(I_A \otimes H_B), \tag{A.18}$$

$$\tilde{V}_{n,AB} = (H_A \otimes H_B)V_{n,AB}(I_A \otimes H_B). \tag{A.19}$$

Doing the same calculation as in equation (A.10), we get

$$\begin{aligned} \Big|\langle\Phi|(I_{A'B'} \otimes \tilde{U}^{\dagger}_{AB}\tilde{V}_{n,AB})|\Phi\rangle\Big|^2 &= \frac{1}{16}\left|\sum_{x,x'=0}^{1} \langle xx'|_{AB} O_{AB}\tilde{U}^{\dagger}_{AB}\tilde{V}_{n,AB}O^{\dagger}_{AB}|xx'\rangle_{AB}\right|^2 \\ &= \frac{1}{16}\left|\sum_{x,x'=0}^{1} \langle xx'|_{AB} U^{\dagger}_{AB}V_{n,AB}|xx'\rangle_{AB}\right|^2, \end{aligned} \tag{A.20}$$

where in the last line we have used equations (A.14), (A.18) and (A.19). The end result is the same as in the calculation (A.10).

For calculating the success probability in this case, we use the input state (A.15) and tracing over the transformed basis states

$$(H_A \otimes H_B)|x_{t_A} x'_{\omega_B}\rangle \tag{A.21}$$

for all $x, x' \in \{0, 1\}$ (using the definitions of the Hadamard operators (2.84) and (2.85)). We do the same calculation as in equation (A.12) and get

$$\begin{aligned} P_{\text{suc,CJ}} &= \frac{1}{4N_{\text{r}}} \sum_{x,x'=0}^{1} \sum_{y,y'=0}^{1} \int\int \left| \langle x_{t_A} x'_{\omega_B}| (H_A \otimes H_B) \tilde{V}_{n,AB} O^{\dagger}_{AB} |yy'\rangle_{AB} \right|^2 \mathrm{d}t_A \, \mathrm{d}\omega_B \\ &= \frac{1}{4N_{\text{r}}} \sum_{x,x'=0}^{1} \sum_{y,y'=0}^{1} \int\int \left| \langle x_{t_A} x'_{\omega_B}| V_{n,AB} |yy'\rangle_{AB} \right|^2 \mathrm{d}t_A \, \mathrm{d}\omega_B, \end{aligned} \tag{A.22}$$

which is the same as equation (A.4).

A.4 Fidelity of entanglement swap

To calculate the fidelity of entanglement swap, we use equations (2.35), (2.37), (2.38) and (2.83). (Also we call the input state $|\psi_{\text{in}}\rangle$ by $|\Phi\rangle$, since it is the same as the input state for Choi-Jamiolkowski fidelity, as discussed in section 2.4.4.) We can write

$$F_{xx'} = \frac{1}{P_{\text{suc},xx'}} \langle \phi^{xx'}|_{A'B'} \mathrm{tr}_{AB} \Big((I_{A'B'} \otimes P_{xx',AB}) \rho_{\tilde{\mathcal{V}}} (I_{A'B'} \otimes P_{xx',AB})^{\dagger} \Big) |\phi^{xx'}\rangle_{A'B'}, \tag{A.23}$$

where the success probability is given by equation (2.40). Using the Bell basis representation (2.48) of the initial state $|\Phi\rangle$, we have

$$\begin{aligned} \rho_{\tilde{\mathcal{V}}} &= \mathcal{I}_{A'B'} \otimes \tilde{\mathcal{V}}_{AB} \big(|\Phi\rangle\langle\Phi| \big) \\ &= \frac{1}{4} \sum_{y_1,y_2=0}^{1} \sum_{y_3,y_4=0}^{1} \mathcal{I}_{A'B'} \otimes \tilde{\mathcal{V}}_{AB} \big(|\phi^{y_1 y_2}\rangle_{A'B'} |\phi^{y_1 y_2}\rangle_{AB} \langle\phi^{y_3 y_4}|_{A'B'} \langle\phi^{y_3 y_4}|_{AB} \big) \\ &= \frac{1}{4} \sum_{y_1,y_2=0}^{1} \sum_{y_3,y_4=0}^{1} |\phi^{y_1 y_2}\rangle_{A'B'} \langle\phi^{y_3 y_4}|_{A'B'} \otimes \tilde{\mathcal{V}}_{AB} \big(|\phi^{y_1 y_2}\rangle_{AB} \langle\phi^{y_3 y_4}|_{AB} \big) . \end{aligned} \tag{A.24}$$

Using this and carrying out the projections onto $|\phi^{xx'}\rangle_{A'B'}$ in equation (A.23), it can be written

$$F_{xx'} = \frac{1}{4P_{\text{suc},xx'}} \mathrm{tr}_{AB} \left(P_{xx',AB} \tilde{\mathcal{V}}_{AB} \Big(|\phi^{xx'}\rangle_{AB} \langle\phi^{xx'}|_{AB} \Big) P^{\dagger}_{xx',AB} \right). \tag{A.25}$$

Using equation (2.77) and the assumption (2.78), it can be further simplified to

$$F_{xx'} = \frac{1}{4N_r P_{\mathrm{suc},xx'}} \sum_{n=1}^{N_\mathrm{r}} \int\int \left| \langle x_{t_A} x'_{\omega_B} | \tilde{V}_{n,AB} | \phi^{xx'} \rangle_{AB} \right|^2 \mathrm{d}t_A \, \mathrm{d}\omega_B, \tag{A.26}$$

where $\tilde{V}_{n,AB}$ is defined in terms of $V_{n,AB}$ by equation (A.19).

The expressions for the success probabilities $P_{\mathrm{suc},xx'}$ can be written starting from equation (2.40), which gives

$$P_{\mathrm{suc},xx'} = \mathrm{tr}_{A'B'AB}\Big((I_{A'B'} \otimes P_{xx',AB}) \rho_{\tilde{\mathcal{V}}} (I_{A'B'} \otimes P_{xx',AB})^\dagger \Big). \tag{A.27}$$

Using equation (A.24), this becomes

$$P_{\mathrm{suc},xx'} = \sum_{y,y'=0}^{1} \mathrm{tr}_{AB}\left(P_{xx',AB} \tilde{\mathcal{V}}_{AB}\Big(|\phi^{yy'}\rangle_{AB} \langle \phi^{yy'}|_{AB} \Big) P^\dagger_{xx',AB} \right). \tag{A.28}$$

Using equation (2.77) and the assumption (2.78), it can be further simplified to

$$P_{\mathrm{suc},xx'} = \frac{1}{4N_\mathrm{r}} \sum_{n=1}^{N_\mathrm{r}} \sum_{y,y'=0}^{1} \int\int \left| \langle x_{t_A} x'_{\omega_B} | \tilde{V}_{n,AB} | \phi^{yy'} \rangle_{AB} \right|^2 \mathrm{d}t_A \, \mathrm{d}\omega_B. \tag{A.29}$$

To find the expressions for equations (A.26) and (A.29) we first calculate the states $V_{n,AB}(I_A \otimes H_B)|\phi^{yy'}\rangle_{AB}$. Using the definition of the Bell basis (2.18) and the real evolution given by equation (2.79), they are

$$\begin{aligned} V_{n,AB}(I_A \otimes H_B)|\phi^{00}\rangle_{AB} = \frac{1}{2} \int\int & \phi_B(\omega_B) \big(t_\mathrm{b} \phi_{A,\mathrm{out},n,0}(t_A) |0_{t_A} 0_{\omega_B}\rangle \\ & + R_{0,n}(\omega_B) \phi_{A,\mathrm{out},n,0}(t_A) |0_{t_A} 1_{\omega_B}\rangle \\ & + t_\mathrm{b} \phi_{A,\mathrm{out},n,10}(t_A) |1_{t_A} 0_{\omega_B}\rangle \\ & - \phi_{A,\mathrm{out},n,11}(t_A, \omega_B) |1_{t_A} 1_{\omega_B}\rangle \big) \, \mathrm{d}t_A \, \mathrm{d}\omega_B, \end{aligned} \tag{A.30}$$

$$\begin{aligned} V_{n,AB}(I_A \otimes H_B)|\phi^{01}\rangle_{AB} = \frac{1}{2} \int\int & \phi_B(\omega_B) \big(t_\mathrm{b} \phi_{A,\mathrm{out},n,0}(t_A) |0_{t_A} 0_{\omega_B}\rangle \\ & - R_{0,n}(\omega_B) \phi_{A,\mathrm{out},n,0}(t_A) |0_{t_A} 1_{\omega_B}\rangle \\ & + t_\mathrm{b} \phi_{A,\mathrm{out},n,10}(t_A) |1_{t_A} 0_{\omega_B}\rangle \\ & + \phi_{A,\mathrm{out},n,11}(t_A, \omega_B) |1_{t_A} 1_{\omega_B}\rangle \big) \, \mathrm{d}t_A \, \mathrm{d}\omega_B, \end{aligned} \tag{A.31}$$

$$\begin{aligned} V_{n,AB}(I_A \otimes H_B)|\phi^{10}\rangle_{AB} = \frac{1}{2} \int\int & \phi_B(\omega_B) \big(t_\mathrm{b} \phi_{A,\mathrm{out},n,0}(t_A) |0_{t_A} 0_{\omega_B}\rangle \\ & + R_{0,n}(\omega_B) \phi_{A,\mathrm{out},n,0}(t_A) |0_{t_A} 1_{\omega_B}\rangle \\ & - t_\mathrm{b} \phi_{A,\mathrm{out},n,10}(t_A) |1_{t_A} 0_{\omega_B}\rangle \\ & + \phi_{A,\mathrm{out},n,11}(t_A, \omega_B) |1_{t_A} 1_{\omega_B}\rangle \big) \, \mathrm{d}t_A \, \mathrm{d}\omega_B, \end{aligned} \tag{A.32}$$

$$V_{n,AB}(I_A \otimes H_B)|\phi^{11}\rangle_{AB} = \frac{1}{2}\int\int \phi_B(\omega_B)\big(t_\mathrm{b}\phi_{A,\mathrm{out},n,0}(t_A)|0_{t_A}0_{\omega_B}\rangle - R_{0,n}(\omega_B)\phi_{A,\mathrm{out},n,0}(t_A)|0_{t_A}1_{\omega_B}\rangle - t_\mathrm{b}\phi_{A,\mathrm{out},n,10}(t_A)|1_{t_A}0_{\omega_B}\rangle - \phi_{A,\mathrm{out},n,11}(t_A,\omega_B)|1_{t_A}1_{\omega_B}\rangle\big)\,\mathrm{d}t_A\,\mathrm{d}\omega_B. \tag{A.33}$$

The states $V_{n,AB}(I_A\otimes H_B)|\phi^{yy'}\rangle_{AB}$ are then projected onto the states $(H_A\otimes H_B)|x_{t_A}x'_{\omega_B}\rangle$ in the integrands of equations (A.26) and (A.29). The latter states can be written

$$(H_A \otimes H_B)|0_{t_A}0_{\omega_B}\rangle = \frac{1}{2}\left(|0_{t_A}0_{\omega_B}\rangle + |0_{t_A}1_{\omega_B}\rangle + |1_{t_A}0_{\omega_B}\rangle + |1_{t_A}1_{\omega_B}\rangle\right), \tag{A.34}$$

$$(H_A \otimes H_B)|0_{t_A}1_{\omega_B}\rangle = \frac{1}{2}\left(|0_{t_A}0_{\omega_B}\rangle - |0_{t_A}1_{\omega_B}\rangle + |1_{t_A}0_{\omega_B}\rangle - |1_{t_A}1_{\omega_B}\rangle\right), \tag{A.35}$$

$$(H_A \otimes H_B)|1_{t_A}0_{\omega_B}\rangle = \frac{1}{2}\left(|0_{t_A}0_{\omega_B}\rangle + |0_{t_A}1_{\omega_B}\rangle - |1_{t_A}0_{\omega_B}\rangle - |1_{t_A}1_{\omega_B}\rangle\right), \tag{A.36}$$

$$(H_A \otimes H_B)|1_{t_A}1_{\omega_B}\rangle = \frac{1}{2}\left(|0_{t_A}0_{\omega_B}\rangle - |0_{t_A}1_{\omega_B}\rangle - |1_{t_A}0_{\omega_B}\rangle + |1_{t_A}1_{\omega_B}\rangle\right). \tag{A.37}$$

Using the above expressions, the success probability in equation (A.29) becomes

$$P_{\mathrm{suc},xx'} = \frac{1}{64N_\mathrm{r}}\sum_{n=1}^{N_\mathrm{r}}\int\int |\phi_B(\omega_B)|^2\Big(\big|f_1+f_2+f_3-f_4\big|^2 + \big|f_1-f_2+f_3+f_4\big|^2 + \big|f_1+f_2-f_3+f_4\big|^2 + \big|f_1-f_2-f_3-f_4\big|^2\Big)\,\mathrm{d}t_A\,\mathrm{d}\omega_B, \tag{A.38}$$

where

$$\begin{aligned} f_1(t_A,\omega_B) &= t_\mathrm{b}\phi_{A,\mathrm{out},n,0}(t_A),\\ f_2(t_A,\omega_B) &= R_{0,n}(\omega_B)\phi_{A,\mathrm{out},n,0}(t_A),\\ f_3(t_A,\omega_B) &= t_\mathrm{b}\phi_{A,\mathrm{out},n,10}(t_A),\\ f_4(t_A,\omega_B) &= \phi_{A,\mathrm{out},n,11}(t_A,\omega_B), \end{aligned} \tag{A.39}$$

and the arguments of f_1, f_2, f_3 and f_3 in the integrand of equation (A.38) are omitted for brevity. Note that the success probability (A.38) is independent of x and x'. Using the parallelogram law,

$$|a|^2 + |b|^2 = \frac{1}{2}(|a+b|^2 + |a-b|^2), \tag{A.40}$$

in two stages, we see that

$$\begin{aligned} 4\left(|f_1|^2+|f_2|^2+|f_3|^2+|f_4|^2\right) &= 2\left(|f_1+f_2|^2+|f_1-f_2|^2+|f_3+f_4|^2+|f_3-f_4|^2\right)\\ &= |f_1+f_2+f_3-f_4|^2+|f_1-f_2+f_3+f_4|^2\\ &\quad +|f_1+f_2-f_3+f_4|^2+|f_1-f_2-f_3-f_4|^2, \end{aligned} \tag{A.41}$$

Hence, we can further simplify equation (A.38) to

$$P_{\mathrm{suc},xx'} = \frac{1}{16N_{\mathrm{r}}} \sum_{n=1}^{N_{\mathrm{r}}} \int\int |\phi_B(\omega_B)|^2 \Big(|f_1|^2 + |f_2|^2 + |f_3| + |f_4|^2 \Big) \, \mathrm{d}t_A \, \mathrm{d}\omega_B, \tag{A.42}$$

such that the success probability $P_{\mathrm{suc},xx'}$ is is the success probability (2.87) divided by 4. Hence, the total success probability for a Bell measurement (2.41) is the same as equation (2.87). Hence, together with the result (A.13) we have shown that

$$P_{\mathrm{suc,CJ}} = P_{\mathrm{suc,Bell}} = P_{\mathrm{suc,swap}}. \tag{A.43}$$

The fidelities $F_{xx'}$ (equation (A.26)) can also be shown be be independent of x and x' in the same way as the success probabilities $P_{\mathrm{suc},xx'}$ above. All $F_{xx'}$ result in the equation (2.88), such that the same equation trivially gives the average entanglement swap fidelity (2.42).

Appendix B

Numerical methods for the continuum model

The truncations of both equations (3.33) for the Λ-type scheme and equations (3.51) for the dual-color scheme can be written

$$0 = M\boldsymbol{\sigma} + g\sqrt{2\pi}V\boldsymbol{\mathcal{E}}, \tag{B.1}$$

where

$$\boldsymbol{\sigma} = \begin{pmatrix} \vdots \\ \sigma_{ac}^{(+2)} \\ \sigma_{ab}^{(+1)} \\ \sigma_{ac}^{(0)} \\ \sigma_{ab}^{(-1)} \\ \sigma_{ac}^{(-2)} \\ \vdots \end{pmatrix}, \quad V = \begin{pmatrix} \vdots & \vdots \\ 0 & 0 \\ 1 & 0 \\ 0 & 0 \\ 0 & 1 \\ 0 & 0 \\ \vdots & \vdots \end{pmatrix}, \quad \boldsymbol{\mathcal{E}} = \begin{pmatrix} \mathcal{E}_+ \\ \mathcal{E}_- \end{pmatrix}, \tag{B.2}$$

and the definition of the matrix M depends on whether we consider equations (3.33) or equations (3.51). For equations (3.33), we have

$$M = \begin{pmatrix} \ddots & \vdots & \vdots & \vdots & \vdots & \vdots & \iddots \\ \cdots & \delta & \Omega_0^*/2 & 0 & 0 & 0 & \cdots \\ \cdots & \Omega_0/2 & \tilde{\Delta} & \Omega_0/2 & 0 & 0 & \cdots \\ \cdots & 0 & \Omega_0^*/2 & \delta & \Omega_0^*/2 & 0 & \cdots \\ \cdots & 0 & 0 & \Omega_0/2 & \tilde{\Delta} & \Omega_0/2 & \cdots \\ \cdots & 0 & 0 & 0 & \Omega_0^*/2 & \delta & \cdots \\ \iddots & \vdots & \vdots & \vdots & \vdots & \vdots & \ddots \end{pmatrix}. \tag{B.3}$$

For equations (3.51), we subtract $n\Delta_{\mathrm{d}}$ (n is the number of the row such that the middle one has $n = 0$) from the diagonal elements of the above matrix.

We can write the equations for the electric field as

$$\begin{pmatrix} \frac{q}{n_0} & 0 \\ 0 & -\frac{q}{n_0} \end{pmatrix} \boldsymbol{\mathcal{E}} = \frac{g\sqrt{2\pi}}{c} V^{\mathrm{T}} \boldsymbol{\sigma}, \tag{B.4}$$

where V^{T} is the transpose of the matrix V. Using equation (B.1) and defining

$$M_{\mathcal{E}} = (\Gamma_{1\mathrm{D}}/2) V^{\mathrm{T}} M^{-1} V, \tag{B.5}$$

equations (B.4) become

$$\begin{pmatrix} M_{\mathcal{E},11} + \frac{q}{n_0} & M_{\mathcal{E},12} \\ M_{\mathcal{E},21} & M_{\mathcal{E},22} - \frac{q}{n_0} \end{pmatrix} \boldsymbol{\mathcal{E}} = \begin{pmatrix} 0 \\ 0 \end{pmatrix}, \tag{B.6}$$

where $M_{\mathcal{E},kl}$ are the elements of $M_{\mathcal{E}}$. This equation is the equivalent of equation (3.37), but more general, since it is possible that $M_{\mathcal{E},11} \neq M_{\mathcal{E},22}$ (for the dual-color scheme). For equation (B.6) to have non-trivial solutions, the determinant of the matrix on the left hand side should be equal to zero. Hence, we get the equation

$$\left(\frac{q}{n_0}\right)^2 + \frac{q}{n_0}(M_{\mathcal{E},11} - M_{\mathcal{E},22}) - \det(M_{\mathcal{E}}) = 0, \tag{B.7}$$

where $\det(M_{\mathcal{E}})$ is the determinant of $M_{\mathcal{E}}$. The dispersion relation is found by solving equation (B.7).

Appendix C

Effective mass for the regularly placed Λ-type scheme

In this appendix, we derive the expression for the effective mass (3.100). For the single-mode case, we have that

$$\mathrm{tr}(T_{\mathrm{cell}}) = \lambda + 1/\lambda, \tag{C.1}$$

where $\mathrm{tr}(T_{\mathrm{cell}})$ is the trace of T_{cell}, and λ is one of the eigenvalues of T_{cell}. Since the length of the unit cell is $L_{\mathrm{u}} = \pi/k_0$, equation (C.1) together with equation (3.93) implies that

$$\cos(qL_{\mathrm{u}}) = -\frac{1}{2}\mathrm{tr}(T_{\mathrm{cell}}), \tag{C.2}$$

The right hand side of this equation is a function of δ. We will solve it perturbatively to find δ as a function of q. Then the mass is found as the coefficient of the second order term in q in the series expansion.

For small δ and $\Omega_0 \neq 0$, the scattering coefficient β_j (given by equation (3.62) with $\Omega(z_j) = \Omega_0 \cos(k_0 z_j)$) can be approximated by

$$\beta_j \approx -i\frac{\Gamma_{1\mathrm{D}}}{2|\Omega_0|^2\cos^2(k_0 z_j)}\delta. \tag{C.3}$$

The precise condition for this approximation to be valid is that

$$\delta \ll \frac{|\Omega_0|^2}{|\tilde{\Delta}|}\cos^2(k_0 z_j) \tag{C.4}$$

has to be fulfilled for all the atoms in the unit cell which experience non-vanishing classical drive, i.e. the frequency has to be within their EIT windows. The right hand side of equation (C.4) is smallest for the atoms placed at $k_0 z_j = \pm(\pi/2 - \pi/N_{\mathrm{u}})$ (see figure 3.4). This leads to the condition given by equation (3.98) of the main text.

For the chosen unit cells in figure 3.4 and numbering the atoms from the left (such that the leftmost atom in the unit cell has index $j = 1$), we have within the approximation

above that β_j for $1 \leq j \leq N_\mathrm{u} - 1$ is inversely proportional to the classical field strength. We define

$$\beta_\mathrm{c} = -i\frac{\Gamma_\mathrm{1D}}{2|\Omega_0|^2}\delta, \tag{C.5}$$

so that for the chosen unit cells we have

$$\beta_j \approx \frac{\beta_\mathrm{c}}{\cos^2((j - N_\mathrm{u}/2)k_0 d)} \tag{C.6}$$

with $d = \pi/(N_\mathrm{u}k_0)$.

On the other hand, the last atom in the unit cell, which is positioned at the node of the standing wave of the classical drive, will instead be described by equation (3.62) with $\Omega(z_j) = 0$, i.e.

$$\beta_{N_\mathrm{u}} \approx \frac{\Gamma_\mathrm{1D}}{\Gamma' - 2i\Delta_\mathrm{c}}, \tag{C.7}$$

where we have approximated $\Delta \approx \Delta_\mathrm{c}$, since we assume $\delta \ll \Delta_\mathrm{c}$. This last atom effectively behaves as a two-level atom.

The claim now is that in this approximation and for even N_u, we have to first order in β_c that

$$\frac{1}{2}\mathrm{tr}(T_\mathrm{cell}) \approx -1 - 2(N_\mathrm{u} - 1)\beta_{N_\mathrm{u}}\beta_\mathrm{c}. \tag{C.8}$$

We will prove this claim below, but first we show how it leads to the desired expression for the effective mass (3.100). If we expand the left hand side of equation (C.2) around $qd = 0$, we find

$$\cos(qL_\mathrm{u}) = \cos(N_\mathrm{u}qd) \approx 1 + \frac{1}{2}N_\mathrm{u}^2\,(qd)^2\,. \tag{C.9}$$

Then, using equations (C.8) and (C.9) for respectively the right hand side and the left hand side of equation (C.2) together with equations (C.7) and (C.5), we get

$$\frac{1}{2}\,(qd)^2 \approx -\frac{(N_\mathrm{u} - 1)\Gamma_\mathrm{1D}^2}{2N_\mathrm{u}^2(\Delta_\mathrm{c} + i\Gamma'/2)|\Omega_0|^2}\delta. \tag{C.10}$$

Comparing this expression with equation (3.99), we find the mass given by equation (3.100).

Now we prove the claim (C.8). The transfer matrices for the atoms have elements given by equations (3.86) with the scalar β_j given by either equation (C.3) or equation (C.7). We first find the product of the transfer matrices for the atoms with $1 \leq j \leq N_\mathrm{u} - 1$ and free propagation between them. If $T_{\mathrm{a},j}$ is the transfer matrix for the atom with β_j, and T_f is the free propagation matrix given by equation (3.89) with $d = \pi/(N_\mathrm{u}k_0)$, then we can recursively define the partial product by $T^{(j)} = T_\mathrm{f}T_{\mathrm{a},j}T^{(j-1)}$

for $2 \leq j \leq N_{\mathrm{u}} - 1$, and $T^{(1)} = T_{\mathrm{f}} T_{\mathrm{a},1}$. In terms of the elements of the matrix $T^{(j)}$ we have to first order in β_j that

$$T_{11}^{(j)} \approx \left(1 - \sum_{j'=1}^{j} \beta_{j'}\right) e^{ijk_0 d} \tag{C.11a}$$

$$T_{22}^{(j)} \approx \left(1 + \sum_{j'=1}^{j} \beta_{j'}\right) e^{-ijk_0 d} \tag{C.11b}$$

$$T_{21}^{(j)} \approx \sum_{j'=1}^{j} \beta_{j'} e^{i(2j'-j-2)k_0 d} \tag{C.11c}$$

$$T_{12}^{(j)} \approx -\sum_{j'=1}^{j} \beta_{j'} e^{-i(2j'-j-2)k_0 d} \tag{C.11d}$$

We can now find

$$\mathrm{tr}(T_{\mathrm{cell}}) = \mathrm{tr}\Big(T_{\mathrm{f}} T_{a,N_{\mathrm{u}}} T^{(N_{\mathrm{u}}-1)}\Big). \tag{C.12}$$

After writing the matrix product out, taking the trace and using $\exp(iN_{\mathrm{u}}k_0 d) = -1$ we get

$$\mathrm{tr}(T_{\mathrm{cell}}) \approx -2 - 4\beta_{N_{\mathrm{u}}} \sum_{j=1}^{N_{\mathrm{u}}-1} \beta_j \cos^2((j - N_{\mathrm{u}}/2)k_0 d) \tag{C.13}$$

Using equation (C.6), the above simplifies to

$$\mathrm{tr}(T_{\mathrm{cell}}) \approx -2 - 4\beta_{N_{\mathrm{u}}} \sum_{j=1}^{N_{\mathrm{u}}-1} \beta_{\mathrm{c}}, \tag{C.14}$$

which is the same as equation (C.8).

Bibliography

[1] S. Das, A. Grankin, I. Iakoupov, E. Brion, J. Borregaard, R. Boddeda, I. Usmani, A. Ourjoumtsev, P. Grangier, and A. S. Sørensen, "Photonic controlled-phase gates through rydberg blockade in optical cavities," Phys. Rev. A **93**, 040303 (2016).

[2] S. Das, A. Grankin, I. Iakoupov, E. Brion, J. Borregaard, R. Boddeda, I. Usmani, A. Ourjoumtsev, P. Grangier, and A. S. Sørensen, "Photonic controlled-phase gates through rydberg blockade in optical cavities," (2015), arXiv:1506.04300 .

[3] H. L. Sørensen, J.-B. Béguin, K. W. Kluge, I. Iakoupov, A. S. Sørensen, J. H. Müller, E. S. Polzik, and J. Appel, "Coherent backscattering of light off one-dimensional atomic strings," Phys. Rev. Lett. **117**, 133604 (2016).

[4] I. Iakoupov, J. R. Ott, D. E. Chang, and A. S. Sørensen, "Dispersion relations for stationary light in one-dimensional atomic ensembles," Phys. Rev. A **94**, 053824 (2016).

[5] I. Iakoupov, J. Borregaard, and A. S. Sørensen, "Controlled-phase gate for photons based on stationary light," (2016), arXiv:1610.09206 .

[6] H. J. Kimble, "The quantum internet," Nature **453**, 1023 (2008).

[7] L.-M. Duan and H. J. Kimble, "Scalable photonic quantum computation through cavity-assisted interactions," Phys. Rev. Lett. **92**, 127902 (2004).

[8] D. E. Chang, A. S. Sorensen, E. A. Demler, and M. D. Lukin, "A single-photon transistor using nanoscale surface plasmons," Nat Phys **3**, 807 (2007).

[9] H. Kim, R. Bose, T. C. Shen, G. S. Solomon, and E. Waks, "A quantum logic gate between a solid-state quantum bit and a photon," Nat Photon **7**, 373 (2013).

[10] W. Chen, K. M. Beck, R. Bücker, M. Gullans, M. D. Lukin, H. Tanji-Suzuki, and V. Vuletić, "All-optical switch and transistor gated by one stored photon," Science **341**, 768 (2013).

[11] T. G. Tiecke, J. D. Thompson, N. P. de Leon, L. R. Liu, V. Vuletić, and M. D. Lukin, "Nanophotonic quantum phase switch with a single atom," Nature **508**, 241 (2014).

[12] B. Hacker, S. Welte, G. Rempe, and S. Ritter, "A photon–photon quantum gate based on a single atom in an optical resonator," Nature **536**, 193 (2016).

[13] J. Volz, M. Scheucher, C. Junge, and A. Rauschenbeutel, "Nonlinear [pi] phase shift for single fibre-guided photons interacting with a single resonator-enhanced atom," Nat Photon **8**, 965 (2014).

[14] A. V. Akimov, A. Mukherjee, C. L. Yu, D. E. Chang, A. S. Zibrov, P. R. Hemmer, H. Park, and M. D. Lukin, "Generation of single optical plasmons in metallic nanowires coupled to quantum dots," Nature **450**, 402 (2007).

[15] J. Claudon, J. Bleuse, N. S. Malik, M. Bazin, P. Jaffrennou, N. Gregersen, C. Sauvan, P. Lalanne, and J.-M. Gérard, "A highly efficient single-photon source based on a quantum dot in a photonic nanowire," Nat Photon **4**, 174 (2010).

[16] A. Goban, C.-L. Hung, S.-P. Yu, J. D. Hood, J. A. Muniz, J. H. Lee, M. J. Martin, A. C. McClung, K. S. Choi, D. E. Chang, O. Painter, and H. J. Kimble, "Atom–light interactions in photonic crystals," Nat Commun **5** (2014).

[17] I. Söllner, S. Mahmoodian, S. L. Hansen, L. Midolo, A. Javadi, G. Kiršanskė, T. Pregnolato, H. El-Ella, E. H. Lee, J. D. Song, S. Stobbe, and P. Lodahl, "Deterministic photon–emitter coupling in chiral photonic circuits," Nat Nano **10**, 775 (2015).

[18] K. Hammerer, A. S. Sørensen, and E. S. Polzik, "Quantum interface between light and atomic ensembles," Rev. Mod. Phys. **82**, 1041 (2010).

[19] M. Saffman, T. G. Walker, and K. Mølmer, "Quantum information with rydberg atoms," Rev. Mod. Phys. **82**, 2313 (2010).

[20] O. Firstenberg, C. S. Adams, and S. Hofferberth, "Nonlinear quantum optics mediated by rydberg interactions," Journal of Physics B: Atomic, Molecular and Optical Physics **49**, 152003 (2016).

[21] D. E. Chang, L. Jiang, A. V. Gorshkov, and H. J. Kimble, "Cavity qed with atomic mirrors," New Journal of Physics **14**, 063003 (2012).

[22] M. Hafezi, D. E. Chang, V. Gritsev, E. Demler, and M. D. Lukin, "Quantum transport of strongly interacting photons in a one-dimensional nonlinear waveguide," Phys. Rev. A **85**, 013822 (2012).

[23] F. Le Kien, V. I. Balykin, and K. Hakuta, "Atom trap and waveguide using a two-color evanescent light field around a subwavelength-diameter optical fiber," Phys. Rev. A **70**, 063403 (2004).

[24] E. Vetsch, D. Reitz, G. Sagué, R. Schmidt, S. T. Dawkins, and A. Rauschenbeutel, "Optical interface created by laser-cooled atoms trapped in the evanescent field surrounding an optical nanofiber," Phys. Rev. Lett. **104**, 203603 (2010).

[25] A. Goban, K. S. Choi, D. J. Alton, D. Ding, C. Lacroûte, M. Pototschnig, T. Thiele, N. P. Stern, and H. J. Kimble, "Demonstration of a state-insensitive, compensated nanofiber trap," Phys. Rev. Lett. **109**, 033603 (2012).

[26] J.-B. Béguin, E. M. Bookjans, S. L. Christensen, H. L. Sørensen, J. H. Müller, E. S. Polzik, and J. Appel, "Generation and detection of a sub-poissonian atom number distribution in a one-dimensional optical lattice," Phys. Rev. Lett. **113**, 263603 (2014).

[27] B. Gouraud, D. Maxein, A. Nicolas, O. Morin, and J. Laurat, "Demonstration of a memory for tightly guided light in an optical nanofiber," Phys. Rev. Lett. **114**, 180503 (2015).

[28] M. Bajcsy, S. Hofferberth, V. Balic, T. Peyronel, M. Hafezi, A. S. Zibrov, V. Vuletic, and M. D. Lukin, "Efficient all-optical switching using slow light within a hollow fiber," Phys. Rev. Lett. **102**, 203902 (2009).

[29] F. Blatt, L. S. Simeonov, T. Halfmann, and T. Peters, "Stationary light pulses and narrowband light storage in a laser-cooled ensemble loaded into a hollow-core fiber," Phys. Rev. A **94**, 043833 (2016).

[30] J. H. Shapiro, "Single-photon kerr nonlinearities do not help quantum computation," Phys. Rev. A **73**, 062305 (2006).

[31] J. Gea-Banacloche, "Impossibility of large phase shifts via the giant kerr effect with single-photon wave packets," Phys. Rev. A **81**, 043823 (2010).

[32] I. Friedler, D. Petrosyan, M. Fleischhauer, and G. Kurizki, "Long-range interactions and entanglement of slow single-photon pulses," Phys. Rev. A **72**, 043803 (2005).

[33] E. Shahmoon, G. Kurizki, M. Fleischhauer, and D. Petrosyan, "Strongly interacting photons in hollow-core waveguides," Phys. Rev. A **83**, 033806 (2011).

[34] A. V. Gorshkov, J. Otterbach, M. Fleischhauer, T. Pohl, and M. D. Lukin, "Photon-photon interactions via rydberg blockade," Phys. Rev. Lett. **107**, 133602 (2011).

[35] D. Tiarks, S. Schmidt, G. Rempe, and S. Dürr, "Optical π phase shift created with a single-photon pulse," Science Advances **2** (2016), 10.1126/sciadv.1600036.

[36] A. Albrecht, T. Caneva, and D. E. Chang, "Changing optical band structure with single photons," (2016), arXiv:1603.05432 .

[37] R. Dum, A. S. Parkins, P. Zoller, and C. W. Gardiner, "Monte carlo simulation of master equations in quantum optics for vacuum, thermal, and squeezed reservoirs," Phys. Rev. A **46**, 4382 (1992).

[38] J. Dalibard, Y. Castin, and K. Mølmer, "Wave-function approach to dissipative processes in quantum optics," Phys. Rev. Lett. **68**, 580 (1992).

[39] A. Gilchrist, N. K. Langford, and M. A. Nielsen, "Distance measures to compare real and ideal quantum processes," Phys. Rev. A **71**, 062310 (2005).

[40] E. Knill, R. Laflamme, and G. J. Milburn, "A scheme for efficient quantum computation with linear optics," Nature **409**, 46 (2001).

[41] P. Kok, W. J. Munro, K. Nemoto, T. C. Ralph, J. P. Dowling, and G. J. Milburn, "Linear optical quantum computing with photonic qubits," Rev. Mod. Phys. **79**, 135 (2007).

[42] L.-M. Duan, M. D. Lukin, J. I. Cirac, and P. Zoller, "Long-distance quantum communication with atomic ensembles and linear optics," Nature **414**, 413 (2001).

[43] N. Sangouard, C. Simon, H. de Riedmatten, and N. Gisin, "Quantum repeaters based on atomic ensembles and linear optics," Rev. Mod. Phys. **83**, 33 (2011).

[44] B. Schumacher, "Sending entanglement through noisy quantum channels," Phys. Rev. A **54**, 2614 (1996).

[45] M. A. Nielsen, "A simple formula for the average gate fidelity of a quantum dynamical operation," Physics Letters A **303**, 249 (2002).

[46] M.-D. Choi, "Completely positive linear maps on complex matrices," Linear Algebra and its Applications **10**, 285 (1975).

[47] A. Jamiołkowski, "Linear transformations which preserve trace and positive semidefiniteness of operators," Reports on Mathematical Physics **3**, 275 (1972).

[48] L. V. Hau, S. E. Harris, Z. Dutton, and C. H. Behroozi, "Light speed reduction to 17 metres per second in an ultracold atomic gas," Nature **397**, 594 (1999).

[49] M. D. Lukin, "*Colloquium* : Trapping and manipulating photon states in atomic ensembles," Rev. Mod. Phys. **75**, 457 (2003).

[50] C. Liu, Z. Dutton, C. H. Behroozi, and L. V. Hau, "Observation of coherent optical information storage in an atomic medium using halted light pulses," Nature **409**, 490 (2001).

[51] D. F. Phillips, A. Fleischhauer, A. Mair, R. L. Walsworth, and M. D. Lukin, "Storage of light in atomic vapor," Phys. Rev. Lett. **86**, 783 (2001).

[52] M. Fleischhauer and M. D. Lukin, "Dark-state polaritons in electromagnetically induced transparency," Phys. Rev. Lett. **84**, 5094 (2000).

[53] J. T. Shen and S. Fan, "Coherent photon transport from spontaneous emission in one-dimensional waveguides," Opt. Lett. **30**, 2001 (2005).

[54] A. V. Gorshkov, A. André, M. D. Lukin, and A. S. Sørensen, "Photon storage in Λ-type optically dense atomic media. I. Cavity model," Phys. Rev. A **76**, 033804 (2007).

[55] A. V. Gorshkov, A. André, M. D. Lukin, and A. S. Sørensen, "Photon storage in Λ-type optically dense atomic media. II. Free-space model," Phys. Rev. A **76**, 033805 (2007).

[56] R. H. Hadfield, "Single-photon detectors for optical quantum information applications," Nat Photon **3**, 696 (2009).

[57] H. J. Briegel, D. E. Browne, W. Dur, R. Raussendorf, and M. Van den Nest, "Measurement-based quantum computation," Nat Phys , 19 (2009).

[58] Y. Li, P. C. Humphreys, G. J. Mendoza, and S. C. Benjamin, "Resource costs for fault-tolerant linear optical quantum computing," Phys. Rev. X **5**, 041007 (2015).

[59] I. Iakoupov, *Photon gates in atomic ensembles*, Master's thesis, University of Copenhagen (2013).

[60] A. André and M. D. Lukin, "Manipulating light pulses via dynamically controlled photonic band gap," Phys. Rev. Lett. **89**, 143602 (2002).

[61] M. Bajcsy, A. S. Zibrov, and M. D. Lukin, "Stationary pulses of light in an atomic medium," Nature **426**, 638 (2003).

[62] D. E. Chang, V. Gritsev, G. Morigi, V. Vuletić, M. D. Lukin, and E. A. Demler, "Crystallization of strongly interacting photons in a nonlinear optical fibre," Nat Phys **4**, 884 (2008).

[63] S.-P. Yu, J. D. Hood, J. A. Muniz, M. J. Martin, R. Norte, C.-L. Hung, S. M. Meenehan, J. D. Cohen, O. Painter, and H. J. Kimble, "Nanowire photonic crystal waveguides for single-atom trapping and strong light-matter interactions," Applied Physics Letters **104**, 111103 (2014).

[64] D. Witthaut and A. S. Sørensen, "Photon scattering by a three-level emitter in a one-dimensional waveguide," New Journal of Physics **12**, 043052 (2010).

[65] D. E. Chang, A. H. Safavi-Naeini, M. Hafezi, and O. Painter, "Slowing and stopping light using an optomechanical crystal array," New Journal of Physics **13**, 023003 (2011).

[66] S. A. Moiseev and B. S. Ham, "Quantum manipulation of two-color stationary light: Quantum wavelength conversion," Phys. Rev. A **73**, 033812 (2006).

[67] F. E. Zimmer, J. Otterbach, R. G. Unanyan, B. W. Shore, and M. Fleischhauer, "Dark-state polaritons for multicomponent and stationary light fields," Phys. Rev. A **77**, 063823 (2008).

[68] S. A. Moiseev, A. I. Sidorova, and B. S. Ham, "Stationary and quasistationary light pulses in three-level cold atomic systems," Phys. Rev. A **89**, 043802 (2014).

[69] K. R. Hansen and K. Mølmer, "Stationary light pulses in ultracold atomic gases," Phys. Rev. A **75**, 065804 (2007).

[70] G. Nikoghosyan and M. Fleischhauer, "Stationary light in cold-atomic gases," Phys. Rev. A **80**, 013818 (2009).

[71] Y.-W. Lin, W.-T. Liao, T. Peters, H.-C. Chou, J.-S. Wang, H.-W. Cho, P.-C. Kuan, and I. A. Yu, "Stationary light pulses in cold atomic media and without bragg gratings," Phys. Rev. Lett. **102**, 213601 (2009).

[72] J.-H. Wu, M. Artoni, and G. C. La Rocca, "Decay of stationary light pulses in ultracold atoms," Phys. Rev. A **81**, 033822 (2010).

[73] J.-H. Wu, M. Artoni, and G. C. La Rocca, "Stationary light pulses in cold thermal atomic clouds," Phys. Rev. A **82**, 013807 (2010).

[74] T. Peters, S.-W. Su, Y.-H. Chen, J.-S. Wang, S.-C. Gou, and I. A. Yu, "Formation of stationary light in a medium of nonstationary atoms," Phys. Rev. A **85**, 023838 (2012).

[75] M. W. Sørensen and A. S. Sørensen, "Three-dimensional theory for light-matter interaction," Phys. Rev. A **77**, 013826 (2008).

[76] S. Arlinghaus and M. Holthaus, "Generalized acceleration theorem for spatiotemporal bloch waves," Phys. Rev. B **84**, 054301 (2011).

[77] M. Holthaus, "Floquet engineering with quasienergy bands of periodically driven optical lattices," Journal of Physics B: Atomic, Molecular and Optical Physics **49**, 013001 (2016).

[78] N. Stephen, "Transfer matrix analysis of the elastostatics of one-dimensional repetitive structures," Proceedings of the Royal Society of London A: Mathematical, Physical and Engineering Sciences **462**, 2245 (2006).

[79] I. H. Deutsch, R. J. C. Spreeuw, S. L. Rolston, and W. D. Phillips, "Photonic band gaps in optical lattices," Phys. Rev. A **52**, 1394 (1995).

[80] G. Bertocchi, O. Alibart, D. B. Ostrowsky, S. Tanzilli, and P. Baldi, "Single-photon sagnac interferometer," Journal of Physics B: Atomic, Molecular and Optical Physics **39**, 1011 (2006).

[81] M. Bradford, K. C. Obi, and J.-T. Shen, "Efficient single-photon frequency conversion using a sagnac interferometer," Phys. Rev. Lett. **108**, 103902 (2012).

[82] N. Sangouard, C. Simon, B. Zhao, Y.-A. Chen, H. de Riedmatten, J.-W. Pan, and N. Gisin, "Robust and efficient quantum repeaters with atomic ensembles and linear optics," Phys. Rev. A **77**, 062301 (2008).

[83] J. Borregaard, P. Kómár, E. M. Kessler, M. D. Lukin, and A. S. Sørensen, "Long-distance entanglement distribution using individual atoms in optical cavities," Phys. Rev. A **92**, 012307 (2015).

[84] T. Caneva, M. T. Manzoni, T. Shi, J. S. Douglas, J. I. Cirac, and D. E. Chang, "Quantum dynamics of propagating photons with strong interactions: a generalized input–output formalism," New Journal of Physics **17**, 113001 (2015).